THE APPLICATION OF STREAMLINE RESERVOIR SIMULATION CALCULATIONS TO THE MANAGEMENT OF OILFIELD SCALE

The Thesis by

Tharwat Fawzi Ragheb Hassane

Submitted for the Degree of

Doctor of Philosophy in Petroleum Engineering

Institute of Petroleum Engineering

Heriot-Watt University

Edinburgh, Scotland, UK

June 2013

ABSTRACT

Inorganic scale may precipitate in oilfield systems, down hole in the reservoir, in the production flow tubing, and in surface facilities, as a consequence of thermodynamic changes that affect the flowing brines. These changes may be induced by temperature or pressure changes, or by mixing of incompatible brines. While much work has been performed to study the effect of thermodynamic changes such as pressure decrease or temperature increase on scale precipitation, it is only recently that a body of work has been developed on the impact that the dynamics of brine mixing in the reservoir has on scale precipitation *in situ*. Much of this work has been conducted using finite difference simulators, which are handicapped with regard to these calculations in that numerical dispersion effects can be orders of magnitude greater than physical dispersion. The introduction of chemical reaction calculations into streamline simulation models presents a very significant opportunity for improving the accuracy of such calculations. While numerical dispersion effects for immiscible calculations (eg water displacing oil) can be countered by pseudoisation of the relative permeability functions, in finite difference models it is difficult to control numerical dispersion for miscible displacements e.g. seawater (with a Sulphate concentration) displacing formation water (with a Barium concentration), which may lead to scaling in the reservoir (Barium Sulphate precipitation). Streamline simulation reduces the numerical errors for both miscible and immiscible displacement, thus making the scaling calculations much more accurate. The objective of this PhD project was to study the application of a streamline simulator, which has the appropriate chemistry modeling capabilities, to realistic reservoir scenarios. The project consisted of two stages:

1) Study of synthetic systems to identify the impact of brine mixing in simple scenarios (eg single layer and multi-layer quarter five spot patterns)

2) Application of the technique to full field reservoir systems to improve the capability of making scale management decision during the project Front End Engineering and Design (FEED) phase.

The calculations performed demonstrate where, and under what conditions, scale precipitation takes place in situ in the reservoir, and what the resulting impact on the chemical composition of the produced brine will be. This information is key in the planning of the management of oilfield scale.

ACKNOWLEDGEMENTS

I would like to express my sincere gratitude to my supervisor, Professor Eric Mackay, for his invaluable guidance, motivation and support throughout the course of my PhD. It would have been very difficult for me to have reached this point in my academic journey, without his leadership and technical criticism, which is highly appreciated. He has been a constant source of inspiration throughout this research.

My endless gratitude goes to my parents for their prayers and patience throughout the course of my study. I would like to thank my brother, sisters, relatives, friends, and well-wishers for their help and encouragement for which I am deeply grateful.

I am also grateful to British Petroleum (BP) and Schlumberger for their support both technical and financial. Without their financial contribution towards the cost of my PhD at Heriot-Watt University, Edinburgh, UK, I would not have been able to complete this study. My sincere gratitude also goes to FAST sponsors (Baker Petrolite, BP, BG Group, BWA Water Additives, Champion Technologies, Chevron, Clariant Oil Services, Conoco-Phillips, Halliburton, MI Swaco, Nalco, PETROBRAS, PETRONAS, PTT, REP, Rhodia, Saudi Aramco, Shell, Statoil Hydro, Talisman Energy, ThermPhos and Total) for their invaluable feedback.

I would like to thanks also Allan Thomson from Schlumberger who helped in obtaining valuable references. Furthermore, I would like to thank Dr. Fazrie Wahid for his technical support, which was of great assistance during this research during my job with Schlumberger. Needless to say, I would like to express my sincere gratitude to all the members of the Flow Assurance and Scale Team (FAST) for making my stay at Heriot-Watt a memorable one. Prof. Eric Mackay deserves further praise for the guidance and motivation he provided, on both academic and non-academic issues. I would like to acknowledge my manager in BP Egypt, Mr. Barry and Mr. Mick Mactier, for their financial support for my stay in Edinburgh. Special thanks go to Heather O'Hara of FAST for her administrative help.

Finally, I am sincerely grateful to my beloved wife Reham, and my children, Engy, Rana, Malak and Gana. Reham made a unique contribution at every step during the period of my research, providing constant support and encouragement.

TABLE OF CONTENTS

LIST OF FIGURES

LIST OF TABLES

NOMENCLATURE

1D	One-dimensional
2D	Two-dimensional
3D	Three-dimensional
Ba	Barium
$BaSO_4$	Barium sulphate (barite)
C	Tracer concentration (mg/l)
$CaSO_4$	Carbonate sulphate (anhydrite)
$CaSO_4.2H_2O$	Calcium sulphate (gypsum)
CFL	Courant-Friedrichs-Lewy constraint
C_o	Initial injected tracer concentration (mg/l)
CW	Connate water
FDM	Finite difference methods
FOPR	Field Oil Production Rate (bbl/day)
FWPR	Field Water Production Rate (bbl/day)
FPR	Field Average Pressure (psia)
IMPES	Implicit pressure explicit saturation
IW	Injected water
K	Permeability (mD)
L	System length (ft)
NaCl	Sodium chloride (halite)
Pb	Bubble point pressure (psia)
PDE	Partial differential equations
PV	Pore Volume
PVI	Pore Volume Injection

PERMX	Permeability in x Direction
PERMY	Permeability in y Direction
PERMZ	Permeability in z Direction
Q	Fluid rate (bbl/day)
$SrSO_4$	Strontium sulphate (celestite)
SiO_2	Silicone dioxide (quartz)
S_w	Water saturation
S_{wc}	Connate water saturation
t	Time, (days)
TOF	Time of Flight
u	Total velocity, $u=Q/A$ (ft/day)
v	Fluid velocity (Darcy velocity) $v=u/\phi$ (ft/day)
WWIT	Well Water Injection Total (bbl)
WWCT	Well Water Cut
x	Distance (ft)
X_D	Dimensionless distance, $X_D=x/L$
Δt	Length of time step (days)
ϕ	Porosity
ρ_o	Oil density (lb/ft^3)
SO_4	Sulphate
λ_t	Total mobility
λ_g	Total gravity mobility
G_j	the velocity due to gravity effects

CHAPTER 1: INTRODUCTION

1.1 INTRODUCTION AND OBJECTIVES

Scale is the hard crystalline deposit resulting from the precipitation of mineral compounds present in water. Oilfield scale consists of one or more types of inorganic deposit along with other debris. There are various types of scale: one of them occurs when the fluid is undergoing production and this causes a reduction in the solubility of carbon dioxide (CO_2), due to decrease in pressure. As the brine passes through the bubble point pressure (Pb), carbon dioxide is evolved. As carbon dioxide is produced the pH increases, and the solubility with respect to various carbonate minerals decreases rapidly. A precipitate is formed with divalent ions such as iron and more commonly calcium as outlined in the following equation.

$$Ca(HCO_3)_2 = CaCO_3 + CO_2 + H_2O$$

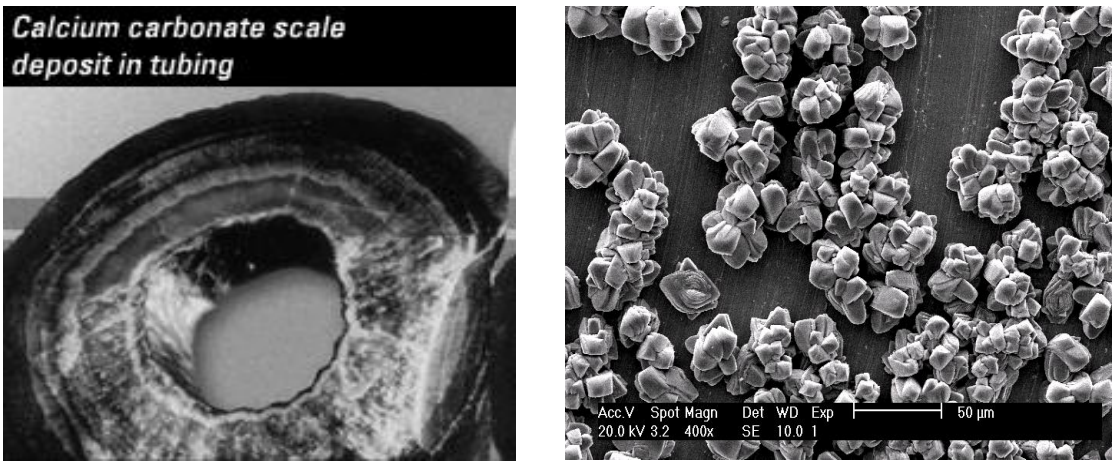

(a) (b)

Figure 1.1: Images of scale formed in the oil and gas industry (a) cross section of a partially blocked tube (b) scale crystals formed on a metal surface.

If the brine pressure does not drop below the carbon dioxide bubble point pressure until the brine is in the production well, then the calcium carbonate scale will not form in the reservoir. However, if the bubble point migrates down the tubing and into the reservoir

as a result of the reservoir pressure depletion, calcium carbonate may precipitate in the reservoir (Mackay, 2003).

There are many factors contributing to scale deposition and different scales may be subjected to different influencing factors, so the common causes of oilfield scale include the following:-

- Alteration in pressure and temperature.
- Evaporation.
- Comingling of incompatible brines.

1.1.1 Alteration in Pressure and Temperature

The solubility of a mineral scale changes with pressure and temperature. For example $CaCO_3$ solubility decreases with pressure drop and $BaSO_4$ solubility decreases with temperature decline. Therefore, the respective scale may precipitate out from the fluid produced as it flows from the wellbore up to the wellhead due to pressure depletion or temperature drop. Carbonate scale formation is mainly caused by pressure reduction.

1.1.2 Evaporation

If brines presents in the reservoir come into contact with continuous gas stream evaporation may take place. The most abundant ions are normally sodium and chloride and so halite (NaCl) precipitation may occur. And at the same time CO_2 gas is released from the produced water, increasing the pH which further decreases the solubility of $CaCO_3$. Therefore, carbonate scale can be deposited from single brine. High temperatures and the presence of particles may accelerate crystal growth, which will increase the precipitation rate.

1.1.3 Comingling of Incompatible Brines

The research presented here will focus on this type of scale formation. The principle cause of sulphate scale is the mixing of incompatible brines. Waterflooding is one of the most common methods of oil recovery, although it does lead to certain production problems after water breaks through e.g. corrosion, scaling etc. Most commonly, barium (Ba) ions present in the formation water can interact with Sulphate ions (SO_4) present in the injected water, and the brine mixes to form barium sulphate ($BaSO_4$).

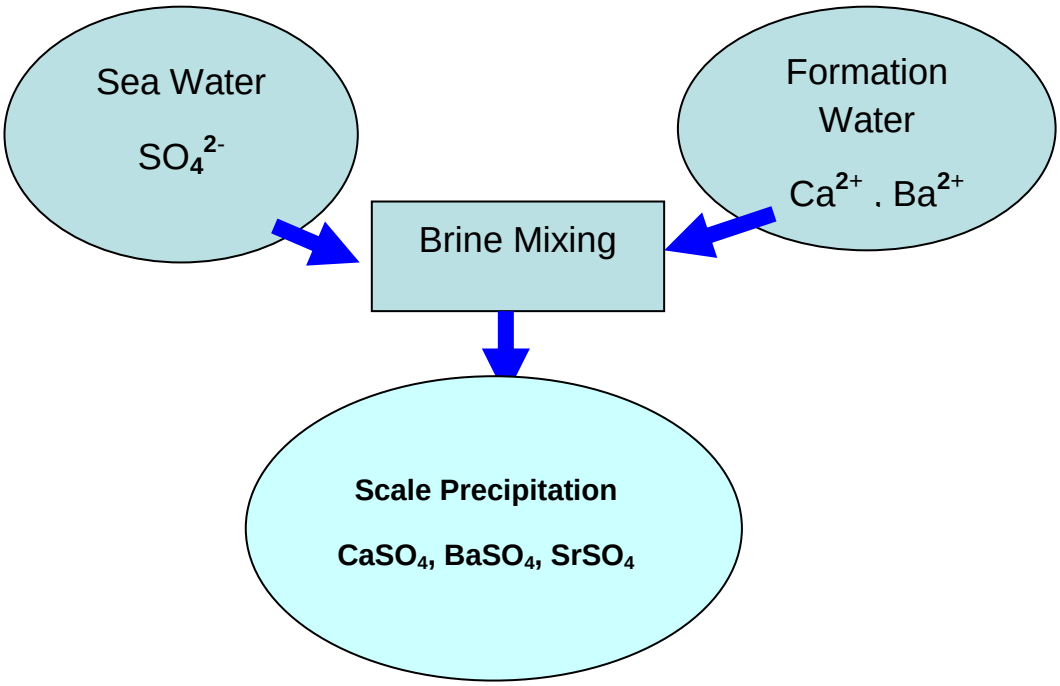

Figure 1.2: Mixing of brines that lead to precipitation of Sulphate scales.

Precipitation of sulphate scale is a complex process and is governed by factors like the compositions of various water patterns of water mixing, formation of geological structure, kinetics of precipitation, temperature and pressure environment, areal placement of the injectors and type of producer (i.e. horizontal or vertical). It is understood that the area with the greatest propensity for scale precipitation is the near wellbore formation adjacent to production wells, where turbulent flow regimes, water coning and flow convergence increase the potential for brine mixing (Mackay 2003).

Barium sulphate is the least soluble and hardest common scale, as shown in Table 1.1. It also exhibits an extremely high thermodynamic stability when formed. These factors make barium sulphate the most difficult scale to remove and it is commonly considered the most difficult to prevent. Barium sulphate is the most common acid insoluble scale but there are others: strontium sulphate (celestite – $SrSO_4$) and calcium sulphate (anhydrite – $CaSO_4$, gypsum – $CaSO_4$.2H2O), which are all collectively referred to as sulphate scales.

Name	Synonym	Formula	Hardness (Mohs)	Solubility		
				cold water (mg/l)	hot water (mg/l)	other
Common Scales						
barium sulphate	barite	$BaSO_4$	3.3	2.2	3.4	60 mg/l in 3% HCl
calcium carbonate	calcite	$CaCO_3$	3	14	18	acid soluble
strontium sulphate	celestite	$SrSO_4$	3	113	140	slightly acid soluble
calcium sulphate	anhydrite	$CaSO_4$	3	2090	6190	acid soluble
calcium sulphate	gypsum	$CaSO_4.2H_2O$	2	2410	2220	acid soluble
sodium chloride	halite	NaCl	2	357000	391200	(insoluble in HCl)
Sand Grains						
silicone dioxide	quartz	SiO_2	7	insoluble	insoluble	HF soluble
NOTE: Mohs hardness scale from 1 (soft) to 10 (hard)						

Table 1.1: Properties of commonly occurring scales. Note low solubility of barium sulphate scale. (After Mackay et al. 2004)

Oilfield scales that precipitate from brine solution adhere to solid surfaces in the reservoir, production tubing or surface facilities. Scale accumulation causes problems such as constriction of fluid flow, production impairment and damage of down hole equipment.

1.2 TYPES OF SCALE

There are basically two main types of oilfield scale: carbonate and sulphate scales.

1.2.1 **Carbonate Scales**

Carbonate scales usually result from a reduction in pressure or an increase in temperature which may cause calcium and bicarbonate ions to precipitate as calcium carbonate (calcite $CaCO_3$). The drops in fluid pressures that occur in the wellbore are the most common cause of $CaCO_3$ precipitation, although mixing of two brines, where one is rich in calcium ions and the other rich in bicarbonate ions may also lead to precipitation. Mechanical constrictions in the well cause greater pressure drops and as a result these are particularly prone to scaling. Electrical Submersible Pumps (ESPs), reacting to the heat generated from the pump, create greater pressure drops and increase the temperature and therefore will be doubly at risk. Carbonate scales generally appear early in the field life, when formation waters are produced.

1.2.1.1 Characteristics of Carbonate Scales

Carbonate scales are typically softer than other types of scale, and they tend to be soluble. These two features mean that they can be removed from the wellbore by washing using appropriate dissolvers.

If the reservoir is being depleted, the CO_2 bubble point may migrate down the production string and into the formation, which makes the scaling problem more complicated to treat. The application of chemical inhibitors can prevent carbonate scale accumulation in the wellbore and in the formation at the location where the chemical is applied, say by a scale inhibitor squeeze treatment. Figure 1.3(a) shows an image of a pipe partially obstructed by $Caco_3$, and Figure 1.3(b) shows a pipe with a mixed $CaCO_3$ / $BaSO_4$ scale.

(a) (b)

Figure 1.3: Section of tubing pulled from wells due CaCO3 and due to mixed $BaSO_4$ scale damage.

1.2.2 Sulphate Scales

Greater attention will be placed on sulphate scales, because these are the topic of the research in this thesis. As already mentioned, sulphate scales tend to form as a result of mixing of incompatible brines. Figure 1.4 shows an example of $BaSO_4$ precipitation occupying the space between sand grains in a rock sample.

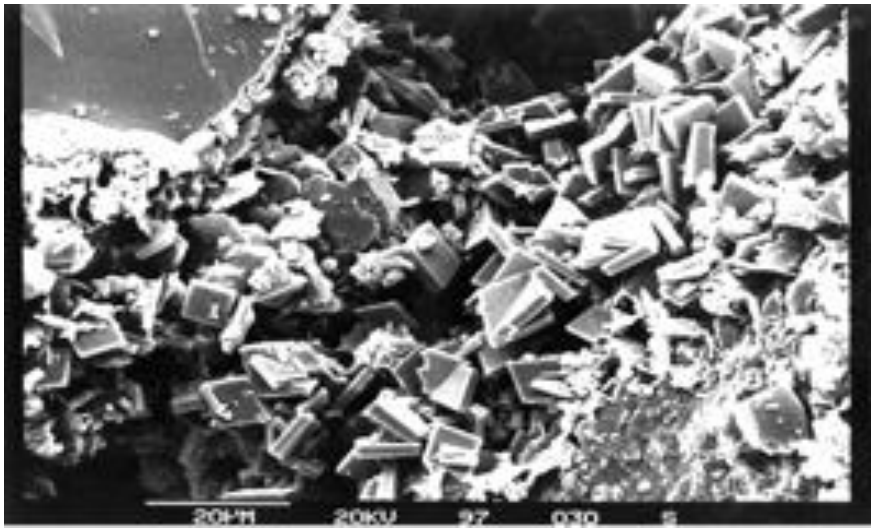

Figure 1.4: $BaSO_4$ crystals plugging the pore space between two sand grains, which are located top left and bottom right.

(a) (b)

Figure 1.5: Show two pictures, one of the baffles in a separator covered in $BaSO_4$ (a) and the second ones shows the baffles ones the scale has been removed (b).

Improvement in reservoir performance is often achieved by injecting water, which achieves two purposes: driving oil towards the production well and maintaining the reservoir pressure. Pressure maintenance is important because it ensures the oil remains above the bubble point pressure, and so gas remains in solution .Were gas to come out of solution then both phases would compete for the pore space and oil mobility would be reduced. In addition, pressure maintenance by water injection ensures a greater drawdown (or differential between the reservoir pressure and the production well

bottom hole pressure) in the production well, and that maintains higher production rates. In its natural state $BaSO_4$ arising from seawater injection, is difficult to dissolve. Applying inhibitors (mostly by squeeze treatment) is the most effective method of managing it. Continuous injection of inhibitor in the well by capillary string through the annulus or via the gas lift mandrel are alternative forms of down hole protection. Continuous injection is frequently used topsides. An alternative method is a sulphate reduction plant to remove most of the SO_4 ions before water injection. This alternative method is deployed when the application of inhibitors may be problematic for operational reasons, such as difficulty accessing the well or problems with chemical placement. If brine mixing is what causes the sulphate scale precipitation, then it is necessary to identify where the mixing is taking place. For example, if injection water (IW) is rich in sulphate ions, and this water displaces hydrocarbon and the connate water (CW), then an IW/CW mixing zone will be established.

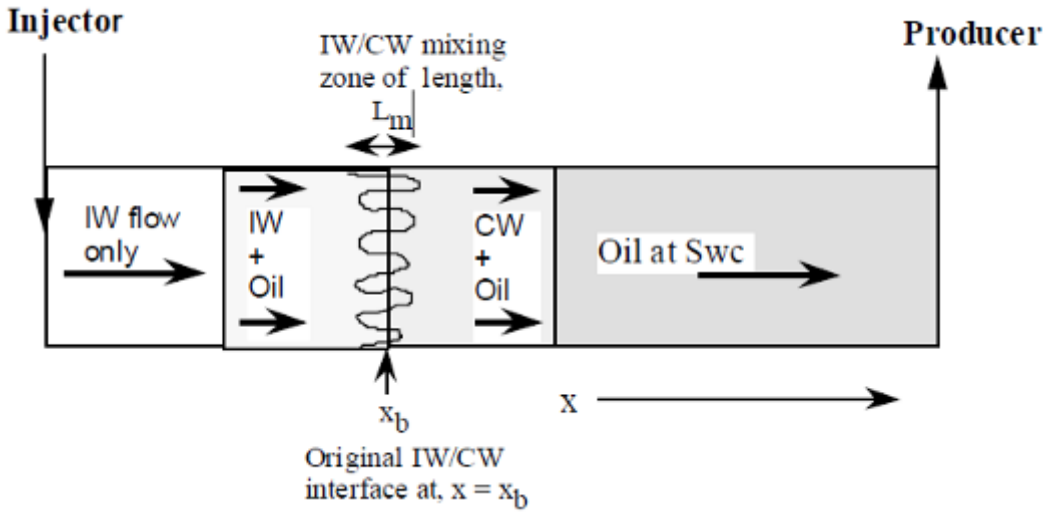

Figure 1.6: Linear Waterflooding showing the development of IW/ CW interface (after Sorbie and Mackay, 2003)

If the connate water contains barium ions, then tracking this mixing zone will allow us to identify where $BaSO_4$ precipitation takes place, as shown in Figure 1.6. Brine mixing usually refers to the mixing of injected water with the previous water in the reservoir. Seawater that has not undergone sulphate reduction will have SO_4 concentrations of approximately 3,000 ppm. Hydrocarbon bearing-rock will usually contain irreducible water saturation, the previously mentioned connate water. However, an aquifer containing water that occupies the entire pore space below the free water level can

underlie the hydrocarbon-bearing layers at the same time. Although the brine composition is usually homogeneous throughout the reservoir before production commences, quite different compositions can be found in different layers or between the hydrocarbon-bearing layers and aquifer zones. The identification of scaling potentials is more complicated in these situations, and brine mixing calculations need to take account not only of IW/CW mixing, but also of mixing between the various formations waters.

1.3 PROBLEMS CAUSED AND LOCATIONS

As noted scale precipitation may occur wherever there is brine mixing between incompatible brines.

Brines may mix at any of the following locations (Figure 1.7).

(a) Prior to injection, for example, if sea water is supplement by produced water re-injection (PWRI).

(b) Around the injection well, as injected brine enters the reservoir, contacting formation brine.

(c) Deep in the formation, caused by displacement of formation brine by injected brine, or converging flow paths.

(d) As the injection brine and formation brine converge towards the production well, and within the radius of a squeeze treatment.

(e) As the injection brine and formation brine converge towards the production well, but beyond the radius of squeeze treatment.

(f) In the completed interval of a production well, as one type of brine enters the completion, while the other type of brine follows up the tubing from a lower section.

(g) At the junction of a multilateral well, where one branch is producing one type of brine and the other branch is producing another type of brine.

(h) At the subsea manifold, where one well is producing one type of brine and the other branch is producing another type of brine.

(i) At the surface facilities, where one production stream is flowing there is one type of brine and where another production stream is flowing there is another type of brine.

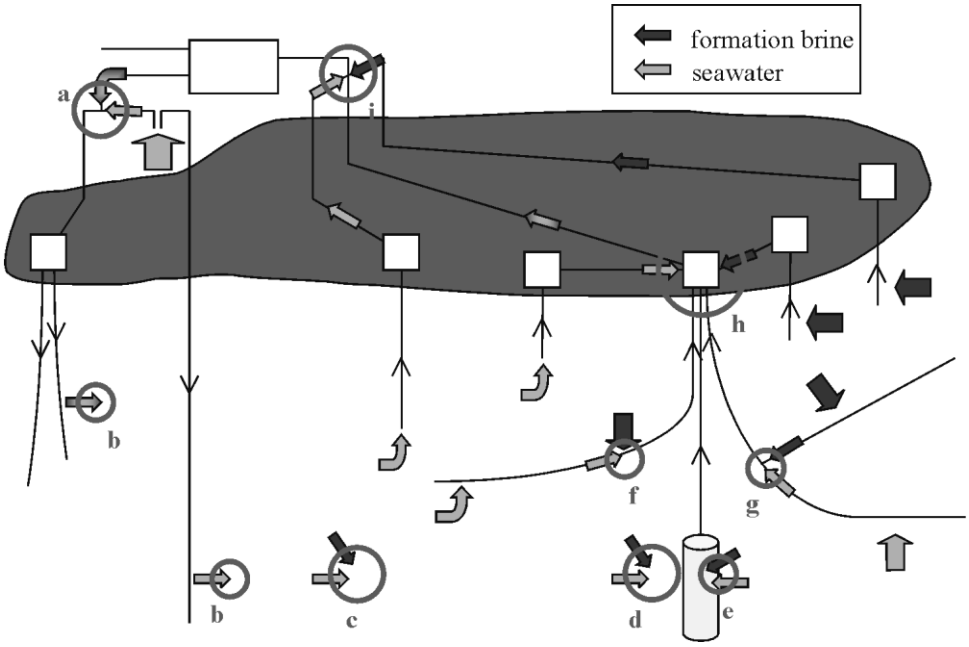

Figure 1.7: Locations of scale deposition. (After Mackay, 2003)

After $CaCO_3$, $BaSO_4$ is the most commonly reported scale in oilfield systems, particularly in provinces where seawater is injected for pressure maintenance. However, some reservoirs experience no scale issues, and more are affected by other scales.

1.3.1 Other types of oilfield scale

Other types of oilfield scale include:

• Iron carbonate (siderite; $FeCO_3$) – often due to corrosion products and bicarbonate in formation brine;

• Iron sulphides (pyrite; FeS, FeS_2) – often due to corrosion products and sulphate reducing bacteria;

• Iron oxide of various types (including Fe $(OH)_2$, $Fe^{2+}O_3$, $Fe^{3+}O_4$) – often due to corrosion products and oxygen rich injected water.

As well as due to corrosion, iron may be found in formation brines. Moreover, due to the very low solubility of iron beaming minerals even lower than BasSO_4 concentration in formation brines tend to be low.

Barium sulphate has the lowest solubility of the sulphate scales, but depending on the composition of the formation water, other sulphate scales may occur as well as or instead of $BaSO_4$.

• Strontium sulphate (Celestite; $SrSO_4$ strontium in formation water and sulphate commonly in injected seawater;

• Calcium sulphate (> 110oC anhydrite, $CaSO_4$ < 110oC gypsum, $CaSO_4$.2H2O)-calcium in formation water and sulphate commonly in injected seawater;

• Mixed barium/strontium sulphate ((Ba,Sr)SO_4) - barium and strontium in formation water and sulphate commonly in injected seawater.

In the Middle East, $SrSO_4$ is more common than $BaSO_4$ due to regional variation in formation water compositions.

Exotic scale types such as barium carbonate (witherite), strontium carbonate (strontianite), calcium fluorite (fluorite), sodium chloride (halite) and magnesium hydroxide (brucite) are the more unusual scales associated with high temperatures, high pressure (HT/HP) reservoirs of the North Sea and other oil/gas.

1.4 THE PROBLEMS OF BARIUM SCALE

1.4.1 The Peculiarities Concerning the Problem

The formation of scale, particularly barite, is a common problem in the North Sea (UK) and in other regions where sea water flooding is used, including the deep water developments in the Campos Basin (Brazil) and the oil production fields in the South China Sea (Malaysia, Indonesia and Brunei). In all these cases, the continuous mixing of incompatible waters has led to the precipitation of sulphate scale, in production equipment, completion tubing, at the periphery of production wells, or within the reservoir itself. The formation of scale has long been known to lead to a reduction in flow capacity (Vetter 1975), and lessons learnt in immature provinces are having to be applied in regions where sea waterflooding has started relatively recently such as the Gulf of Mexico and offshore West Africa. Furthermore, barium sulphate scale also has

the potential to contain co-precipitated radium, which results in the occurrence of naturally occurring radioactive material (NORM) (He et al. 1994), Thus there is a health and safety risk where ever barium sulphate precipitation occurs.

Evaluation of squeeze treatments allows the assessment of scale inhibition by monitoring the inhibitor return rate during this process. At the molecular level, the process of scale inhibition is usually discussed in terms of the thermodynamics or the atomic kinetics of the inhibitor in the aqueous medium (Tromp et al. 2002). In addition to this, the presence of auxiliary ions, found in abundance in the oilfield-scaling environments can also affect the efficiency of scale inhibitors, for example through the formation of complexes and defects. The influence of auxiliary ions on the growth and morphology of barite was predicted as early as 1955, (Hartman et al. 1955). In environments where the concentration of auxiliary ions is high, the influence of divalent cations on both barite growth and inhibition cannot be neglected. Several works have demonstrated the importance of incorporating the effects of divalent cations in their studies, for example Pina et al. (2000) in predicting the formation of a solid solution of Sr^{2+} ions in the barite crystal lattice and Hennessy et al. (2002) in elucidating the physical effects of introducing Ca^{2+} and Mg^{2+} ion defects in the barite lattice structure. Benton et al. (1993) for example, details the influence of thermodynamics and kinetics on barite growth and inhibition in the presence of auxiliary ions. In addition, publications by Graham et al. (2003) on inhibitor efficiency of barite inhibition in the presence of auxiliary ions and that of Yuan et al. (1991 and 1994) for the developments of scale formation prediction are more industrially related.

1.5 AIM

This thesis aims to improve the understanding of scale precipitation due to brine mixing and to focus on barium sulphate scale in particular as a case study. We model this type of scale using the streamline simulation for the first time with a view to improve the accuracy of simulation of precipitation, and hence of our understanding.

1.6 OBJECTIVES

The main focus of this thesis is to examine the mechanisms of brine mixing leading to cases of barium sulphate that had been covered in previous publications and at the same time to better understand the more accurate modelling of these mechanisms using streamline simulation. In brief, the objectives are:-

• Logical configuration of the problem and the method of addressing the problem.

• Evaluation of generic barium sulphate scale formation using simple 1D, 2D and 3D streamline models.

• Using modern technology such as appropriate adapted streamline simulation to address the field scale problem.

1.7 THESIS OUTLINE

There is extensive literature published in both the petroleum engineering and crystal science literature that deals with the problems associated with scale formation and modelling. This PhD investigation has started with an introduction to scale in general (Chapter 1) which is followed by a literature review on scale in general (Chapter 2). This literature review deals with previous work that was conducted in the area of scale formation and parameters that influence barium sulphate formation. Chapter3 is a review of the development in computer modelling techniques for simulation of waterflooding, focusing on brine mixing and in situ precipitation. Chapter 4 describes the finite difference and streamlines simulations. In this chapter calculations are presented that have been run to show the result of the dispersion effect and its impact on the results of water breakthrough. Furthermore, in this chapter we address a number of points as follows:-

1. In 1D linear water flood displacements FrontSim has effectively shown minimal numerical dispersion, producing similar results to ECLIPSE with grid block sizes approximately 100 times bigger than in ECLIPSE. This allows a detailed study of the location of the mixing front.

2. Numerical calculations in a 2D areal model have shown that injected water will arrive at the producer at different times, determined by the areal flow paths taken by the streamlines. Hence, the mixing of different brines is expected in the near production wellbore region for an extended period, which can lead to continuous scale deposition. Similar effects regarding brine mixing at the producers have been quoted for 2D heterogeneous layered models. FrontSim results for the 2D areal systems always produced sharper brine mixing zones than finite difference solutions. This relatively short mixing zone advances through the reservoir from the injector with minimal scale dropout in the oil bearing layers and thus with no significant permeability impairment.

However, near the producers, the continuous supply of scaling ions that mix in this turbulent flow zone provides favorable conditions for significant formation damage as a result of scale. The extent to which more accurate modelling of precipitation deep in the reservoir limits ion depletion, therefore ensuring more ions remain in solution, leads to more precipitation being predicted around the wellbore is investigated.

3. Mixing within the aquifer may be a possible explanation for the low barium concentrations measured at the production wells. Scale formation in the aquifer would have a limited effect on permeability, and indeed it helps to relieve the scaling problem near the producers. The location of scale precipitation in the oil leg versus in the aquifer or near the oil water contact is studded here. It is clear from the overall results obtained that streamline simulation can be a useful alternative and complementary tool to mitigate the problems of numerical dispersion inherent in standard simulators. In particular, since a streamline simulation preserves sharp fronts, it can be very helpful in gaining a better understanding of where the scaling problem may be occurring, which is important when the aim is to prevent any loss in productivity due to scale.

The advantage of a 3D streamline simulation is that it may produce more reliable brine mixing calculations in heterogeneous reservoir systems. Therefore, relatively fine grid models with proper heterogeneous descriptions would explicitly model physical dispersion due to heterogeneity. It is this future of streamline simulation that is exploited in this work.

Throughout this work, because most of the reservoir simulators are based on fluid flow calculations and they do not account for kinetic reactions, it was assumed that when complete mixing of the brines occurred, all the barium in the formation water had dropped out to form $BaSO_4$ in the reservoir. It would be very advantageous if in the near future a reaction kinetics model was incorporated into the streamline simulation codes to account for the chemical reactions between the species and therefore allowing more accurate predictions of the mass of scale that can precipitate in the reservoir. However , in this work it is consider that the reaction kinetics are generally fast relative to rate of displacement deep in the reservoir, and thus the equilibrium assumption does not create large error.

Chapter 5 deals with how we model scale in a streamline simulator by using the new keywords that describe the chemical interactions. In this chapter the 1D, 2D and 3D

models have been used to demonstrate the results. SPE-119605 describes in summary the contents of this chapter. In developing new simulation technique, it is always important to test methodology in generic synthetic systems that one relatively easy to interpret. However, the most interesting learning are often obtained when an approach is applied in a real field scenario, albeit with various parameters. This is undertaken in Chapter 6 by application of this method to Field X. Chapter 7 provides the conclusions and outline of future work to be conducted on this subject.

CHAPTER 2: LITERATURE REVIEW ON BARIUM SULPHATE SCALE FORMATION

2.1 INTRODUCTION

This chapter provides a review of the crystallography of barite formation, beginning with nucleation and growth, crystal imperfections, barite inhibition and the way all these factors interconnect. Research on inhibitor chemistry and proposed mechanism is also outlined.

2.2 CRYSTALLOGRAPHY OF BARIUM SULPHATE

The word barite is a derivative of the Greek word 'Baros' meaning heavy and is sometimes called heavy spar. The barite crystal is typically characterised by its faces and its crystallographic three-dimensional axes. Barium sulphate crystals have three pairs of parallel faces, since the crystals in each pair are different sizes they are categorised under the orthorhombic crystal system. The three axes are at right angles to one another, but with different lengths (Deer et al. 1992). Barite is also categorised under the Pnma space group, which includes strontium sulphate or celestite as well. The orthorhombic unit cell comprises four barium ions and four sulphate molecules. The sulphate molecule is presumed to be a regular tetrahedral, positioned with the S and the two oxygen atoms on mirror planes at y=1/4 and ¾. According to Deer et al. (1992) the other two oxygen atoms are equidistant from and on opposite sides of the different SO_4^{2-} structure. The unit cell of barium is illustrated by Figure 2.1.

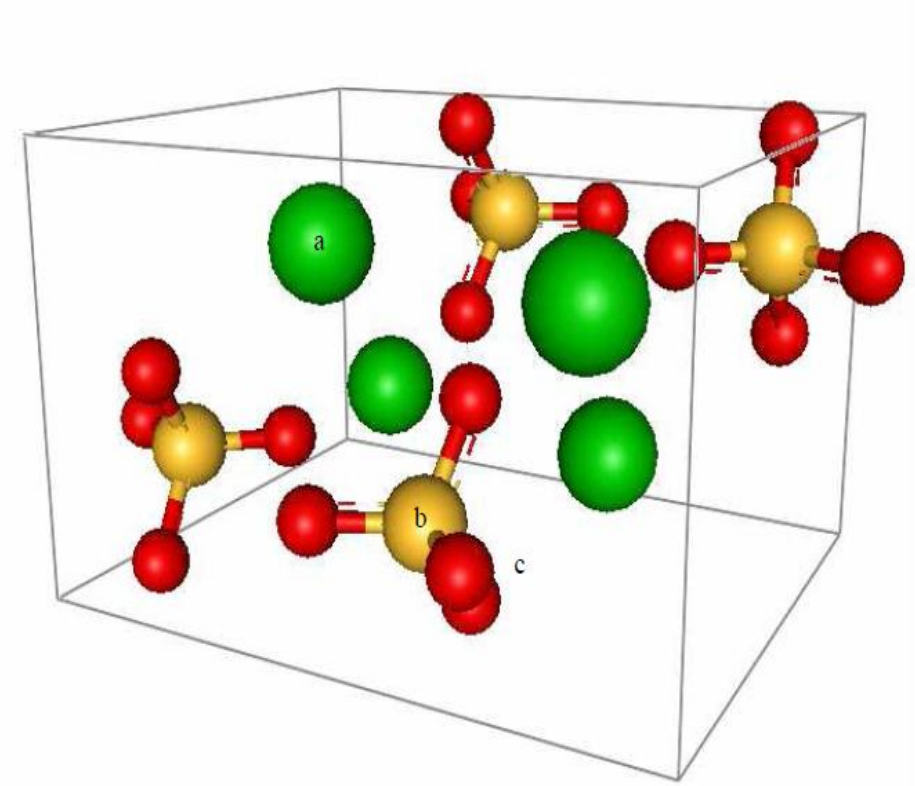

Figure 2.1: An illustration of the unit cell of barite. The barium ions are denoted (a), the sculphur atom denoted (b) and the oxygen atoms denoted (c).

2.3 NUCLEATION AND GROWTH OF BARITE

Barium sulphate is created when there is an excess of barium ions and sulphate molecules resulting from incompatible waters mixing. Two theories of formation have been proposed. According to Oddo et al. (1994), the resulting barium sulphate crystals form as the solubility product of barium sulphate is exceeded and they deposit. Earlier, Vetter (1975) concluded that the barium sulphate formed and was transported in the solution from the rock formation into the equipment. It entered the equipment as a supersaturated barium sulphate solution. Furthermore, this supersaturation takes place during the displacement process. Both methods are accepted as valid and are attributed to different conditions. Vetter (1975) noted that variations in pressure and

Temperature could also cause barite self-scaling, which leads to the question of whether the precipitation of $BaSO_4$ crystals should modeled as mobile or as depositing. In this work it is assumed that very few crystals would travel further than the length scale of a grid block, and hence it is assumed all crystals deposited within the grid in which they form. It is accepted that the size of the critical nucleus required to produce a secondary nucleation changes according to the system conditions, in other words, supersaturation and temperature. According to Pina et al. (2000) the crystallisation process happens at moderate to high levels of supersaturation. Earlier work by Walton and Hlabse (cited in Weintritt 1967) proposed that the nucleation of barium sulphate is a 'spontaneous' process resulting from its low solubility rather than depending on excesses of barium or sulphate ions.

Fischer (1951) concluded that the aging of barium sulphate crystals does not change their size or habits when in contact with the mother liquid except for when the initial aging barium sulphate crystal is less than 1 micron in diameter. In such cases, the 'Ostwald ripening effect' takes place. Ostwald ripening (Ostwald 1896,1897, for empirical evidence see Ng 1996) is when a large number of small crystals form in a system before most of them disappear gradually, leaving others to grow larger. The larger crystals are favoured more energetically than those that are smaller, and as they increase in size the smaller crystals surrounding them begin to vanish.

The formation of these smaller crystals is kinetically favoured, in other words it is easier for them to nucleate. However, larger crystals are favoured thermodynamically. Therefore, from the perspective of dynamics, while many small crystals can be nucleated more easily they have a greater surface area to volume ratio when compared to larger crystals. Surface molecules are not as energetically stable as those that are well ordered and within the bulk of the liquid. Conversely, larger crystals have a greater volume to surface area ratio and a lower energy rate. As a result those smaller crystals that grow will achieve lower energy rates; this is noted in the Ostwald ripening effect.

Fischer (1951) also suggested that protuberances would appear on the crystal surfaces if any foreign electrolytes were produced during the precipitation process. Examples of such electrolytes are sodium chloride, sodium nitrate or ferric chloride. He proposed that it was the presence of defect ions on barite that caused this. Weintritt (1967) highlighted that two of the most significant factors that have an effect on barium sulphate deposition and control are the low solubility, which impacts on growth and the

Thermodynamics of the system which controls how the crystal forms. It is therefore critical that any reservoir model of in situ scaling must include the correct thermodynamics.

Pina et al. (2000) have also identified two main factors controlling actual ionic distribution during barite's growth process. These are firstly the supersaturation state of the multi-component solution that comes into contact with the crystal as it grows, secondly the growth mechanism, which occurs on the surface of the crystal. This is in agreement with methods proposed by Weintritt (1967). Two factors need to be considered when analysing the growth of a particular surface. The first is the dominant manner in which the crystal grows and secondly the amount of energy necessary for the molecules to attach themselves to the surface. These criteria correlate to each other.

The work of Nancollas and Purdie (1963) provides an example; it reported a rapid growth of barium sulphate when supersaturated barium sulphate solution was seeded at 25^0C. Von Weiman (in a review paper published by Weintritt 1967) concluded that there is a direct correlation between the kinetics of barium sulphate growth and supersaturation. Furthermore, he noted a greater number of particles formed when the kinetics of the growth process increased. This was confirmed by Weintritt (1967) who proposed that as well as supersaturation levels, the absolute magnitude of the ionic concentration is important.

Furthermore, Liu et al. (1976) studied the rate of rate of crystallization and dissolution by Scanning Electron Microscopy (SEM). They concluded that after a secondary nucleation, which is characterized by a second increase in growth, the rate of crystallization is in proportion to the square of the supersaturation. This shows a controlled growth on the surface. In addition, they found that the dissolution rate follows a similar rule. This suggested that fluid dynamics do not affect growth processes, and thus, in our reactive transport models, the rate of precipitation does not need to be made a function of fluid advection rate. This is in contrast to Marchisio et al.'s (2002) study, which concluded that the mixing process was a significant factor in barite crystal formation and had an important role in generating the supersaturation effect. The significance of fluid dynamics has also been emphasized regarding its impact on the nucleation and growth phase of barite. This means that although in this work we do not conceder kinetics in detail, it remains an open question as to whether kinetics should be linked to flow velocity. It has also been proposed that aggregation affects barite growth. During the aggregation process, a transport mechanism brings

particles close to the crystal's surface. It is the balance between the forces of repulsion and attraction (both Van der Waals and double layer repulsion) of the particles and the surface that will determine the attachment of new molecules onto the surface of the crystal. It is thought that speciation in ionic adsorption and the differential solutions of ions causes inter particle attraction. Thus, the different conclusions arrived at by Liu et al. (1976) and Marchisio et al. are believed to be the result of the different parameters of their respective studies.

Furthermore, it has been noticed that the growth of barite in oilfields is more likely to happen through a heterogeneous process. In other words, when a surface is present it could be manmade such as metal tubing, pipelines or equipment or within porous rock materials and sand particles. This is because crystallisation happens at lower levels of supersaturation since the activation energy is relative to the primary nucleation (see Markov 1996 and Nancollas 1985, for examples of this). The fact that auxiliary ions are present in downhole conditions can also have an impact on crystal growth and its properties.

Hartman and Perdok (1955) proposed that the presence of auxiliary ions could affect the (011) surface of barium sulphate. In similar findings, Benton et al. (1993) proposed that the barite (001) surface was also affected by the existence of molecular impurities. As early as 1922 Mellor, reported that when a system of barium sulphate was precipitated in the presence of a Pb^{2+} ion containing small levels of impurities, the Pb^{2+} ion will systematically replace certain barium ion sites on the barium lattice. This results in a non-morphological change, in other words a solid solution. According to Butler (1971) this only occurs at very high temperatures. As it modifies the physical and geometric features of the host it can be an important factor in inhibition.

The same occurrence is also evident when strontium is substituted into barium sulphate as the fact that as both lead and strontium contain the same sulphate structure as barium suggested that because of the similarities in crystal structure, a perfect transformation from barite to celestite takes place during the solid solution replacement as the strontium is replaced by the barium ion within the barium sulphate crystal. As this defective structure becomes closer to a celestite, they are termed 'barytocelestine', while those closer to barite are termed 'strontiobarytes'. According to Deer et al.(1992) the presence of a Sr^{2+} ion defect in the structure of the barium sulphate structure would cause diminished density in the material. The limited substitution of the Ca-$BaSO_4$

system in comparison to a Sr-$BaSO_4$ system can be ascribed to the differences in structure of calcium sulphate and barium sulphate.

Redfern et al. (1998) studied the defects at the surface, namely strontium and calcium. Binding with surface sulphate they form calcium sulphate or strontium sulphate respectively. The findings from this study demonstrated that surface energy levels including a layer of strontium sulphate into barium sulphate were lower than that containing calcium sulphate. Growth in both calcium and strontium sulphate disrupted the surface structure. The level of disruption caused on the barite surface was greater for calcium sulphate than for strontium sulphate. This was ascribed to the fact that strontium and barite sulphate have greater similarities in ionic radii and structure when compared to calcium sulphate. Furthermore, it has been proposed that this overgrowth in calcium and strontium sulphate on the barite surface is energetically non-viable.

Using X-ray diffraction, Hennessy et al. (2002) showed that the presence of the Ca^{2+} ion causes an increase in the lattice volume of the barium sulphate precipitate with a significant amount of Ca^{2+} ion identified in the lattice structure of barite in a barium sulfate nucleating system. This occurs with or without an inhibitor present. A description was not provided regarding the presence of Ca^{2+} ion on the surface of barite. However, they noted that the presence of Mg^{2+} instead of Ca^{2+} resulted in a marked reduction of the barium sulphate lattice parameter in the same system. Hennessy et al. (2002) also showed that the presence of magnesium in barite that was otherwise pure and in an inhibitor system would cause a reduction in inhibition efficiency when compared to a placebo in which there is no magnesium ion is present. It is interesting to note that this X-ray diffraction study also demonstrates that the lattice parameter of barite has grown by a certain magnitude and no magnesium ion was found present in the precipitate. The study proposed that when magnesium and calcium ions were present, the solubility of barium sulphate is modified, thus causing more Ca^{2+} ion to be integrated into the bulk structure.

Davey et al [1991] suggested that removing Ca^{2+} and Mg^{2+} ions from the test solution would produce dendritic morphologies. This shows the controlling effect these ions have on barite growth and suggests the presence of both these ions act as a growth suppressant for the barite crystal. Dendritic growth refers to uncontrolled growth of a crystal, which results in surface roughness. Markov (1996) proposed that from the standpoint of thermodynamics, a rough surface implies that there is an increase in the Gibbs free energy of the surface while there is an increase in the local entropy of the

surface. If the system is at high supersaturation levels but below its thermodynamic critical temperature, the same phenomenon can also occur. In such situations, as the rate of formation of the 2-D nuclei increases significantly, it will overtake the surface growth of the preceding one leading to multilayer growth (Markov 1996). Chernov (1973) had previously argued that in certain cases, when the density of the nuclei grows very large, the mean rough surface edges would become similar to the interatomic distance, and therefore, atoms can practically be integrated at any site as they arrive. This in turn would result in uncontrolled crystal growth.

Davey et al. (1991) found that dendritic growth occurred when in the Ca^{2+} ion was absent. Hennessy et al. (2002) found that dendritic growth happened when calcium ions were present during barium sulphate precipitation, however, not vice versa. The different experimental parameters may account for these different results as could the final content of the bulk solution system. The modifications in morphology found in Hennessy et al.'s research point to the fact the scaling process had increased rapidly during the absence of cations in the solution.

The surface charge of the barite surface can also be affected by the presence of both Ca^{2+} ions and Mg^{2+} ions (Collins 1999). Furthermore, both these factors could result in the provision of a better medium for both surface growth (dendritic growth occurrence) and the inclusion of defects in the bulk lattice (increased Ca^{2+} concentration in the bulk lattice of barite). Collins [1999] has demonstrated that the electrokinetic properties of barite can be influenced by both the quality and quantity of the ion present in the bulk and pH of the medium. He demonstrated that when Ca^{2+} and Mg^{2+} ions are present in the suspending liquid, the surface electrical property of barium sulphate was altered considerably. However, the scale of the effects depends on the ionic concentration and on the pH of the system. In this case, two pH values were selected for the system; 4.5 and 5.6 for simulating the downhole conditions of the Miller and Forties oilfields in the North Sea respectively. Changes in the surface electrical charge are believed to have created a better adsorption site for the inhibitor on the surface of the barium sulphate. This was achieved by a reduction in the magnitude from a positively charged surface or an increase in the magnitude from a negatively charged barite surface. The impact was more marked when Mg^{2+} ions were present compared to Ca^{2+} ions. Furthermore, it was found that a barite precipitated when calcium was present has a marked difference in its

electro kinetic property compared to a barite precipitated in a pure system in the absence of any external cationic auxiliaries.

Gallardo et al. (2000) measured mobility as a function of calcium concentration at a fixed pH of 5.5 and the findings revealed that when the calcium ion was present in the bulk solution it was sufficient to alter the surface electrical properties of barite. At 20mM of calcium, the sign of the zeta potential (ς-potential) was reversed from -3mV to +10mV with the point of zero charge reached at around 4mM calcium. It can be suggested that calcium ions are specifically adsorbed into/onto the barium sulphate lattice and the solubility of barium sulphate can be changed when metal ions are present in the solution. Hennessy et al. (2002) findings were in agreement. Research conducted by Collins (1999) and Gallardo et al. (2000) put forward the importance of taking Ca^{2+} ion defects in the barite lattice into consideration when studying the barite growth and inhibition process.

This literature review has emphasized the relationship of the various parameters that impact on barite crystal growth process. It is important to understand the growth mechanism of barite scale for two main reasons. The first enables better scale prediction to be conducted in order to identify measures to mitigate the problem systematically and secondly, to enhance the understanding of the mechanics of surface growth inhibition which would help in the provision of a better scale inhibitor. However, when modeling scale precipitation deep into the reservoir, certain choices have to be made about which processes and interactions to include, and which cannot be modeled, or are not relevant. The first conclusion of this literature survey is that accurate modelling of the thermodynamics is very important. Solubility products for typical reservoir conditions are generally well known, and then modelling of the thermodynamics is also feasible. One limitation is that it has been demonstrated that other ions interfere with the stability of the main crystals forming. While it would possible to track all the relevant ions (e.g. strontium, calcium, magnesium, even lead), a look up table approach would be required to take proper account of how they interfere with the $BaSO_4$ crystal lattice. The kinetics of barite precipitation is also more difficult to accurately. While temperature fronts can be tracked in streamline simulation (by use of an appropriately retarded tracer) the impact of temperature on kinetics is less easy to determine, as is the impact of fluid velocity and turbulence. Surface areas are very important in determining rate of crystal growth. However, there are affected by the presence of impurities in the crystal, and by other solid surfaces present such as fines, metal tubing, corrosion products, let alone the

Important of the organic precipitation such as waxes and asphaltine and even the impact of wettability. Thus in real reservoir systems, accurate modelling of the various components that combine to give reaction rate is too difficult. However, as always

noted, for barium sulphate at typical reservoir temperatures, an equilibrium assumption is probably sufficient deep within the reservoir where reaction rates are low and there is time for the barium to reach equilibrium at local grid block conditions within the time steps, and so the equilibrium assumption has been used in the work presented in this thesis.

CHAPTER 3: LITERATURE REVIEW ON MODELLING OF SCALE PRECIPITION DUE TO BRINE MIXING

Not many people have worked on the subject of scale modelling in the reservoir before. The majority of the work on this subject has been conducted using the finite different method calculation used in the CMG STARS software (Mackay 2003). The following review of publications explains the developments in the subject.

"Modeling of In-Situ Scale Deposition: The Impact of Reservoir and Well Geometries and Kinetic Reaction Rates" by Mackay, EJ, paper SPE 81830, *SPE Production & Facilities (Feb2003) (1) 45-56*

This paper extends earlier research describing the modelling of brine mixing and the reasons for scale deposition being mainly a problem at production wells. The purpose was to explain the application of reservoir simulation calculations *including chemical (scaling) reactions*, and to show the impacts these reactions would have on the resulting brine chemistry as the fluids flow through the reservoir. The site of the greatest levels of scale deposition and the ensuing brine compositions at the production well are provided for a variety of sensitivities. These include: reservoir geometry (1D, 2D areal, 2D vertical, 3D), well geometry (location and orientation within the field and with regard to other wells and the aquifer), and reaction rate (this ranges from no precipitation to equilibrium). The paper shows that in systems that have no aquifer, maximum scale deposition happens in the immediate vicinity of the production wellbore, and thus low produced cation concentrations show squeeze treatments that are inadequate. In systems where water injection occurs, low cation concentrations may also be the result of deposition deeper within the reservoir or the aquifer. In addition, maximum scale dropout still takes place, as the fluids near the production well are sufficiently far from the wellbore that they are not affected by squeeze treatments, nor do they have any significant effect on productivity. The reaction rate is crucial in ascertaining how much scale has been deposited, but even under equilibrium conditions, adequate concentrations of scaling ions are brought into the production well thus requiring the well to be squeezed, although lower volumes of inhibitor are necessary. Once cation concentrations have been decreased, the paper proposes that they will never increase again. In addition, some of the limitations of this type of modelling are provided such as

the determination of the kinetic reaction rates, size of the mixing zone, and the effect on permeability. Although the thermodynamics are fairly well understood, kinetics are far harder to establish. The size of the mixing zone is impacted by numerical dispersion, and currently, computationally intensive techniques are necessary to solve this problem, which is why the streamline approved adopted in this thesis is of such great importance.

Predicting In-Situ Sulphate Scale Deposition and the Impact on Produced Ion Concentrations" by Mackay, E.J., Trans IChemE (March2003) 81 (A) 326-332.

This paper builds on work discussed in the previous paper. It examines the effect of brine mixing and scaling on the complete reservoir flow system, starting with injection, through to displacement through the reservoir, to the production wells and up to the surface flow facilities. It studies the impact of brine mixing and scale deposition in different locations in the reservoir, including close to the injection well, in the oil leg, in the aquifer, and as fluids approach the production well, first outside an inhibitor treated zone and then within the treated zone. Each configuration has a different effect on the chemistry of the brine. This would be observed by the analysis of brine samples taken from the production well. This paper also considers the effects of desulphation and produced water re-injection on scale deposition in the reservoir. Finally, the fact it is necessary to protect injection and/or production wells in these circumstances is also examined. Identification of the various zones where deposition may take place is of particular relevant to current work, and Figure 1.6 is taken from this paper.

Predicting Brine Mixing Deep Within the Reservoir, and the Impact on Scale Control in Marginal and Deepwater Developments" by Mackay, E.J., Jordan, M.M. and Torabi, F., paper SPE 85104, SPE Prod. & Facilities (Aug 2003) 18 (3) 210-220.

This paper provides the field data and results of reservoir simulation calculations from three North Sea fields demonstrating that the formation of scale deep within the reservoir can clarify why there are low cation concentrations at production wells. This deposition, however, has very little negative effect on oil production and flow within the near wellbore region if the wells are treated sufficiently. The extent and effect of the deposition is different throughout the reservoir and can be estimated. In addition, the paper demonstrates that the ability to model brine mixing and stripping of the scaling ions before the fluids reach the production wellbore has an important impact on the

economic assessment of marginal fields and deepwater developments (where technical challenges and associated costs of scale control might mean that development is uneconomic). An outline of the data requirements and methodology used allowing such an assessment to be made is also provided.

"Integrated Risk Analysis for Scale Management in Deepwater Developments" by Mackay, E.J., Jordan, M.M., Feasey, N., Shah, D., Kumar, P. and Ali, S., paper SPE 87459, SPE Prod. & Facilities (May 2005) 20 (2) 138-154.

This paper discusses the techniques developed in the previous publications and how they are applied to the scale management decision-making during the FEED stage of a development in a deepwater environment. The paper looks at how the risk analysis process should be conducted. There is a focus on the necessity for all the available production chemistry and reservoir engineering data to be integrated. The full field reservoir simulation model was first adapted to calculate potential seawater breakthrough and the length of seawater production. The findings were then used to ascertain the timing, duration and volume of squeeze treatments for scale control. The process required the use of flow profiles obtained from the reservoir simulation model. These were subsequently applied in a near well squeeze simulator to calculate treatment performance to minimum inhibitor concentration. This was followed by an analysis of predicted seawater production profiles and total water production rates for each well in turn. The aim was to identify the potential for the accurate placement of inhibitor by bullhead treatments in zones that were threatened by scale deposition. Further modifications were made to the reservoir model to study the effects of scale deposition on the brine chemistry at the production wells, and as a result the requirements for inhibitor squeeze treatments were revised. An economic analysis of the options available for scale management was also conducted. This compared sulphate reduction with inhibitor squeezing, based on those treatment specifications identified. It is clear from this paper that a cross discipline approach using reservoir engineering and production chemistry can promote a more thorough assessment of the scale risk. Furthermore, the most financially viable control programmes can also be selected with this approach.

This body work is very interesting and has proved valuable to the industry. It is clear from the papers the main weak point in the work is the method that was used in the simulation for the calculation, namely the finite difference method (FDM). This method can result in a major problem known as numerical dispersion error. This error will be covered in Chapter 4 of this thesis. The most commonly used reservoir flow models are conventional finite difference simulators. In these models, the reservoir is discretised into grid cells, in which properties such as permeability, porosity, net to gross, pressure and saturation are averaged. The pressure in each grid cell is calculated, taking account of sources and sinks, such as wells and aquifers. Next, the volumetric flow of each phase between the cells is calculated, followed by a calculation of the saturation change in each cell. Since pressure is dependent on saturation, the calculation is iterative. Reservoir simulation models are developed for most reservoirs that rely on injection and/or aquifer waters for sweep and pressure maintenance. While the principal objective is to calculate potential hydrocarbon recovery, all such models must, out of necessity, also be able to calculate water flows and fluid pressures. Many reservoir simulation models may also be adapted to track different brines, such as formation and injected waters, and to calculate where these mix. This type of calculation may be used to explain one of the reasons why scale deposition is principally a problem at production wells, and not, in general, at injection wells.

The advantage of this type of calculation is that it may be used to identify where the greatest risk of scaling is likely to occur, and hence an appropriate scale management strategy may be developed to address this risk.

The finite-difference approach gives us a great deal of flexibility in handling the non-linear partial differential equation, in addition to the property distribution in heterogeneous systems for which an analytical solution is not feasible. In the finite difference methods we describe elements or cells to describe the geometry of our reservoir. We calculate the flux into and out of each cell and then accumulate volume or mass. We speak of tanks or gridblocks discritised in x, y and z, and connected at intersecting faces (interblock transmissibility). We divide the time into discrete increments, chosen so that saturation change in any gridblock during each time step is

not excessive (Δsw less than 20%). However, this method has a weak point which is the numerical dispersion which we discuss below.

First, the numerical dispersion is essentially an error due to the fact that we use the grid block approximation for solving the flow equations. The results from this effect will give us a wrong estimation of the water breakthrough and as well the scaling timing in the reservoir. There are some techniques to solve this problem, such as by using the pseudo relative permeability curves and these can work well sometimes but we have to keep in mind that relative permeability curves work for oil water phases but not for components within a phase. We are dealing with two incompatible waters which are part of one phase, thus not two phases such as oil and water, then pseudoisation can not solve of the numerical dispersion problem. This work has overcome this numerical error by using the streamline modelling approach. A new code was added by one of the FrontSim developers to an existing streamline model to allow scale interaction in the simulator. This is the first time streamline simulation has been used to model scale. The comparison between the two methods, finite difference simulation and streamline will be presented with many examples in Chapter 4. The basic procedure in a streamline simulation for a given permeability field is to calculate the pressure distribution by solving conventional pressure equations. From this the iso-potential (pressure contours) can be calculated. The gradient of the pressure locally perpendicular to the isopotentials are the streamlines. The full detailed description for the streamline method and how the codes were added in the streamline simulation will be presented in Chapter 5, but it is sufficient to note here that components, such as barium and sulphate can be transported along the streamline also.

CHAPTER 4: FINITE DIFFERENCE AND STREAMLINE SIMULATION

4.1 INTRODUCTION AND OBJECTIVES

Streamline and streamtube-based flow simulation have been considered to be among the most important new reservoir engineering tools for several years. They have been used in the oil industry since the 1950s. The techniques have proved to be a very useful contribution to substantial progress in the oil field. The recent renewed interest has been to a large extent driven by new developments in reservoir characterization. For the past two decades, there has been a tremendous growth in the ability of the petroleum industry to develop fine-scale static models that integrate 3D geological models and geophysical data. The multimillion cell geological models are now routine and can be generated by general purpose commercial codes. This has led to some considerable challenges. First, the gap between the geological modelling and flow simulation has widened, because flow simulation cannot cope with the resolution possible for geological modelling.

Secondly, the increase in model resolution results in increased acknowledgment of their uncertainty. We must understand and quantify the impact of the unknown element of the static model on fluid flow and transport for prudent reservoir management. Recent deployment in streamline simulation offers significant potential to meet some of these challenges. Many of these developments will be stated and explained in detail later in this chapter.

Streamline is one of the great techniques in oil engineering providing us with a tool for fast flow simulation and rapid screening and ranking of 3D reservoir models. The evaluation of the flood fronts and their interaction with heterogeneity can be visualized easily by using streamline models. Streamlines are also intuitively appealing because they naturally delineate the fast and slow flow paths in turn, providing a natural means for dynamic reservoir characterization. The speed and the accuracy of the streamline simulation also leads to a host of other applications: for example, rate allocation and flood front measurements, integration of water-cut and tracer data into reservoir descriptions, upgrading from fine scale model, multiphase up scaling through the use of

pseudo relative permeabilities, and flexible grid generation during reservoir simulation, to name just a few.

The purpose of this chapter is to provide a broad overview of the current streamline technology: its foundation and its historical precedents (streamline and front tracking) and the comparison with the finite difference methods by using different examples for 1D, 2D and 3D models. Also the strengths and the limitations of the streamline models compared with conventional finite difference simulation will also be discussed in this chapter.

4.2 BACKGROUND AND HISTORY

The foundation of potential flow theory can be traced back to the 19th century. Modelling fluid flow and transport using streamlines dates back to the seminal work of Muskat (1937). Since then, several authors have applied and extended the underlying concepts for applications to petroleum reservoir modelling. Notable among these are Fay and Pattes (1951), Higgins and Leighton (1962), Moral-Seytox (1966), Pitts and Crawford (1970), LeBlance and Caudle (1971), and Martin and Wegner (1979). Many of these early applications used analytical or numerical stream tube-based approaches to model multiphase displacement, primary waterflooding. The flow domain is divided into a number of stream tubes, and fluid saturation calculations are performed along these stream tubes. The motivation behind stream tube modelling was the lack of numerical dispersion and computational advantages associated with a slowly varying velocity field during a waterflooding process. The direct extension of the stream tube approach to 3D flow, however, is nontrivial because of the complexities associated with tracking tube geometries in 3D space. Lake et al. (1981) adopted a hybrid approach whereby they combined an aerial stream tube model with cross-sectional finite-difference simulator to model large scale micellar-polymer flooding. Some of the subsequent successful applications of this hybrid approach were reported by Emanuel et al. (1989). Mathews et al. (1989), Hewett and Behrens (1991), and Emanuel and Milliken (1997). Two other commonly used methods for convective transport are Lagrangian particle–tracking (Schafer-Perini and Wilson, 1991) and level set methods (Sethian, 1996).

Particle-tracking replaces frontal contours altogether, for example, tracer concentration, with statistically significant collection of particles. Each particle represents a finite parcel of fluid, either mass or volume. The particle is then moved by solving the velocity equations along the appropriate path lines. Dispersion can be accounted for using an algorithm developed by Chorine (1973); after convection each particle is repositioned with variance in position apportioned to dispersion. In general, the Lagrangian approach works well near steep fronts but not as well for smooth profiles. Another drawback associated with such schemes is the loss of resolution of the front with the progression of time and the statistical variance of the concentration response.

The front-tracking method is a composite Eulerian–Lagrangian approach that introduces interfaces as degree of freedom in the computations. A Lagrangian approach is used to move the frontal contours. Away from the front a Eulerian approach is used. spatial discretisation is used to evolve the solution. The primary limitations of the front tracking approach are the computational burden associated with complications arising from the closed approach or intersecting contours. An alternative to the front tracking method is the level set method, which represents propagating interfaces as a zero level set of higher–dimensional functions.

The streamline methods use concepts from particle tracking to define paths in 3D space (Datta-Gupta 1998), the approach does not required the tube geometries to be explicitly evaluated and is thus ideally suited for modelling flow and transport in three dimensions: (Batycky et al. 1997). This has been greatly facilitated by the introduction of the streamline "time of flight" as a spatial variable (Datta-Gupta 1995). The time of flight is the travel time of a natural tracer along the streamlines. The time of flight formulation decouples the effect of the geological heterogeneity from the transport (saturation) calculation. This decoupling is accomplished by recasting the saturation equations that are now reduced to a series of 1D calculations along the streamline that are decoupled from the underlying geological grid. This greatly facilitates the saturation calculation. Currently this calculation is sufficiently general to model time –varying velocity fields, compressible flow, gravity, compression and fracture flow and pattern conversion. The simplicity, computational efficiency and ready generalisation to 3D summarise the power of the streamline approach.

4.3 FINITE DIFFERENCE METHODS (F.D.M)

The most commonly used reservoir flow models are conventional finite difference simulators. In these models, the reservoir is discretised into grid cells, in which properties such as permeability, porosity, net to gross, pressure and saturation are averaged. The pressure in each grid cell is calculated, taking account of sources and sinks, such as wells and aquifers. Next, the volumetric flow of each phase between the cells is calculated, followed by a calculation of the saturation change in each cell. Since pressure is dependent on saturation, the calculation is iterative. Reservoir simulation models are developed for most reservoirs that rely on injection and/or aquifer waters for sweep and pressure maintenance. While the principal objective is to calculate potential hydrocarbon recovery, all such models must, out of necessity, also be able to calculate water flows and fluid pressures. Many reservoir simulation models may also be adapted to track different brines, such as formation and injected waters, and to calculate where these mix. This type of calculation may be used to explain one of the reasons that scale deposition is principally a problem at production wells, and not, in general, at injection wells.

The advantage of this type of calculation is that it may be used to identify where the greatest scaling risk is likely to occur, and hence an appropriate scale management strategy may be developed to address this risk.

The finite-difference approach gives us a great deal of flexibility in handling the non-linear partial differential equation, in addition to the property distribution in heterogeneous systems for which an analytical solution is not feasible. In the finite difference methods we describe elements or cells to describe the geometry of our reservoir (Figure. 4.1). we calculate the flux into and out of each cell and then accumulate volume or mass.

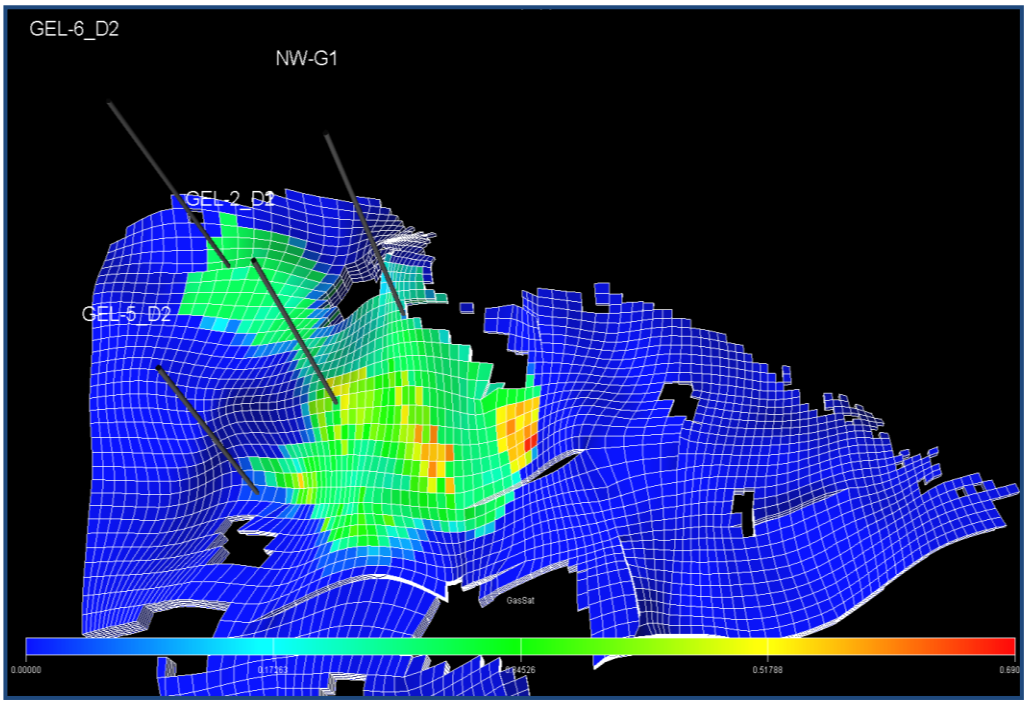

Figure 4.1: Finite difference discretization.

4.4 STREAMLINE SIMULATION OVERVIEW

Streamline simulations approximate 3D fluid flow calculations by the sum of 1D solutions along streamlines. The choice of the streamline directions for 1D calculation makes the approach extremely effective for modelling convection-dominated flows in the reservoir. This is typically the case when heterogeneity is the predominant factor governing the flow behavior. The geometry and the density of the streamlines reflect the impact of geology on fluid paths providing better resolution in regions of faster flow.

4.4.1 Streamlines

Streamlines are instantaneous lines that are everywhere tangential to velocity fields (see Figure 4.2).

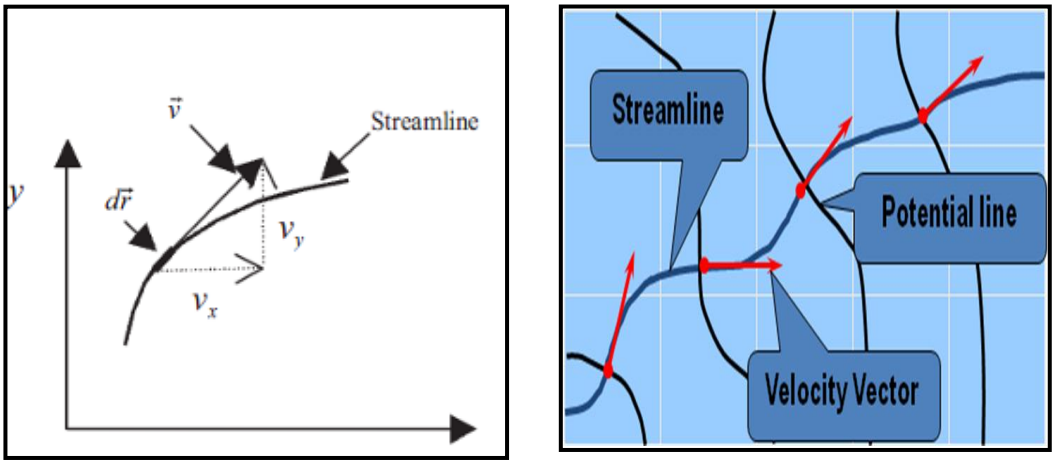

Figure 4.2: The concepts of the streamlines.

There is no specification associated to "velocity" in this definition. Restrictions by which the velocity can be in a steady state are also not mentioned. Incompressibility of the fluid is not necessarily required. In a very simple and succinct way, streamlines are defined once we have a velocity field. For our applications the velocity will always be the total interstitial velocity. This is the total multiphase Darcy velocity divided by porosity.

We do not consider streamlines separately for different phases or for different components. We do not vary this definition when considering compressible fluids. If the velocity varies in relation to time, then we take an instantaneous snapshot to consider a definition for the streamline. Once the streamlines are calculated, they define a spatial discretisation of the flow field. This form of discretisation naturally places a higher resolution in regions of faster flow, analogous to the local grid refinement in finite–difference simulations.

These concepts will now be elaborated on using a single example. Figure 4.3 shows different permeability distributions with distinct characterisation ranging from uniform permeability to an almost stratified pattern. This example is of water injection in a 2D cross section with an injector on the left and a producer on the right. The streamlines for these three cases are also shown in the same figure.

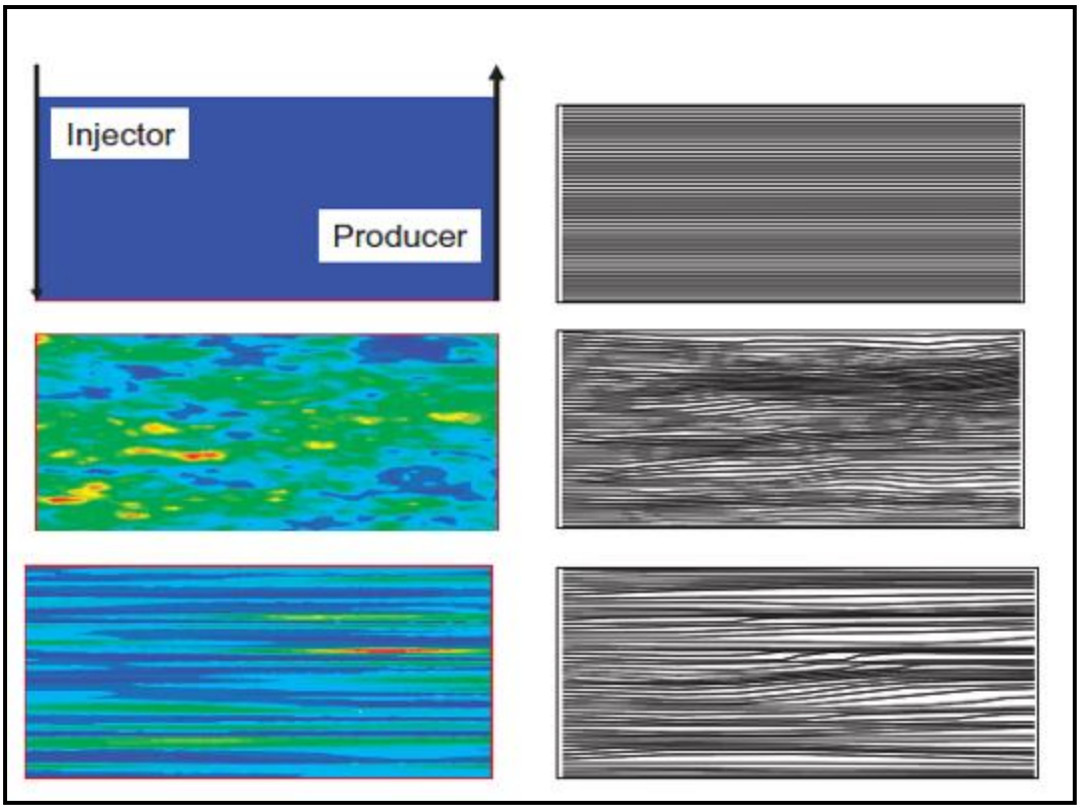

Figure 4.3: Three permeability heterogeneity patterns (left) and their impact on the streamline geometry and density (right).

It was observed that for the homogeneous case, the streamlines are uniformly distributed. However, for the heterogamous cases the streamline geometry and density reflect the underlying permeability distribution. The streamline particularly tends to cluster in the region of high flow and is sparsely distributed in low-permeability regions thus providing a higher transverse resolution in regions of faster flow.

4.4.2 Time of Flight (T.O.F)

The time of flight is either the time required for a fluid particle to travel along a streamline from the starting point of the streamline to the current position, or it is the travel time of the natural tracer particle along a streamline, or it is the distance along the streamline divided by the particle velocity.

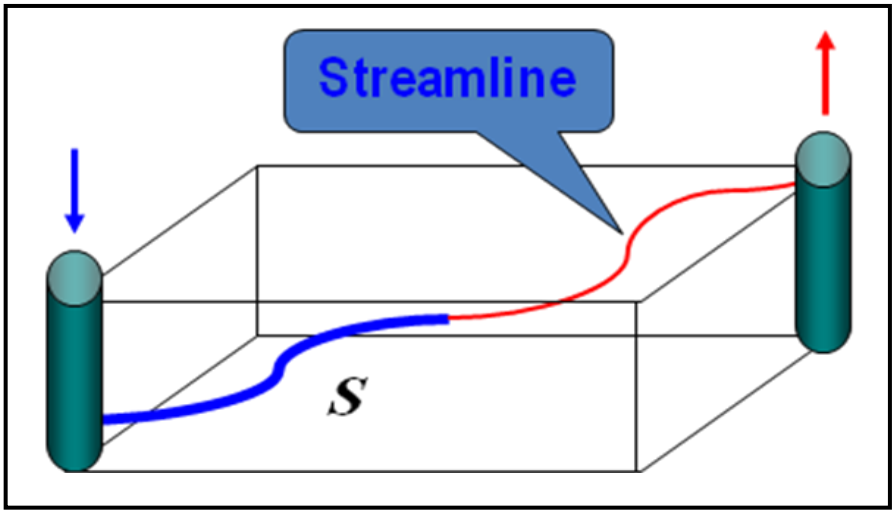

Figure 4.4: The time of flight.

The time of flight is used to transform the 3D saturation equation to multiple 1D equation that are solving along the streamlines. The significance of the Time of Flight (T.O.F) will become apparent as we explore the concepts of the streamline in Chapter 5 later. But for now note that given a velocity field and thus, a fixed set of streamlines, the time of flight can be thought of as a measure of spatial distance along the streamlines.

4.5 COMPARISON BETWEEN STREAMLINE AND FINITE DIFFERENCE

Comparative analysis between streamline and finite difference is of great importance in oil engineering. It enriches and enhances the simulation of oil production techniques. It also gives wide explanatory scope and diversity in oil fields. There are various methods of establishing differentiation between streamline and finite difference calculations. Moreover, to demonstrate the effect of the numerical dispersion in a finite difference solution, there are three different models with different sizes of cells has been used. To simplify the problem, a 1D model has been used with different numbers of cells; 10, 100 and 1000 cells respectively to demonstrate the numerical dispersion effect. It is very important to initially clarify what we mean by the numerical dispersion effect. Its importance lies in the fact that this type of clarification adds to the positive quality of our analysis of oil field techniques and mechanisms. The numerical dispersion is essentially an error due to the fact that we use the grid block approximation for solving the flow equations.

4.5.1 1D Model Oil and Water Including 10 Cells Grid

The base case model consists of a 1-layer system with a pair of producers/injectors as shown in Figure 4.5. The model consist of 10 cells with total model length of 1000 ft., similar to the sizes employed in fine scale full field geological modeling was used. We have used a constant permeability for all cells 10 mD and the constant porosity 20 %. The injector appears on the left side and the producer on the right hand side of Figure 4.5. The figure shows the oil saturation after a certain period of time during the simulation; that is it analyses in detail how water has been displaced at that instantaneous time. The saturation process is not always the same in different models. It varies most of the time from one model resolution to another.

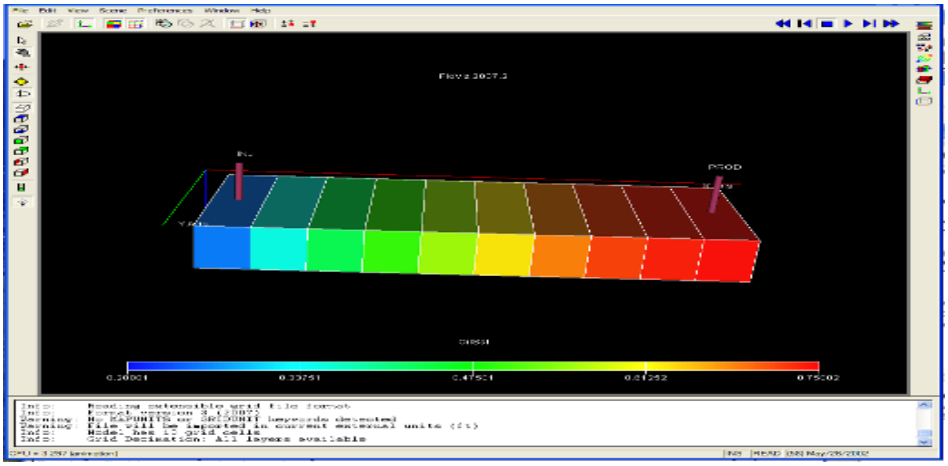

Figure 4.5 : Base 1D Model (10x1x1 cell). Oil Saturation.

The results of this model are shown in Figure 4.6 on the following page. The figure reveals the outcome of what could be the various conditions and circumstances surrounding the experiments that can be carried out in this type of model. This model for instance, as shown below, indicates the field oil production rate (FOPR) which is represented by the red line and the field water cut (FWCT) that is denoted by a blue-line. Furthermore, it is clear that the water starts to break through after 120 days.

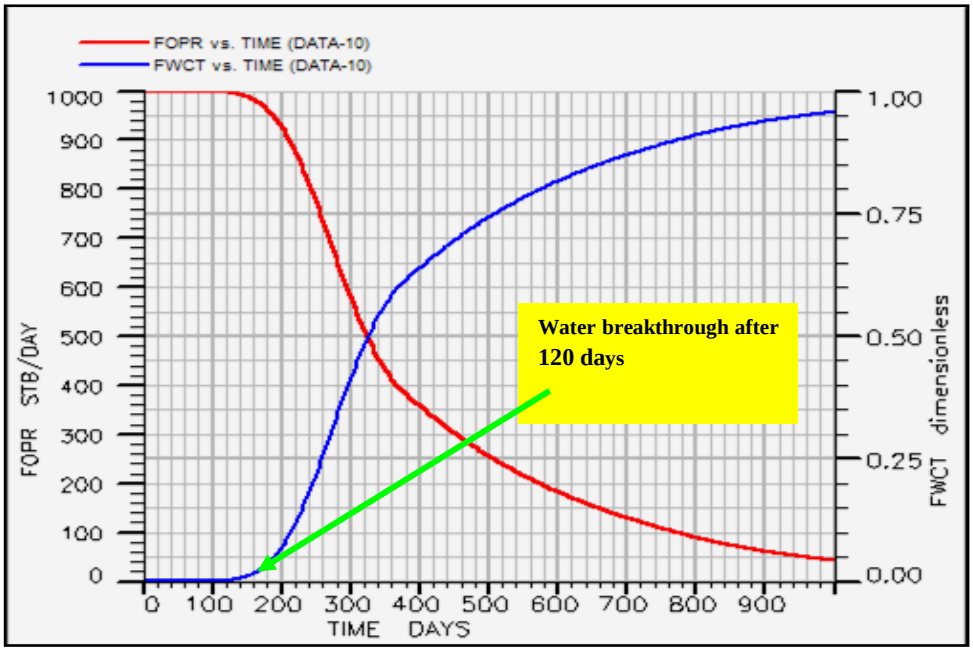

Figure 4.6: Water breakthrough at 120 days.

4.5.2 1D Model of Oil and Water Including a 100 Cells Grid

The new model again consists of a 1-layer system with a pair of producers/injectors as shown in Figure 4.7. The model consist of 100 cells with total model length of 1000 ft, similar to the sizes employed in routine full field simulations was used. Again have used constant permeability for all cells of 10 mD and the constant porosity 20 %.

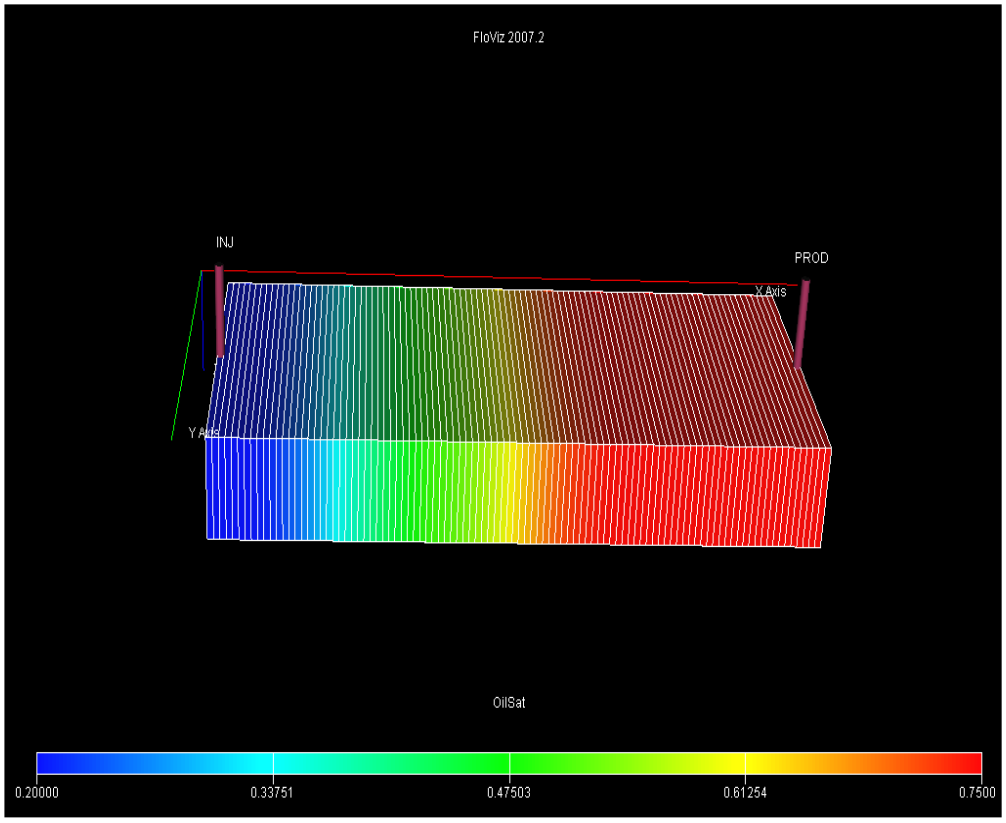

Figure 4.7: 1D Model (100x1x 1 cell). Oil Saturation.

The results of this model are shown in Figure 4.8; the figure indicates the field oil production rate (red-line) and the field water cut (blue-line). Furthermore, it is clear that water breakthrough starts after 240 days. We can easily see that the water breakthrough process is not always identical in FDM even in the models that have the same overall dimensions, as in the two cases just presented. A difference of water breakthrough timing of 120 days is very significant.

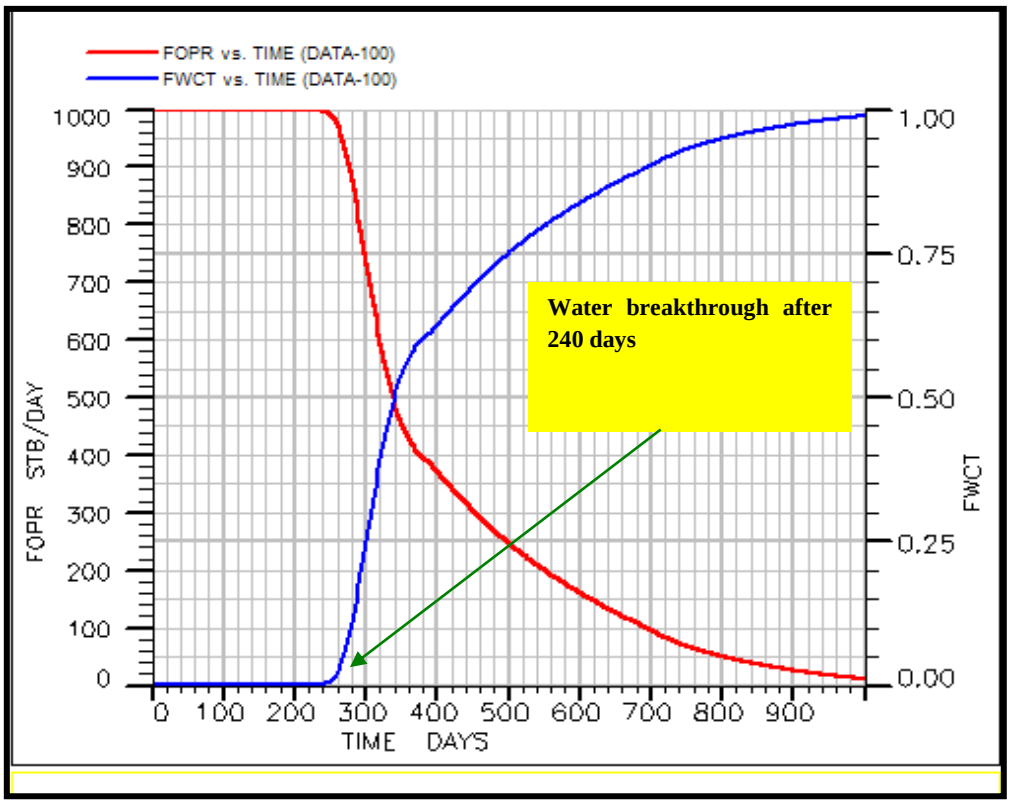

Figure 4.8: Water breakthrough at 240 days.

4.5.3 1D Model of Oil and Water Including a 1000 Cells Grid

This model consists of a 1-layer system with a pair of producers/injectors as shown in Figure 4.9. The model consists of 1000 cells with total model length of 1000 ft. similar to the sizes employed in routine coarse scale full field simulation was used. We have used constant permeability for all cells 10 mD and the constant porosity 20 %.

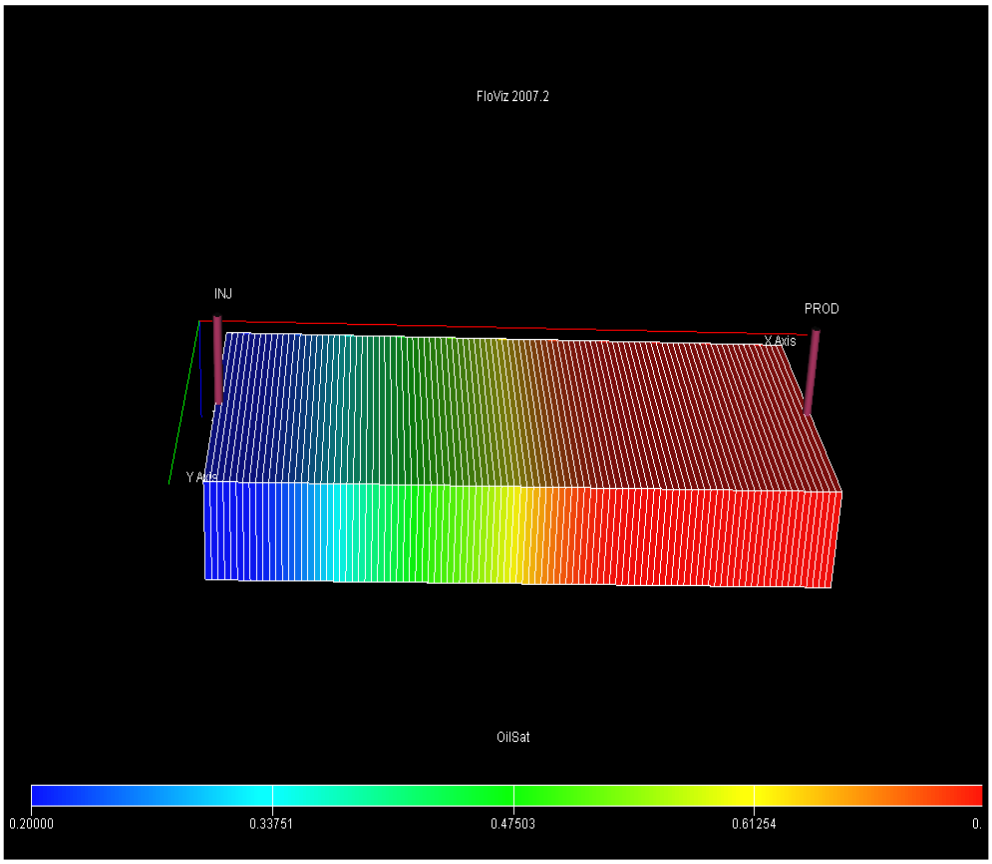

Figure 4.9: 1D Model (1000x1x 1 cell). Oil Saturation.

The results of this model are shown in Figure 4.10; the figure indicates the field oil production rate (red-line) and the field water cut (blue-line). Furthermore, it is clear that water breakthrough starts after 270 days.

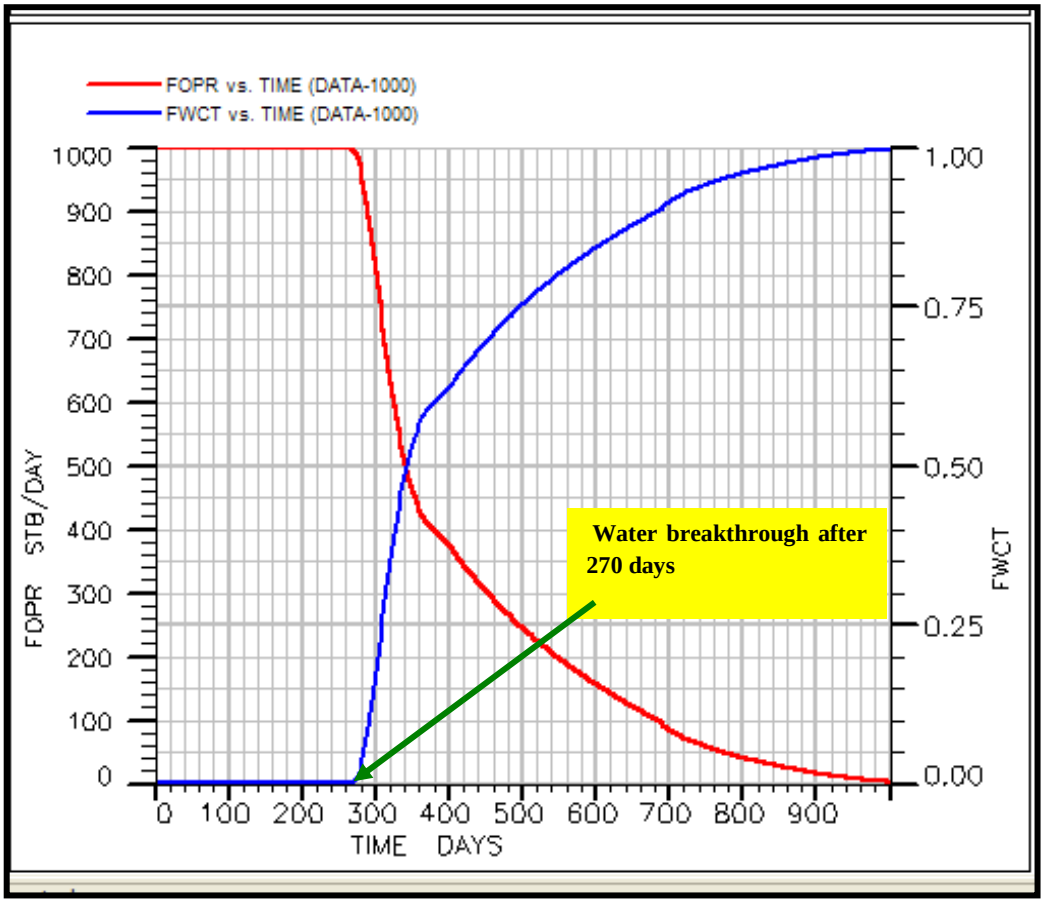

Figure 4.10: Water breakthrough at 270 days.

4.7.3 STREAMLINE MODEL

This model consists of a 1-layer system with a pair of producers/injectors as shown in Figure 4.11. The model consists of 100 cells. Similar to the sizes employed in routine full field simulations was used. We have used constant permeability for all cells 10 mD and the constant porosity 20 %.

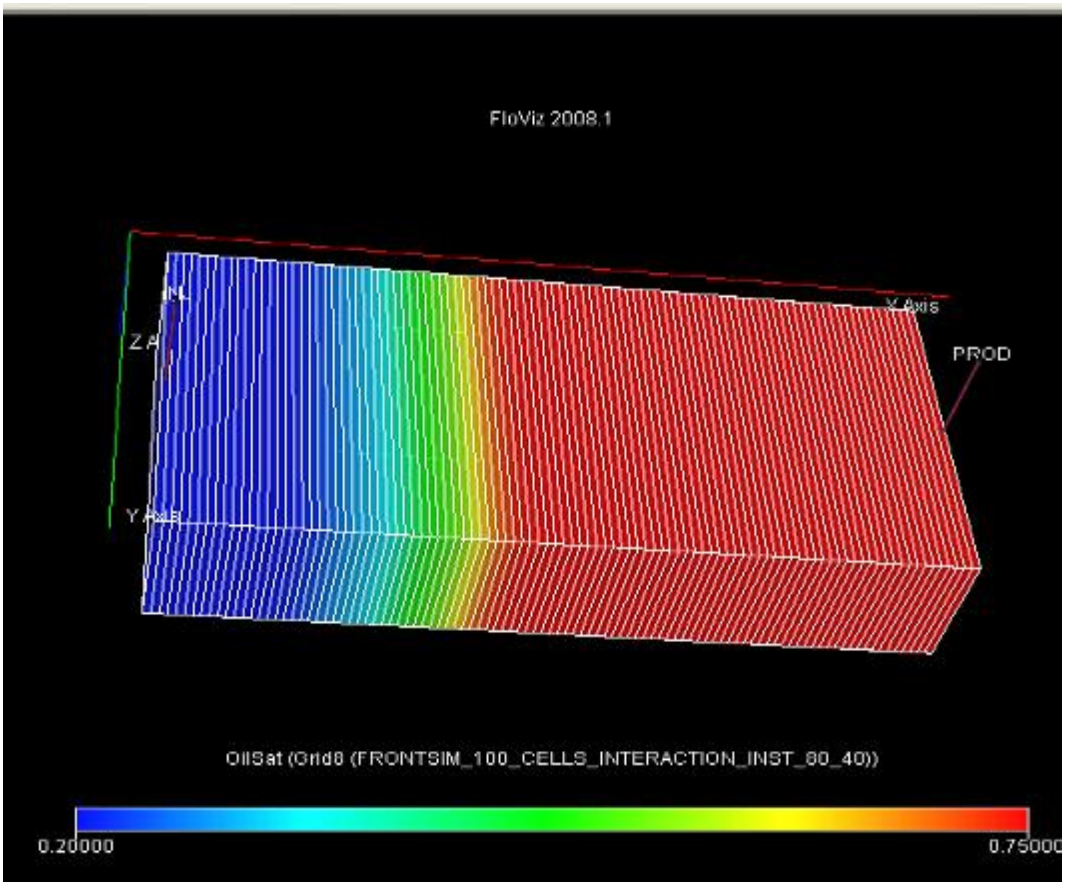

Figure 4.11: 1D Model (100x 1x 1 cell) Streamline Oil Saturation.

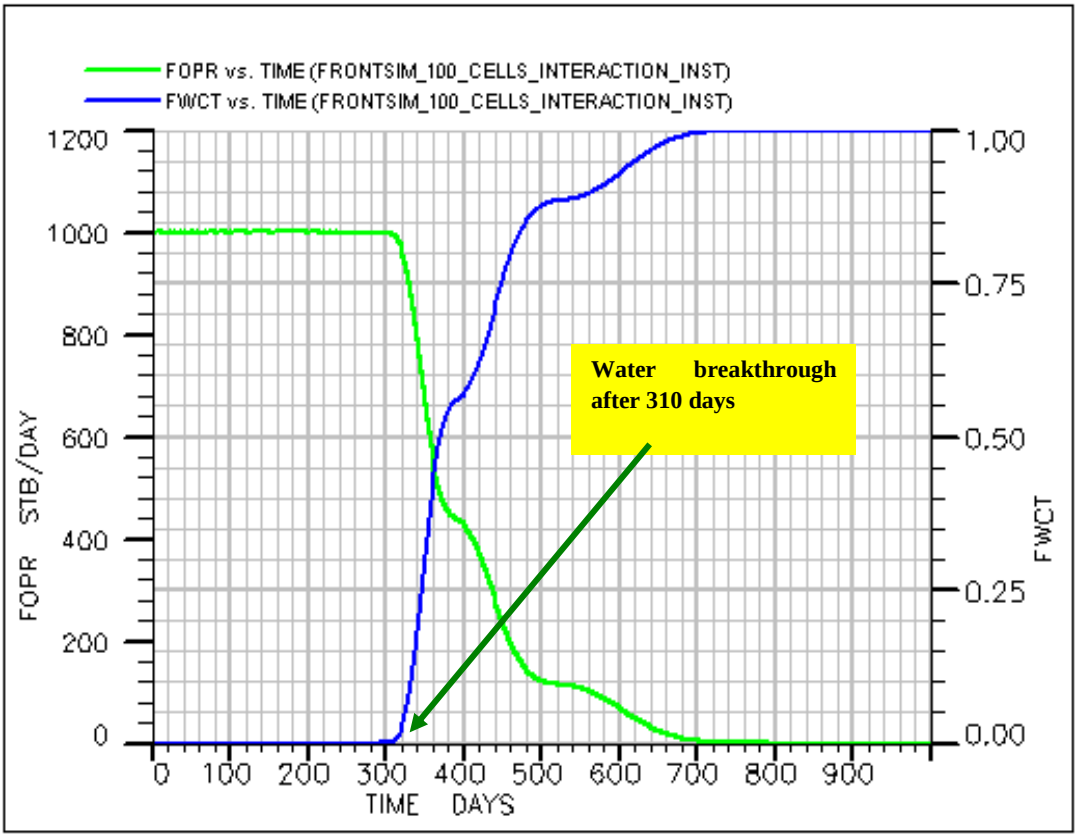

Figure 4.12: Water Breakthrough at 310 days.

The results of this model are shown in Figure 4.12. The figure indicates the field oil production rate (red-line) and the field water cut (blue-line). Furthermore, it is clear that water break through starts after 310 days.

As we can observe from the results of the four different models, they show differences in the time in which water breakthrough takes place (Figure 4.13). Water breakthrough occurs later in the streamline model compared with the other results from the finite difference models. Since all the models simulate essentially the same system, the only difference in the level of dispersion, with the streamline model inhibiting the lowest dispersion of all the calculations.

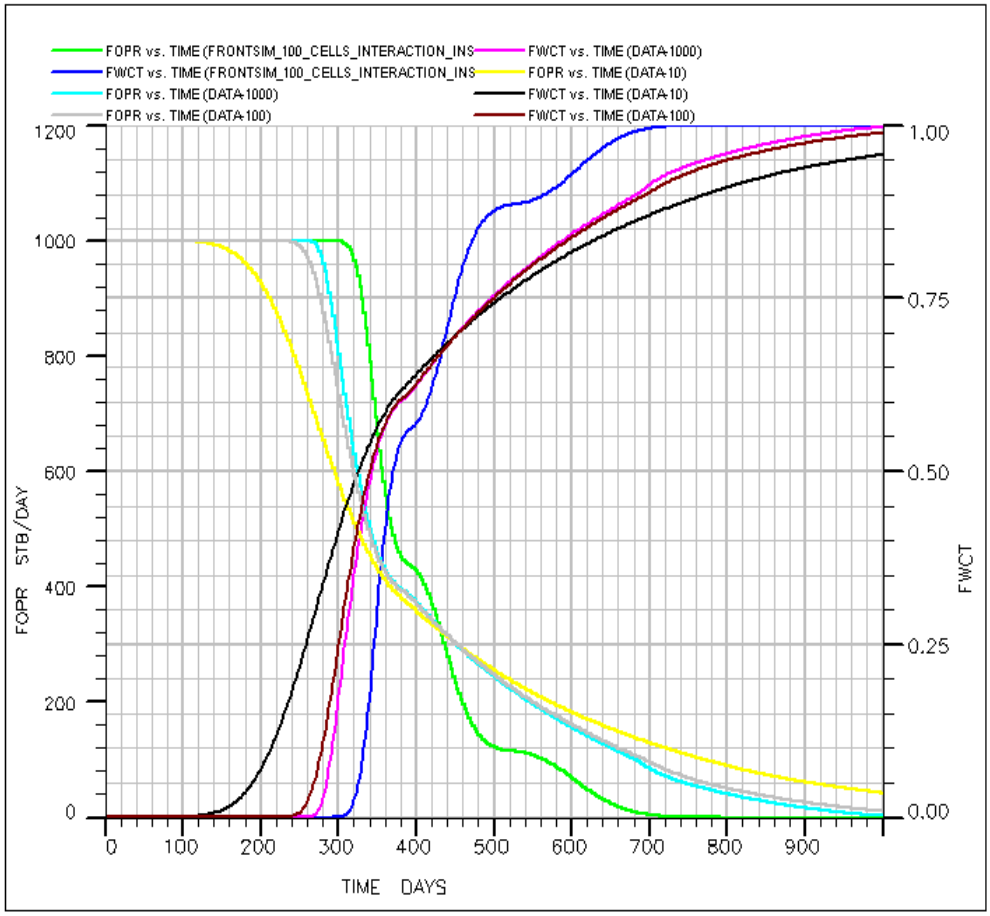

Figure 4.13: Oil production rate and water breakthrough time for the four models.

The results of this model are shown in the Table 4.1 below.

Model	**Number of cells**	**Water Breakthrough time (Days)**
1 D FDM	**10**	**120**
1 D FDM	**100**	**240**
1 D FDM	**1000**	**270**
1 D Streamline	**100**	**310**

Table 4.1: illustrates the different model grid and different times of water breakthrough.

If we assume that the model that leads to the latest prediction of water breakthrough time is probably the most accurate for one dimensional flow in homogenous system, then increasing grid resolution has a very significant impact on the accuracy of the calculations, but that a lower resolution streamline model is more accurate than any of the FDMs.

4.7 AREAL DISPLACEMENTS IN TWO-DIMENSIONAL GEOMETRY

4.7.1 Oil/Water Displacement and Water Mixing in Waterflooding

An area of (2D) waterflooding can be regarded as a sequence of 1D displacement which arrives at different times according to the length of the physical streamlines travelled by the fluids. In this scenario, injected water will flow relatively quickly in a direct line between the wells, but will travel slowly as it spreads out in the corners of the field as shown in Figure 4.14 (note that this is a FDM). In this way, as injected water is produced, there will still be connate water to be delivered from the flanks of the field by the streamlines that go through the corners of the field. This will cause the mixing of the two brines near the production wellbore due to the convergence of different streamlines travelling from various zones in the field. (We refer to these as physical streamlines, although here we are using a FDM, not Streamline simulation)

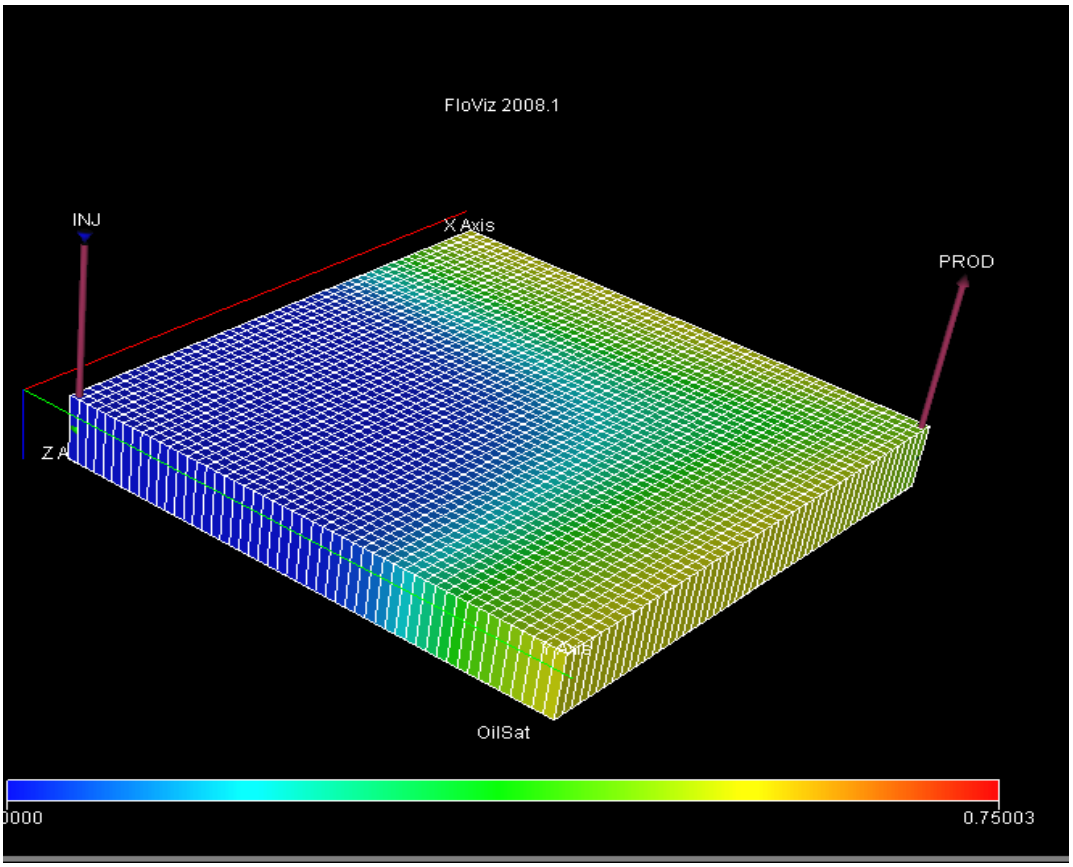

Figure 4.14: Areal (2D) with 50x50x1 cells water flood. Injected water displacement in finite difference model.

It has been concluded that a 2D areal model of a homogeneous reservoir is the an appropriate method for studying the mechanisms of areal displacements by both finite difference method (F.D.M) and streamline method. Simulation grids 50x50x1 (50 ft cells) are used to illustrate the results. Figure 4.14 shows a 2D Areal model with uniform permeability and the same porosity of 20% for all the cells. This figure shows the oil saturation as water is displaced from the injection well on the left of the figure to the produced well on the right of the figure. The permeability in x and y directions is 1000 mD.

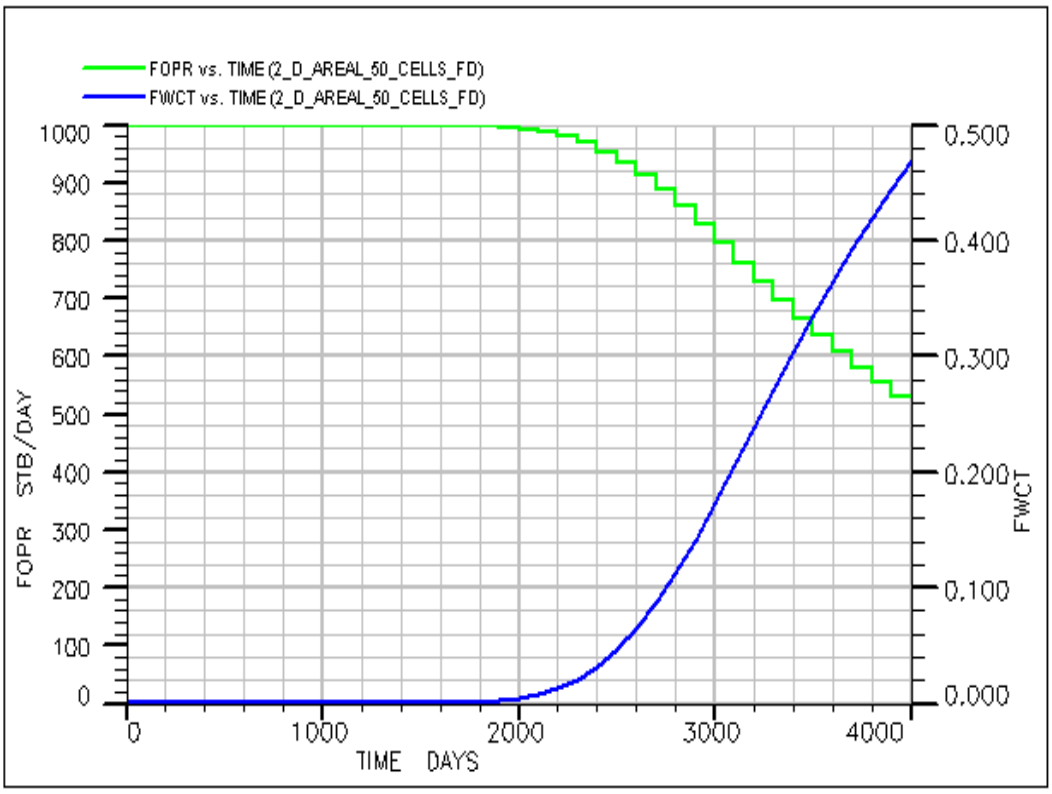

Figure 4.15: Areal (2D) Water flood. Field and production rate are water cut from ECLIPSE calculation for 50x50 grid blocks.

The results of this model are shown in Figure 4.15 above. The figure illustrates the field oil production rate FOPR (green line) and the field water cut FWCT (blue line). Furthermore, it is clear that water breakthrough started after 1900 days.

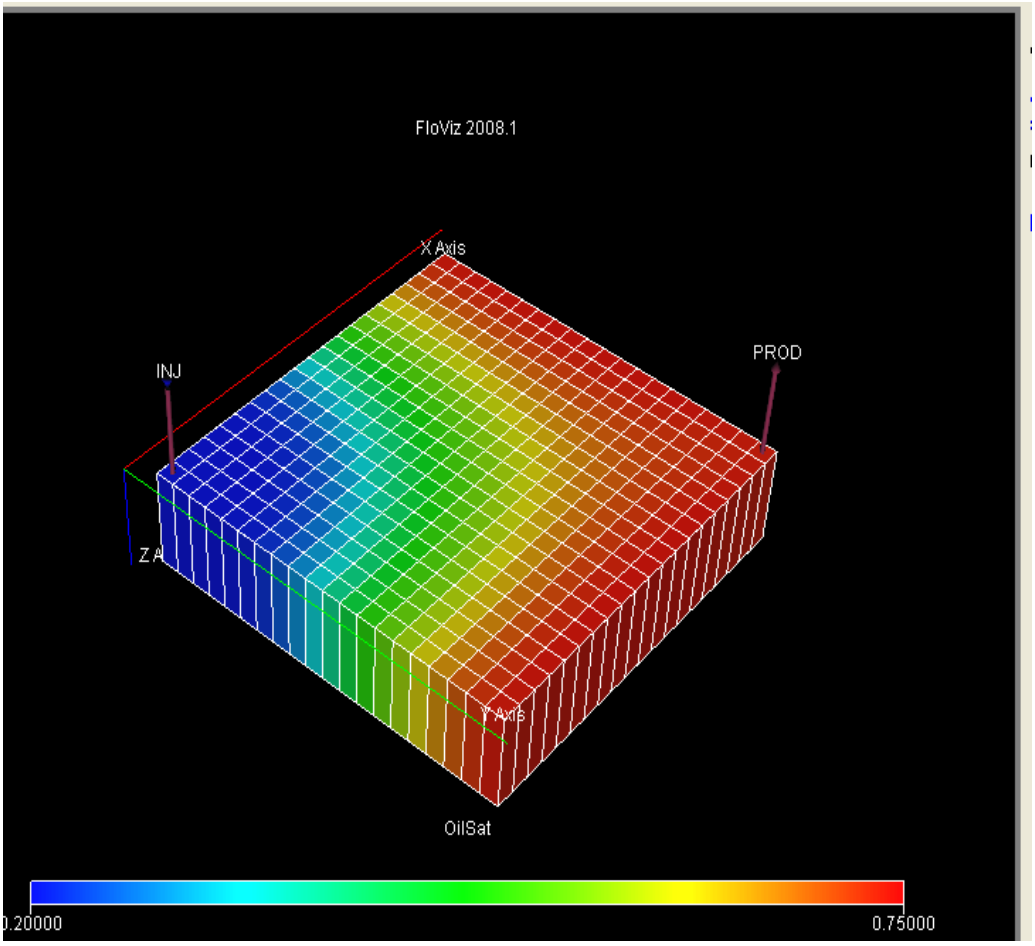

Figure 4.16: Areal (2D) Water flood. Injected water displacement, finite difference model with 20x20x1 cells.

A simulation grid with 20x20x1 same as in 50x50x1 model was used to illustrate the impact of the grid resolution. Figure 4.16 shows the oil saturation at an earlier time than in Figure 4.14, but the extent of the mixing is greater.

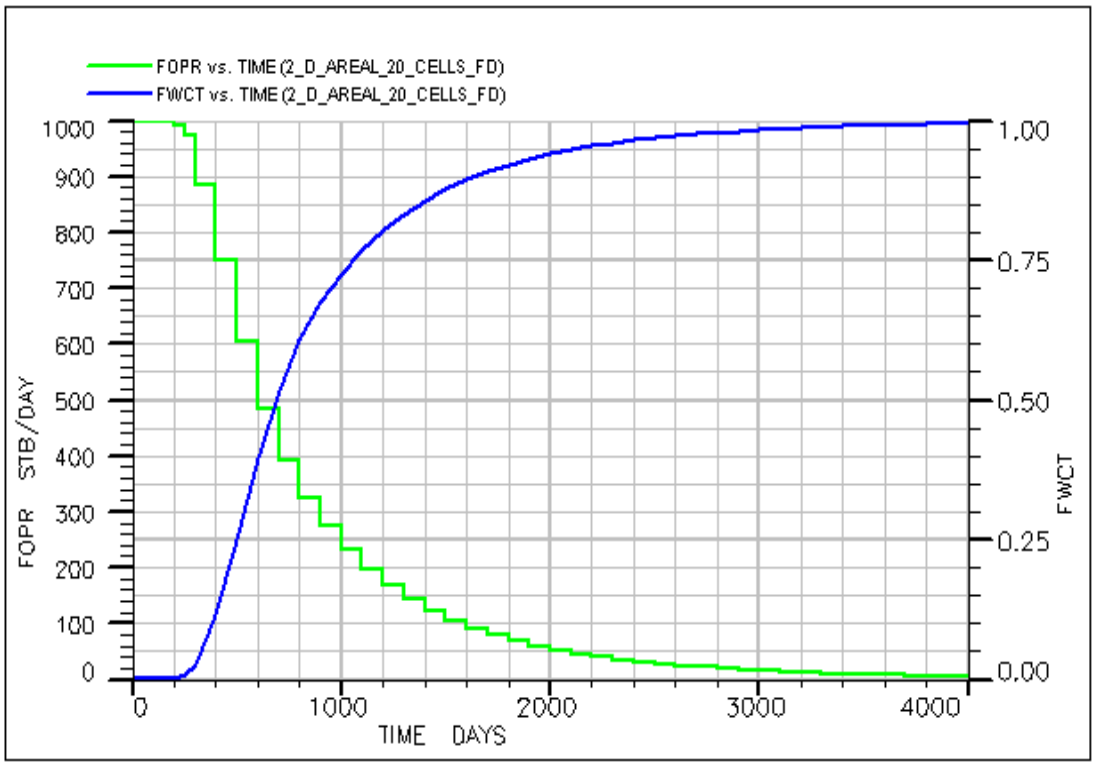

Figure 4.17: Areal (2D) waterflood. Field and production rate and water cut injected from ECLIPSE for 20x20x1 grid blocks.

The results of this model are shown in Figure 4.17 above. The figure illustrates the field oil production rate FOPR (green line) and the field water cut FWCT (blue line). Furthermore, it is clear that water breakthrough started after 200 days. (The rise in water cut tends to be more gradual in the 2D models than in the 1D model.)

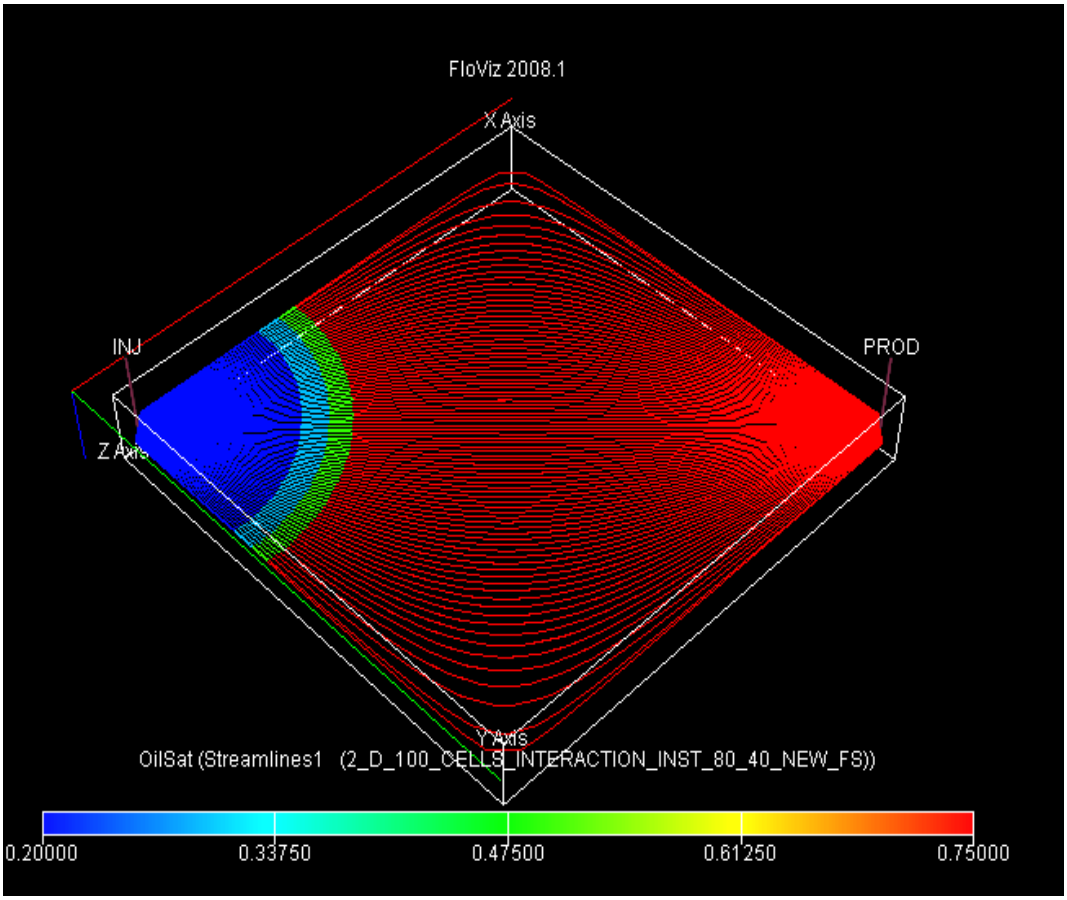

Figure 4.18: Areal (2D) Waterflood. Injected water displacement calculated using Frontsim.

A 2D areal model of the same homogeneous reservoir was also modeled using the streamline method. Simulation grids and 20x20x1 (50 ft cells) was used. Figure 4.18 shows the oil saturation at earlier time than for the other models, but it is clear the front is much sharper in this case.

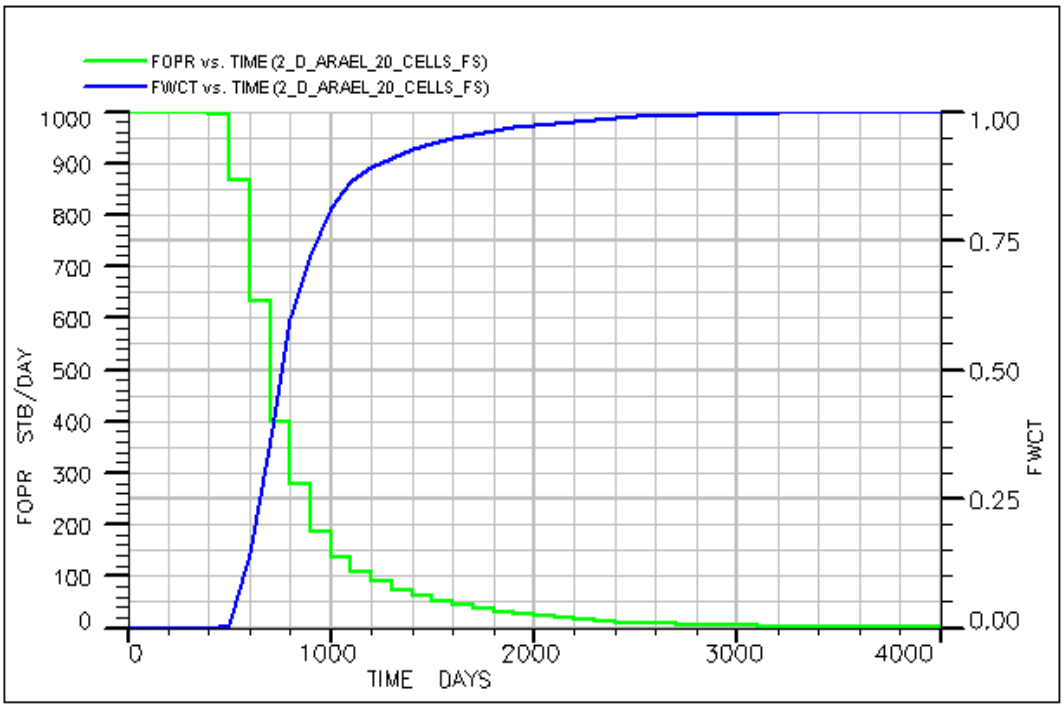

Figure 4.19: Areal (2D) Waterflood, oil production rate and water cut from FrontSim model with 20x20 grid blocks.

The results of this model are shown in the Figure 4.19 above. The figure illustrates the field oil production rate FOPR (green line) and the field water cut FWCT (blue line). Water breakthrough occurs after 500 days, some 300 days later than in the coarse 2D model.

The results and the work that has been conducted will now be summarized as follows:-

A 2D areal model with a homogeneous reservoir was chosen for studying the mechanisms of areal displacements by both finite difference and streamline method. Simulation grids with 20x20x1 (50 ft) cells, 50x50x1 (50 ft) cells for finite difference and 20x20x1 (50 ft) cells for FrontSim are used to illustrate the results.

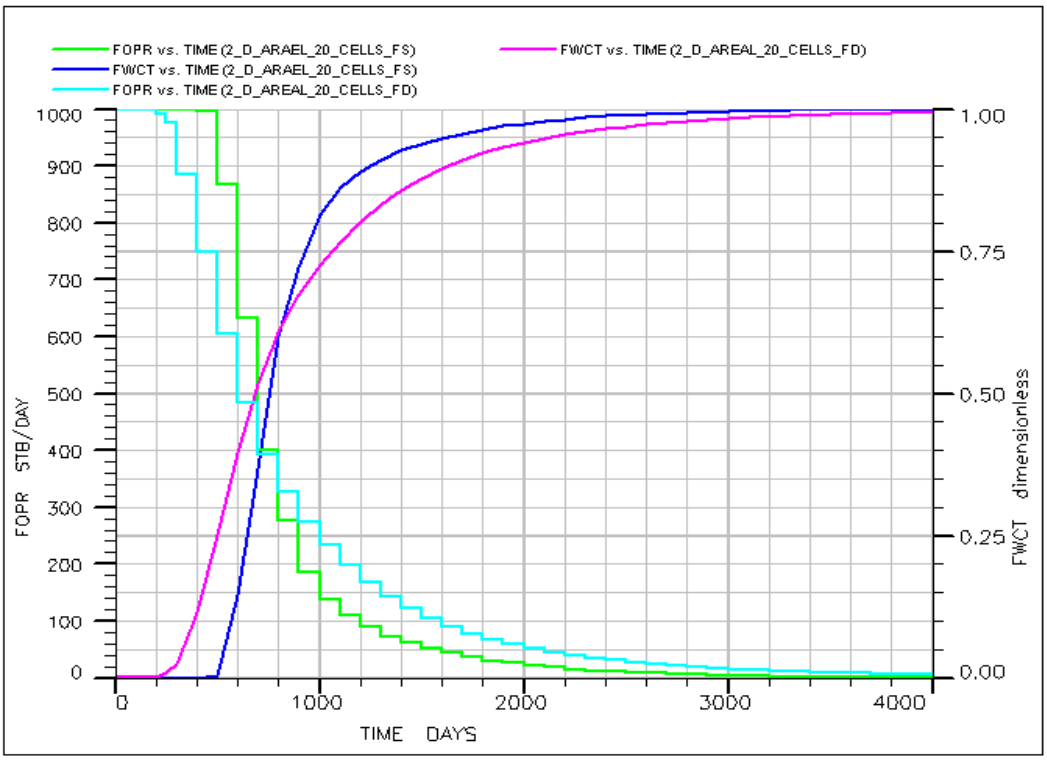

Figure 4.20: Areal (2D) Waterflood. Oil production rate and water from Frontsim for 20x20 and the finite difference model with same number of grid blocks and the same grid sizes.

In Figure 4.20 we have shown the results of the FrontSim model and the finite difference model for the same grid sizes and the same properties to simulate the numerical dispersion effect in the 2D areal model. We can also observe that the time of the water breakthrough for FrontSim is 500 days, whereas the time breakthrough of the finite difference is 200 days. Therefore we can conclude again that streamline simulation reduces the degree of numerical displacement.

We can see that so far this has concerned models with 1 or 2 dimensions. We have discussed different things that can be experimented on in the model, and have identified that the reduction in numerical dispersion in the streamline models significantly reduces the degree of numerical dispersion.

Now that 1D and 2D areal models have been dealt with 3D models are used and the results compared with the previous models. However, before that heterogeneity is introduced by means of a random permeability model.

4.7.2 2D Areal Random Permeability Model

In this chapter we have used a 2D homogeneous model to analyze the effects of injected and connate water mixing. The other extreme was depicted using a non-correlated random permeability field in the reservoir. The distribution of random permeability is illustrated in Figure 4.21.

In order to show the effects of permeability variation, Figure 4.22 provides a comparison of ECLIPSE and FrontSim results regarding the injected/connate water mixing zone over different periods of time. Once more, the results have revealed less numerical dispersion, providing sharper results when compared with the finite difference solution. The most significant effect of heterogeneity has been the marked smearing of the mixing zone. This extends the area impacted by incompatible waters being mixed, particularly the area next to the production well.

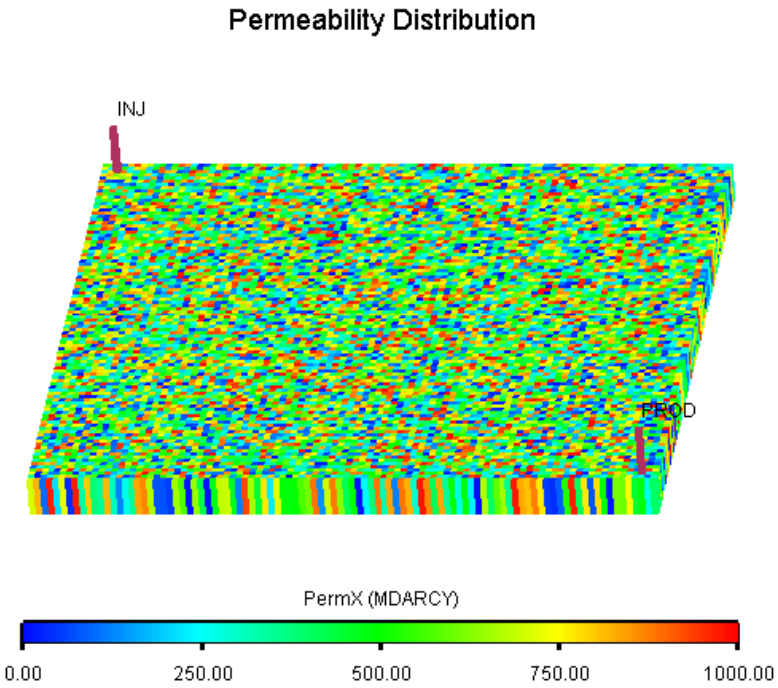

Figure 4.21: Non-correlated permeability distribution for the 2D areal model (100x100 grid blocks).

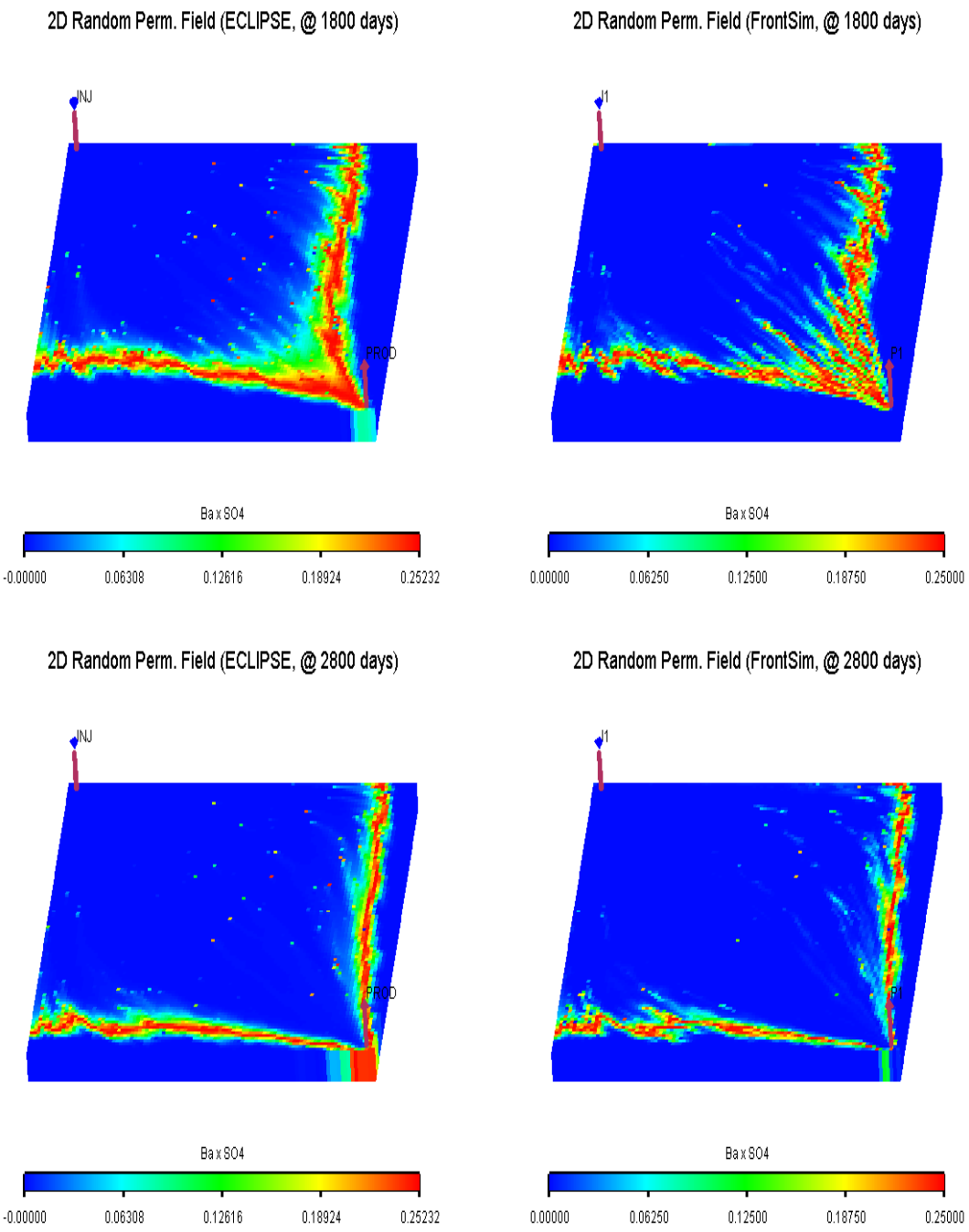

Figure 4.22: Ba and SO_4 mixing zone at 1800 and 2800 days for ECLIPSE and FrontSim for a 2D non-correlated random permeability model.

In addition to areal heterogeneity, vertical heterogeneity may also have an important role, and in fact may produce some mixing in the formation depending on the well and reservoir geometries. For example, the partial completion of a well may cause the convergence of flows from different layers leading to some mixing in the near wellbore

region, or coning of bottom water mixing with a different type of water coming from further up. In summary, permeability layering can be regarded as a combination of several 1D displacements in different layers, causing connate water banking and different injected water breakthrough times in each layer. This situation may be complicated further by the presence of an aquifer (with possibly a different water composition), which may also be responsible for the low barium ion concentrations due to scale deposition within the aquifer itself.

4.7 Three-Dimensional Geometry

A 3D model with constant cell size of 250x250x50 ft. was used to illustrate the numerical dispersion effects. The base case model consists of a 3-layer system (10, 10, 3) cells with producer/injector pair as shown in Figure 4.23. The permeability distribution is shown in figure 4.23 (b), and the relative permeability curves in Figure 4.23 (c).

The solution to this problem obtained in ECLIPSE is compared with the FrontSim solution in Figure 4.24. The results show the effect of numerical dispersion in finite difference simulation, where the breakthrough occurs at 200 days, instead of 300 days in streamline simulation.

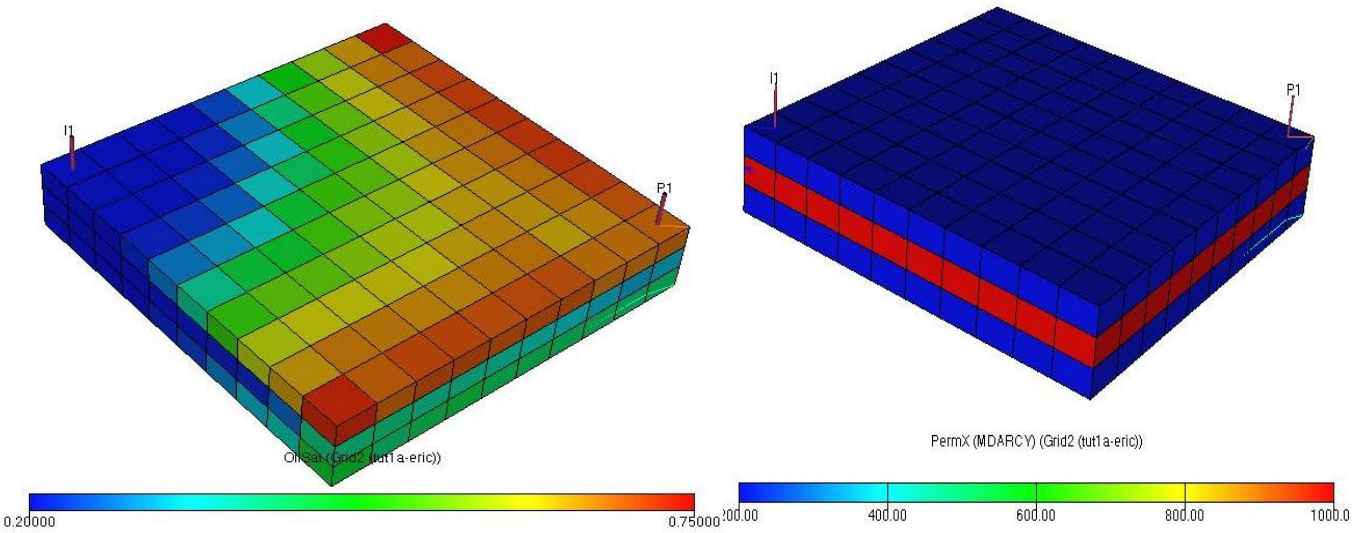

(a) (b)

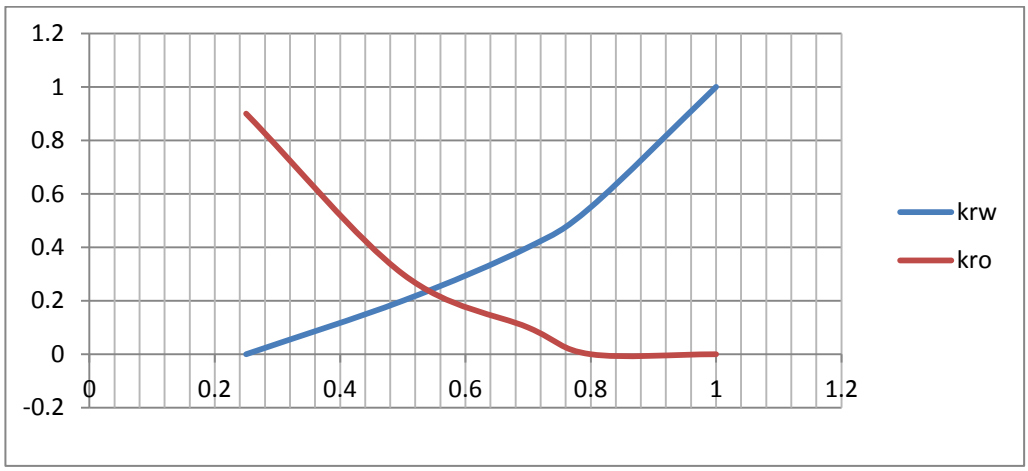

(c)

Figure 4.23: (a) Base 3D Model (10x10x3 cells) oil saturation; (b) Permeability Distribution and (c) relative permeability functions.

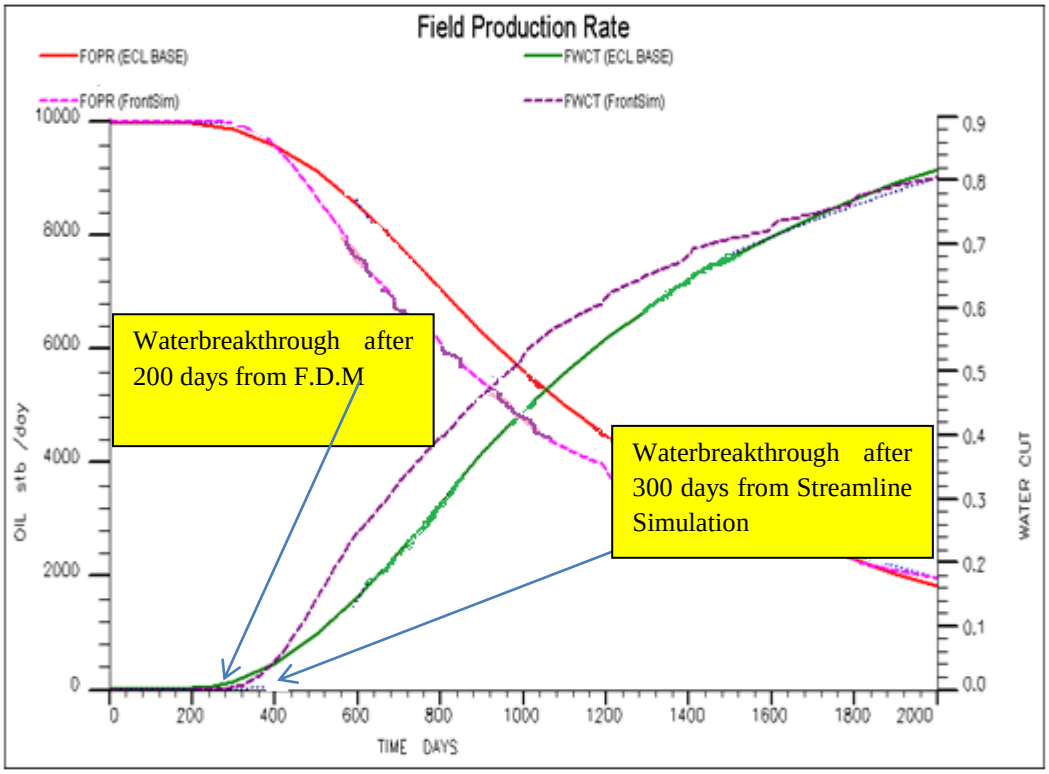

Figure 4.24: the 3D Model production rates and water cut

4.7 CONCLOSION & DISCUSSION

Over the last few years, the use of streamline simulations has become more common in the industry due mainly to significant savings in computation time and reduced numerical dispersion. In this study, a finite difference based model (ECLIPSE) and a streamline simulator (FrontSim) have been compared for tracking the flow of injected water through a series of one, two and three-dimensional systems to address the problem of numerical dispersion exhibited by finite difference methods, particularly when predicting water and injected water breakthrough times. Recent calculations using FDM have been performed regarding injected, connate and aquifer water mixing in waterflooding and its consequences in scale dropout within the reservoir. In this work, those conclusions have been closely used as a base framework to contrast with streamline simulation. Basic 1D, 2D and 3D geometries and model studies have confirmed the numerical dispersion problem that occurs in FDM when compared with streamline modelling. These differences lead to the following conclusions concerning dispersion in waterflood, mixing of injected and formation water in the reservoir

- In 1D linear waterflood displacements, FrontSim has effectively shown minimal numerical dispersion, producing similar results to ECLIPSE with grid block sizes that are approximately 100 times bigger.

- Streamline simulation is more effective and faster than F.D.M., and can model using very fine gridblocks, with shorter run times and with minimal numerical dispersion.

- The results clearly show that streamline simulations can be an effective substitute or complementary tool in alleviating the issues regarding numerical dispersion that are inherent in standard simulators. As streamline simulation maintains sharp fronts, this can help gain a better insight into where the problem of scaling may be arising. This is crucial when the aim is to avert a drop in productivity that could occur because of scale.

- By utilizing the 3D streamline model we prove that the streamline simulation produce more accurate water breakthrough times compaired to the Finite difference methods.

- Numerical calculations in a 2D areal model have shown that injected water will arrive at the producer at different times, determined by the areal flow paths taken by the streamlines. Hence, the mixing of different brines is expected in the near production wellbore region for an extended period, which can lead to continuous scale deposition. Similar effects regarding brine mixing at the producers have been observed for a 2D heterogeneous model. FrontSim results for the 2D areal systems always produced sharper brine mixing zones than finite difference solutions.

CHAPTER 5: SIMULATION OF SCALE DEPOSITION USING STREAMLINE SIMULATION

5.1 INTRODUCTION AND BACKGROUND

Waterflooding is a common method of providing pressure support for oil reservoirs. Certain production problems may arise after water breakthrough. One of the biggest problems is that of scale formation. This problem of scale formation can occur if the injected water contains ions. For example, as already noted if sea water, which is rich in Sulphate ions (SO_4), is injected into formation water that is rich in Barium (Ba), Barium Sulphate may form in the formation or the production well. Understanding where the scale forms is important as the formation of scale close to the well or in the well can reduce the productivity of the well or in extreme cases cause the loss of the well. The location of the formed scale will determine whether the near well treatment will succeed or not. If, on the other hand, scale forms deep in the reservoir it may have a negligible effect on the well production.

In 1999 White et al. identified that wells in a North Sea field were producing lower than expected levels of barium. This occurred because the scale was being formed in the formation (in other words the barium was consumed in the formation). The well had, however, been successfully squeezed and there was no apparent loss of production. This suggests that the scale is being deposited some distance from the well. Sorbie and Mackay(2005) and Mackay and Sorbie (2000) pointed out that mixing deep in the reservoir, particularly in the aquifer could lead to reduced production of scaling ions without any impact on the productivity of production wells. Clearly, by identifying where scale is formed we want to understand the movement of scale forming ions in the context of a full field simulation. Over the last few years various approaches have been investigated (e.g. Mackay and Graham 2003.). In general, it is quite difficult to do this in a standard reservoir simulator such as ECLIPSE. Although, the propagation of ions through the reservoir using tracers is easy, most simulators do not provide any way to model the interaction of the ions. As discussed in Chapter 4, finite difference simulators tend to introduce numerical dispersion and it is therefore difficult to model the narrow

ion depleted region between injected and connate water without using a very fine grid. Simulations can consequently be very time consuming.

There are two basic approaches to $BaSO_4$ scale mitigation. Either by removing the sulphate ions from the injected water or using squeezes treatments to prevent scale formation close to the well. (E.J. Mackay et al. 2003). From a financial point of view, the cost of running a simulation study using a pre-existing simulation model is negligible. The cost of installing a sulphate treatment plant is typically in the region of $20million to $100 million dollars. The cost of a squeeze treatment using coiled tubing intervention in a deep water environment can typically range from $0.5million to $10 million and has to be repeated. Clearly, if we can predict that scale will form deep in the reservoir rather than close to the producer, then the savings that can be made are valuable.

As indicated before in Chapter 4 the scale formation modelling by using the ECLIPSE finite difference method tends to create numerical dispersion effects in addition to the fact that we cannot simulate the chemical interaction. A new technique using an adaptation of an existing streamline simulation with new keywords that model the chemical interactions has been developed. The central work of this thesis is to apply that code to identify the impact on scale management. First we detail the methodology and some of the equations associated with streamline simulation, and then we describe the new thermodynamics modelling addition.

5.2 STREAMLINE SIMULATION

5.2.1 **Basic Concepts**

Streamlines are instantaneous lines that are everywhere tangential to a velocity field, with no restriction that velocity be in a steady state and no requirement that fluids be incompressible. For our applications, the velocity will always be the total interstitial velocity. This is the multiphase Darcy velocity divided by the porosity. If the velocity varies with time, then we think in terms of an instantaneous snapshot to define the streamlines.

This section will now discuss time of flight (T.O.F) for three different permeability distributions with distinct characteristics ranging from uniform permeability to an almost stratified pattern. We studied water injection in a 2D areal cross-section with the injector on the left and the producer on the right. As shown in Figure 5.1**,** for homogeneous cases, the tracer front moves uniformly and all particles arrive at the producer at the same time. For the heterogeneous cases, we can easily see the interaction between the heterogeneity and flow field. In high permeability regions, the tracer moves faster, leading to early breakthrough.

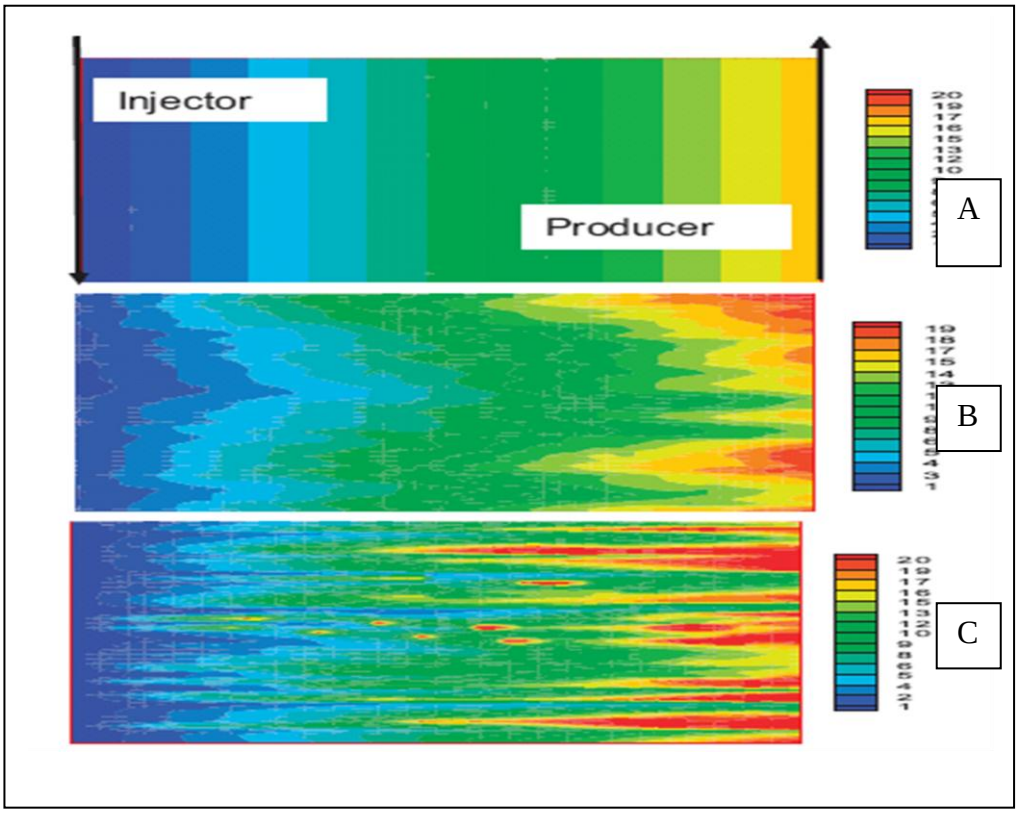

Figure 5.1: Streamline time of flight for three heterogeneity patterns.

A key underlying concept in streamline simulations is to isolate the effects of geological heterogeneity from the details of the physics of fluid calculations. Mathematically, this is accomplished by using the streamline time of flight as a spatial coordinate variable. From a computational point of view, we have now moved to a coordinate system where all streamlines are straight lines and the distance along the streamlines has been replaced by the corresponding time of flight. The impact of heterogeneity is embedded

in the time of flight distribution. The physical process calculations are now reduced to 1D solutions along streamlines with the time of flight being the spatial variable as shown in Figure 5.2. For example, we can carry out 1D water flood calculations along each streamline and simply sum up the contributions of all the streamlines at the producer to get the overall response. We can also contour the saturation distribution along each streamline to obtain a snapshot of saturation variations in the reservoir, shown in Figure 5.3.

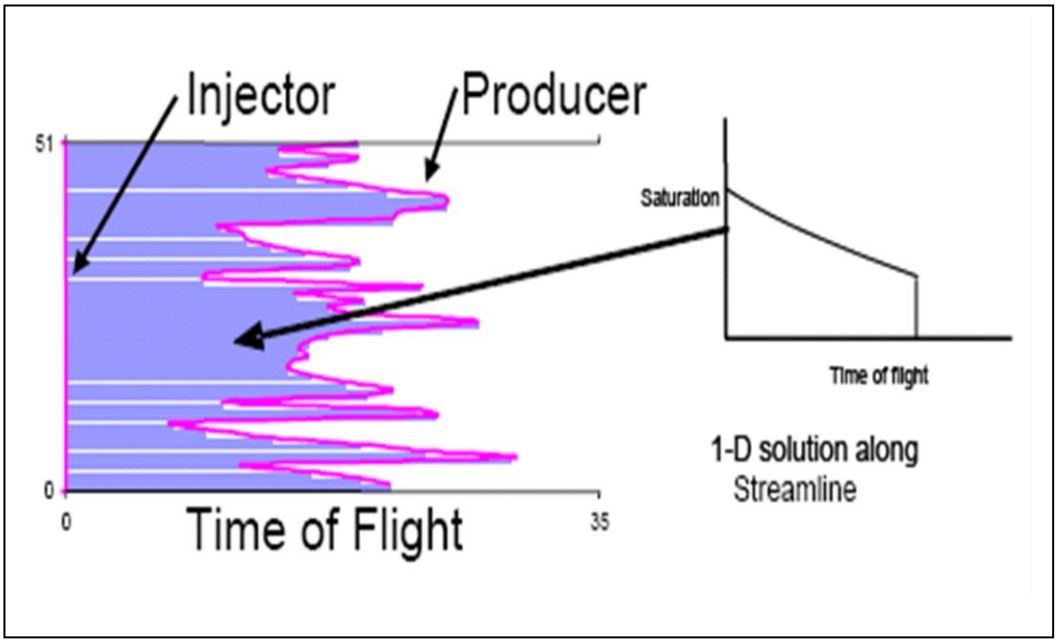

Figure 5.2: Streamline saturation calculations. The multidimensional calculations are reduced to a series of 1D calculations. With the time of flight as the spatial variable

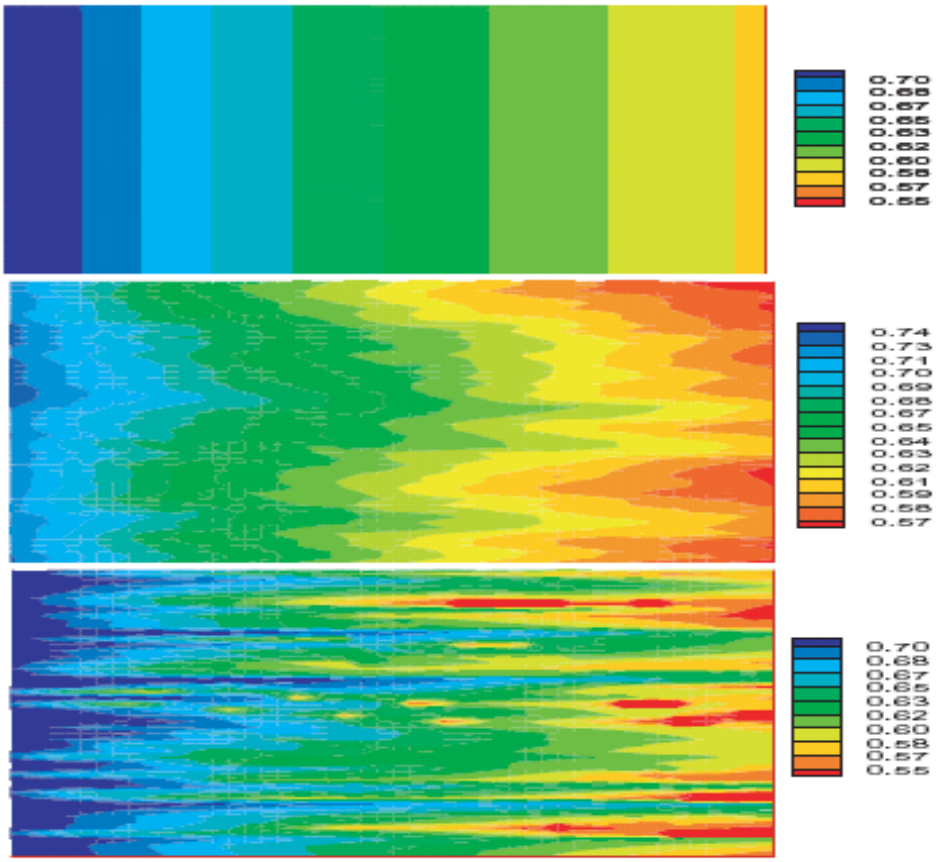

Figure 5.3: Saturation profile at 0.55 PVI for the three heterogeneity distributions in Figure 5.1.

5.3 STREAMLINE SIMULATION STEPS

We will illustrate these steps using waterflooding in a heterogeneous five-spot pattern with infill drilling. The permeability distribution and well configuration are shown in Figure 5.4. Waterflooding is carried out until 0.35 PV is injected and then four wells are drilled to convert the pattern to a nine-spot.

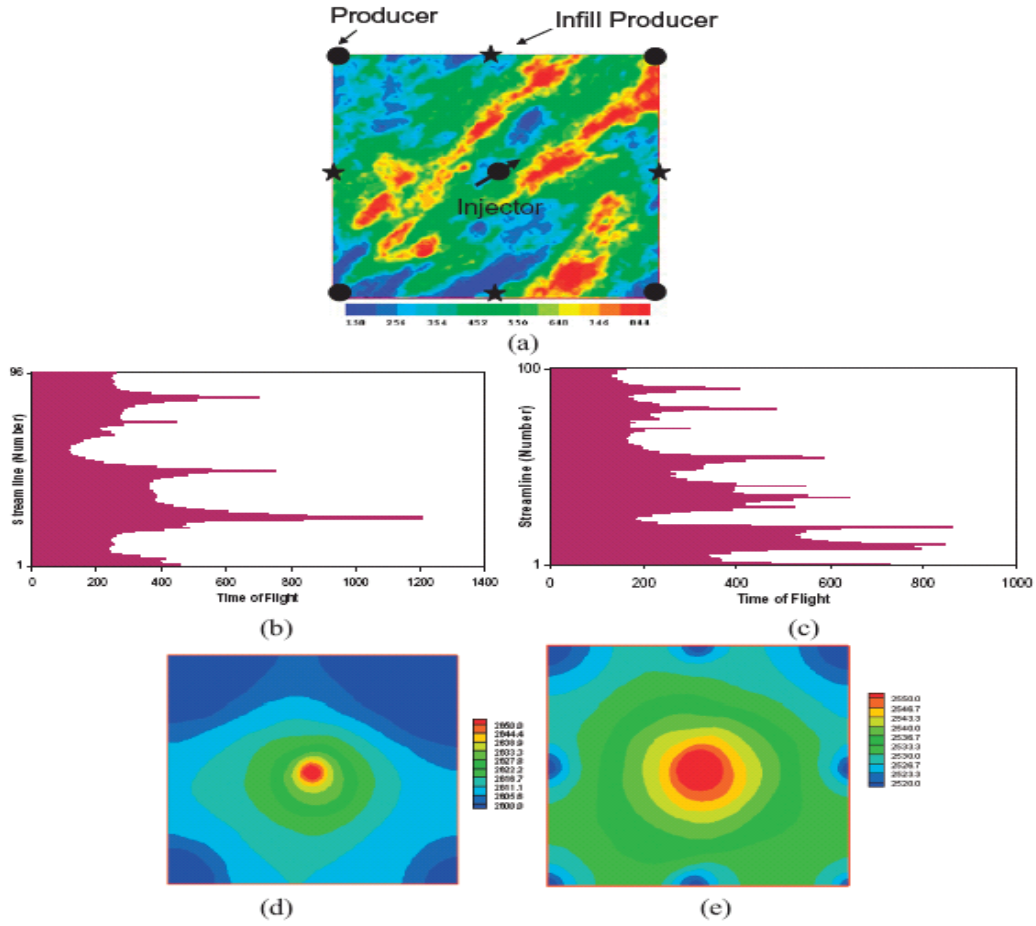

Figure 5.4: Permeability distribution and well configuration: five-spot to nine-spot conversion via infill drilling. (a) Permeability and wells, (b) Time to flight for five-spot, (c) Time to flight for nine-spot, (d) Pressure distribution for the five spot, (e) Pressure distribution for nine-spot.

In Figure 5.4 (b), the streamline time of flight to producers is plotted for this heterogeneous five-spot pattern. Because we are in streamline coordinates, we have what appears to be a linear flood *along each streamline*. The only indication that this is a pattern flood is the appearance of stagnation lines at the balance points between the different producers. (No specific streamline reaches a stagnation point, and so the maximum observed time of flight remains finite). In Figure 5.4 (c), we show the time of flight per streamline after the nine-spot conversion. Again, we have what appears to be a linear flood, but with more evidence for stagnation. Finally, the pressure maps for the five-spot and nine-spot are shown in Figure 5.4 (d), (e). So, we can summarize the main stages of the streamline simulation, following Datta-Gupta, 2007:-

- Given a grid with initial reservoir properties distribution such as porosity, permeability, net to gross, and boundary conditions then the pressure and fluid velocity are obtained from numerical solution of the pressure equation and application of Darcy's law. As a result they permit a flexible treatment of spatial heterogeneity, compressibility, and source and sink terms as a conventional finite-difference simulation.

- The streamlines are traced following the total fluid velocity of the field. This is illustrated in Figure 5.5 (a) for the heterogeneous five-spot pattern. The streamlines tend to cluster along the high permeability streaks, providing higher resolution along preferential flow paths.

- The particle travel time or the time of flight (T.O.F.) along the streamlines is computed. Figure 5.5 (b) shows contours of travel time or time of flight along streamlines. The time of flight contours correspond to tracer fronts in the reservoir. Clearly, the time of flight coordinate provides us with a quantitative form of flow visualization that is a very powerful aspect of streamline simulation.

- A 1D numerical technique is used to solve the transport equations (saturation and concentration) along the streamlines using the time of flight (T.O.F) as spatial, effectively decoupling heterogeneity effects and significantly simplifying the calculations. The result of this step is illustrated in Figure 5.5(c).

- The streamlines are updated periodically to account for mobility effects or changing well conditions. This is illustrated in Figure 5.5 (d) for a pattern conversion from a five-spot pattern to a nine-spot pattern. Once the streamlines are regenerated, the model recomputes the time of flight along the new streamlines, as shown in Figure 5.5 (e). Finally, a saturation calculation is resumed using the updated time of flight Figure 5.5 (f).

- Pressures, velocities, and streamlines are updated during the calculation. The simulations are not restricted to steady-state, but are instead large time-step IMPES (Implicit Pressure Explicit Saturation) calculations.

- At each pressure update, saturations are resampled from gridblocks to streamlines and vice versa, introducing potential mass balance errors, and to some extent, re-introducing numerical dispersion.

- Operator splitting is used to combine mechanisms and gravity is included routinely in the existing commercial streamline codes. Capillarity has been included within research codes.

- Note that every time streamlines are updated, we need a mechanism to map saturations from the old set of streamlines to the new streamlines. This mapping is a unique feature of streamline simulations and is not required in grid-based simulations. The mapping is also a potential source of error in streamline simulations.

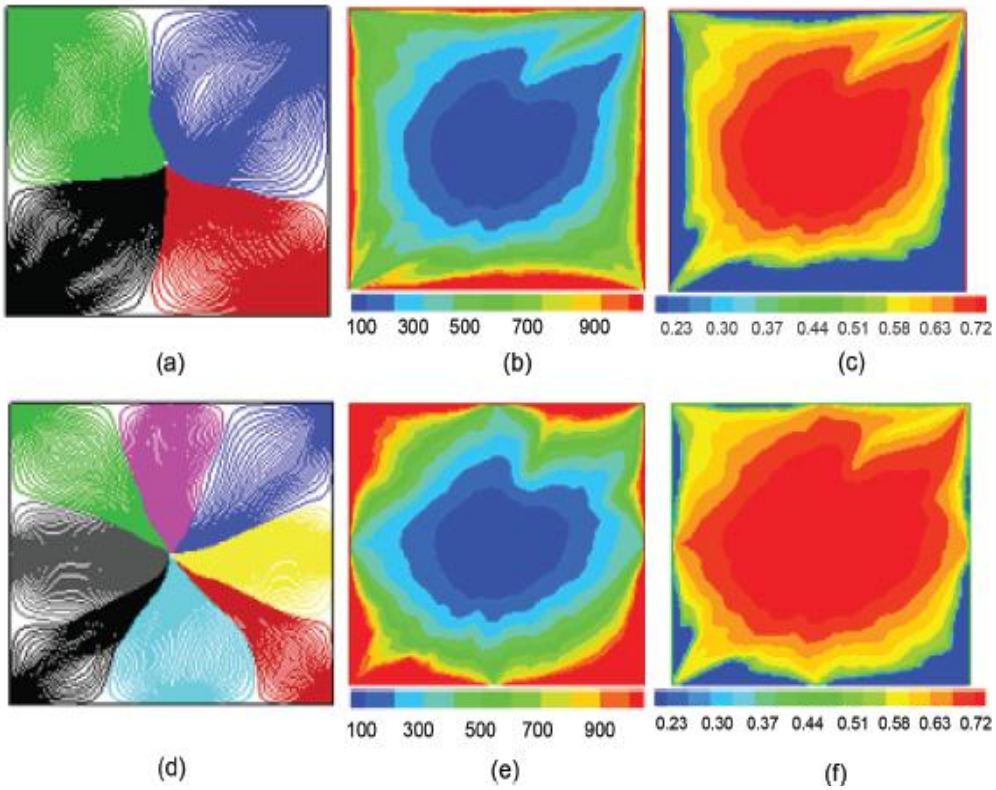

Figure 5.5: A step-wise illustration of streamline simulation: (a) Streamlines, (b) Time of flight, (c) Water saturation at 0.35 PVI, (d) Streamline updating after infill drilling, (e) Updated time of flight, (f) Water saturation at 0.45 PVI. (From Datta-Gupta, 2007)

Streamline-based simulation computation has made it extremely easy to represent longitudinal transport. It is less obvious how to represent gravity segregation, capillarity and diffusion, and unsteady-state velocity effects, all of which transverse the

streamlines. Transverse mechanism techniques exist, whereby the saturation solution is split into two steps: fluxes along streamlines and fluxes across streamlines. Transverse fluxes are more conveniently accounted for by a numerical solution on the grid at the end of the "pressure time step", the time interval at which pressures are recomputed and streams are regenerated. However, if necessary, the streamline time step may be split into several subsidiary time steps, depending on the requirements of the transverse mechanisms. All these steps are illustrated in the flow chart in Figure 5.6.

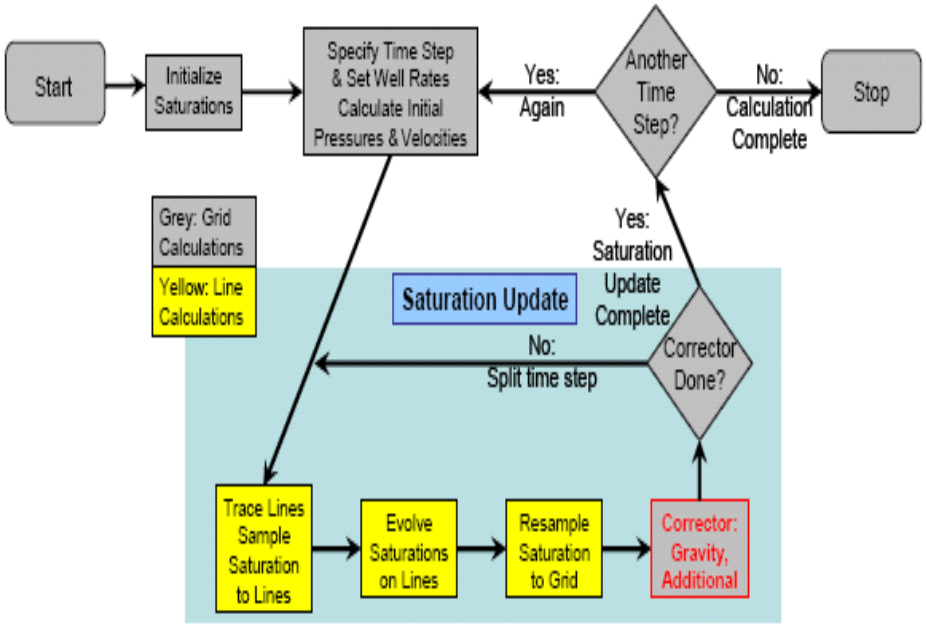

Figure 5.6: The flow chart illustrates steps in streamline simulation Yellow boxes represent calculations along streamlines, whereas the gray boxes represent calculation on the grid.

5.4 STREAMLINES SIMULATION EQUATION

Streamlines are the integrated curves that are locally tangential to the direction of the velocity. The streamline construction is sketched out in two dimensions in Figure 5.7. The components of the velocity vector ν are ν_x and ν_y, and in three dimensions ν_z. The local arc length dr has components dx, dy and dz. Following the sketch in Figure 5.7,

the slope of the streamline at any point is given by the ratio of the components of the velocity at a given instant of time, t_0:

$$\frac{dy}{dx} = \frac{v_y(x,y,z,t_o)}{v_x(x,y,z,t_o)} \quad . \quad \frac{dz}{dx} = \frac{v_z(x,y,z,t_o)}{v_x(x,y,z,t_o)} \qquad \text{(1)}$$

These difference equations may be integrated (analytical or numerically) from a point (x_0,y_0,z_0) to solve for y(x) and z(x), to determine the streamline that runs through this initial point. Alternatively, we can write these equations in the parametric form.

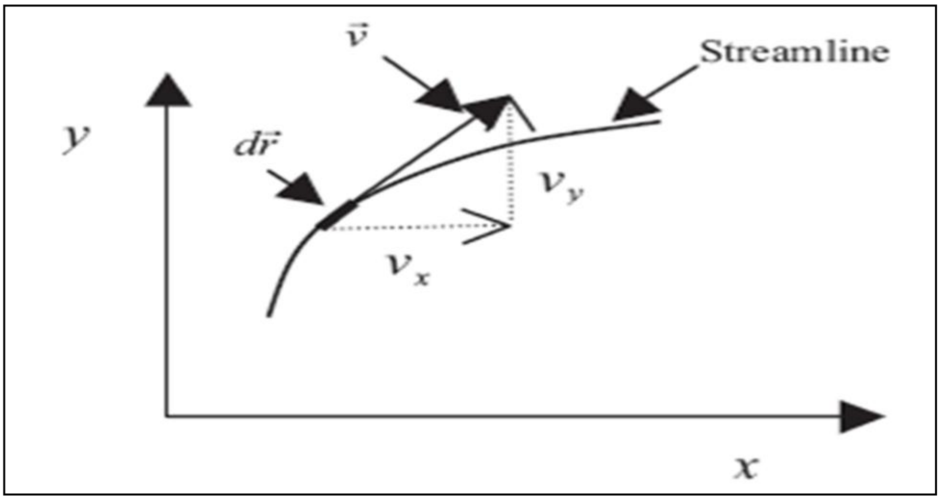

Figure 5.7: Relationship between streamline and velocity in planar flow.

$$dt = \frac{dx}{v_x(x,y,z,t_o)} = \frac{dy}{v_y(x,y,z,t_o)} = \frac{dz}{v_z(x,y,z,t_o)}, \qquad \text{(2)}$$

And determine x(t), y(t), and z(t).

The equation of a physical trajectory (pathline) is very similar, except that the velocity field may be time dependent.

$$dt = \frac{dx}{v_x(x,y,z,t)} = \frac{dy}{v_y(x,y,z,t)} = \frac{dz}{v_z(x,y,z,t)}, \qquad \text{(3)}$$

This difference reminds us that a streamline is defined as a line in space obtained by tracing the instantaneous velocity field. It is not the pathline, which is a physical particle trajectory. This distinction will become important when we examine unsteady-state flow.

A few points are worth emphasising here. We can define streamlines for any velocity. If the velocity in **Eq. (1)** is time-varying, then the streamlines will change with time. For unsteady-state conditions we use a snapshot of the velocity at a time of interest. We often approximate unsteady-state situations as a series of steady-state velocity fields. For defining streamlines, the permeable medium can be homogenous or heterogeneous, isotropic or anisotropic. The fluids can be compressible or incompressible.

There is a relationship between potential and the streamlines, as obtained below for single-phase Darcy's law:

$$\vec{u} = -\frac{1}{\mu}\vec{k}.\nabla\emptyset, \quad \text{..... (4)}$$

Where Ø denotes the fluid potential (the pressure). The streamlines are parallel to the velocity and thus, mathematically,

$d\vec{r} \times \vec{u} = 0$. For the case of isotropic porous media, where the permeability tensor is a scalar,

$$d\vec{r} \times \nabla\emptyset = 0, \quad \text{..... (5)}$$

Hence, the contours of the potential are orthogonal to the streamline for an isotropic medium. Velocity, streamlines, and potential contours for the ¼-five-spot are shown in Figure 5.8. The streamlines are parallel to fluid velocities and orthogonal to the isopotential lines.

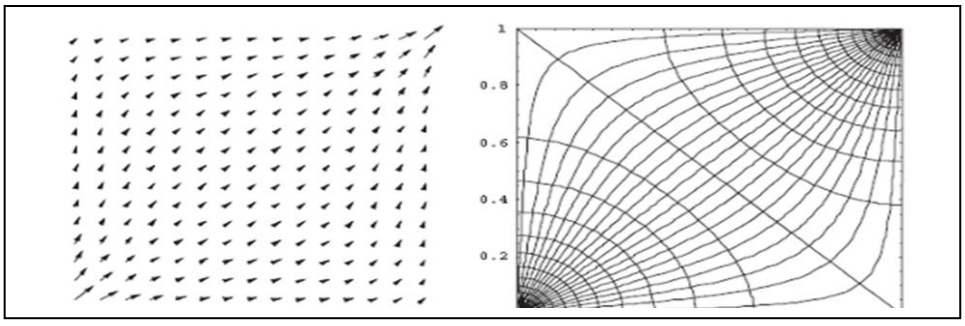

Figure 5.8: Velocity field (left) streamlines, and isopotential lines (right) in homogenous ¼-five-spot pattern for single-phase incompressible flow.

5.5 LINE SOURCE AND SINK SOLUTIONS

As a simple example of the construction of the streamlines, let us consider single-phase incompressible flow in an infinite homogeneous isotropic porous media, with multiple

injectors and producers. In deriving the solutions, the wells are treated as line sources (injectors) and sinks (producers). The pressure distribution can be obtained from a solution of the diffusivity equation and by applying the principle of superposition.

$$P(x,y) = P_m - \frac{\mu}{4\pi kh}\sum_{j=1}^{N_w} Q_i \ln((x-x_i)^2 + (y-y_i)^2) \text{ , } \ldots\ldots\ldots\ldots \text{ (6)}$$

Where P_m refers to the mean reservoir pressure and N_w is the total number of wells. Well j is located at position (x_i, y_i) with injection or production rate Q_i (with appropriate sign conversions, that is, negative for production and positive for injection). Note that in Equation. (6), we assume that the wellbore radius is small compared to the reservoir dimension and the wells are fully penetrating through the entire thickness of the reservoir, which is assumed to be constant. Fluid velocities can be obtained by simply taking the directional derivative of Eq.6 and applying Darcy's Law:

$$v_x = \frac{1}{2\pi h\emptyset}\sum_{j=1}^{N_w} Q_i \frac{x-x_i}{(x-x_j)^2+(y-y_j)^2} \ldots\ldots\ldots\ldots\ldots\ldots\ldots\ldots\ldots\ldots\ldots\ldots\ldots\ldots\ldots\ldots\ldots\ldots\ldots\ldots\ldots\ldots \text{ (7a)}$$

$$v_y = \frac{1}{2\pi h\emptyset}\sum_{j=1}^{N_w} Q_i \frac{y-y_i}{(x-x_j)^2+(y-y_j)^2} \ldots\ldots\ldots\ldots\ldots\ldots\ldots\ldots\ldots\ldots\ldots\ldots\ldots\ldots\ldots\ldots\ldots\ldots\ldots\ldots\ldots\ldots \text{ (7b)}$$

We can see that for incompressible flow, the absolute pressure level does not impact the fluid velocities. Only the difference in pressure matters. The pressure and velocity equations can be extended to anisotropic medium by a coordinate transformation

$$\bar{x} = \frac{x}{\sqrt{k_x}} \; and \; \bar{y} = \frac{y}{\sqrt{k_y}} \ldots\ldots\ldots\ldots\ldots\ldots\ldots\ldots\ldots\ldots\ldots\ldots\ldots\ldots\ldots\ldots\ldots\ldots\ldots\ldots\ldots\ldots\ldots\ldots \text{ (7c)}$$

and the resulting solution is given by (using commonly used field units: Psi, centipoises, millidarcies, feet, and stock-tank barrels per day)

$$P(x,y) = P_m - \frac{70.6\mu\beta}{h\sqrt{k_x k_y}}\sum_{j=1}^{N_w} Q_i \ln((x-x_i)^2 + \frac{k_x}{k_y}(y-y_i)^2) \quad \ldots\ldots\ldots \text{ (8a)}$$

$$v_x = \frac{0.8936\beta}{h\emptyset}\sqrt{\frac{k_x}{k_y}}\sum_{j=1}^{N_w} Q_i \frac{x-x_i}{(x-x_i)^2+\frac{k_x}{k_y}(y-y_i)^2} \ldots\ldots\ldots\ldots\ldots\ldots\ldots\ldots\ldots\ldots\ldots\ldots\ldots\ldots\ldots\ldots\ldots\ldots\ldots\ldots\ldots\ldots (8b)$$

$$\nu_y = \frac{0.8936\beta}{h\emptyset}\sqrt{\frac{k_x}{k_y}}\sum_{j=1}^{N_w} Q_i \frac{y-y_i}{(x-x_i)^2+\frac{k_x}{k_y}(y-y_i} \dots\dots\dots\dots\dots\dots\dots\dots\dots\dots\dots\dots\dots (8c)$$

Equations 8b and 8c describe velocity fields that can be used to define particle trajectories in an infinite domain. These equations are usually solved numerically. For example, the movement of the particle from its current position (x_i,y_i) to a new position (x_{i+1}, y_{i+1}) over a small time increment will be given by

$$x_{i+1} = x_i + (\nu_{xi})\Delta t \dots\dots\dots\dots\dots\dots\dots\dots\dots\dots\dots\dots\dots\dots\dots\dots\dots\dots \text{(9a)}$$

$$.y_{i+1} = y_i + (\nu_{yi})\Delta t \dots\dots\dots\dots\dots\dots\dots\dots\dots\dots\dots\dots\dots\dots\dots\dots\dots\dots \text{(9b)}$$

We can apply these equations repeatedly to trace the particle motion in the flow field. Because we assume steady-state conditions, the particle trajectory will define a streamline and a path line (they coincide). Some simple illustrations of these streamlines are shown in Figure 5.9. The streamline originate ate the injection well terminate at the producing well or open boundaries. In Figure 5.10(a), we start streamlines at the injection well and streamlines are traced up to a fixed time. This depicts the “fronts” or the contour of a fixed time of flight as discussed earlier. Although the line source and sink solutions have been derived for an infinite domain, the same solutions can be used to emulate impermeable boundaries through the application of image wells. As shown in Figure 5.10 (b), a mirror image of wells across a straight line will cause the line to act as no-flow boundary. The principle can be easley applied to generate in bounded domains.

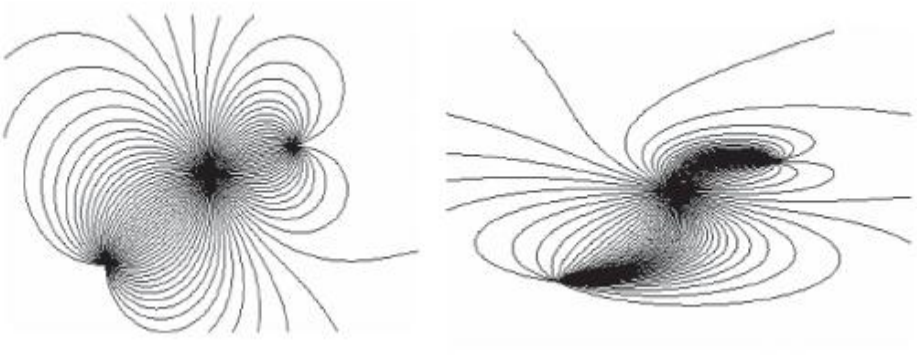

Figure 5.9: Streamlines for central injector and two producers for $K_y=K_x$ (left) and $K_y=0.01\ K_x$(right)

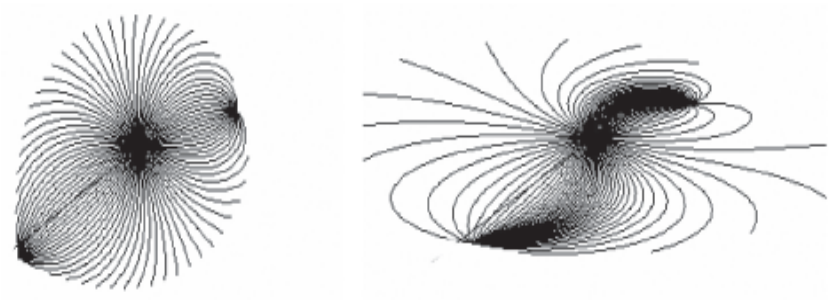

(a)

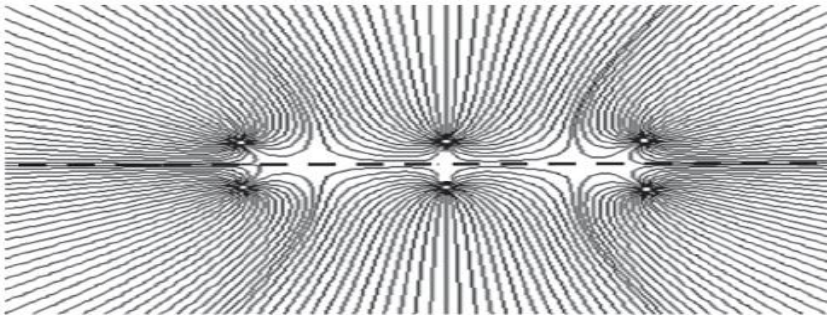

(b)

Figure 5.10: Streamline trajectories until time of flight=5,000 days, $K_y=K_x$ (left) and $K_y=0.1K_x$ (right) (a) and of imposing no-flow boundaries via image wells. Note that no flow occurs across the central horizontal line (b)

5.6 MODELLING GRAVITY IN STREAMLINE SIMULATION

In multiphase flow with gravity, we do not expect individual phase velocities to be aligned with the total velocity, as shown in Fig. 5.11(a). This leads to fluxes transverse to streamlines and results in phase segregation. Gravitational effects can be conveniently included during streamline simulation using the operator splitting techniques. This approach was first implemented in a streamline simulator by (Bratvedt et al., 1996). In the presence of gravity, the phase flux term is composed of two principal directions—the total Darcy velocity and the gravity vector. Thus, we are essentially faced with a 2D problem with streamlines defining one direction and gravity defining the other direction. Even in 3D flows, we are faced with the same 2D problem because the streamlines define a 1D coordinate system. We can solve the 2D problem using an approach analogous to dimensional splitting. The solution here involves a dimensional splitting on a non-orthogonal grid locally spanned by the streamlines and by the direction of gravity (The gravity lines) as shown in Fig. 5.11(b). To illustrate the steps, let us consider the water saturation equation with gravity as below

$$\phi \frac{\partial S_w}{\partial t} + \vec{u}_t \bullet \nabla F_w + \nabla \bullet \left(\Delta \rho g \frac{\lambda_{rw} \lambda_{ro}}{\lambda_{rt}} \vec{\vec{k}} \bullet \nabla D \right) = 0. \quad \text{..... (10)}$$

Where (u_t) is the total velocity, (F_W) is the fractional flow, (*g)* is the gravitational acceleration and (ρ) is the density of phase, (D) represents the Depth, and (k) is the absolute permeability tensor,

Transforming to the streamline time of flight coordinates (τ) we have

$$\frac{\partial S_w}{\partial t} + \frac{\partial F_w}{\partial \tau} + \frac{1}{\phi} \nabla \bullet \left(\Delta \rho g \frac{\lambda_{rw} \lambda_{ro}}{\lambda_{rt}} \vec{\vec{k}} \bullet \nabla D \right) = 0. \quad \text{..... (11)}$$

Where ϕ is the porosity of the formation, and λ_{rt} is the total phase mobility whereas

$\lambda_{rt} = \lambda_{rw} + \lambda_{ro}$

Using the operating splitting, we can reduce the equation (10) to a pair of 1D problems.

The convective component is aligned along the streamline Eq. (12) and the gravity component is aligned vertically, along the gravity lines.

$$\frac{\partial S_w}{\partial t_c} + \frac{\partial F_w}{\partial \tau} = 0. \quad . \quad \text{(12)}$$

$$\frac{\partial S_w}{\partial t_g} + \frac{1}{\phi}\frac{\mathrm{d}}{\mathrm{d}z}\left(\Delta\rho g k_z \frac{\lambda_{rw}\lambda_{ro}}{\lambda_{rt}}\right) = 0. \quad . \quad \text{(13)}$$

The vertical permeability, k_z enter in the expression for flux, also, we have assumed that z-coordinates is aligned with the direction of the gravity points down.

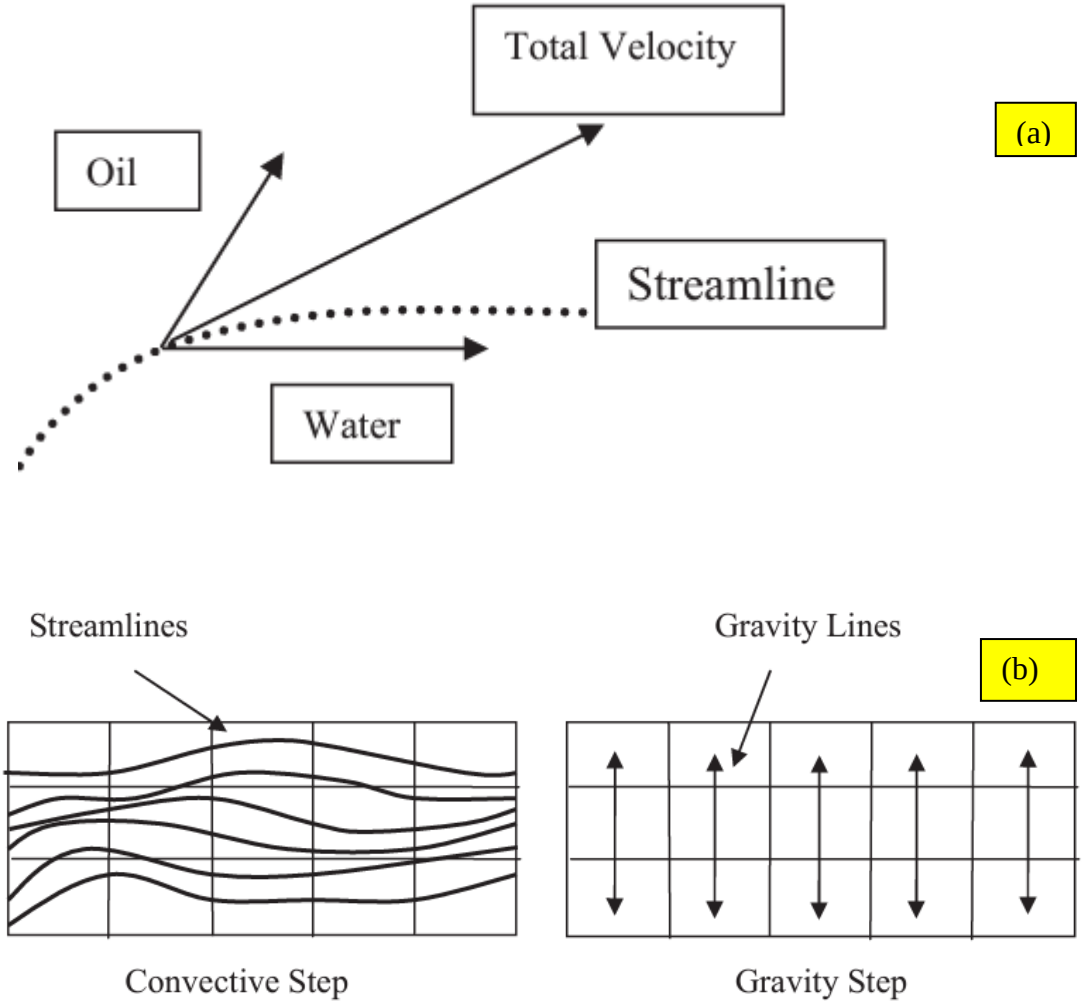

Figure 5.11: The figure show the gravity segregation along the streamline showing the different direction of water, oil and the total flux (a). And the convective streamlines and the vertical gravity lines provide the natural coordinate directions to represent flow with gravity (b).

We can solve the equation (11) using any of the 1D methods. Especially along the streamline we solve the following equation,

$$\frac{\partial S_w^*}{\partial t_c} + \frac{\partial F_w^*}{\partial \tau} = 0, \quad \text{..... (14)}$$

With initial condition $S^*_w(\tau, t_c=0)=Sw(x,y,z,0)$. This initial condition implies that the saturation along the streamline is assigned from the underlying grid. We use the solution of the equation (14), that is $S^*_w(\tau, t_c=\Delta t)$ as the initial data for the gravity step. The saturation is then updated by solving the following equation,

$$\frac{\partial S_w^{**}}{\partial t_g} + \frac{1}{\phi}\frac{\partial}{\partial z}\left(\frac{\Delta\rho\, g\, k_z \lambda_{rw}\lambda_{ro}}{\lambda_{rt}}\right) = 0. \quad \text{..... (15)}$$

Where k_z is the vertical permeability

The solution to solve the above equation, $S_w^{**}(x,y,z,tg=\Delta t)$ gives the approximate solution to equation (10) at time Δt (time step). The solution at any time $t=N\Delta t$ is constructed from a repeated application of the 1D operators. All of the issues associated with saturation mapping will arise in this iteration, and so there is a strong preference to minimize the number of time steps required to reach the final time (t). The selection of the splitting timestep $=\Delta t$ is crucial for the stability and convergence of the solution.

5.7 SCALE PRICIPATION MODEL IN FRONTSIM

We will start by describing the formation of the scale prediction model in FrontSim then evaluate the scale deposition model in two ways. First we will use small, simplified 1 and 2 dimensional models to assess the sensitivity of the scale deposition model to the controlling parameters in terms of the production of scaling ions and the position in which scale is formed. We will then apply the model to simulate a specific field, Field-X. We will then conclude by examining ways of improving and extending the model. However, we will apply the data for this field case in Chapter 6.

5.8 FORMULATION

The modelling of the movement of the barium and sulphate ions is relatively straight forward in that it can be handled by the existing tracer tracking code. The focus of the work is therefore introducing a method of making two tracers interact, one representing the barium ions and one representing the sulphate ions. This method depends on adopting a simpler approach which is to add an additional interaction step at the end of each time step. This is limited in one respect, if the time step is too long it is possible for the zone where scale is being deposited to step over cells so that you get some cells with no scale while their neighbours have more scale than they should have. Provided that the time steps are kept sufficiently short this should only be a minor problem.

5.9 INTERACTIONS

The main problem in the scale modelling is the updating of ion concentrations and the amount of scale deposited in a cell at the end of each time step. The following section will explain two approaches to solving this problem by the concentration of Ba^{2+} and SO_4^{2-} in mg/l at surface conditions in both metric and field unit systems. We divide these by the average molecular weight of the ions to get the tracer concentration in mmol/l at surface conditions. At the end of the process we convert the scale concentration back to kg/rm^3 of pore volume by multiplying the formation volume factor by 10^{-3} * and the molecular weight of $BaSO_4$. If field units are being used this is then converted to lbs/ft^3 before it is output.

5.9.1 Method 1

The simplest method is to say that scale deposition is instantaneous:- we use an equilibrium approach .This is the method that has been used throughout this thesis since

in this work we have not considered the impact of scale damage at production wells, and deep within the reservoir, as already discussed, the reaction rate is not important because the fluid advection rate is slow. Furthermore, reaction rate data was not available for this project. In future work reaction rate effects should be considered, and so Method 2 (see below) will be required.

The basic reaction is:

$$Ba^{2+}(aq) + SO_4^{2-}(aq) = BaSO_4(s)$$

i.e. Ba^{2+} in solution reacts with SO_4^{2-} in solution to produce the solid $BaSO_4$. (We note that the barium could equally well be replaced by calcium or strontium.) In this method we assume at the end of each time-step either all the barium ions or all sulphate ions will be used up in forming scale so if we have N mmol/l of Ba^{2+} and M mmol/l of SO_4^{2-} then if

M>N we have

$$N[Ba^{2+}] + M[SO_4^{2-}] = N[BaSO_4] + (M-N)[SO_4^{2-}]$$

and if N>M

$$N[Ba^{2+}] + M[SO_4^{2-}] = M[BaSO_4] + (N-M)[Ba^{2+}]$$

The residual concentration of the ions still in the solution can of course continue to be transported in the water.

5.9.2 Method 2

This method introduces the concept of a reaction rate. Simply put the modification says that the fraction of the maximum scale that can be formed during a time step is a function of the length of the time step. So that the equations in method 1 become modified as follows

If M>N we have

$$N[Ba^{2+}] + M[SO_4^{2-}] = N(F(dt))[BaSO_4] + (M-N*F(dt))[SO_4^{2-}]$$

$$+(1-F(dt))* [Ba^{2+}]$$

and if N>M

$$N [Ba^{2+}] + M [SO_4^{2-}] = M (F(dt)) [BaSO_4] + (N-M*F(dt)) [Ba^{2+}]$$
$$+ (1-F(dt))* [SO_4^{2-}]$$

Where F(dt) is a function of dt (the time-step length) which varies between 0 and 1.

Two versions of the function F(dt) have been implemented

Version 1

Is a linear function

$F(dt) = dt/T_{scale}$ $dt < T_{scale}$

$= 1$ $dt > T_{scale}$

Version 2

Is an exponential function

$F(dt) = 1-exp(-dt/T_{scale})$

Where T_{scale} is the time to reach equilibrium in the scale formation process.

In practice there is very little difference between the two functions unless $dt >> T_{scale}$.

We can further refine the method by making T_{scale} a function of an assortment of parameters. In this work we have only looked at the effect of making T_{scale} a function of the tracer concentration. However we could make it a function of position, fluid velocity or reservoir temperature. These dependencies are simply input as a table that defines a multiplier to the input value of T_{scale}.

5.10 ADVECTION OF IONS

The modelling of the advective flow of the barium and sulphate ions is handled using the normal tracer tracking option in FrontSim. A full description can be found in the FrontSim Technical Description manual, (FrontSim, 2009). One water tracer is used to

track the barium concentration and a second to track the sulphate concentration. A third tracer is used to hold the $BaSO_4$ concentration. This third tracer does not, however, move with either phase. It simply accumulates further deposits of scale.

5.11 INPUT AND OUTPUT

The ion concentrations are input in g/l. The scale is calculated internally as g/Ml million but is converted to Kg/m3 or lbs/ft3 depending on the unit system in the model. The volumes are ft3 or m3 of pore volume. The ion concentrations are written out at each timestep to the restart files along with the scale concentration. Furthermore, the concentrations of the ions for each well are written out in the summary files and can be displayed in the normal way using the standard ECLIPSE pre and post processor.

5.12 INTERACTION CODE

As mentioned before work has been performed to model the scale deposition deep within the reservoir, however using both streamline and finite difference simulation. It has not, however, been possible to model the interaction between ions in streamline simulators.

The following code has been introduced in the PROPS section in the data file with the following format.

FSSCALE - PROPS SECTION

FSSCALE

BA SO_4 137.4 96 'LINEAR' 1.0 1.0 1.0 /

Item 1 *is the name of the first tracer interacting to give scale*

Item 2 *is the name of the second tracer interacting to produce scale*

Item 3 *is the molecular weight of the first tracer*

Item 4 *is the molecular weight of the second tracer*

Item 5 *defines whether the time dependent behavior is linear or exponential - Default - Linear*

Item 6 *defines the interaction time scale. 0 will indicate that the scale forms instantaneously - Default - 0*

Item 7 *Maximum concentration used to scale values in TSVCxxx for tracer 1 -Default - 1.0*

Item 8 *Maximum concentration used to scale values in TSVCxxx for tracer 2 - Default - 1.0*

TSVCxxx - PROPS SECTION

This code defines a table which allows a multiplier to the scale deposition rate to be defined as a function of the tracer concentration.

TSVCxxx

0 1

1 1 /

Item 1 is the tracer concentration as a fraction of Item 5 or 6 in FSSCALE

Item 2 is the multiplier to be applied to the time scale for scale formation This allows the rate of deposition to be dependent on the concentration of the scaling ion

N:B below is an example of the data file that show how we can fit these key words in props section of the data file.

Other Important Keywords for FrontSim

TUNEFSPR

This keyword sets the tuning options for the pressure solver. The keyword should be followed by the data items described below, terminated with a slash. Default values can be specified before the slash by a null repeat count of the form n*, where n is the number of consecutive items to be defaulted. This keyword is located in schedule section in the data file Refer data file in Appendix (c). For more detail refer to FrontSim manual. In our calculations the default of the frequency of the pressure calculations is every timestep of the simulation (i.e. frequency of pressure recalculations = 1). This is the recommended value for scenarios where gravity segregation is possible. All other values of this keyword are defaulted, except for the maximum material balance error, which is reduced from the default value of 0.02 to 0.01.

TUNEFSSA

This keyword sets the tuning options for the saturation solver. The keyword should be followed by the data items described below, terminated with a slash. Default values can be specified before the slash by a null repeat count of the form n*, where n is the number of consecutive items to be defaulted. This keyword is located in schedule section in the data file Refer data file in Appendix (c). For more details refer to FrontSim manual. The most important number in this keyword is whether or not gravity segregation is included, which in all our 3D modelling it is. The supplied data file for Field X (Chapter 6) used a streamline density of 0.5 (see Appendix C).

5.13 TEST MODELS

A series of one-dimensional, two-dimensional (areal and vertical) and three-dimensional calculations have been run. Sensitivity runs to test the impact of formation water and injection water compositions have been performed. However, in this project we present results for a single formation water composition, with a Ba concentration of 80 mg/l (which when mixed with full sulphate seawater would give a moderate scaling risk) and a base case injection water concentration of SO_4 of 40 mg/l – which corresponds to typical concentration of SO_4 that might be expected from a sulphate reduction plant. This is compared with the results of injecting full sulphate seawater (in which the SO_4^{2-} concentration is 2800 mg/l)

5.12.1 One Dimensional Models

This test model is a 1 dimensional system consisting of 100 cells. It has a connate water saturation of 0.25 with a Ba^{2+} concentration of 80mg/l. The injected water concentration of SO_4 is 40 mg/l. The permeability and porosity are uniform (100 mD and 20% respectively) throughout the model.

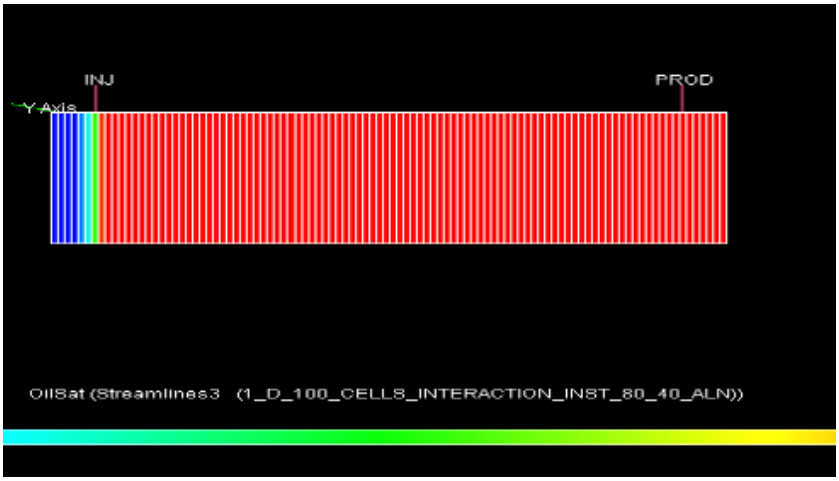

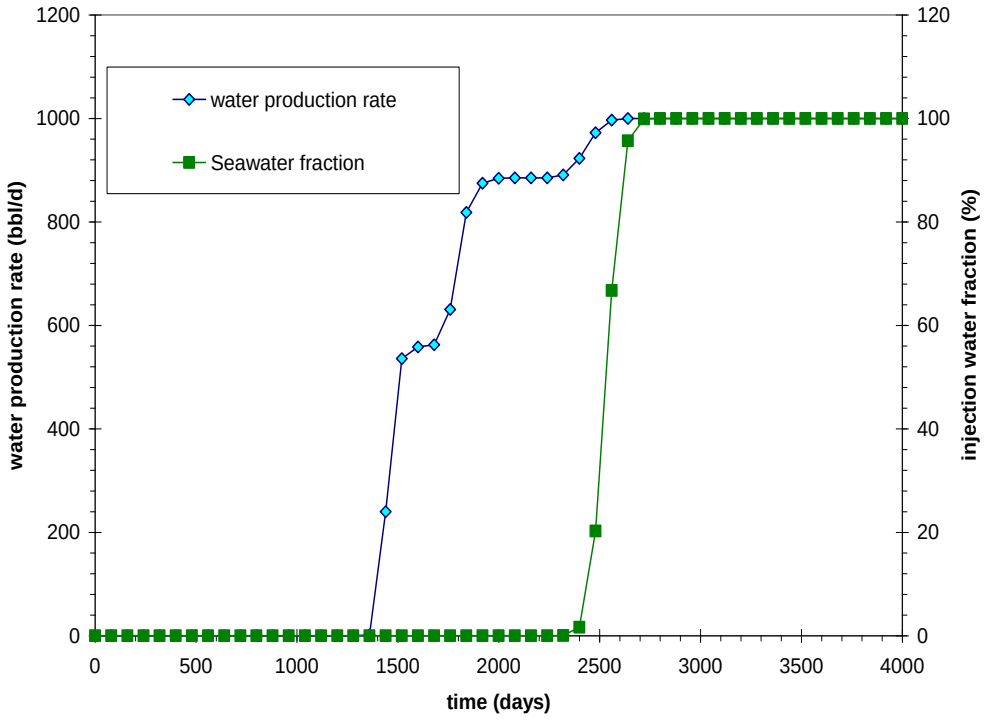

Figure 5.12: Water production rate & percentage of the injected water produced as a function of time.

Figure 5.12 illustrates the water production rate versus the fraction of the injected water produced. As shown in the plot, the sea water starts to breakthrough at the producer after 2300 days whereas the water production breakthrough starts at 1300 days as you can see the formation water breaks through first because the injected seawater not only displaces oil, but also displaces any formation water ahead of it. This formation water

will form a bank of water, which will break through first, as shown here. If inter well distances are large, or the injection water displaces through the aquifer, then the volume of formation water produced before injection water breakthrough can be large.

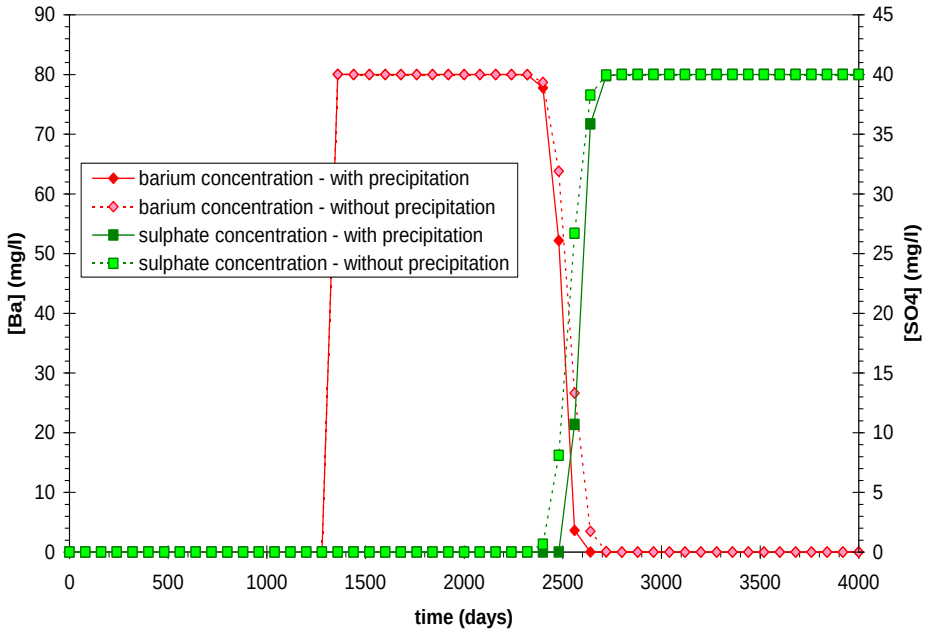

Figure 5.13: Barium and sulphate production with instantaneous precipitation and without precipitation as a function of time for the 1D model.

Figure 5.13 plots the concentration of Ba^{+2} and So_4^{2-} ions versus time with two cases. The first case considers instantaneous precipitation; the second case considers no precipitation of barium sulphate

In the case of no precipitation the concentration of Ba^{+2} is produced in formation water with the maximum concentration of 80 mg/l for up to 2300 days, then the breakthrough occurs and its concentration tends to decrease down to zero mg/l when we produce 100% sea water (see figure 5.13). Furthermore, the concentrations of SO_4^{-2} start to increase after 2300 days (breakthrough time) up to its maximum concentration of 40 mg/l.

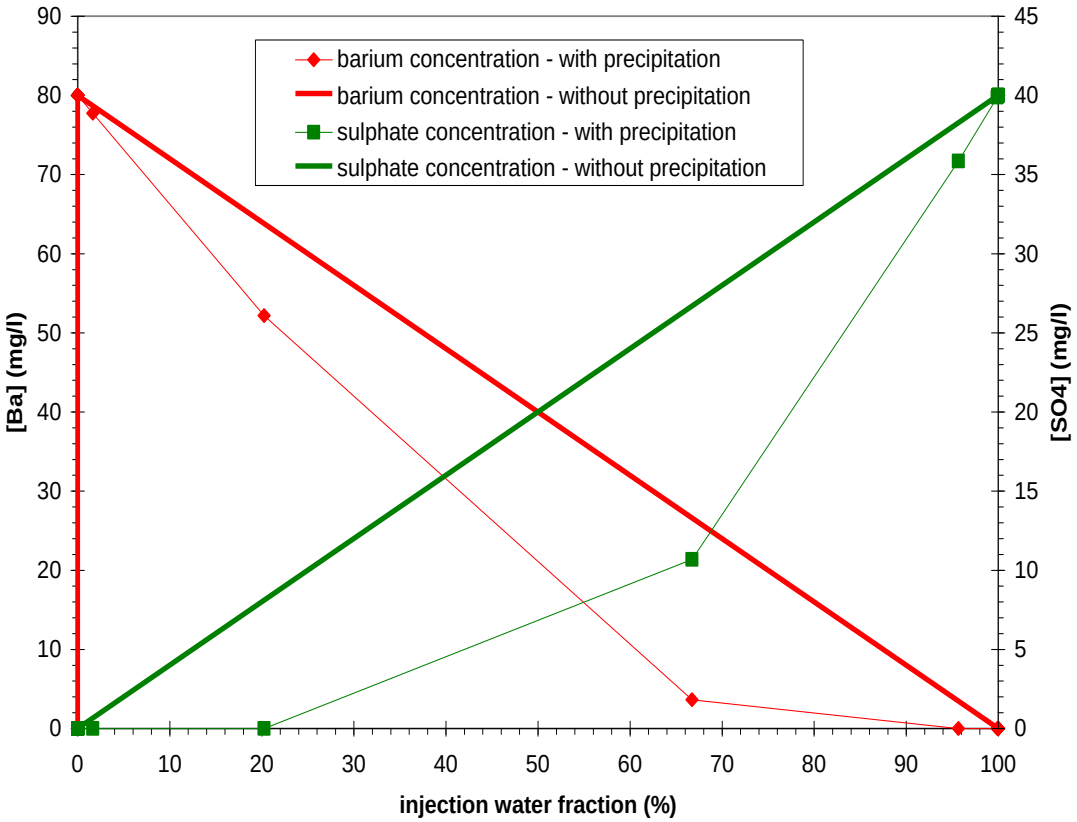

Figure 5.14: The produced barium and sulphate ion concentration as a functions of the produced fraction of sea water.

In case of instantaneous precipitation the concentration of Ba^{2+} reaches zero earlier than the first case. Furthermore, the concentration of SO_4^{2-} starts to increase later than the first case; this is due to the consumption of its ions of Ba^{+2} and SO_4^{-2} to form barium sulphate. This can be clarified in Figure 5.14; the concentration of produced ions in the case of precipitation tends to be lower than in the case of with no precipitation.

5.12.2 Two-dimensional Heterogeneous Model (areal)

This test model is a two-dimensional model consisting of 20x20x1cells. The model has randomly varying permeability values. It has a connate water saturation of 0.25 with a Ba^{2+} concentration of 80 mg/l. The injected water concentration of SO_4^{2-} is 40 mg/l. The results of this model show a more gradual increase in seawater fraction after water breakthrough takes place, as shown in Figure 5.15.

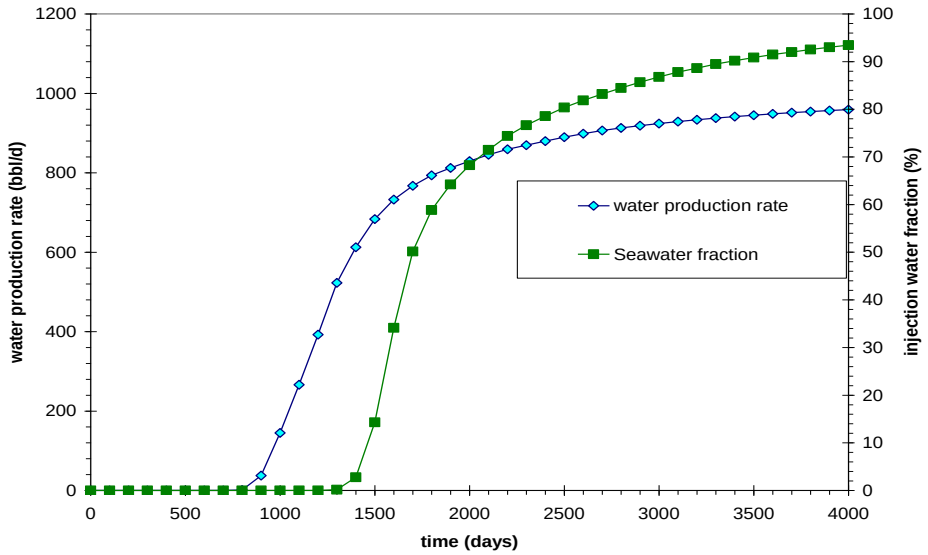

Figure 5.15: Water production rate and seawater fraction for two-dimensional (areal) displacement, showing a more gradual increase in seawater fraction after water breakthrough takes place.

As clarified in Figure 5.16 a significant amount of precipitation may be observed around the producer. Furthermore, by analyzing Figure 5.17 it may be seen that there is a longer time period of co-production of Ba^{2+} and SO_4^{2-} at the production well in this two-dimensional areal displacement model, indicating a greater degree of mixing. This is reflected in the fact that we can now observe that there is a bigger difference between the predicted concentrations with and without in situ precipitation, meaning that precipitation in the reservoir now accounts for a greater degree of ion depletion in the reservoir, and hence the concentrations at the producer are lower than would be observed if there were no in situ precipitation.

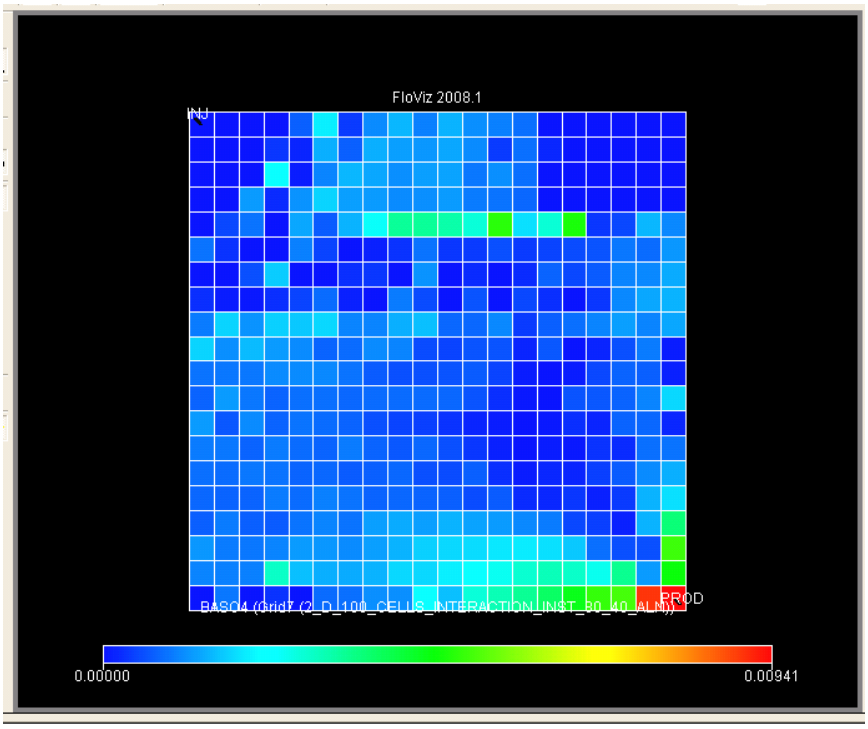

Figure 5.16: $BaSO_4$ distribution in a two-dimensional (areal) model. The injector is at the top left and producer at the bottom right of this quarter-five spot pattern. Note the greatest amount of precipitation is around the producer.

(a)

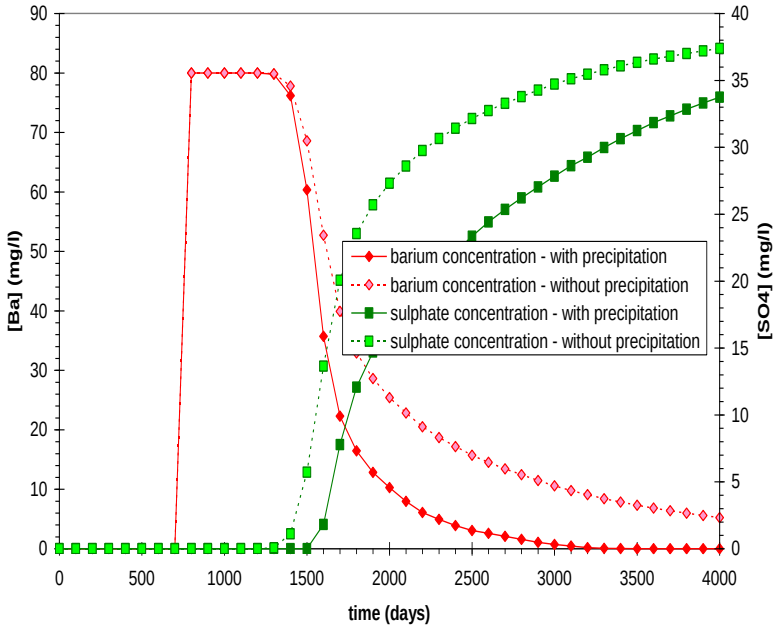

(b)

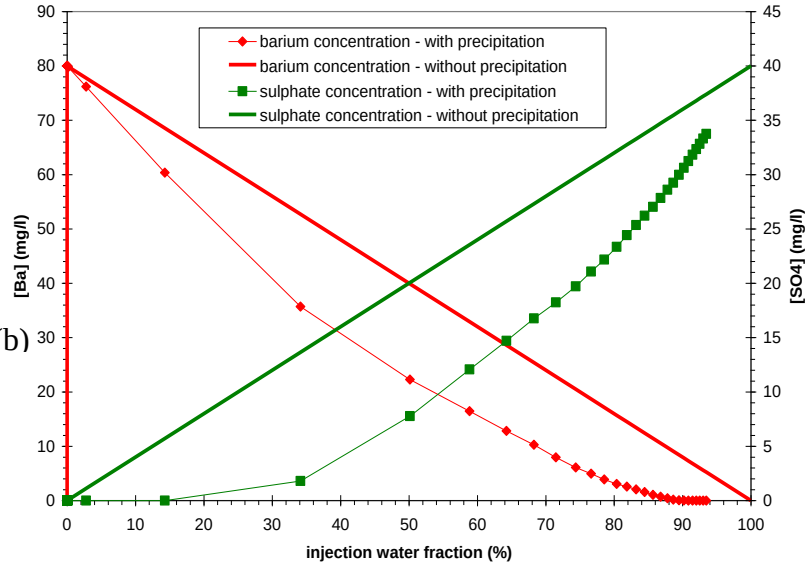

Figure 5.17: Barium and sulphate concentrations at the production well vs. (a) time and (b) % injection water fraction for a two-dimensional areal displacement. Note that there is now a bigger difference between the predicted concentrations with and without in situ precipitation, meaning that precipitation in the reservoir now accounts for a greater degree of ion depletion in the reservoir, and hence the concentrations at the producer are lower than would be observed if there were no in situ precipitation.

5.12.3 Two-dimensional Modelling (vertical)

This test model is a two-dimensional model consisting of 20x1x10 cells; again, the model has randomly varying permeability values, this time constrained by layers. The greatest amount of scale deposition tends to occur in the parts of the reservoir where there is a high volume throughput of mixing brines (such as can occur around production wells), or, as here, near the oil water contact, where due to the presence of an aquifer there is a large amount of mobile formation water (brine at water saturation = 1 and containing barium ions), and where injected water with a large amount of sulphate ions comes into contacts and mixes. See Figure 5.18

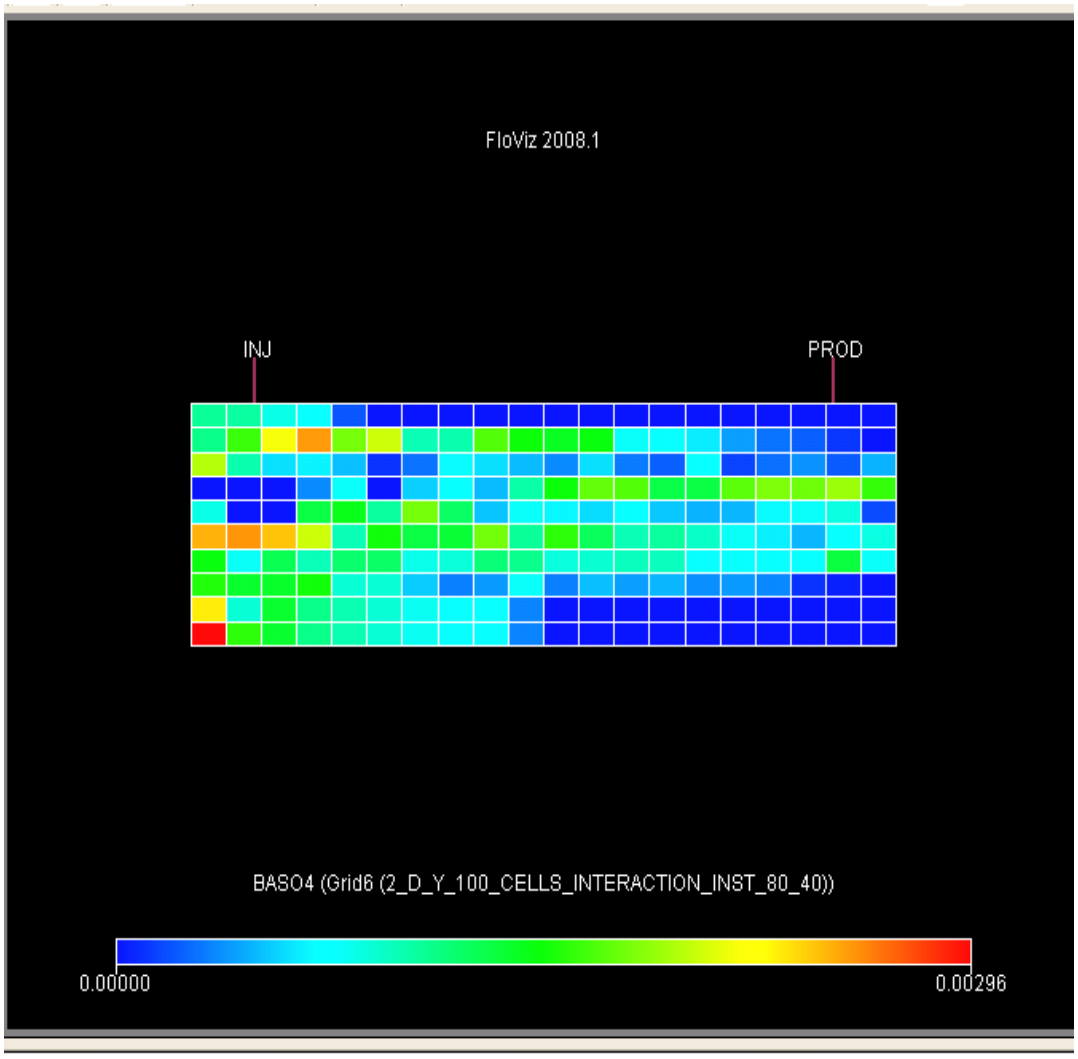

Figure 5.18: $BaSO_4$ distribution in a two-dimensional (vertical) model. The vertical injector is on the left and the vertical producer is on the right of this model. Note precipitation distributed throughout model.

As in the other cases, it has a connate water saturation of 0.25 with a Ba^{2+} concentration of 80 mg/l. The injected water concentration of SO_4^{2-} is 40 mg/l. As shown in Figure 5.19**,** this model has steeper increase in seawater fraction after water breakthrough takes place than the 2-D areal model. Furthermore, in Figure 5.20, we observe that there is a smaller difference between the predicted concentrations with and without in situ precipitation, meaning that there is less precipitation in the reservoir than in the 2D areal system. The impact of this is that there is a greater amount of mixing in the well itself due to brines in different layers breaking through at different times.

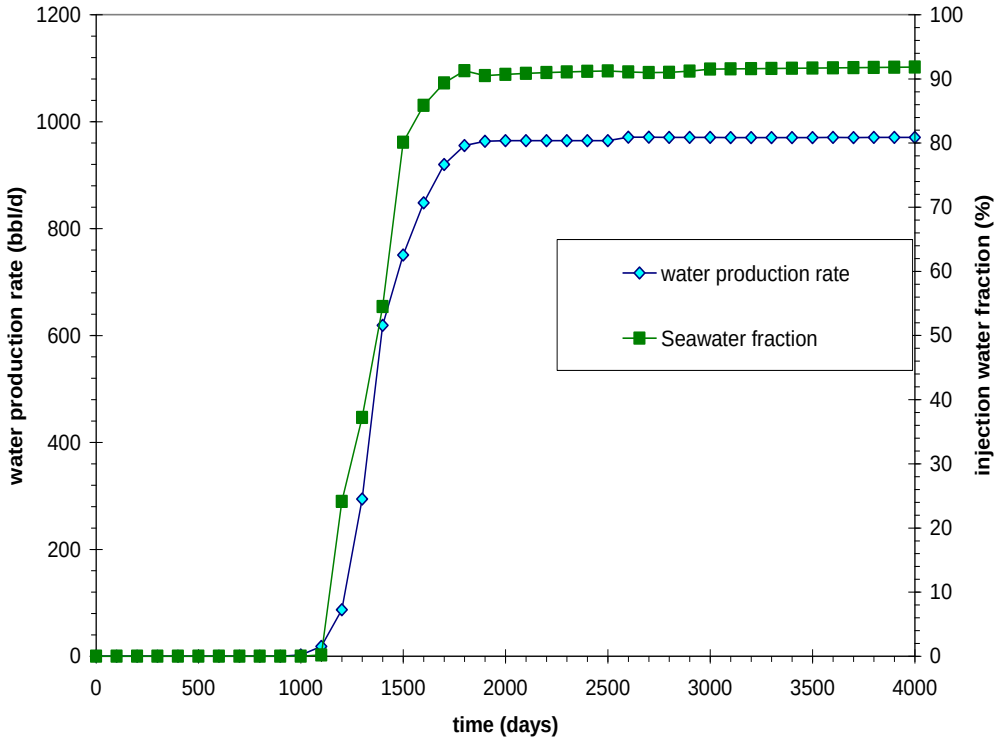

Figure 5.19: Water production rate and seawater fraction for two-dimensional (vertical) displacement, showing steeper increase in seawater fraction after water breakthrough takes place than in the 2D areal model.

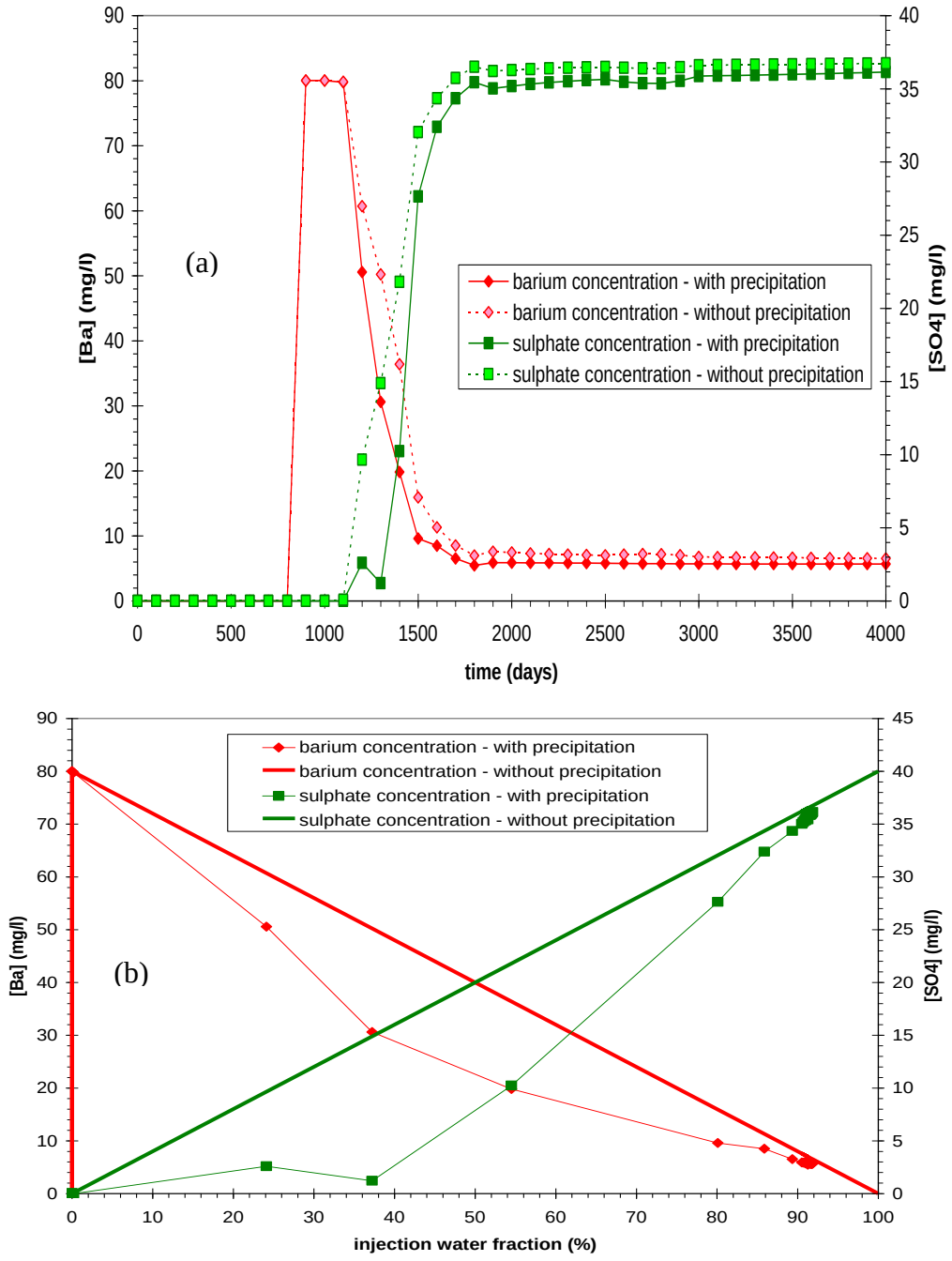

Figure 5.20: Barium and sulphate concentrations at the production well vs. (a) time and (b) % injection water fraction for a two-dimensional vertical displacement. Note that there is a smaller difference between the predicted concentrations with and without in situ precipitation, meaning that there is less precipitation in the reservoir than in the 2D areal system.

5.12.4 Three-dimensional Modelling

This test model is a three-dimensional model consisting of a 20x20x10 cells in a quarter 5 spot pattern. The model has a connate water saturation of 0.25. Various sensitivities have been run to test the impact of injected SO_4^{2-} concentration (40, 80 and 2800 mg/l), but the concentration of Ba^{2+} is kept constant at 80 mg/l. The results of the 40mg/l and 2800 mg/l runs are shown in Figures 5.21 to 5.24. We observed a smaller difference between the predicted concentrations with and without in situ precipitation than that occurring with finite difference models (Mackay, 2003a; Mackay, 2003b, Mackay et al., 2003). This is because streamline simulation introduces less dispersion effects than the finite difference models used previously. In the 2800 mg/l case (corresponding to injection of full sulphate seawater), there is now an abundance of SO_4^{2-} ions, so proportionally more Ba^{2+} ions have been stripped by the reaction (there is more SO_4^{2-} available to react with Ba^{2+} ions). Furthermore, note that the relative loss of SO_4^{2-} ions is now negligible, almost the same with and without precipitation.

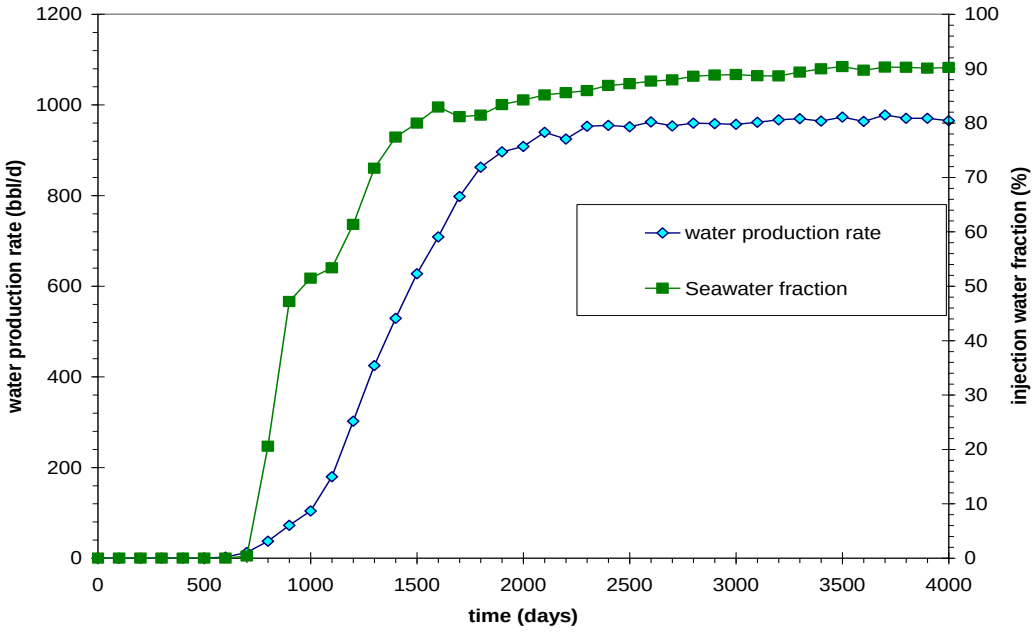

Figure 5.21: Water production rate and seawater fraction for three-dimensional displacement.

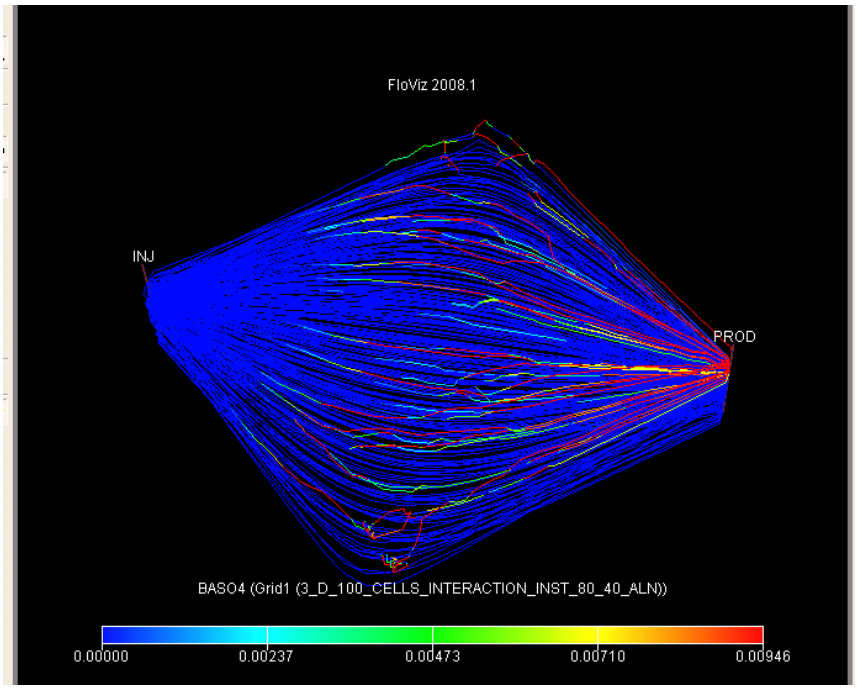

Figure 5.22: Streamline distribution in a three-dimensional model. The vertical injector is on the left and vertical producer is on the right of this quarter-five spot pattern.

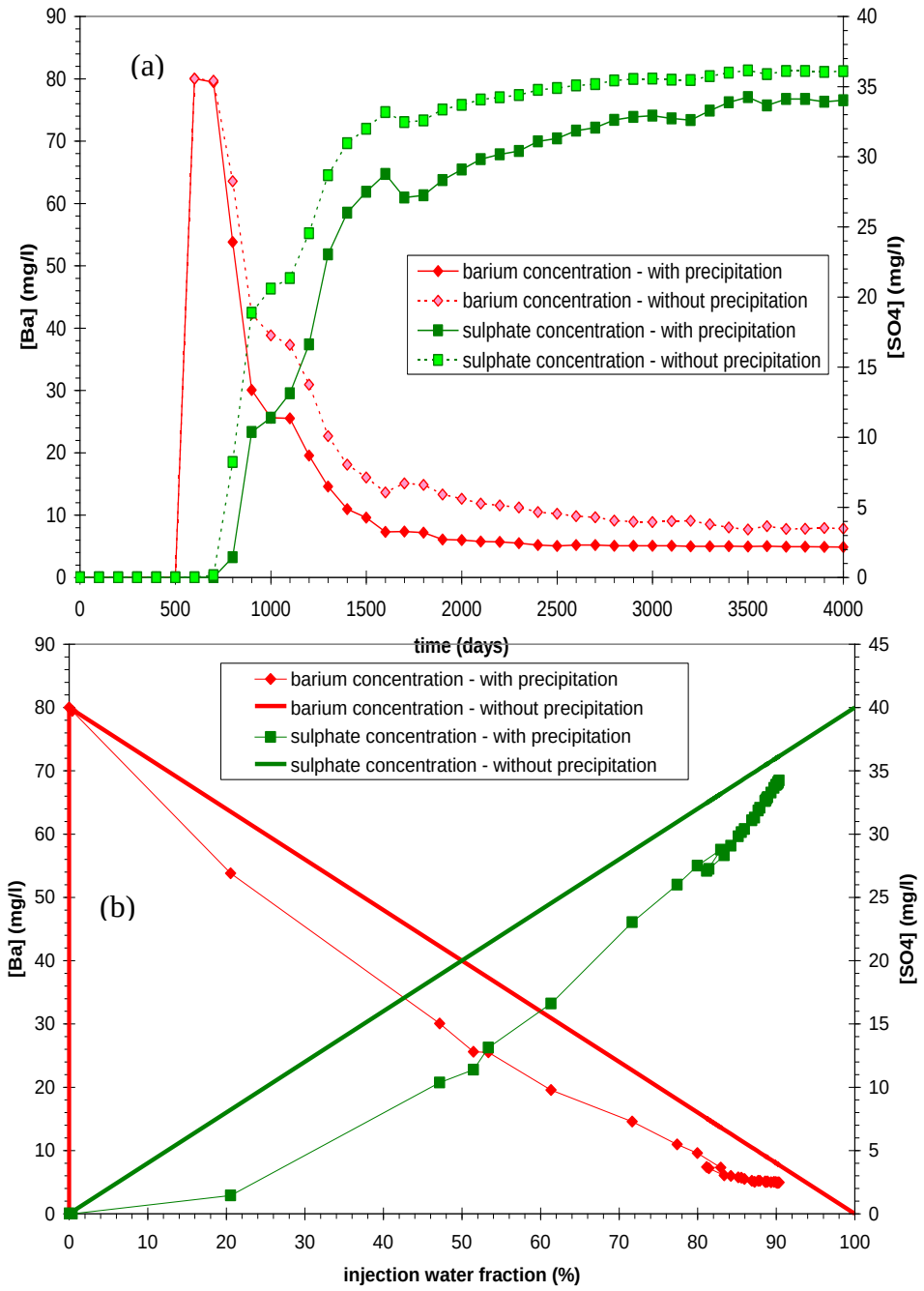

Figure 5.23: Barium and sulphate concentrations at the production well vs. (a) time and (b) % injection water fraction for a three-dimensional displacement for the 40 mg/l SO_4 injection case. Note that there is a smaller difference between the predicted concentrations with and without in situ precipitation than occurs with finite difference models.

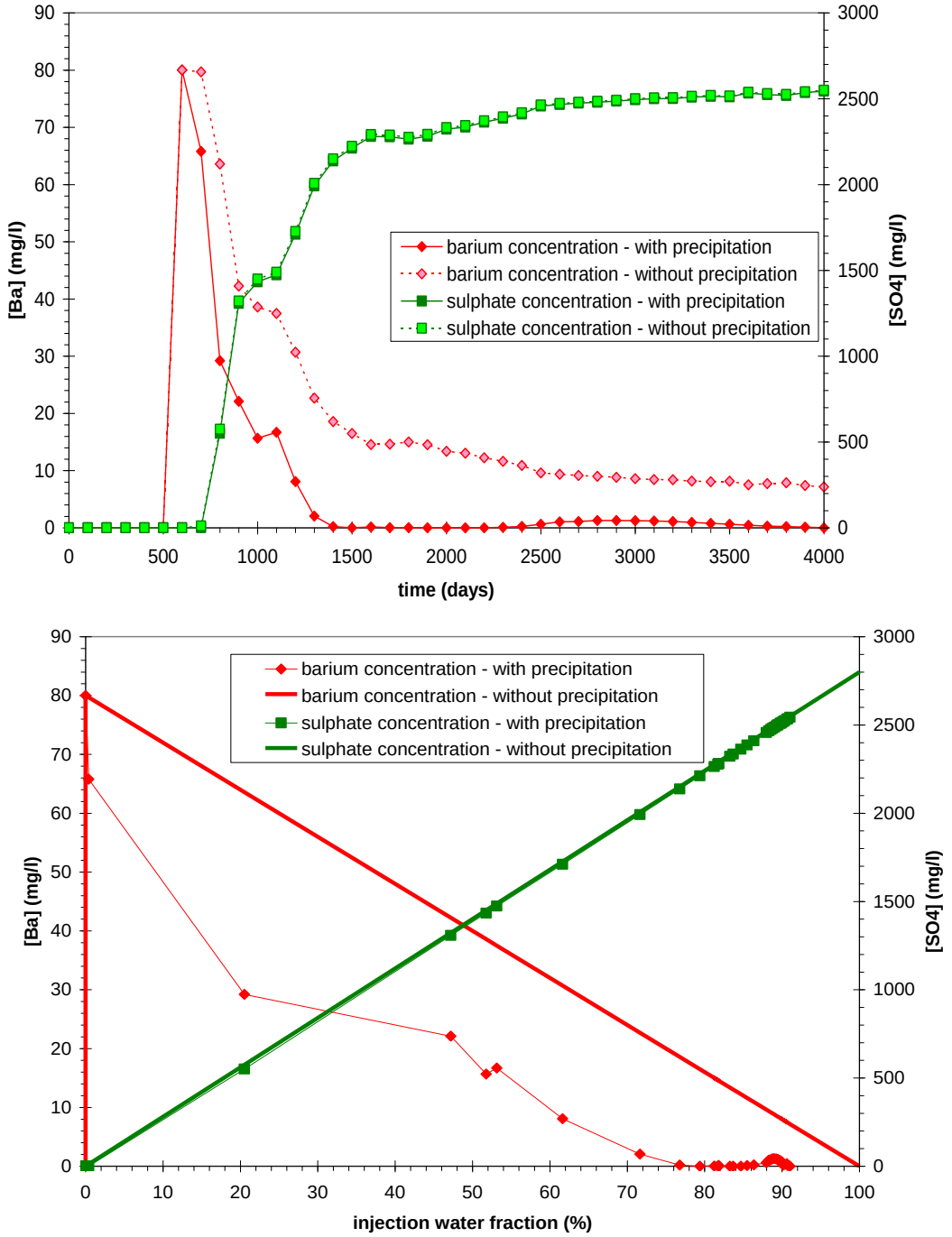

Figure 5.24: Barium and sulphate concentrations at the production well vs. (a) time and (b) % injection water fraction for a three-dimensional displacement, with injection sulphate concentration increased from 40 mg/l (previous cases) to 2800 mg/l (corresponding to injection of full sulphate seawater). Note that there is now an abundance of sulphate ions, so proportionally more barium ions are stripped by the reaction (there is more sulphate available to react with barium ions). Furthermore, note that the relative loss of sulphate ions is now negligible, comparing with and without precipitation.

5.14 IMPACT OF CONVERGING STREAMLINES NEAR A PRODUCTION WELL

Mixing takes place when concentrations are mapped from the streamlines back on to the grid blocks (in the same way that saturation is mapped back from the streamlines onto the grid blocks). Thus, mixing will take place in any grid block through which more than one streamline passes and where one streamline still has formation water, and another has injection water, or in a grid block with only one streamline, but where the injection water front is passing through that grid block. This means that the amount of deposition that would occur near the production well will depend on how frequently the concentrations are mapped back onto the grid blocks, and therefore how frequently the mixing and deposition calculations are performed, which in turn is a function of the frequency with which the global time steps are updated. The advantage of streamline simulation for reducing numerical dispersion is that as well as reducing numerical dispersion in terms of phases (say when water is displacing oil), it also reduced numerical dispersion when one component is displacing another (say seawater is displacing formation water). However, the mixing calculations are performed when the component concentrations in each grid block are calculated from the streamline information, and so these calculations are still susceptible to the impact of grid resolution. Thus the errors in calculating component transport inherent in finite difference modelling are overcome by streamline simulation, but there is still some numerical dispersion introduced when component concentrations are mapped back on to the grid blocks, and the mixing calculations are performed.

As streamlines approach a production well, the density of the streamlines increases, i.e. in any one grid block there will be a greater number of streamlines, and hence the amount of mixing increases (i.e. more streamlines, with potentially different water compositions, results in more mixing). This outcome fairly represents what occurs in nature, where the amount of mixing increases the closer to the wellbore, although this is somewhat dependent on the amount of precipitation and ion stripping that has already taken place further from the well.

In the calculations performed in this work, it is assumed that squeeze treatments are carried out to prevent deposition in the near production well zones, and since this is the zone where most permeability impairment would occur, the calculations performed in this work take into account precipitation and ion stripping or depletion wherever this occurs, but do not consider loss of permeability or well productivity. However, future work could consider the impact of not performing squeeze treatments, and therefore the impact of the calculated deposition near the producers on permeability and well productivity. A sensitivity analysis to the impact of frequency of global timestep updates would be required. In addition, a fine scale grid would be advisable around the production wells.

5.15 EFFECT OF IN-SITU PRECIPITATION ON POROSITY, PERMEABILITY AND ULTIMATELY FLOW PATTERN /SWEEP EFFICIENCY

If the calculations were performed to evaluate the damage occurring around one production well, it is to be expected that once injection water breaks through to one production well, the waterflood advance to this and towards other production wells would be altered. In future work, the extent to which the flood front would be altered could be studied in detail, and an assessment of the extent to which this would impair ultimate recovery (or not, given that the greatest impairment will occur in wells already cutting water). Time step sizes would need to be reduced at the time of injection water break through to, study this effect.

The simulator at this time cannot allow for modelling the impact of scale damage, and further development to the simulator is required. The simulator does calculate the scaling reaction, and the impact on the water composition, and the amount of precipitate formed. Further coding would be required to convert this mass of precipitate in any given grid block into a volume of precipitate, since the density of the mineral barium sulphate is known. From this, the change in porosity could readily be calculated. A change in permeability, however, would probably require the results of experimental tests, since the reduction in permeability would not just

depend on the amount of scale deposited, but on the rock type also. Alternatively, a reduction in well productivity (or an increase in skin) could be calculated, but this would require some knowledge of the extent to which the PI was reduced by a certain amount of scale, which could probably only be identified from history matching analysis. None of these features is currently available in the code, so their impact cannot be demonstrated at this time. However, recommendations will be made to the software to developer to improve the code in this regard.

5.16 REACTION KINETICS

At the injector, the temperature will be lower, and therefore it is to be expected that that the reaction kinetics would be lower than at the production well, or deep within the reservoir, where temperatures will be higher. The rate of deposition is a function of the chemical reaction rate and the volume throughput (the latter is calculated automatically). Since most significant deposition occurs in the hotter zones, it is assumed that using one chemical reaction rate, appropriate for higher temperatures is valid. The simulator does not currently allow for a correlation between chemical reaction rate and fluid temperature, but this is another recommendation that could be made to the software vendor. In addition, impact of other ions (eg sodium, chloride, calcium, magnesium, potassium, strontium, etc.) on the solubility of barium sulphate would be useful.

Deep within the reservoir, the fluid advection rate is relatively slow (order 1 metre per day or lower), and as such, reaction rates do not have much impact, since the fluid has sufficient time to reach equilibrium anyway. However, closer to the wells, the flow rate is higher, and thus fluid may not have time to reach equilibrium. Thus, in any study of the impact of near well deposition, it would be useful to include the effects of varying reaction rates. This is also a recommendation that is being made to the code developers.

5.17 CONCLUSION

This Chapter summarizes how the tracer code was modified inside the streamline simulator FrontSim by adding a simple scale deposition model so that we can model the scale deposition and predict where and when the scale will be formed so we can plan ahead to implement a squeeze treatment operation. We have shown by means of simple one-dimensional, two-dimensional models and later three-dimensional models that we can produce the type of behaviour that we would expect in a reservoir where we have incompatible formation and injected waters. First we have confirmed that the region of the reservoir where scale forms is affected by the rate at which scale forms. In particular, if the time taken for the scale formation process to reach equilibrium is short compared to the time for the injected water to reach the producer, most of the scale is formed deep in the reservoir well away from the producer. We have also confirmed that the concentration of scaling ions produced is affected by the rate at which scale is formed, but only if the timescale for scale formation is comparable with the time for the injected water to breakthrough at the producer. We note that in the 2D model there is significant scale deposition predicted as the streamlines converge near the producer. The mapping process between streamlines and the grid introduces numerical dispersion which will cause diffusion of the ions perpendicular to the streamlines creating additional mixing and therefore scale deposition.

The simple scale precipitation model assumes that one or other of the scaling ions will become completely depleted in each grid cell, and is only appropriate for scales with very low solubilises , such as $BaSO_4$. For other scales which may also occur due to brine mixing. a proper thermodynamics model , including solubility product would be required as future work.

CHAPTER 6: STREAMLINE MODELLING FOR FIELD-X

6.1 INTRODUCTION

The displacement and mixing mechanisms in one, two-dimensional and three-dimensional models were discussed in Chapter 5 based on synthetic data sets. It is important to apply the conclusions drawn to a streamline model of an actual field system to identify the types of observation that can be made. Most reservoirs are best described by a full three-dimensional geometry, where the flow patterns can be described as a combination of the characteristics of the one and two-dimensional systems examined in the previous sections. Factors such as the geometry (areal streamlines) and/or the Lithology (vertical heterogeneity) may cause streamlines of connate water and streamlines of injected water to arrive at the same location (producer) from different directions and hence some mixing is to be expected in the formation around the well. It is this continuous supply of scaling ions into the vicinity of the well and the mixing occurring in this zone of high fluid velocities that creates the potential for scale formation and wellbore damage due to this scale precipitation.

FIELD - X DESCRIPTION

Field X was discovered in 1974 and come on production in 1983; it is the most northerly of the presently producing fields in UKCS. A reservoir map is shown in Figure 6.1 and the relative permeability curves are shown in Figure 6.2. The reservoir is formed by stacked turbidities sandstone of late Jurassic age with (MSM) Magnus sand stone member overlaying the Lower Kimmeridge clay Formation (LKCF) Figure 6.3. The total reservoir thickness is up to 200 mtvt and the depth is 2800 mss. The original water contact is at 3160mss. The trap is a large tilted fault block dipping to the East. Faulting and stratigraphic pitchout has been demonstrated to have impact on the performance of some flow units. STOIP is in the order of 1.5 b/stb of 39 API light sweet crude with bubble point pressure of 2600 psi and solution GOR 775 scf/stb. The MSM has the majority of STIOP (1.2 b/stb) and has a higher expected recovery factor than LKCF. Initial reservoir pressure was 6653 psi at datum 3050 m TVDSS. The reservoir quality improves towards the crest of the structure, with only limited permeability remaining at the oil water contact. The field has light oil with viscosity of 0.5 cp. The

oil formation volume factor ranges from 1.4 and 1.5 rb/stb. Under the pressure, temperature and pH conditions of the reservoir, seawater and formation water incompatibility results in the precipitation of barium sulphate scale. The field has a very clear water oil contact and transition zone. The following table shows the main reservoir properties. The field is currently producing through 38 wells and reservoir pressure is supported by sea water injection through 12 injectors. The production climbed rapidly to plateau in 1985 and the field was constrained by facilities limits to approximately 140 mstbd until the mid-1990s, Figure 6.4 (a). At this time extensive sea water breakthrough occurred. The decline caused by increasing water cuts was expected by the formation of Barium Sulphate scale as a consequence of the mixture of the sea water and formation water. Subsequently a period of extensive activity ensued. Actions included well intervention, future new wells and a change from wells to sidetracks, implementation of gas lift, introduction of additional water injection through subsea wells and change from multi-zone to single completions. These activities successfully slowed the decline rate, Figure 6.4 (b). Figure 6.5 includes the field water injection rate, and when seawater flooding commences, and Table 6.1 has the general reservoir properties. The Field X model is a history matched model, and hence all wells in the model are controlled by flow rates obtained from historical observed data.

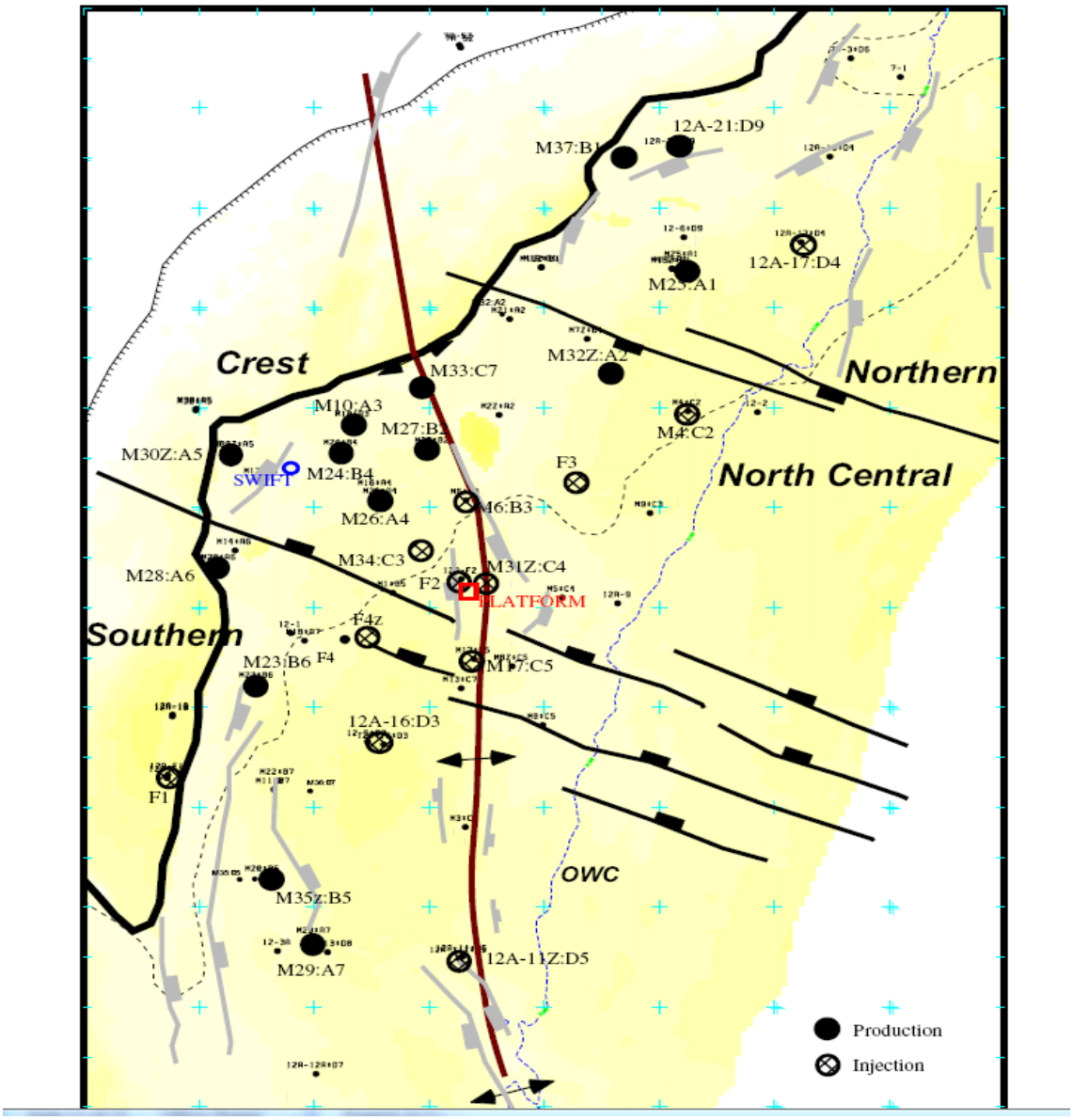

Figure 6.1: Field X Map with areas

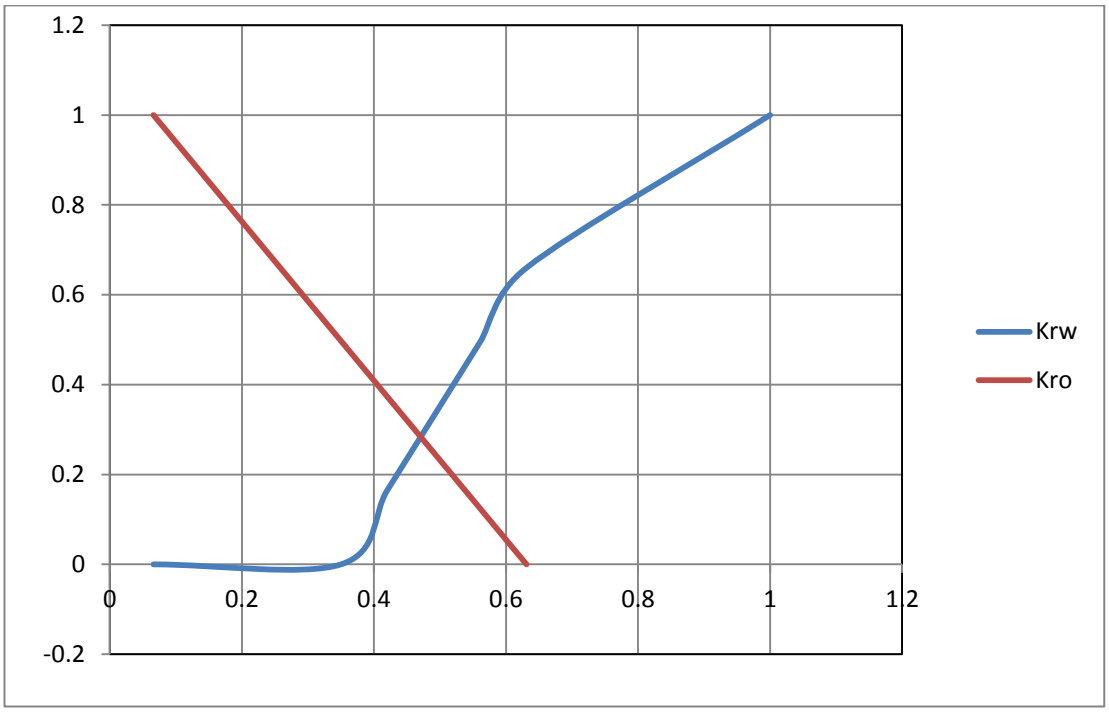
1.2
1
0.8
0.6
0.4
0.2
0
-0.2
0
0.2
0.4
0.6
0.8
1
1.2
Krw
Kro

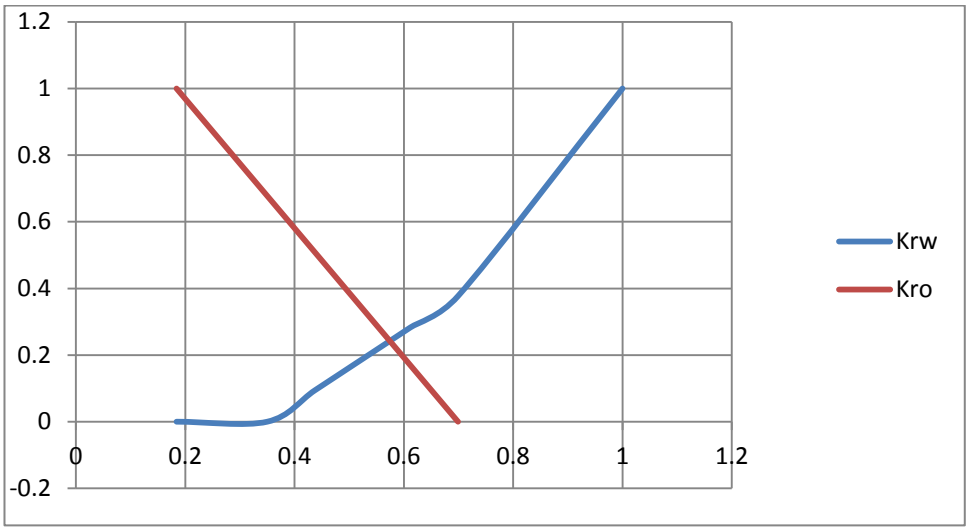
1.2
1
0.8
0.6
0.4
0.2
0
-0.2
0
0.2
0.4
0.6
0.8
1
1.2
Krw
Kro

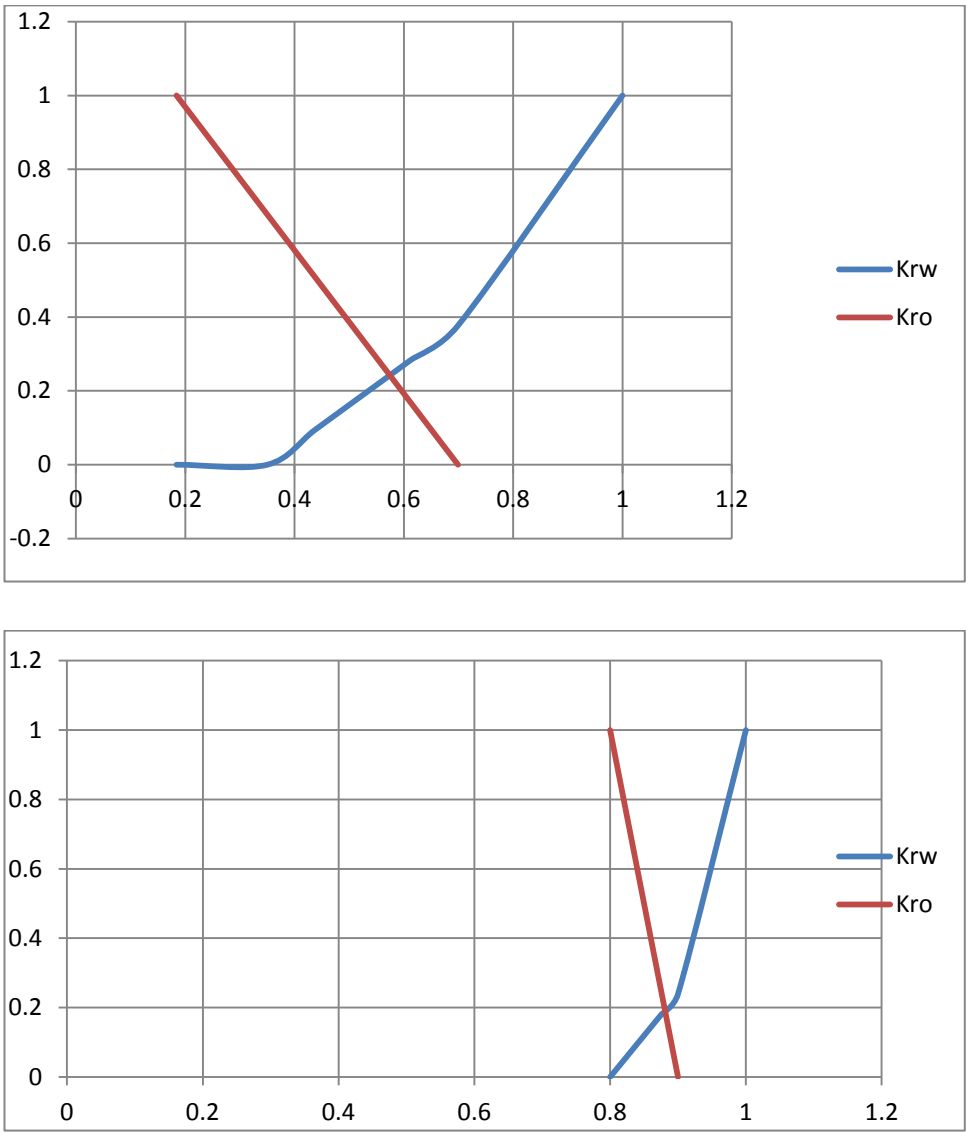

Figure 6.2: Four Relative permeability curves used in the Field X Model.

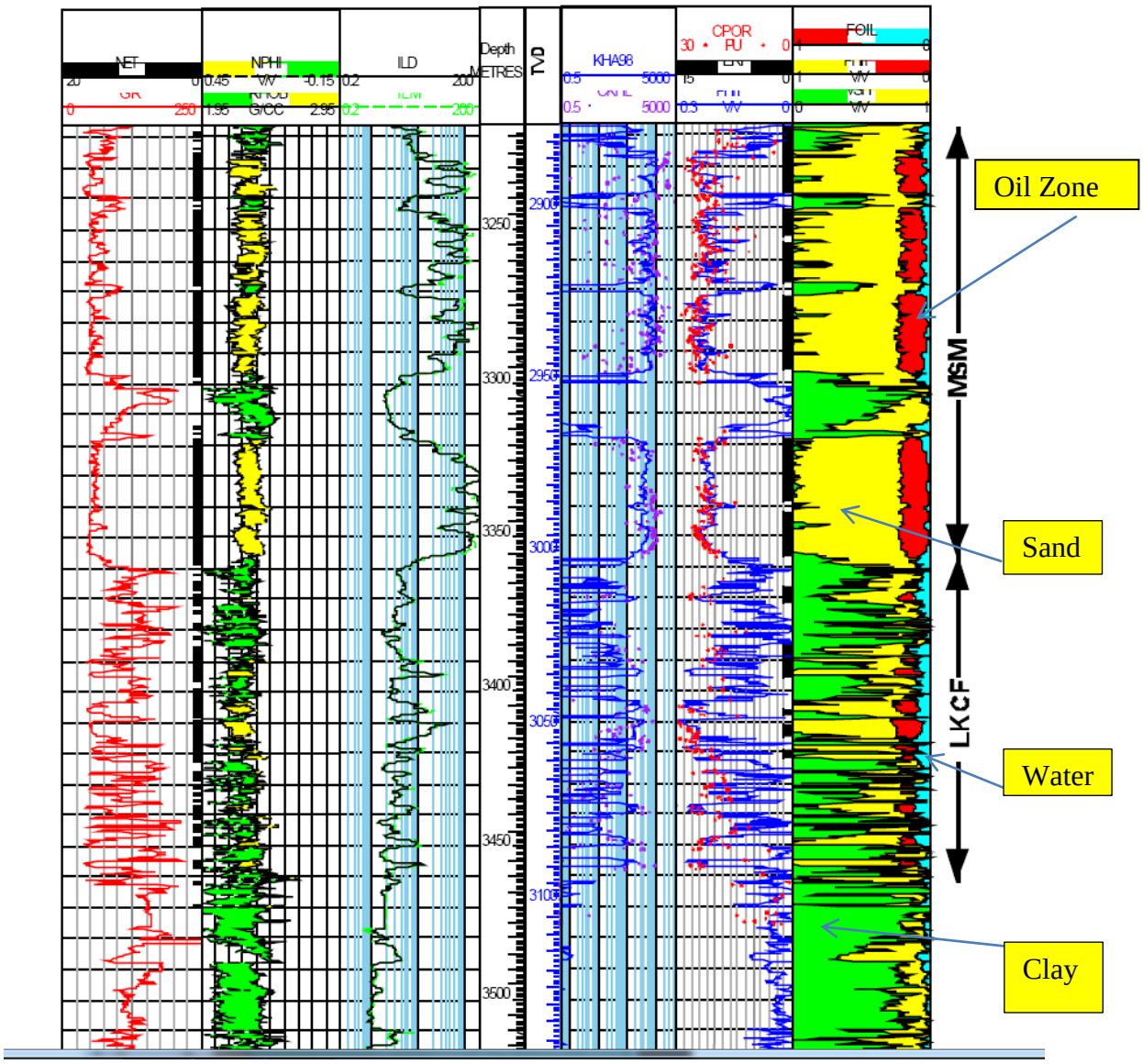

Figure 6.3: Typical log showing MSM and LKCF reservoir for Field x.

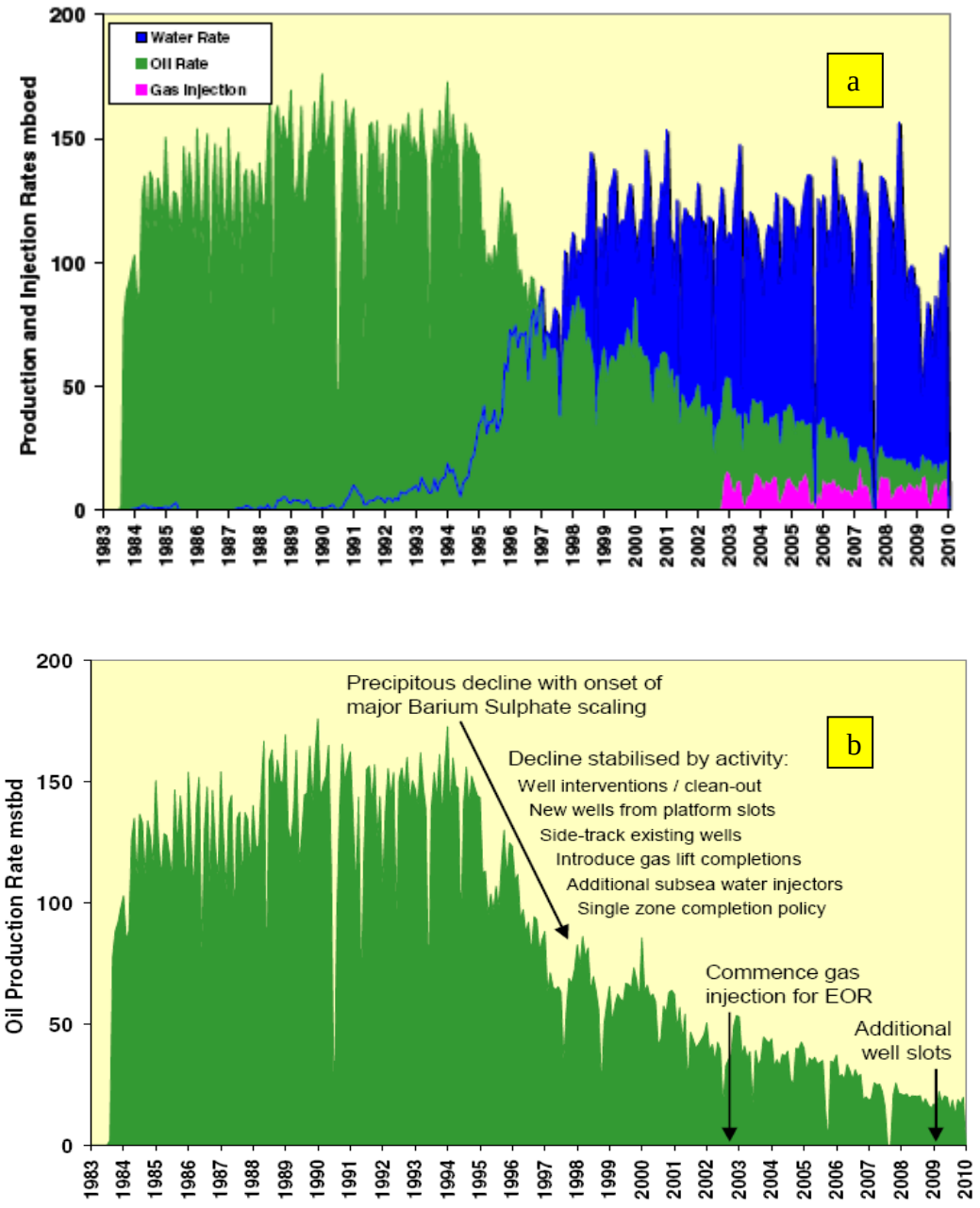

Figure 6.4: (a) Field x oil production and injection history, (b) Production history annotated with major events (SPE-134953)

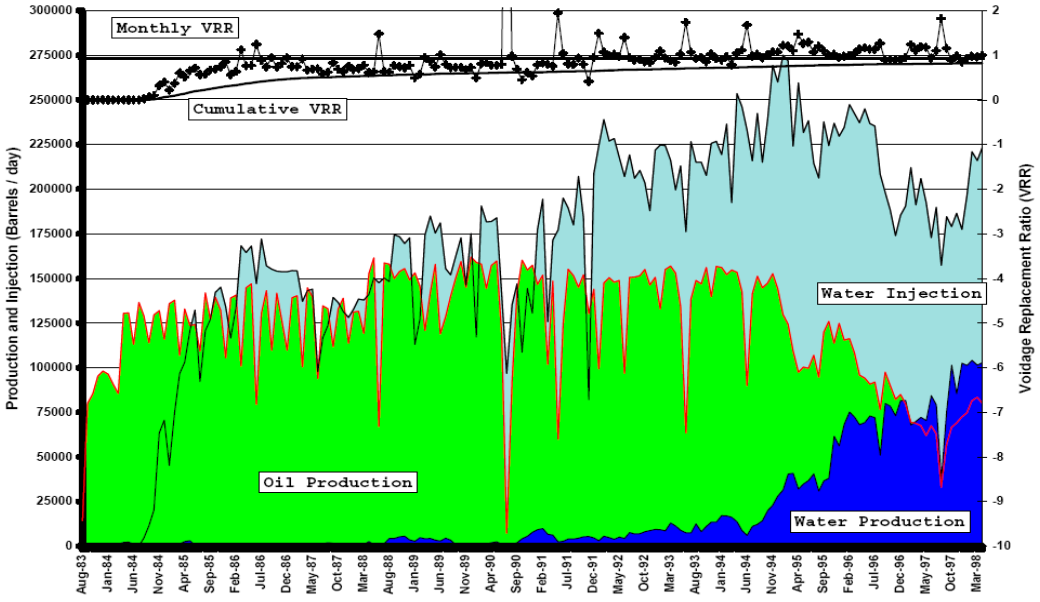

Figure 6.5: Field x oil production history, injection start from 1984 (SPE-49130)

Permeability	**0.01 to 2800 mD**
Porosity	**0.1 to 0.26**
Depth Of Reservoir	**9106 ft**
OWC	**10387 ft**
Initial Pressure	**6653 psia at 10007 ft**
Initial Temperature	**240 F**

Table 6.1 shows the main reservoir properties

Following is a table shows the formation and seawater compositions

Ion	Na	K	Mg	Ca	Sr	Ba	Cl	HCO_3	SO_4	Tem (^{o}c)	pH
Formation Water ppm	**11065**	**210**	**40**	**250**	**45**	**250**	**17350**	**1100**	**0**	**116**	**6.1**
Sea Water ppm	**11470**	**395**	**1340**	**400**	**8**	**0**	**20510**	**155**	**2960**	**NA**	**705**

Table 6.2 shows the formation and seawater compositions

Since the objective of this study is to identify the effectiveness of modelling barium sulphate scaling systems in general, sensitivities will be carried out on a range of formation water barium concentrations ranging from mild to severe, and to two different seawater sulphate concentrations, corresponding to full sulphate seawater and low sulphate seawater.

6.2 STREAMLINE MODEL

A full 3D streamline simulation model of Field X, including the flow rates in the of 12 injector and 38 producer wells, has been provided for this study. The main purpose here is to investigate where scale is likely to form in the reservoir and identify implications for scale control. The streamline model was manipulated to associate tracers to the injected and connate water as indicated by the Field X water compositions, i.e., 3000 mg/l of sulphate (seawater) and 250 mg/l of barium (formation water and aquifer). The product of the concentrations of barium and sulphate has been previously used as an indicator of brine mixing and scaling potential. However, use of the streamline simulation with the scale precipitation model allows us to identify where the scale forms, and the impact on the produced water composition in each well. The model consists of 66220 active grid blocks with average areal cell sizes ranging from 86 to 154 ft and horizontal average thickness of by 5 ft.

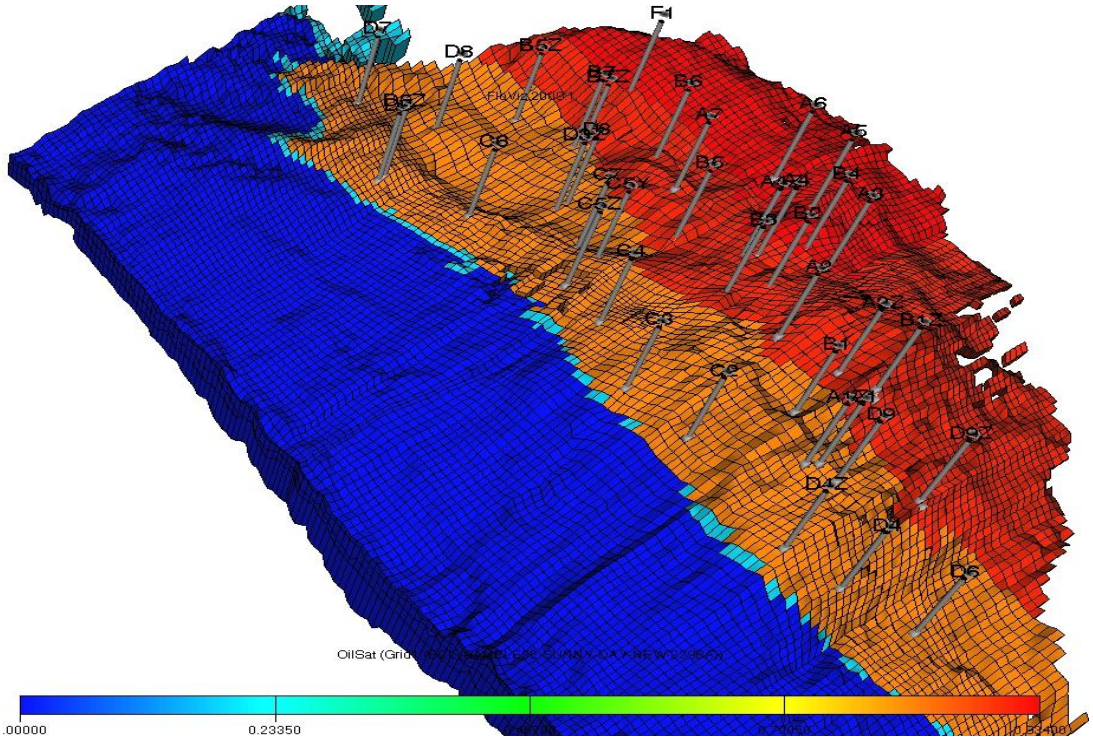

Figure 6.6: Initial oil saturation for 3D Section of Field X. It is evident that there is a large aquifer on the left separated from the oil leg on the right by a transition zone (orange zone), most of the 12 injectors wells are located close the oil water contact.

Initial distribution of oil and water can be seen in Figure 6.1, and Figure 6.7 shows the streamlines connecting the injectors, most of which are located near the water oil contact and the producers. Some of the streamlines originate in the aquifer indicating some of the pressure support from there. Figure 6.8 shows the permeability map.

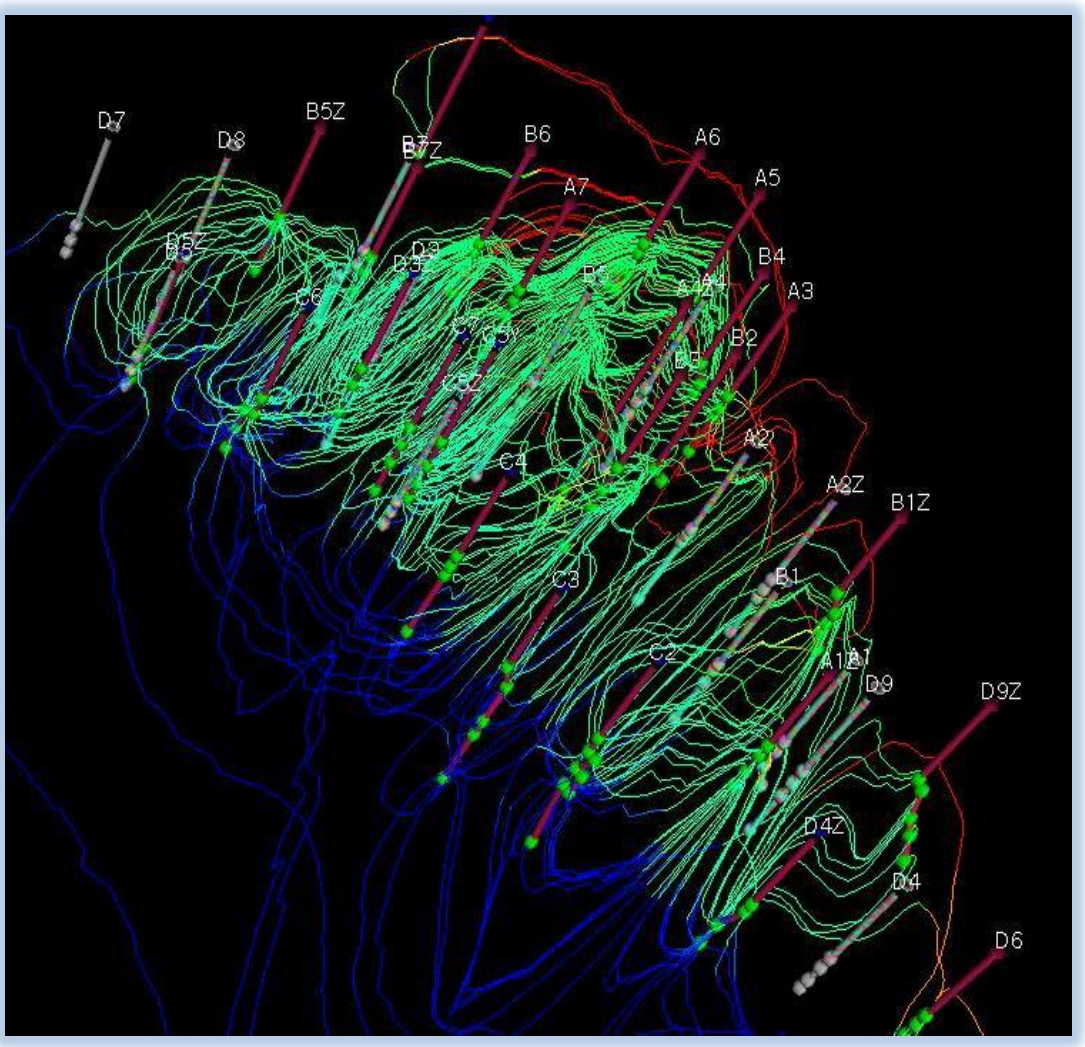

Figure 6.7: Oil saturation for a partial 3D section of Field X showing the streamlines linking injectors and produces, Note that some streamlines originates in the aquifer (bottom left), indicating pressure support from the aquifer is significant.

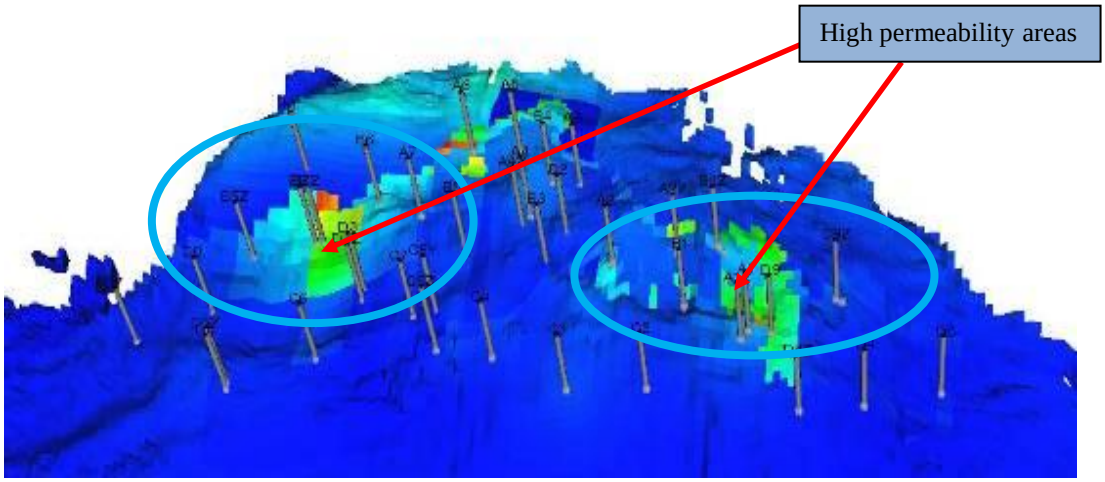

Figure 6.8: 3D section of Field X indicating areas of high permeability.

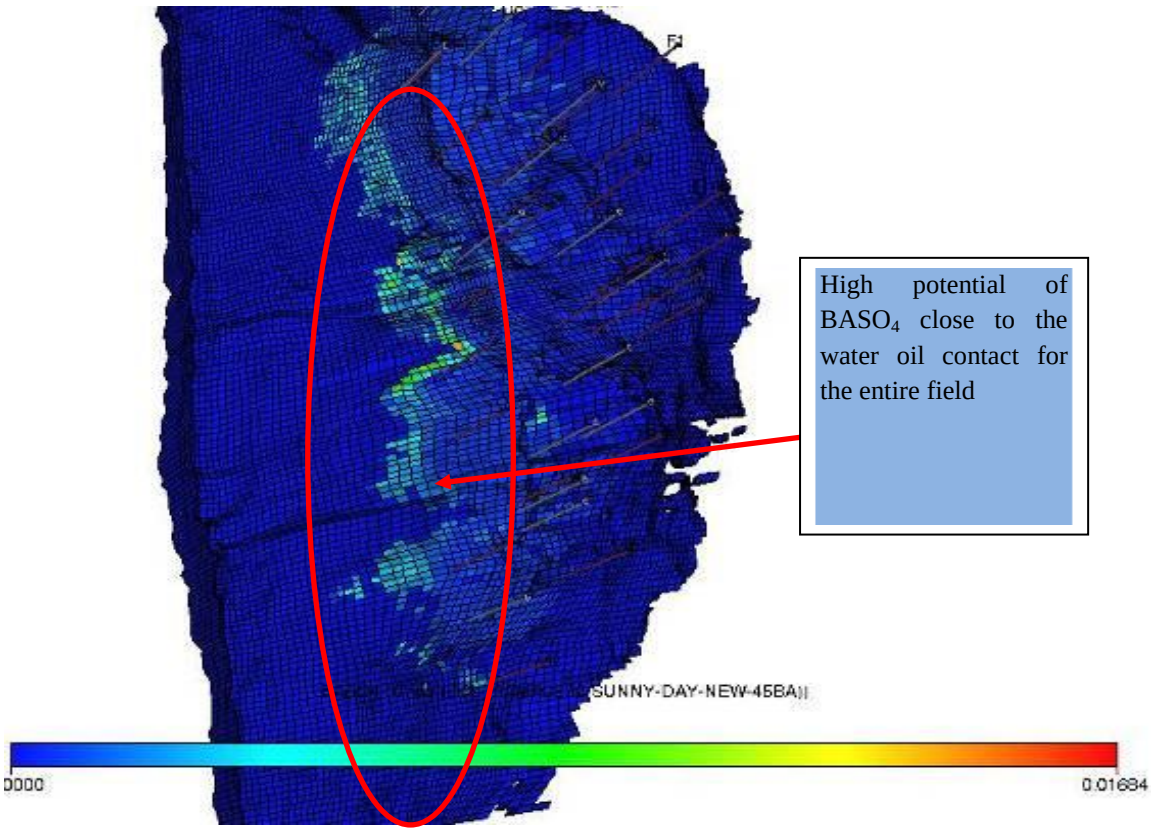

Figure 6.9: 3D section of the Field X indicating that most $BaSO_4$ precipitates close to the oil water contact and water injection wells.

The reason for the deposition occurring mainly near the oil water contact is that injection is mainly into the transition zone while the aquifer is where the greatest saturation of formation water containing the barium ions.

As we can observe in Figure 6.9, there is a higher potential for scale precipitation close to the oil water contact, in addition to the zones of high permeability indicated in figures 6.3, where presumably the higher volume throughput of scaling brines leads to a greater build up of scale. The most important thing to notice is that the maximum build up of scale is 0.017 lb/ft^3 and that is low number relative to rock density (168 lb/ft^3) and so reduction in permeability is probably imperceptible. In addition to that most of the deposition occurs near the oil water contact which means that it is happening away from the production wells.

6.3 RESULTS FOR A SELECTION OF WELLS IN FIELD X

We now discuss the results for a representative selection of production wells of Field X First we present the results for the case in which the barium (Ba) concentration is 250 mg/l and the Sulphate (SO_4) concentration is 3000 mg/l for the most significant scaling wells and later we present the results for different concentrations of barium. The full comprehensive analysis for the other wells will be presented in Appendix A. Different concentrations of (Ba) 45, 80, 229 and 800 mg/l for the wells A1Z, A5, B5Z and D9Z will be presented in Appendix B. Figure 6.10 shows the water production rate in (bbl/day) (blue, left hand vertical axis) and the fraction of the injected sea water (green, right hand vertical axis) versus time (days) in X axis for well A1Z. We observe in Figure 6.10 that the water breakthrough occurs after 4200 days and there is an ensuing sharp rise in the water production rate. The sea water breakthrough occurs after a further 2000 days. From 4200 to 6200 days all the produced water is formation water from the aquifer, whereas sea water breakthrough has not occurred yet during this period and so no reactions have occurred yet between barium and sulphate in the produced water. Even after 8000 days only 10% of the produced water is sea water. Figure 6.11 indicates that there is a high barium concentration with or without precipitation from 4200 to 6000 days which confirms there is no reaction occurring yet between the barium and sulphate, however, after 6000 days the barium concentration decreases due to the interaction with sulphate in the sea water. From Figure 6.12. it is evident that after seawater breakthrough, the seawater fraction only reaches 30%, but despite in situ precipitation reducing the barium concentration, for the entire period after sea water breakthrough there will be a scaling risk with barium concentrations remaining above 10 mg/l at all times, and sulphate concentration rising to above 600 mg/ l. Figure 6.13 indicates that the well A1Z is located lower down the structure so we expect that much of the water production was coming from the aquifer which would explain the slow rise in sea water fraction observed in Figure 6.10. During the period from 4200 to 6000 days most of the produced water came from the aquifer reaching a rate of 6000 to 8000 bbl/d. This well thus mainly produced formation water from the aquifer not injected sea water. However, after 6000 days sea water breakthrough occurred and the reaction took place resulting in scale precipitation, and a scale risk in the well.

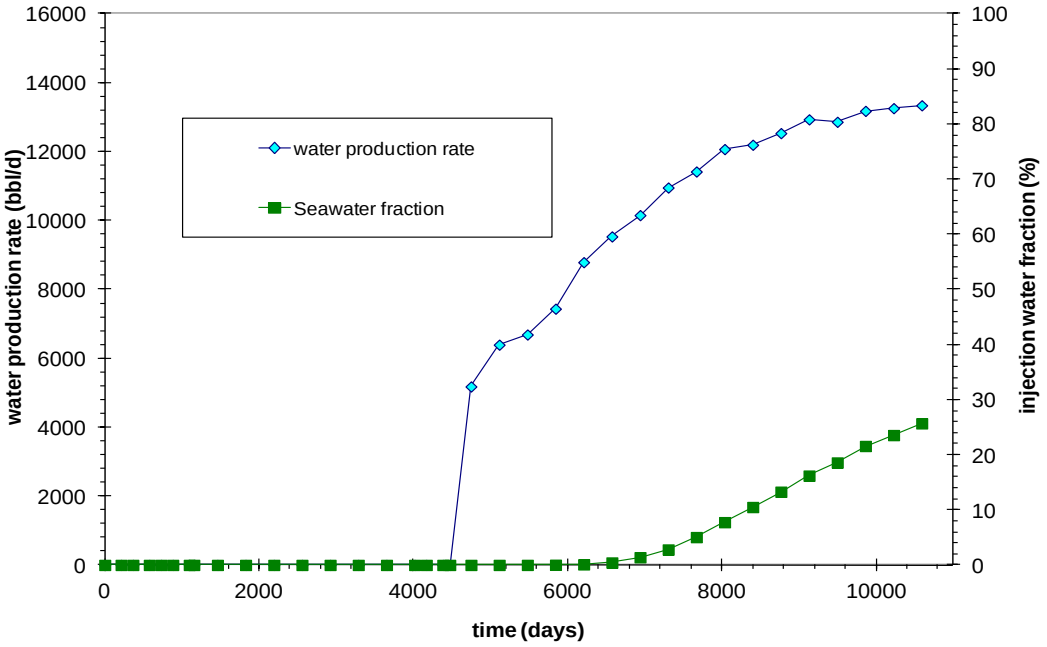

Figure 6.10: Water production rate and percentage of the injected water produced as a function of time for well A1Z. The breakthrough of sea water occurs 2000 days after the formation water breakthrough.

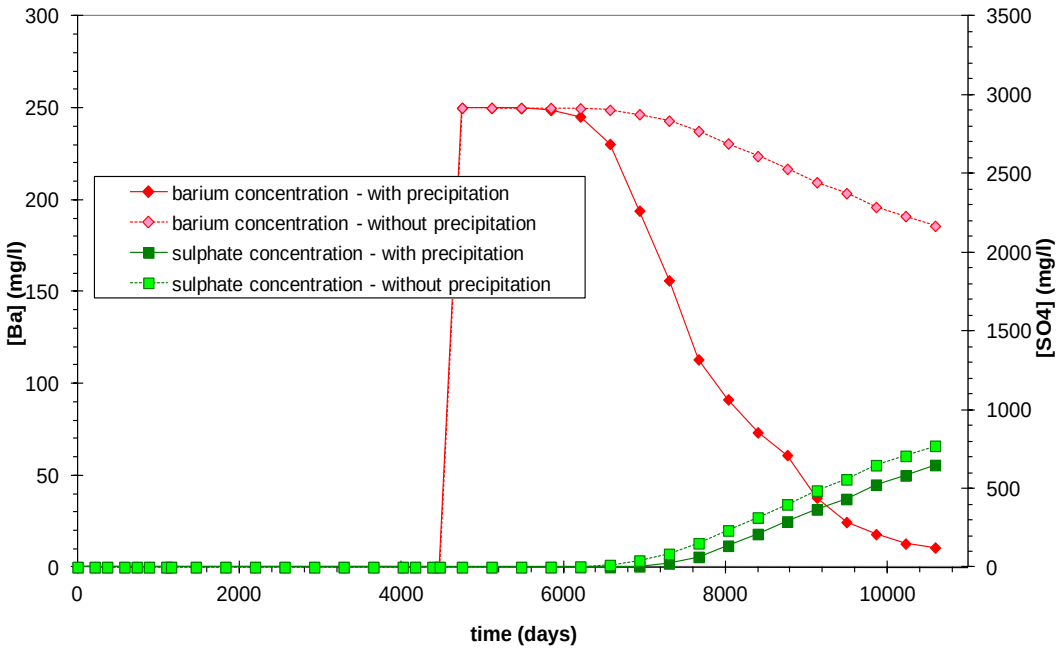

Figure 6.11: Barium and sulphate production with instantaneous precipitation and without precipitation as a function of time for well A1Z. After 6000 days the Ba concentration decreases due to the interaction with SO_4 from sea water. Because of the excess of the SO_4 ions, the relative decrease in SO_4 concentration is much smaller.

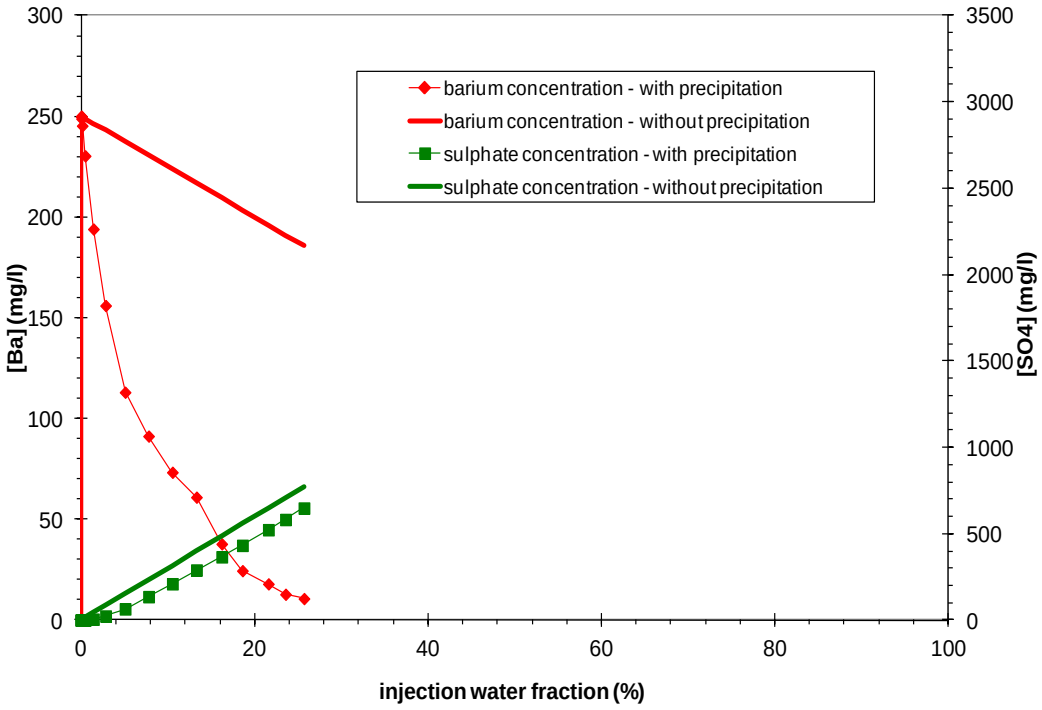

Figure 6.12: The produced concentration of barium and sulphate ions as a function of the sea water fraction in the produced water for well A1Z.

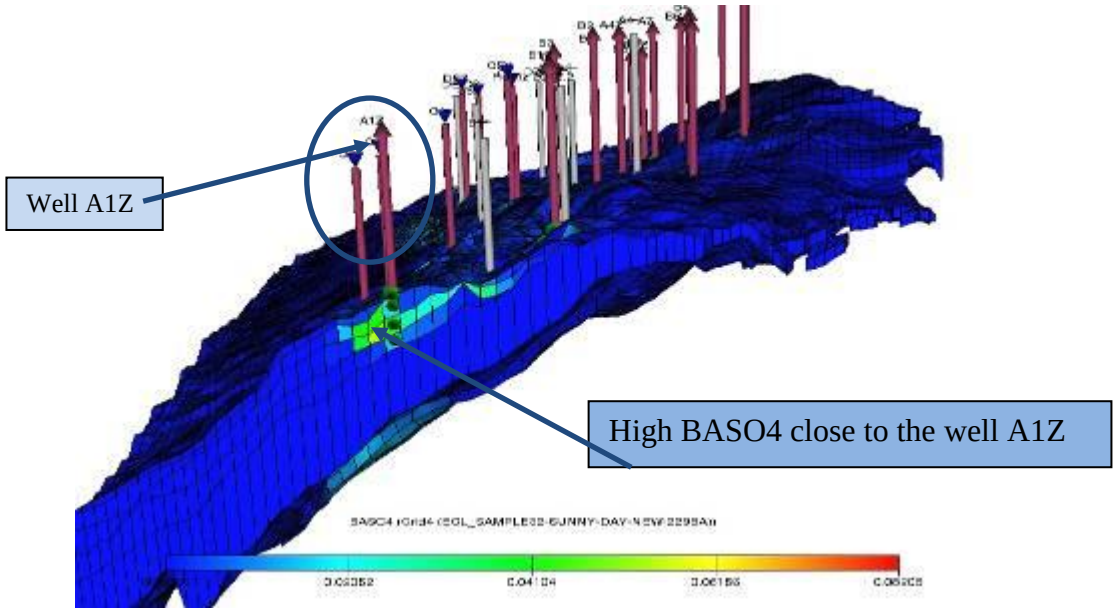

Figure 6.13: The 3D section of Field X indicates $BaSO_4$ deposition for well A1Z. The well is located lower down the structure so we expect the formation water is coming from the aquifer. The figure indicates there is a potential for scale in and around the producer by the end of the period of the simulation.

Well A2 Results:-

The following are the results of the Well A2. Figure 6.14 shows the results for the water production rate in (bbl/day) (blue, left hand vertical axis) and the fraction of the injected sea water (green, right hand vertical axis) versus the time (days) on the X axis. As may be observed in Figure 6.14, the water breakthrough occurs after 1800 days of production water and the water production rate increased very quickly but briefly due to the well being shut in at 4000 days, and there was no more production of water thereafter there is not much scale noticed in this well.

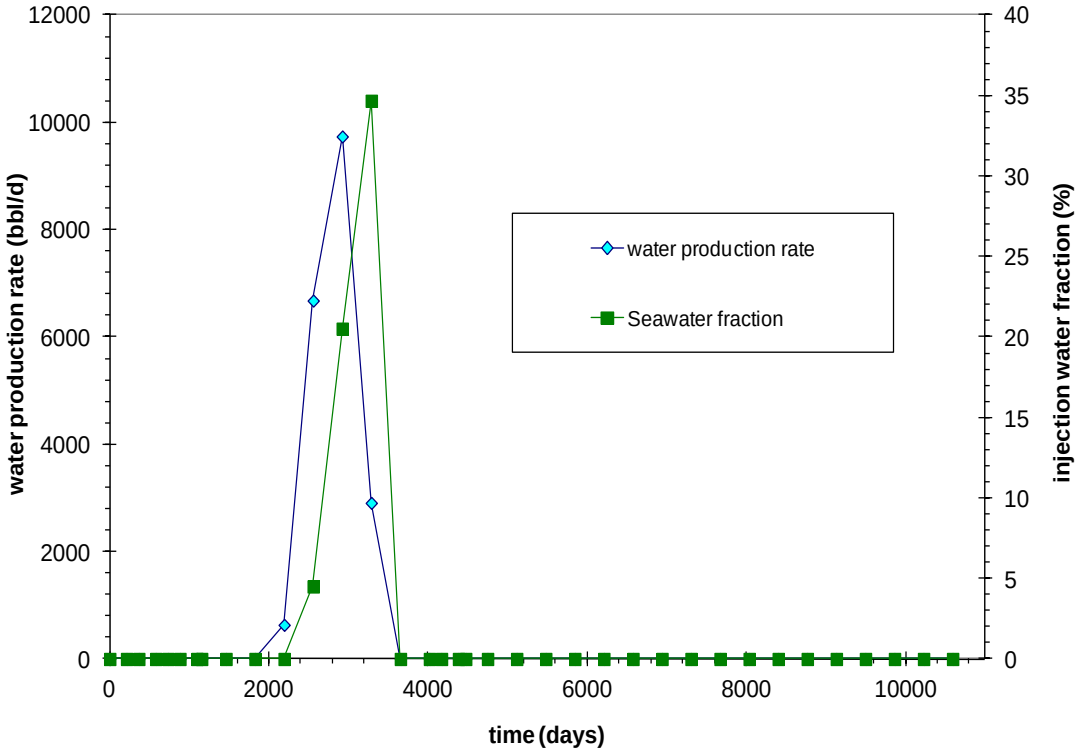

Figure 6.14: Water production rate and percentage of the injected water produced as a function of time for well A2.

Well A2 behaves quite differently from A1Z. Whereas well A1Z experienced sea water breakthrough 2000 days after water breakthrough, and the sea water fraction only rose gradually thereafter, in A2 seawater breakthrough followed very soon after water break through , and within 2000 days had risen to a higher value (35%) than it did after 4000 days in A1Z , This suggests that whenever A1Z was receiving considerable aquifer

support in contrast A2 was receiving negligible aquifer support , and only injection sea water was displaced through the oil leg. This results in much less mixing of seawater and formation water, and hence the stripping of barium ions much is less produced in well A2, as can be seen from Figure 6.15 and 6.16.

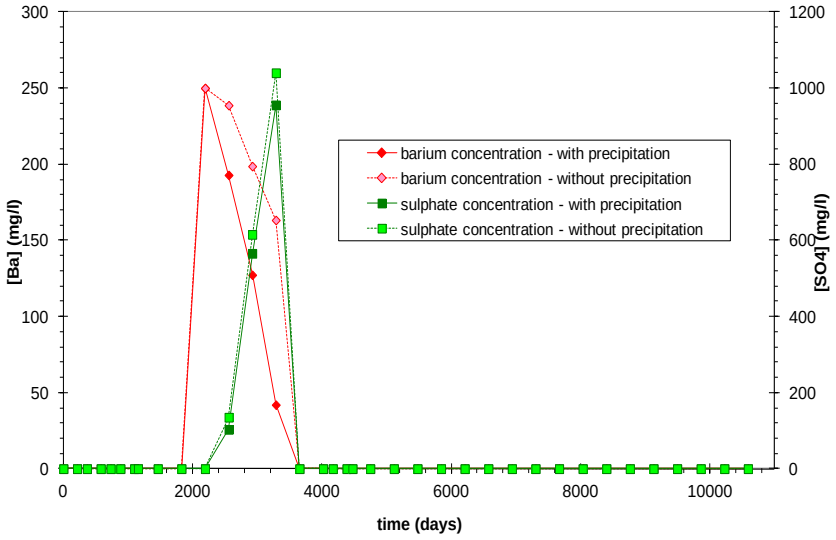

Figure 6.15: Barium and sulphate production with instantaneous precipitation and without precipitation as a function of time for well A2.

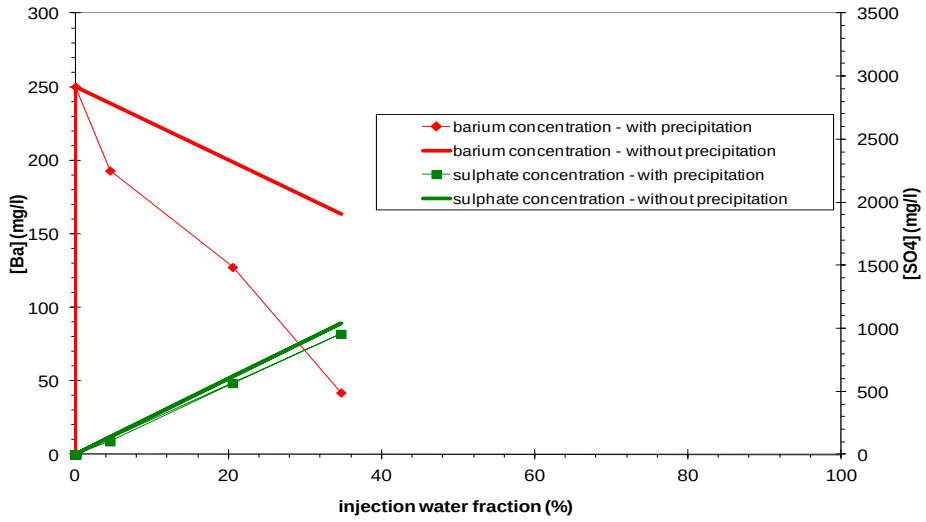

Figure 6.16: The produced concentration of barium and sulphate ions as a function of the produced fraction of sea for well A2.

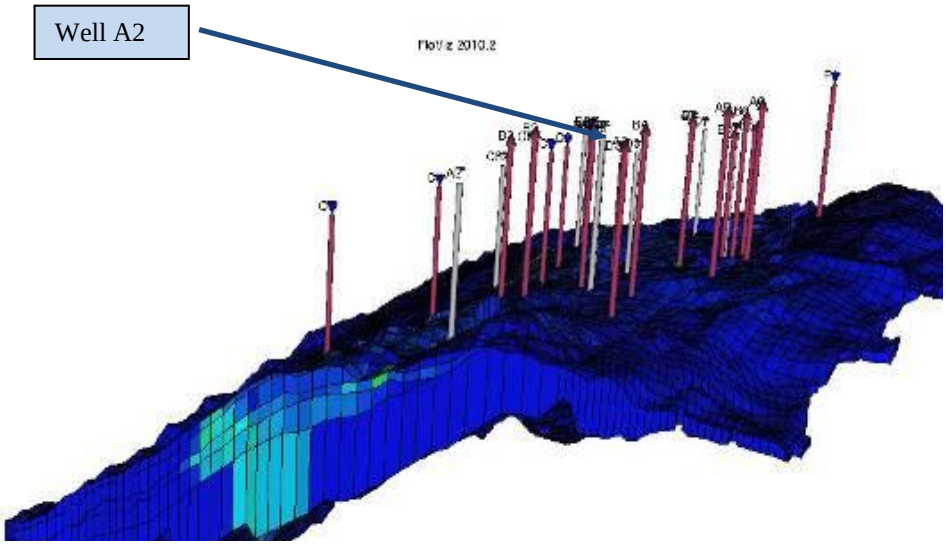

Figure 6.17: The 3D section of Field X $BaSO_4$ location for well A2. The well is located in the oil leg.

Figure 6.17 identifies that well A2 is located further up dip than well A1Z (ref. Figure 6.8), and that there is no evidence of significant scale deposition near A2. Figure 6.15 and 6.16 show the impact that streamline simulation can have, in that were this a conventional finite difference model, the effect of numerical dispersion would have manifested itself as an apparent mixing , and hence more barium stripping would have been predicted due to this numerical dispersion error. This more accurate calculation suggests less barium stripping would be observed in the reservoir, and hence more scaling ions remaining in the reservoir in the brine when it reached the producers, and so a higher scaling risk, albeit for a short period.

Well A3:-

Figure 6.18 shows the results for well A3 of the water production rate in (bbl/day) (blue, left hand vertical axis) and the fraction for the injected sea water (green, right hand vertical axis) versus time (days) on the X axis. As can be observed in Figure 6.13, the water breakthrough for both production water and the sea water happened at the same time, after 5600 days. Figure 6.19 indicates that the barium concentration with precipitation dropped to zero in a very short time of about 500 days and fell to zero by the end of the simulation period. Next to no scale is predicted for this well, and it is clear from Figure 6.21 that the well location is far away from the potential area of scale precipitation which is located near the original oil water contact.

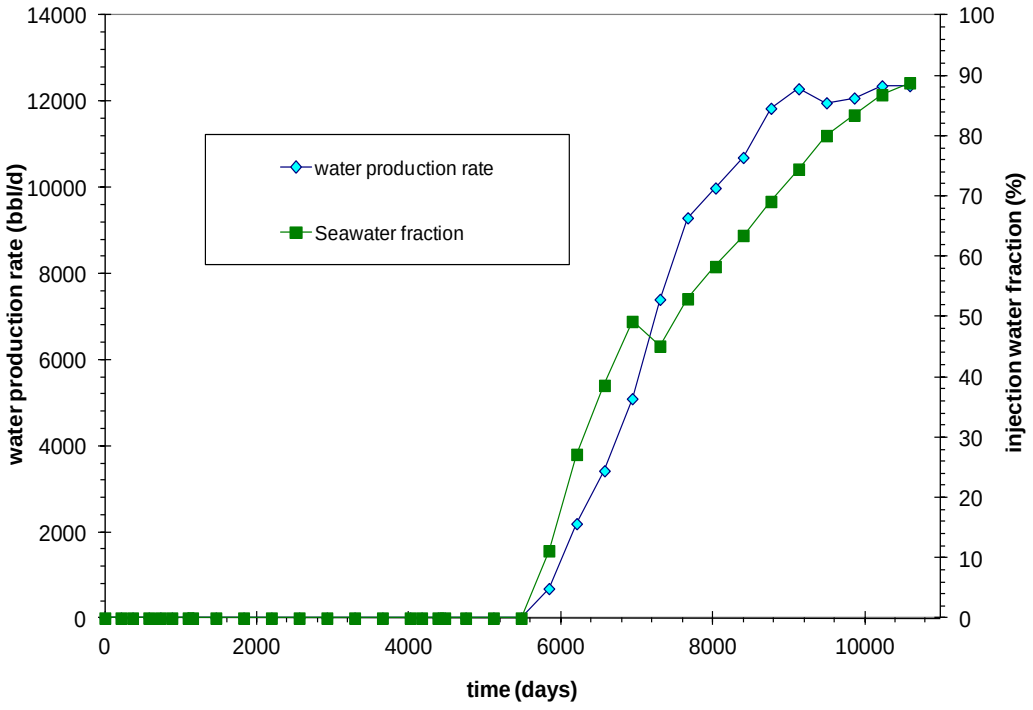

Figure 6.18: Water production rate and percentage of the injected water produced as a function of time for well A3.

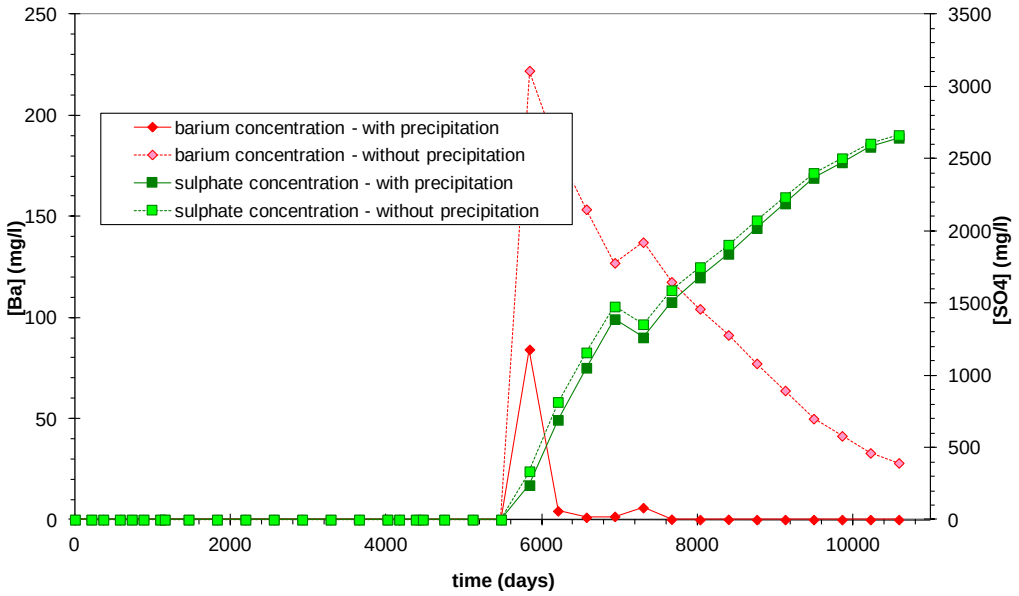

Figure 6.19: Barium and sulphate production with instantaneous precipitation and without precipitation as a function of time for well A3.

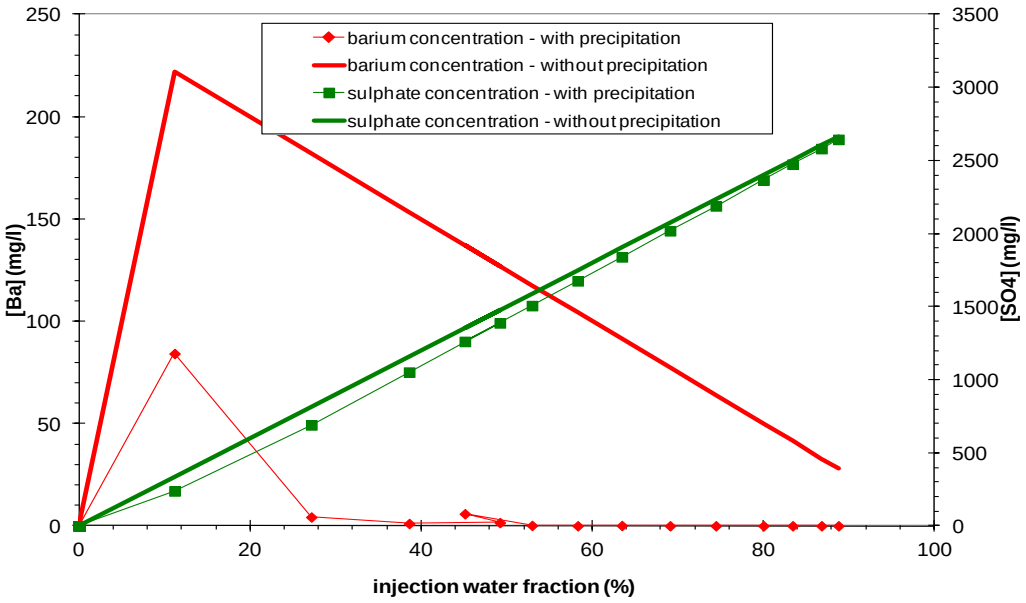

Figure 6.20: The produced concentration of barium and sulphate ions as a function of the produced fraction of sea water for well A3.

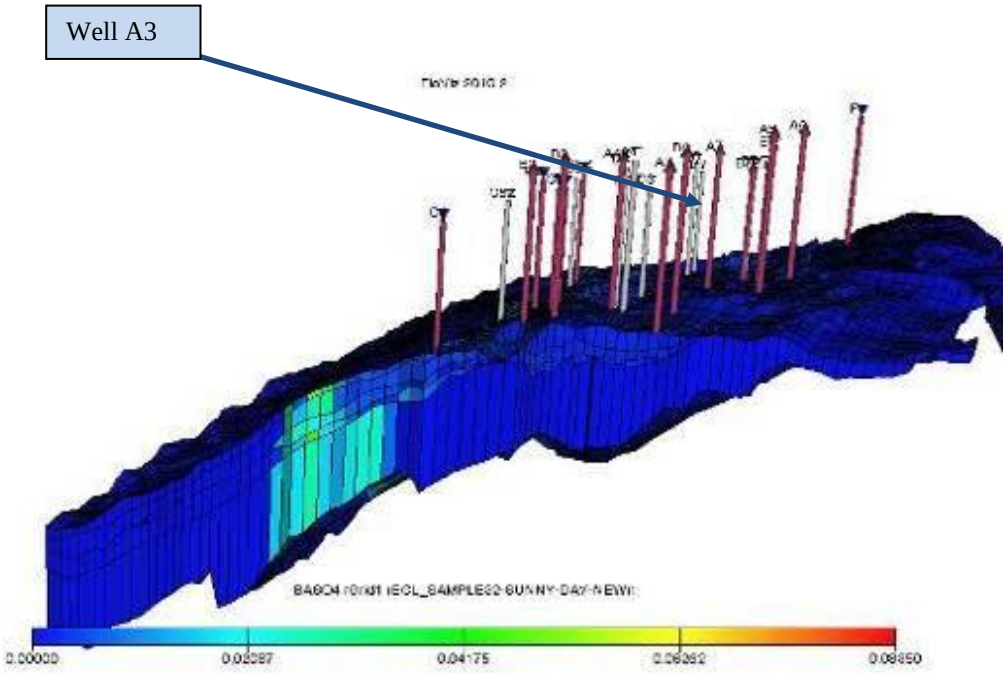

Figure 6.21: The 3D section of Field-X indicates $Baso_4$ location for well A3 which indicates no $BaSO_4$ scale in this well.

It is interesting to compare Well A3 with well A2, in that both have early sea water breakthrough after water breakthrough, indicating little or no influence of aquifer water. For well A2 there is very little in situ precipitation, whereas for A3 there is almost complete barium stripping which means no more barium will precipitate after 7000 days. A clue to explain this perhaps lies in the slight and temporary decrease in sea water fraction this occurs around 7300 days. This suggests breakthrough of water from a different direction, this hypothesis being supported by the increase in the rate of increase of water production at this time (Figure 6.18). If water is arriving at the well from opposite direction, then it is to be expected that the two brines streams will mix before entering the well reducing the scaling potential in the well.

Well A5 Results:-

Figure 6.22 shows the results for Well A5, with the water production rate in (bbl/day) (blue, left hand vertical axis) and the fraction of the injected sea water (green, right hand vertical axis) versus time (days) on the X axis. As can be observed in Figure 6.22, the water breakthrough for both formation water and injected sea water occurred at almost the same time, after 4000 days and most of the water that was produced was the injected sea water and not the aquifer water. The sea water reached 100% by the end of the simulation period. There is a temporary drop in water production to 2830 stb/d at 4748 days, followed by an increase. A likely explanation is that there is a decline in water production if a well is recompleted in an oil bearing zone, or if injection into a high permeability layer is stopped, and so the inflow from that layer into the production well can be reduced (Figure 6.22). Figure 6.23 confirms that the sulphate concentration was almost the same with and without precipitation, but the barium concentration with precipitation dropped to zero in a short time of not more than 400 days after the water breakthrough. Dropping the barium to zero for this short period result in no reaction and no tendency for scale precipitation thereafter. Figure 6.24 indicates that at 20% of the sea water fraction the Ba dropped to zero. It is very clear from figure 6.25, where the well is located in the upper structure of the field in the oil leg and far away from the oil water contact and that significant scale precipitation occurs down dip. No aquifer water was produced and that is why the levels of barium are close to zero, resulting in little scale.

WELL-A5

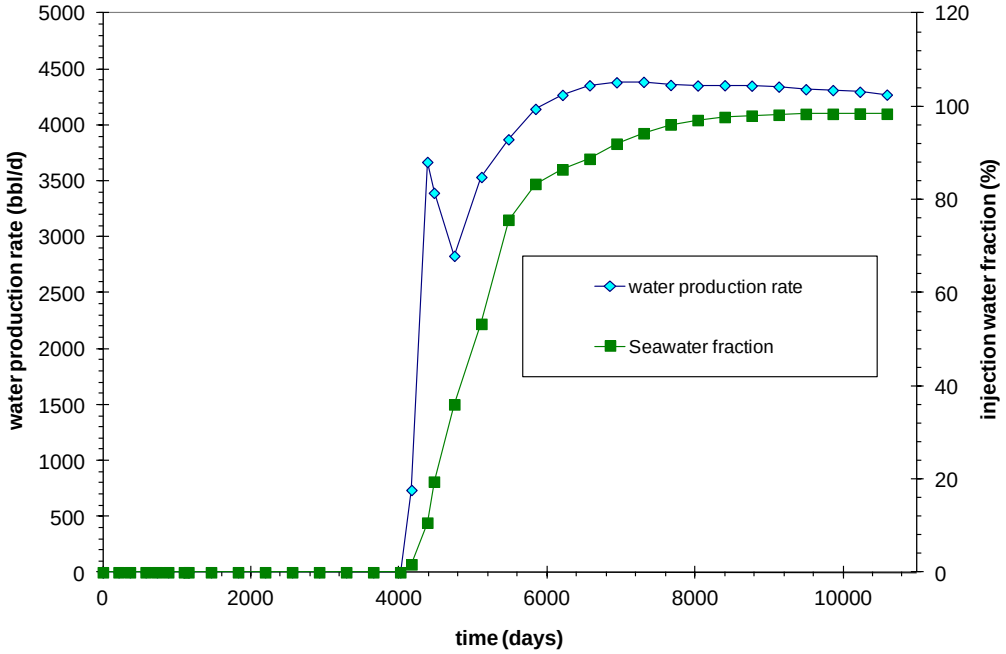

Figure 6.22: Water production rate and percentage of the injected water produced as a function of time for well A5.

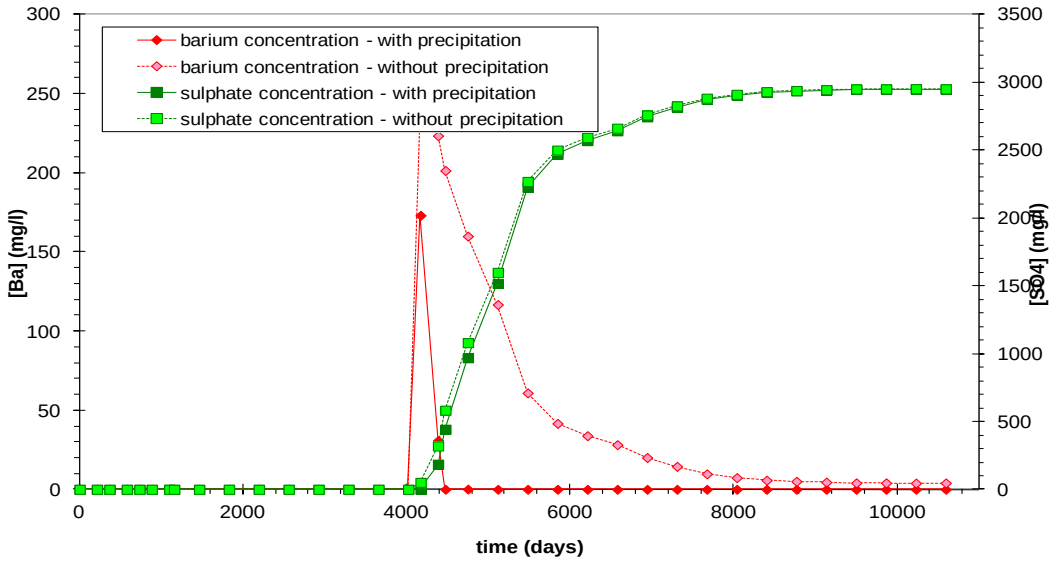

Figure 6.23: Barium and sulphate production with instantaneous precipitation and without precipitation as a function of time for well A5.

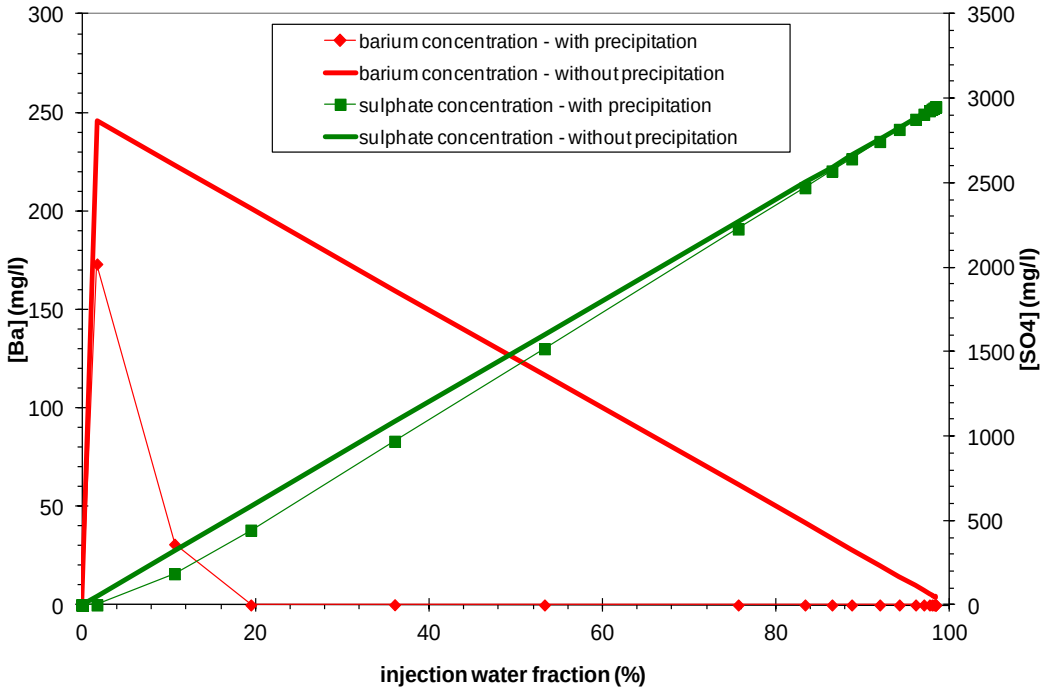

Figure 6.24: The produced concentration of barium and sulphate ions as a function of the produced fraction of sea for well A5.

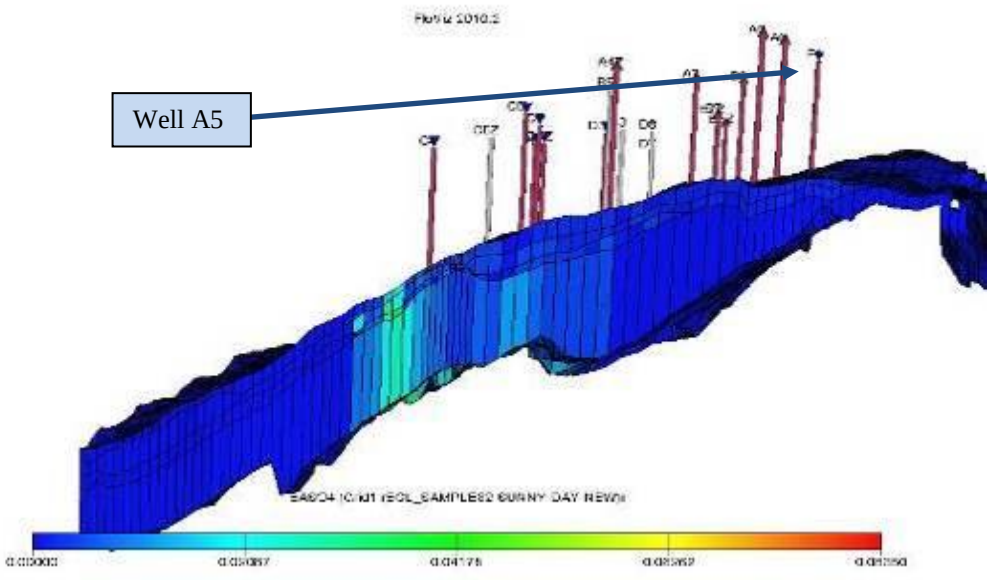

Figure 6.25: The 3D section of Field-X indicates $BaSO_4$ location for Well A5.

Well A6 Results:-

Figure 6.26 shows the results for well A6 with the water production rate in (bbl/day) (blue, left hand vertical axis) and the fraction of the injected sea water (green, right hand vertical axis) versus time (days) in X axis. As can be observed in Figure 6.26, the water breakthrough for both formation water and the injected sea water happened at similar times again, after 3600 days, and most of the water that was produced was the injected water and not the aquifer water. The sea water fraction reached 95% by the end of the simulation period. Figure 6.27 confirms that the sulphate concentration was almost the same with and without precipitation, but the barium dropped to zero after 4200 days. Figure 6.28 indicates that after reaching a sea water fraction of 36% the barium dropped to zero and no further reaction happened. The well is in the oil leg area, and the risk of scale damages is limited to early period after seawater breakthrough. Note that well A6 behaves in a similar way to well A5.

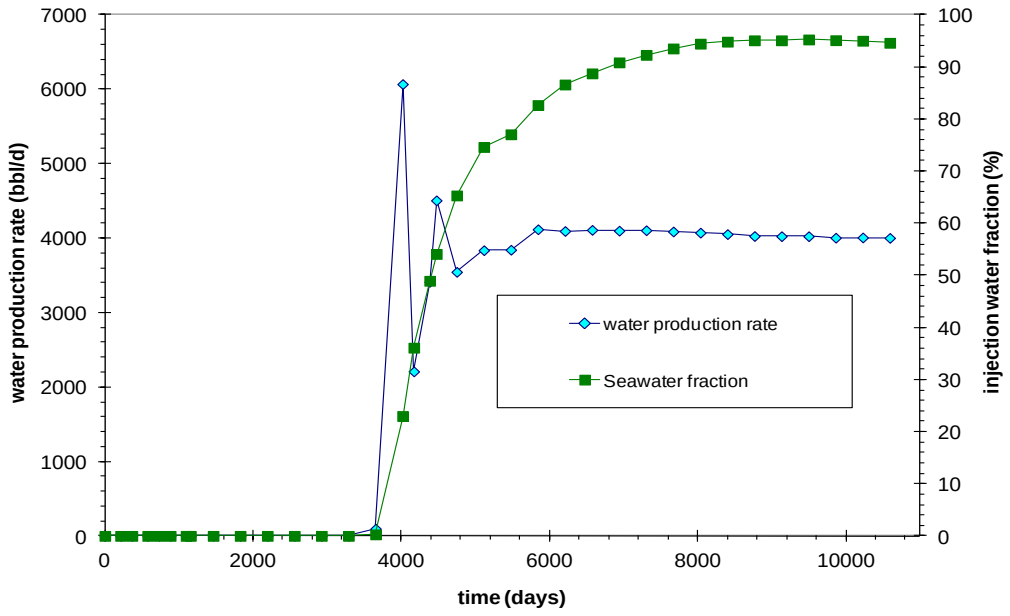

Figure 6.26: Water production rate and percentage of the injected water produced as a function of time for well A6.

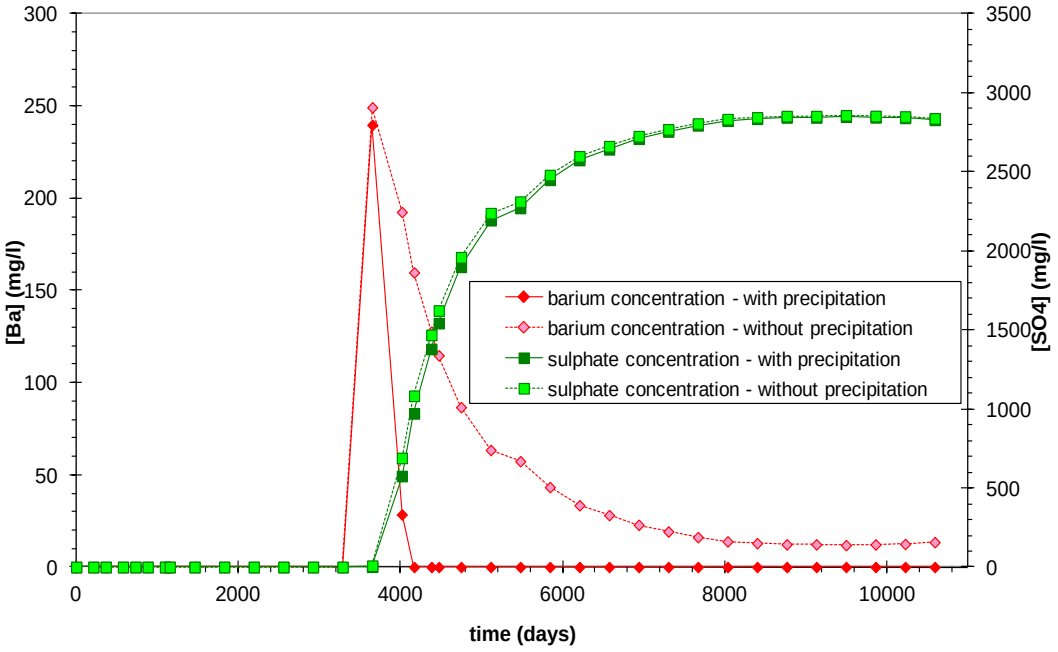

Figure 6.27: Barium and sulphate production with instantaneous precipitation and without precipitation as a function of time for well A6.

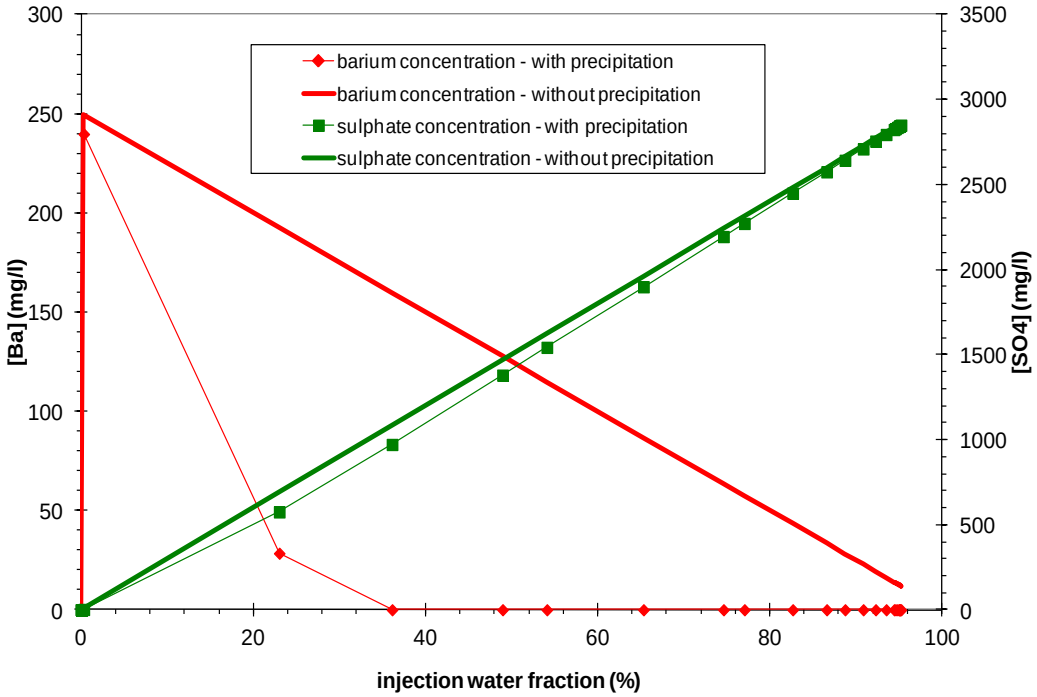

Figure 6.28: The produced concentration of barium and sulphate ions as a function of the produced fraction of seawater for well A6.

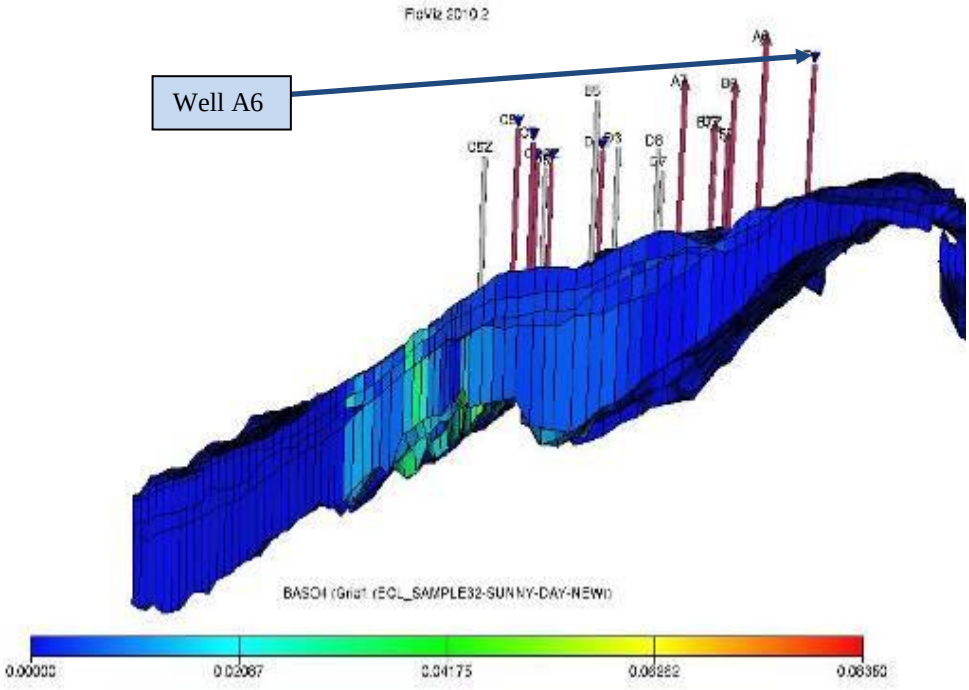

Figure 6.29: The 3D section of Field-X indicates $BaSO_4$ location for well A6. As indicated in the figure the well is far away from the OWC so there is no potential for scale precipitation by the end of the well life.

Well B2 Results:-

The results for the one of the most interesting production wells of Field X will now be discussed. Figure 6.30 shows the results for well B2 with the water production rate in (bbl/day) (blue, left hand vertical axis) and the fraction of the injected sea water (green, right hand vertical axis) versus time (days) in X axis. As can be observed in Figure 6.30 the breakthrough for both sea water and formation water occurs very close together after 4400 days. Note that the water production rate only rises to 2000 bb/d and it takes 6000days to do so. The sea water fraction reaches 50 % after 3000 days but the barium concentration is zero from day one after sea water break through (Figure 6.31 and Figure 6.32). Therefore, there will be no scale problem in this well. The well is quite far from the oil water contact, and thus no aquifer water is produced. The calculation suggests that in this case all the connate water that usually is banked in front of the advancing seawater front is in fact mixing with the sea water, leading to $BaSO_4$ precipitation, and hence no barium is observed at this well, despite the prediction that more than 100 mg/ l would be produced for 3000 days. Figure 6.32 shows that most of the $BaSO_4$ has precipitated quite far down dip, near the oil water contact.

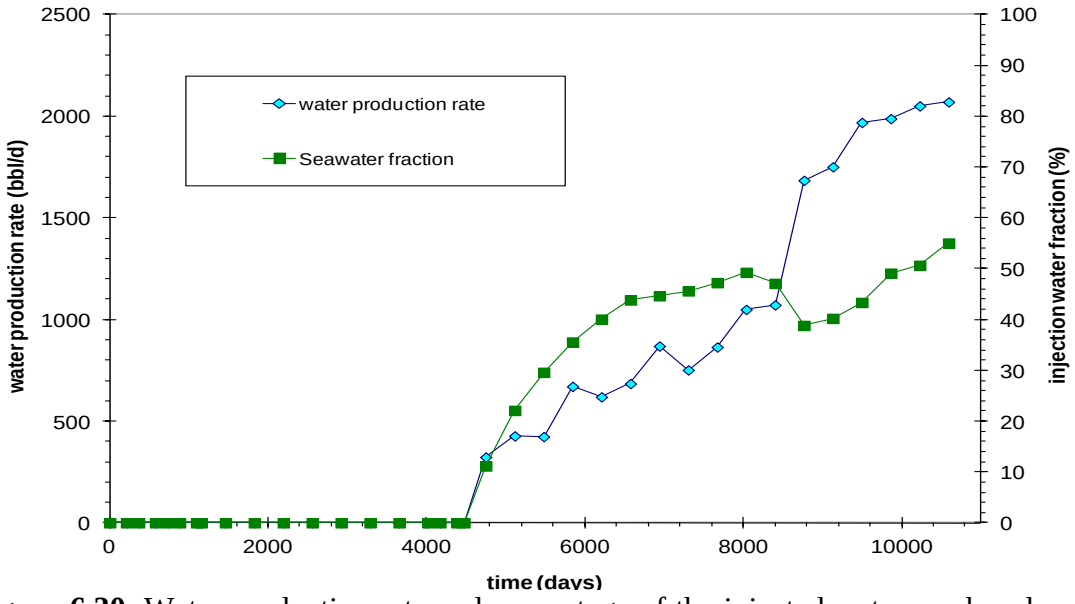

Figure 6.30: Water production rate and percentage of the injected water produced as a function of time for well B2**.**

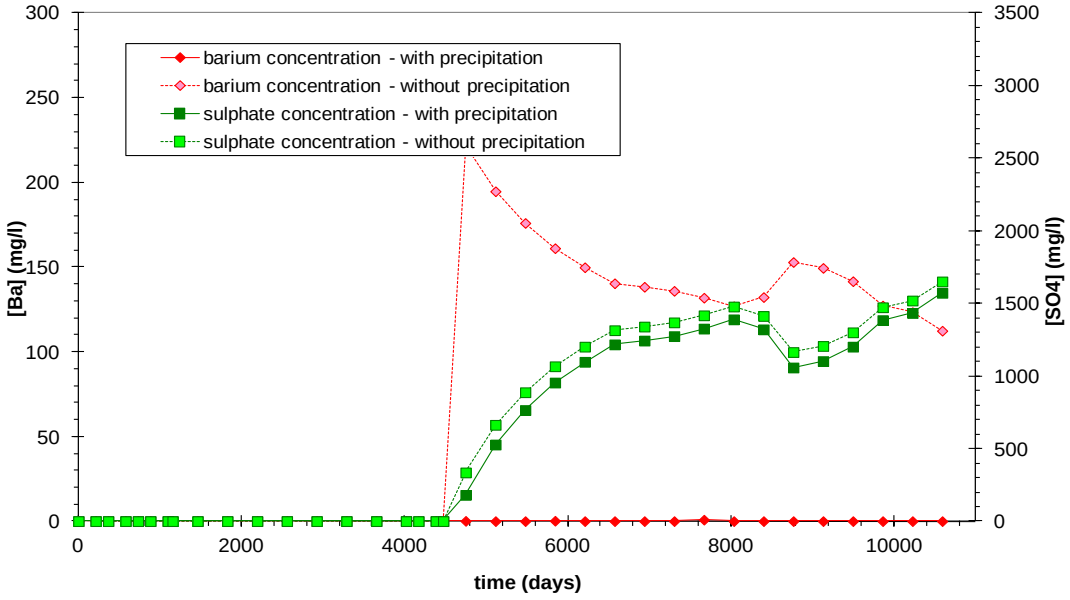

Figure 6.31: Barium and sulphate production with instantaneous precipitation and without precipitation as a function of time for well B2. Note that this with in situ precipitation, no barium at all is expected.

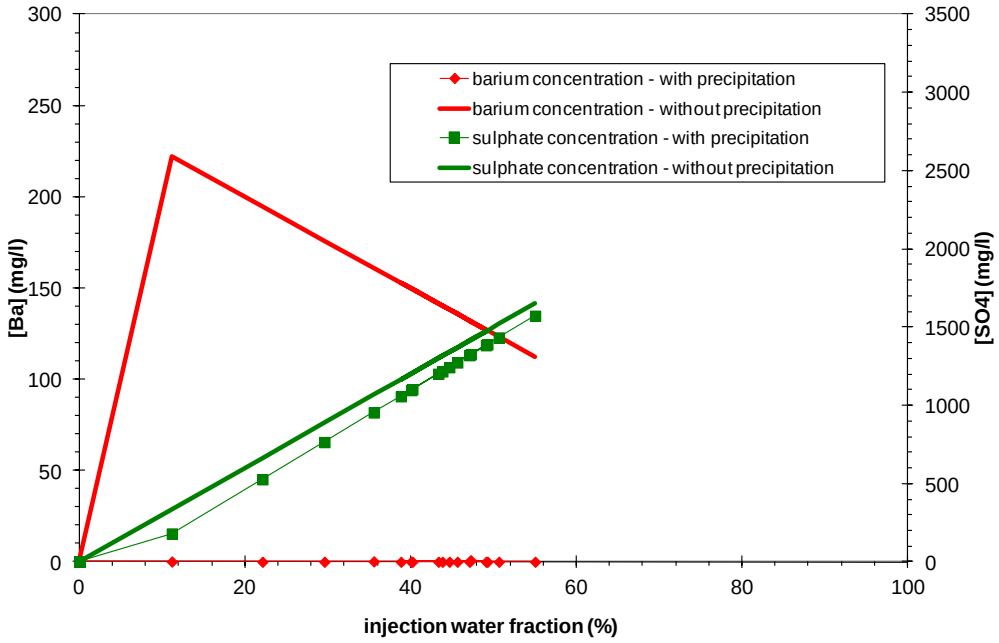

Figure 6.32: The produced concentration of barium and sulphate ions as a function of the produced fraction of sea water for well B2.

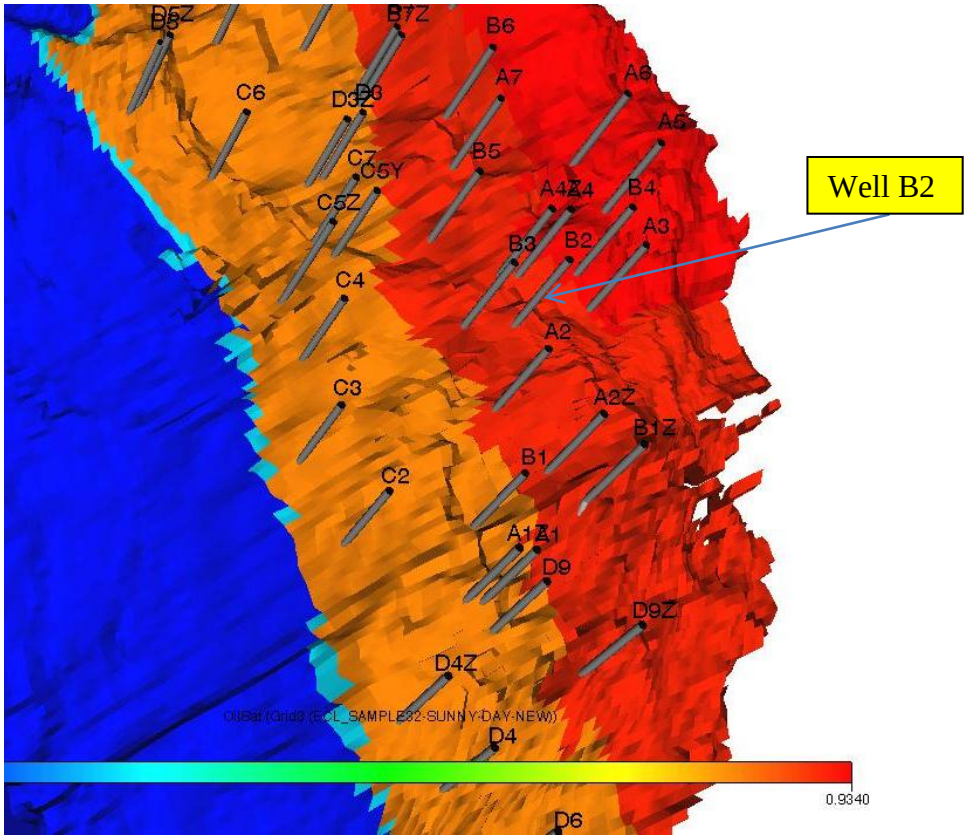

Figure 6.33: The 3D section of Field-X indicates $BASO_4$ location for well B2.

Well B3 Results:-

Figure 6.34 shows the results for well B3 with the water production rate in (bbl/day) (blue, left hand vertical axis) and the fraction of the injected sea water (green, right hand vertical axis) versus time (days) on the X axis. As we can observe in Figure 6.34, the breakthrough of both sea water and formation water occur very close together after 3800 days. The sea water fraction eventually reaches 50% after the water breakthrough, in well B3 much more barium is produced (Figure 6.35 and 6.36). Note that in B3 Sea water breakthrough is very soon, just as in well B2. The water production rate rises to 18000 bbl/d. The high levels of barium above 50 mg/l and the high water production rates will cause significant scale problems. The cause of this is high permeability streaks, which lead to production of relatively unmixed sea water from one direction, and relativity unmixed formation water from other direction, and thus the mixing of

brines and resulting scale risk takes place at the well itself. Figure 6.37 shows that some mixing takes place near the oil water contact, as discuses previously, but perhaps only half of the barium ions have been depleted due to this.

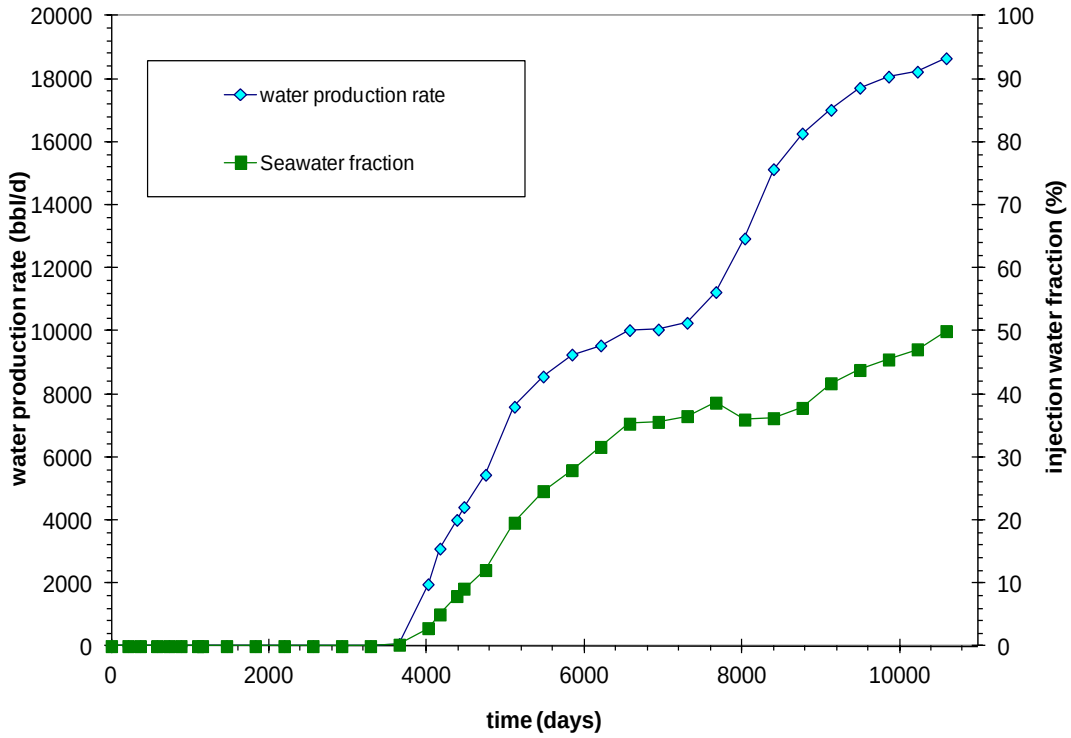

Figure 6.34: Water production rate and percentage of the injected water produced as a function of time for well B3.

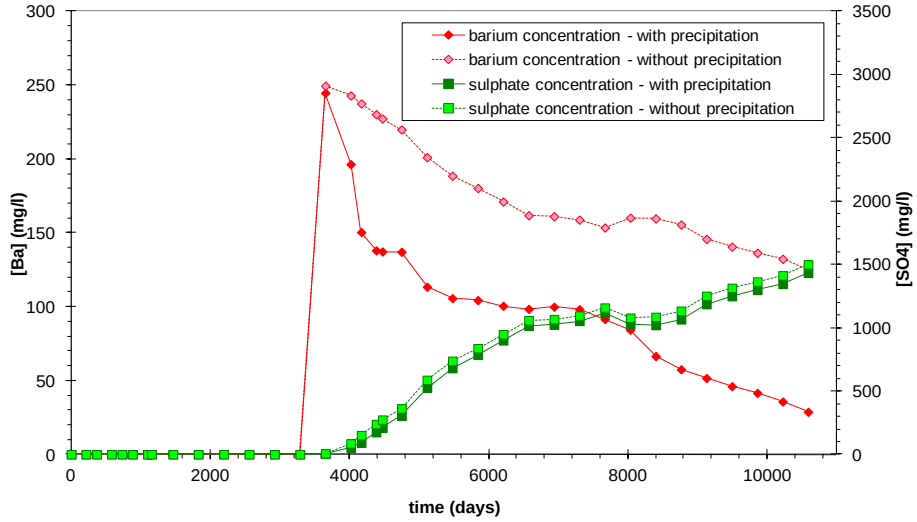

Figure 6.35: Barium and sulphate production with instantaneous precipitation and without precipitation as a function of time for well B3.

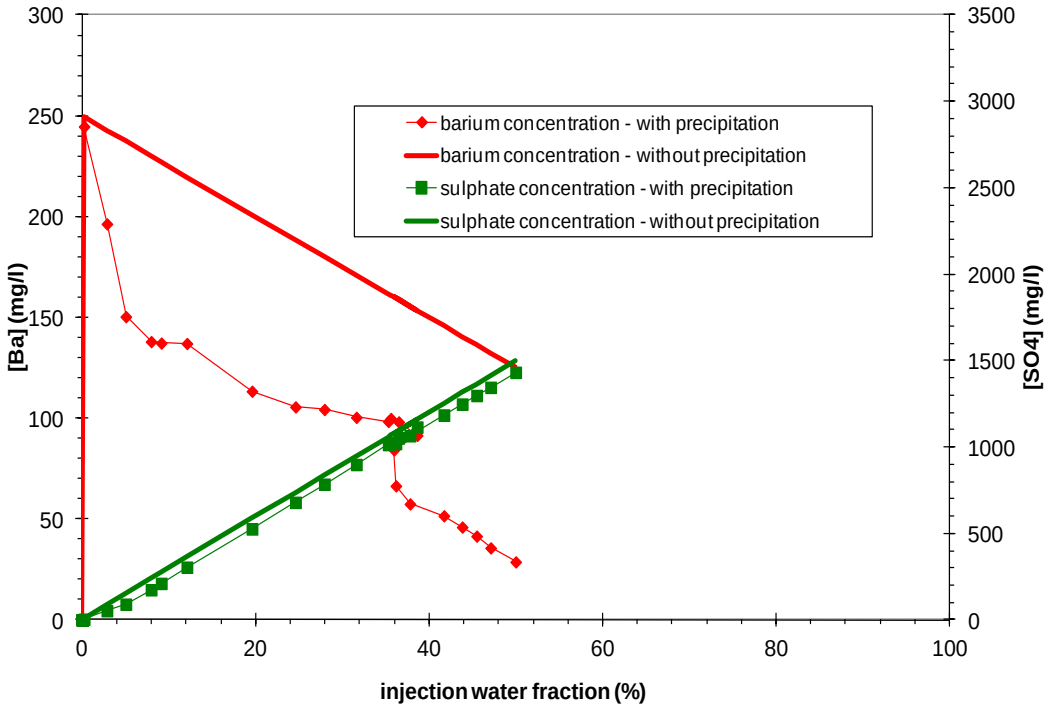

Figure 6.36: The produced concentration of barium and sulphate ions as a function of the produced fraction of sea for well B3.

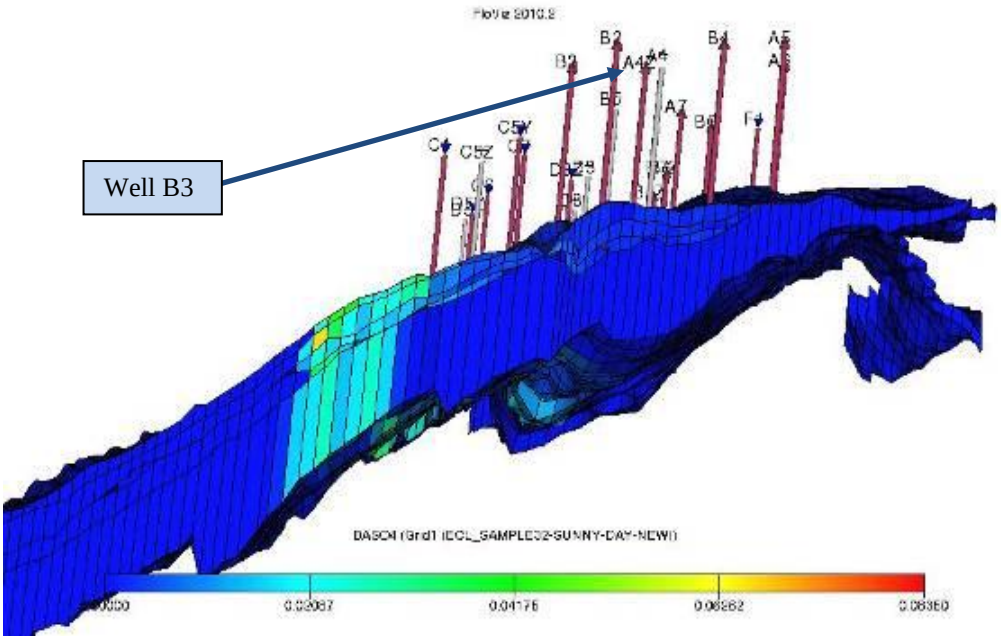

Figure 6.37: The 3D section of Field X indicates $BaSO_4$ location for well B3.

Well B6 Results:-

Figure 6.38 shows the results for well B6 with the water production rate in (bbl/day) (blue, left hand vertical axis) and the fraction of the injected sea water (green, right hand vertical axis) versus time (days) on the X axis. Again we observe that water and the sea water breakthrough occurred at the same time and the sea water fraction sharply increased to over 75%. Figure 6.39 indicates the barium with precipitation increased and reached the maximum value around 5000 days and decreased to zero after 800 days till the end of the simulation period. It is unusual behavior for the sea water to start to increase and decrease suddenly and reach 85 % by the end of the simulation period.

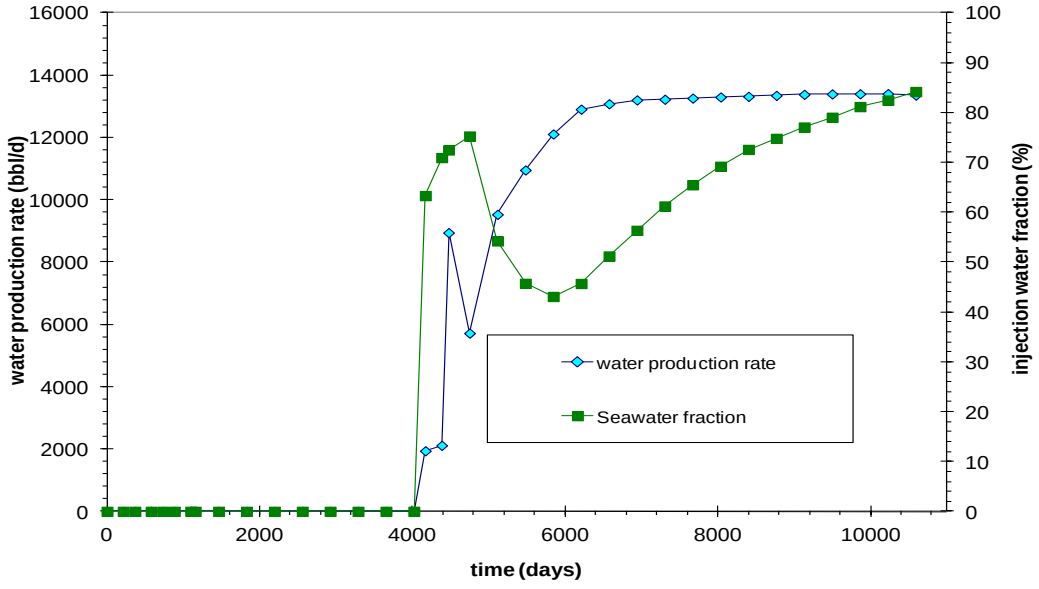

Figure 6.38: Water production rate and percentage of the injected water produced as a function of time for well B6

Figure 6.39 and 6.40 show very unusual behavior in this well. Prior to seawater breakthrough there is almost no water production, and when seawater breakthrough does occur the seawater fraction is above 60%. At this time there is no barium being produced. Moreover, the water production rate decreases temporarily (Figure 6.38) , and this is followed by a reduction in seawater fraction to about 40 % . As this happens the barium levels rise to about 100 mg/l. It is very unusual to observe seawater fraction decreasing and barium raising this could be due to the connected injector being closed, allowing more formation water to reach to the producer.

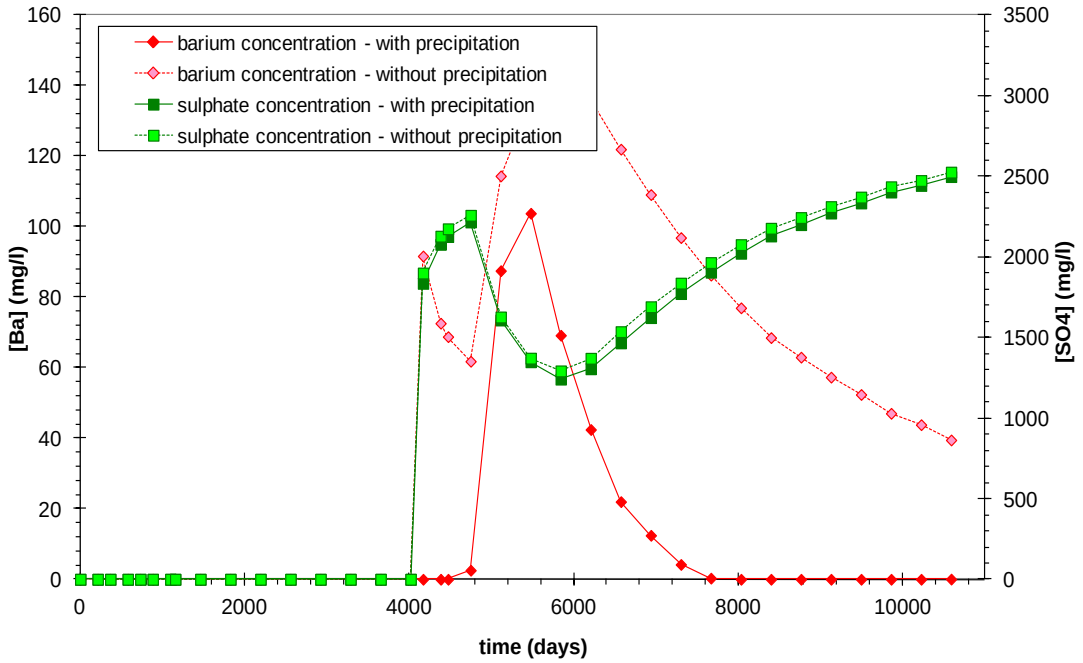

Figure 6.39: Barium and sulphate production with instantaneous precipitation and without precipitation as a function of time for well B6.

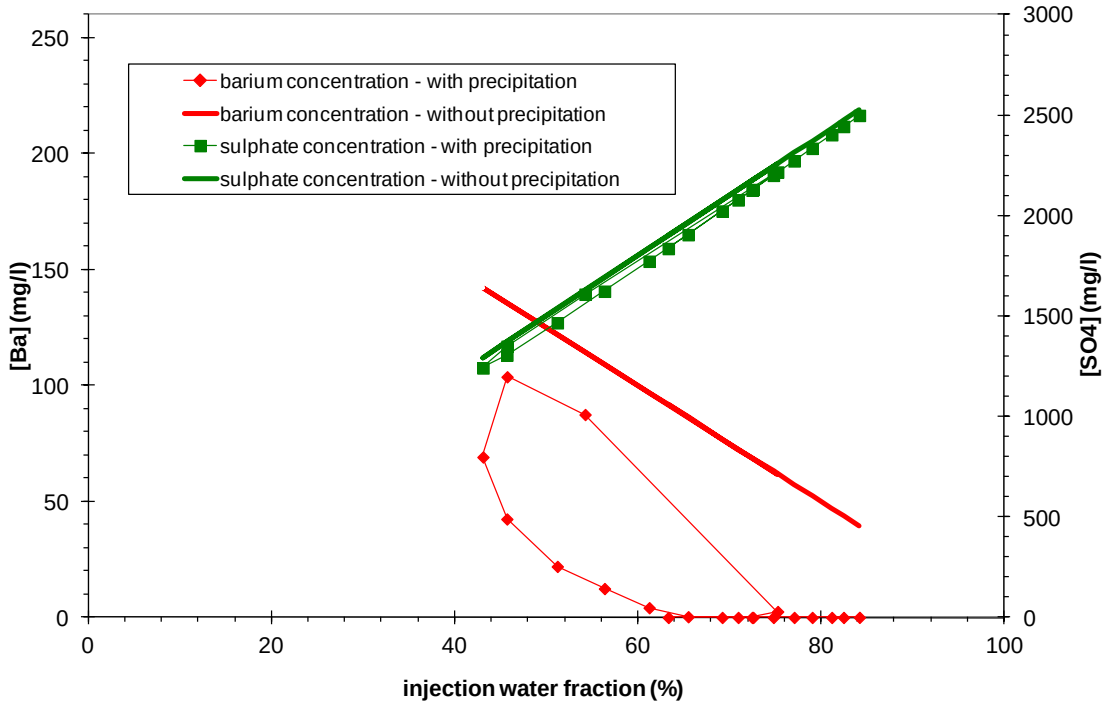

Figure 6.40: The produced concentration of barium and sulphate ions as a function of the produced fraction of sea water for well B6.

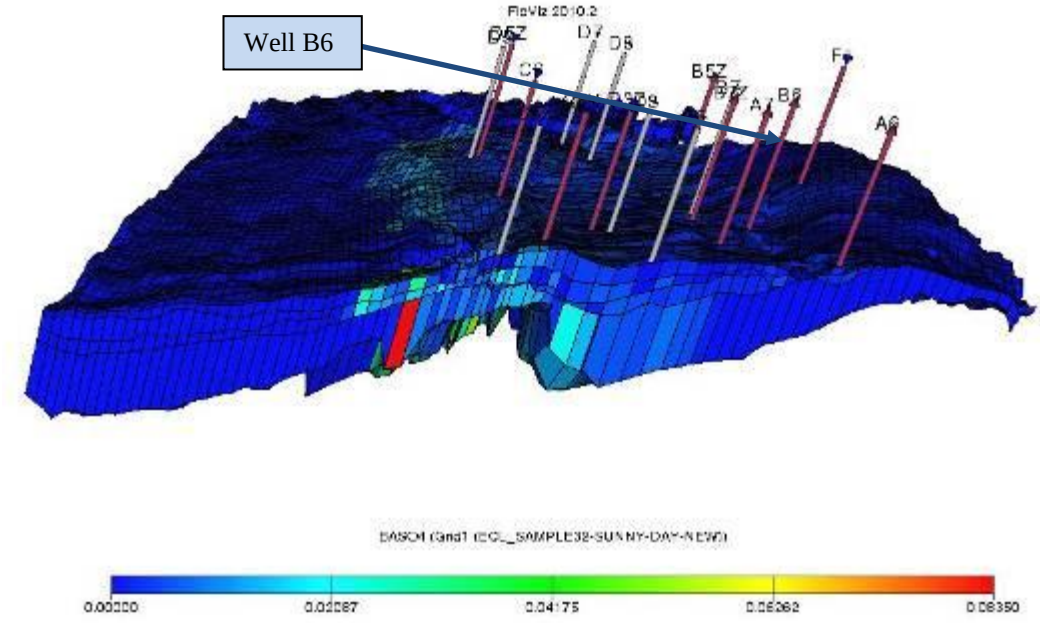

Figure 6.41: The 3D section of field-X indicates $Baso_4$ location for well B6.

This suggests water breakthrough in different layers, quite possibly in different direction, this new water reaching the wellbeing formation water that has not previously conducted seawater. Clearly much caution is required in handling this well. No $BaSO_4$ problems would be expected, and yet after a couple of years the scaling tendency will rise, with up to 100 mg/l of barium being co-produced with 1000 mg/l of sulphate before it eventually decreases again.

Well B7 Results:-

Figure 6.42 shows the results of well B7 with the water production rate in (bbl/day) (blue, left hand vertical axis) and the fraction of the injected sea water (green, right hand vertical axis) versus time (days) on the X axis. As we can observe in Figure 6.42, the water breakthrough started a little earlier than sea water breakthrough. It seems that the well was shut in after 4000 days. Figure 6.43 indicates that when 45% sea water fraction was reached the barium concentration then dropped to zero but it rose to 30 mg/l after that which could contribute toward unexpected scale problems. Figure 6.46 indicates that there is a high permeability streak which could be what causes this change.

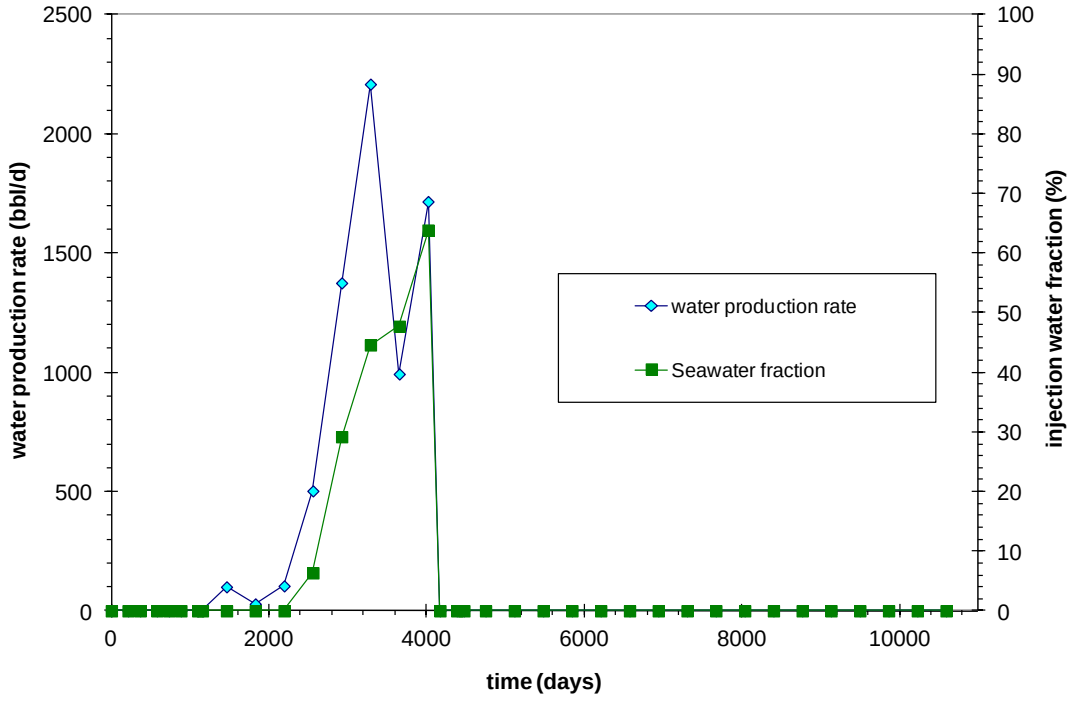

Figure 6.42: Water production rate and percentage of the injected water produced as a function of time for well B7.

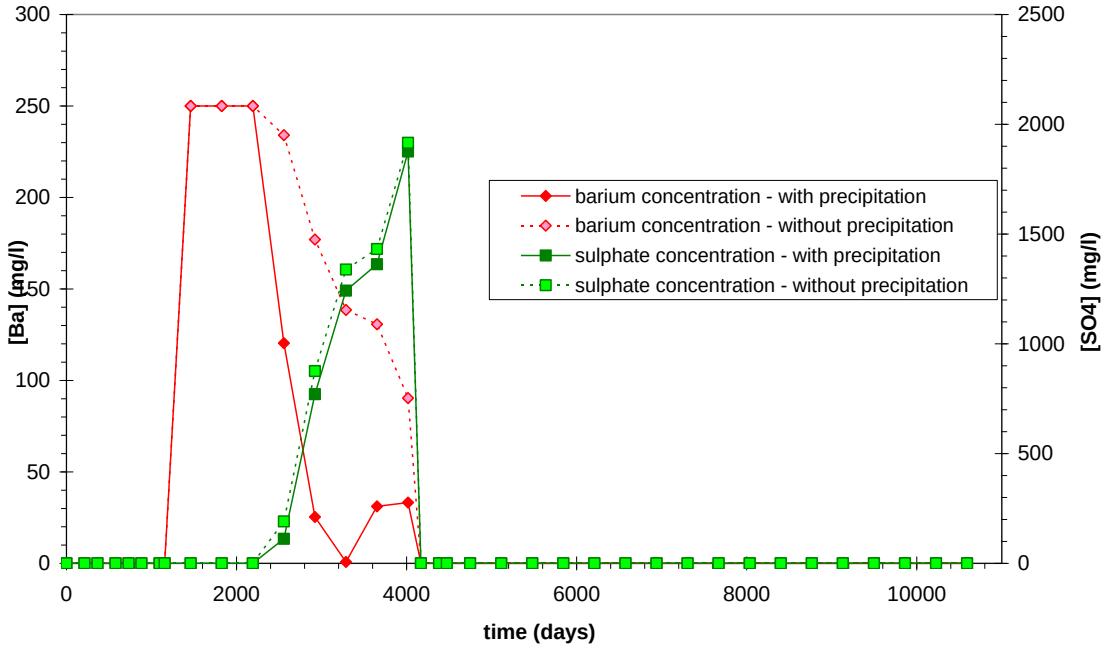

Figure 6.43: Barium and sulphate production with instantaneous precipitation and without precipitation as a function of time for well B7.

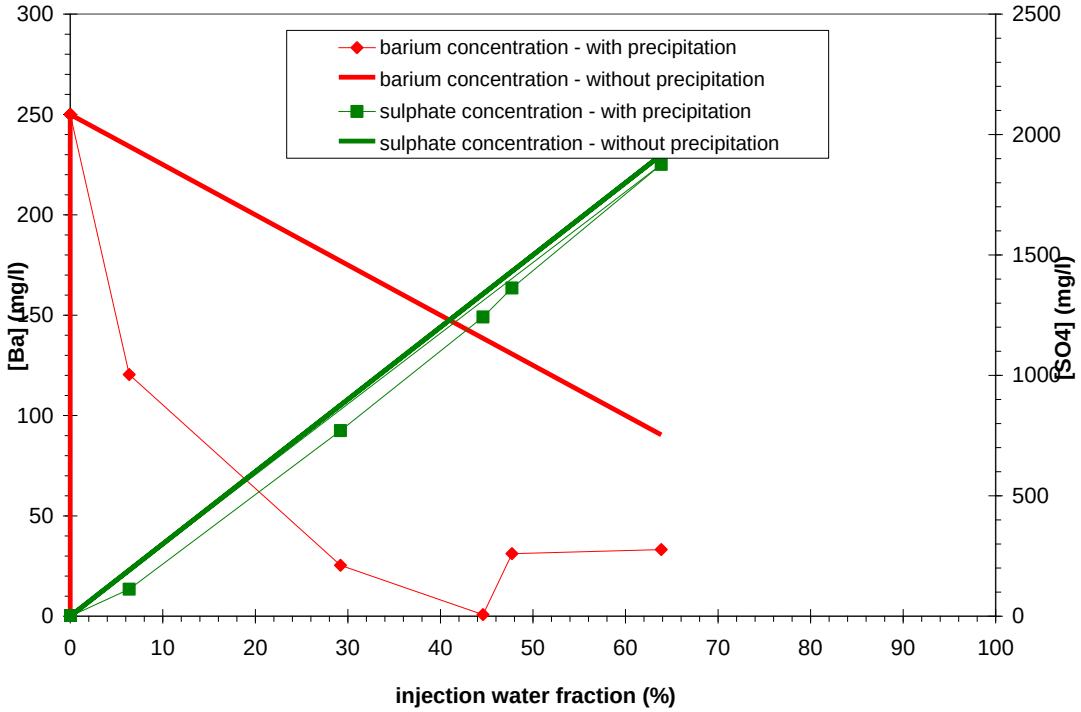

Figure 6.44: The produced concentration of barium and sulphate ions as a function of the produced fraction of sea water for well B7.

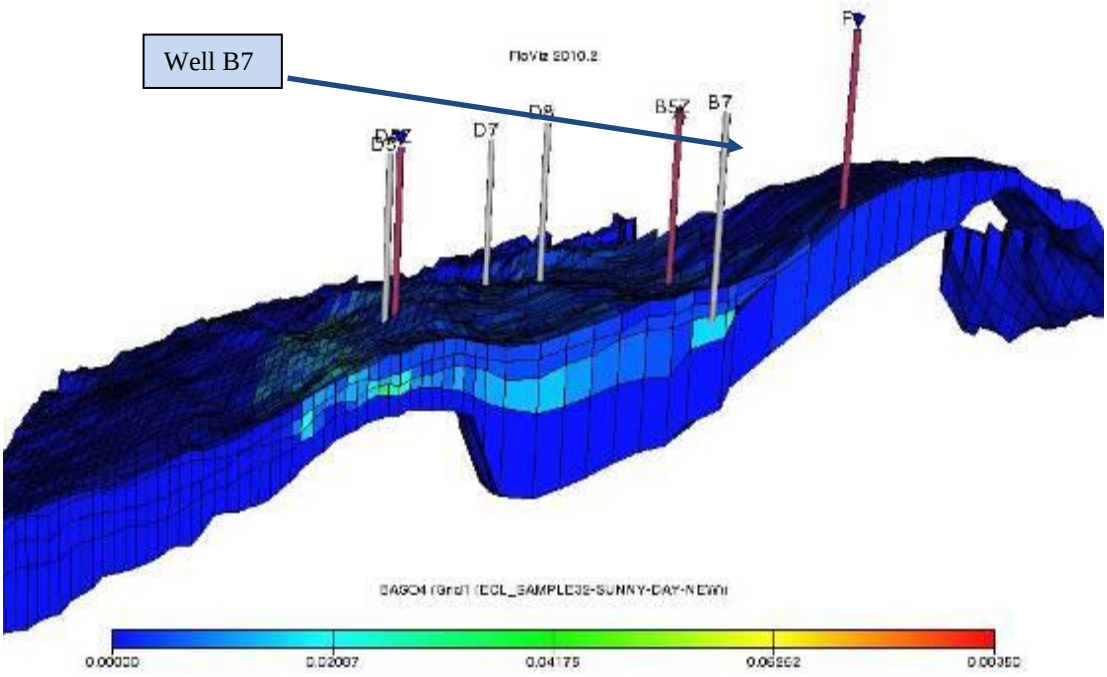

Figure 6.45: The 3D section of Field X indicates $BaSO_4$ location for well B7.

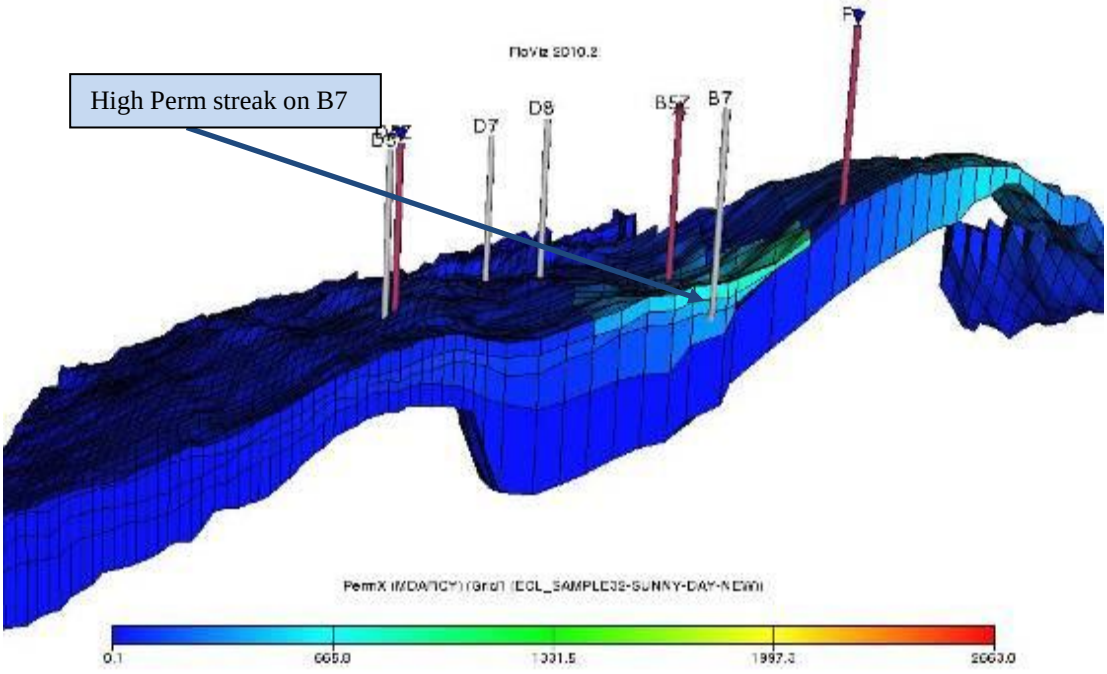

Figure 6.46: The 3D section of Field X indicates a high permeability streak for well B7.

Well D6 Results:-

Figure 6.47 shows the results of well D6 with the water production rate in (bbl/day) (blue, left hand vertical axis) and the fraction of the injected sea water (green, right hand vertical axis) versus time (days) on the X axis. As we can observe in Figure 6.47, the produced water was mainly from the aquifer and is observed within one year. Only after 8000 days do we start to see sea water breakthrough. Figure 6.48 shows that the barium concentration is high and has a constant value which is close to 250 mg/l and after7000 days does the barium concentration start to decrease, although the sea water fraction was still very low and that means no reaction would be occurring in the well. In this situation the operator would have to keep in mind that there is a scale risk and it is a warning that there is sea water coming in and action has to be taken to apply some squeeze jobs to maintain the well so that there is no scaling towards the end of the well's life .

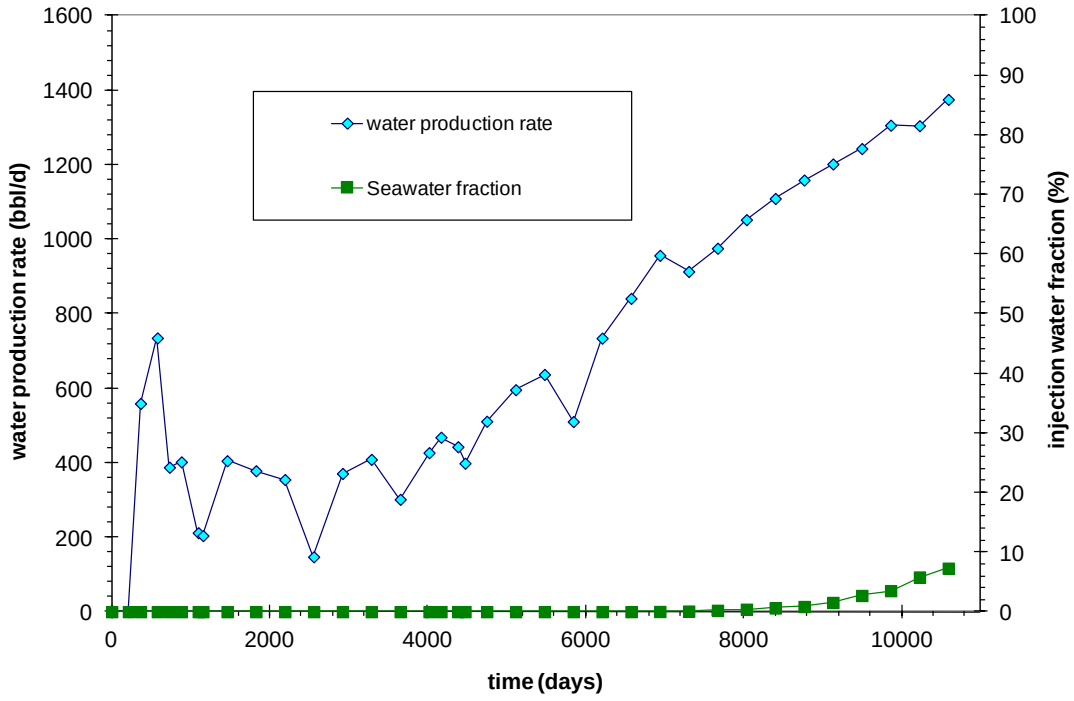

Figure 6.47: Water production rate and percentage of the injected water produced as a function of time for well D6. Production of water from years before sweater injection indicate the impact of aquifer water production.

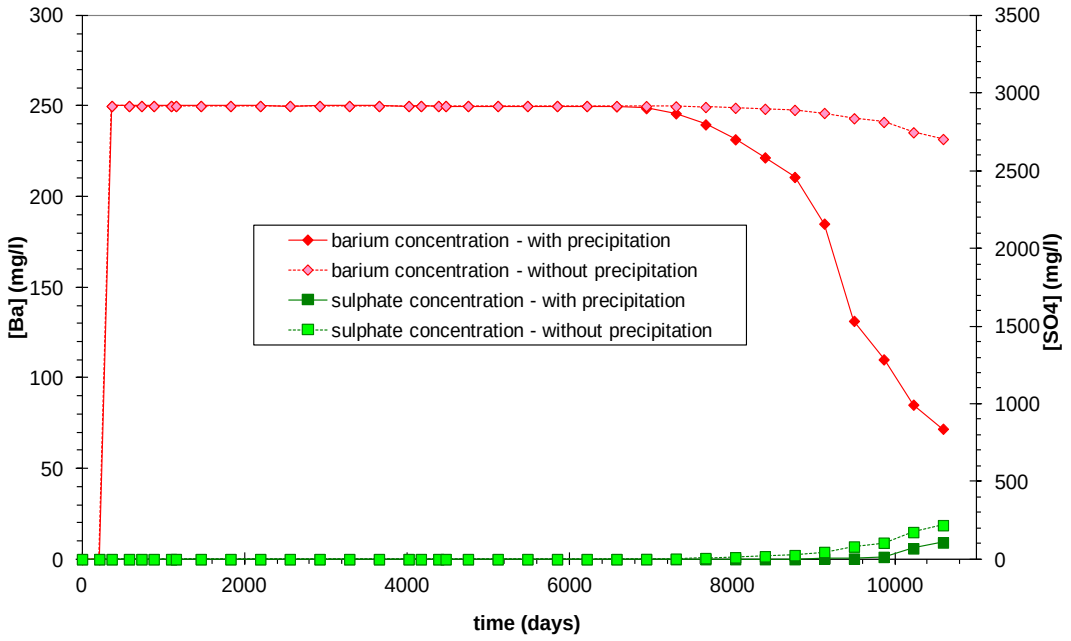

Figure 6.48: Barium and sulphate production with instantaneous precipitation and without precipitation as a function of time for well D6.

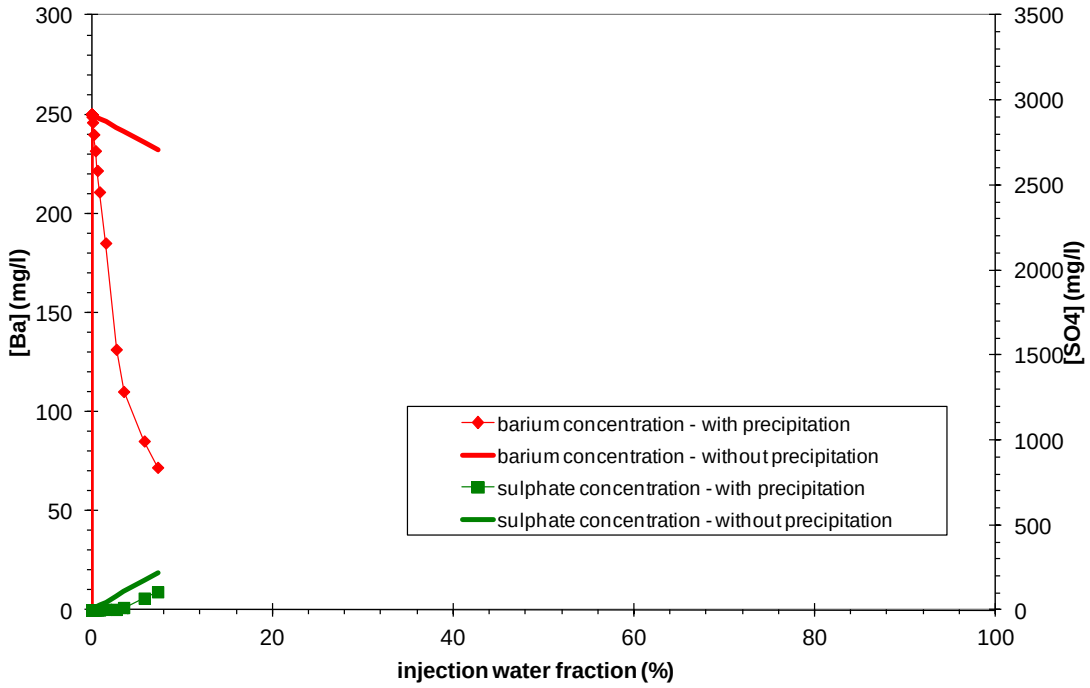

Figure 6.49: The produced concentration of barium and sulphate ions as a function of the produced friction of seawater for well D6.

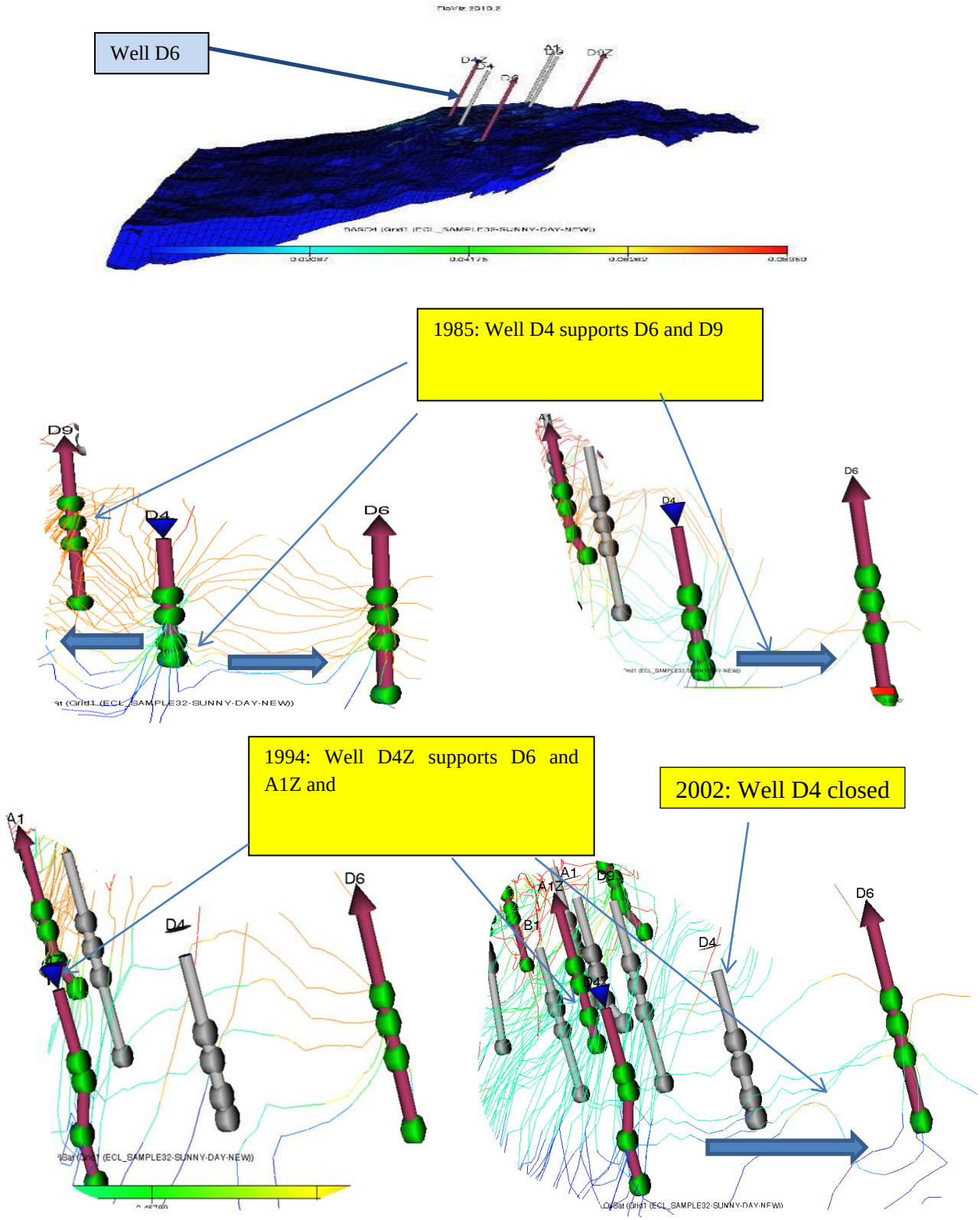

Figure 6.50: Top diagram: location of Well D6. Lower diagrams illustrate streamlines surrounding Wells D6, D9, and D4.

The well D6 was put on production since 1983, and was located in the transition zone, close to the Aquifer. At the beginning of the well life the well was supported by the aquifer since day one; in 1985 after 700 days the well D4 was converted from a producer to an injector to support both D6 and D9 wells, which it did until Jan 1989 which after 2200 days. In Jan 1990 after 2500 days from the production , the well D9 closed due the economic limits and D4 continuing to support D6 and A1Z. In Jan 1991after 3000 days, D4 stopped supporting D6 but was still in contact with A1Z; in 1992 after 3200 days there was little contribution from D4 to D6, in Jan 1994 D4 was shut down and there was not any more support for D6 and thus D6 received its support from the aquifer. Thereafter the well D4Z injector was developed and started to support the well D6, in 2002after 8000 days the seawater starts to increase following water breakthrough.

6.4 IMPACT OF VARYING THE FORMATION WATER BARIUM CONCENTRATION

The following figures show the results for well-A1Z of different concentrations of barium, ranging through 45, 80, 229, 250 and 800 mg/l. All the figures indicate that the barium levels were constant till 6000 days, before seawater breakthrough. Furthermore, after this period the barium started to decrease and the sea water fraction started to increase. Figure 6.51 and Figure 6.52 show that with precipitation barium concentration fell to zero by the end of the simulation interval for the initial barium concentration at 45 and 80 mg/l. However Figure 6.53 and Figure 6.54 indicate that the barium concentration remains above 10 mg/l by the end of the simulation period when the initial barium concentration was 229 or 250 mg/l. Figure 6.55 shows that by end of the simulation period the barium concentration remain above 120 mg/l when the initial barium concentration was 800 mg/l.

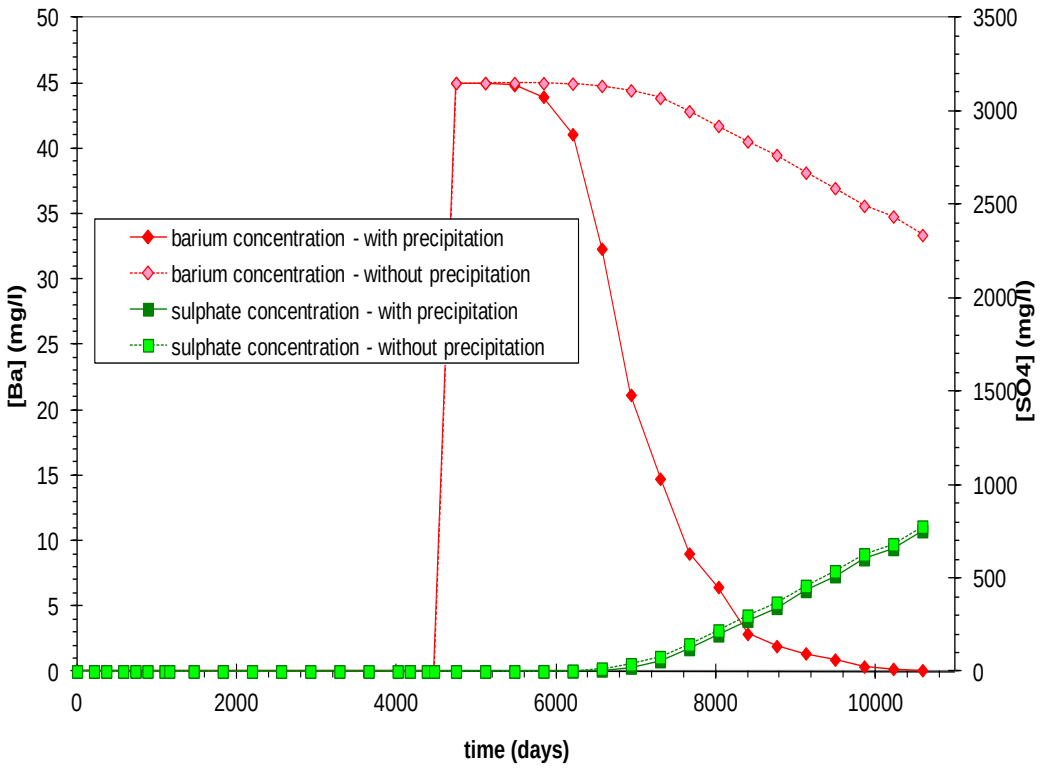

Figure 6.51: Barium and sulphate production with instantaneous precipitation and without precipitation as a function of time for well A1Z, with initial formation water barium concentration set to 45 mg/l.

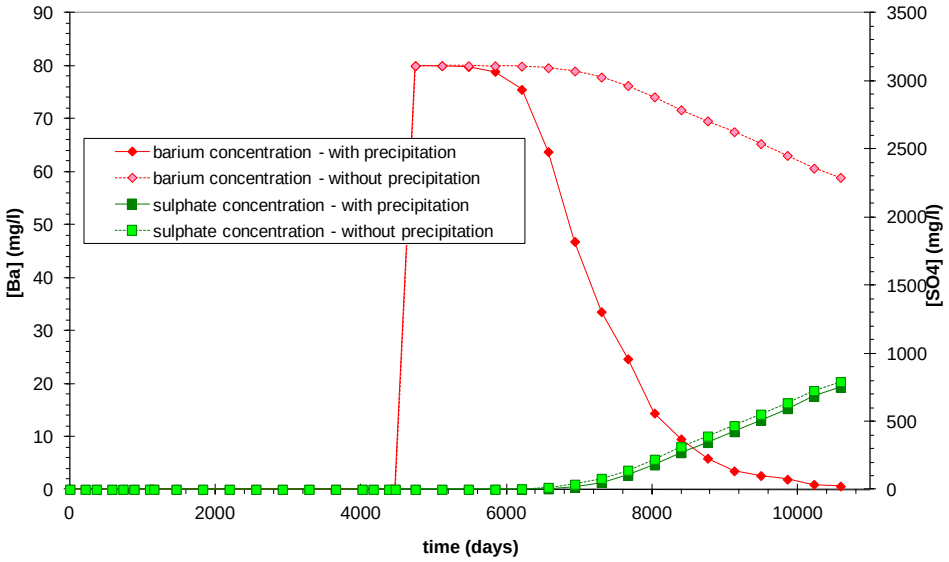

Figure 6.52: Barium and sulphate production with instantaneous precipitation and without precipitation as a function of time for well A1Z, with initial formation water barium concentration set to 80 mg/l.

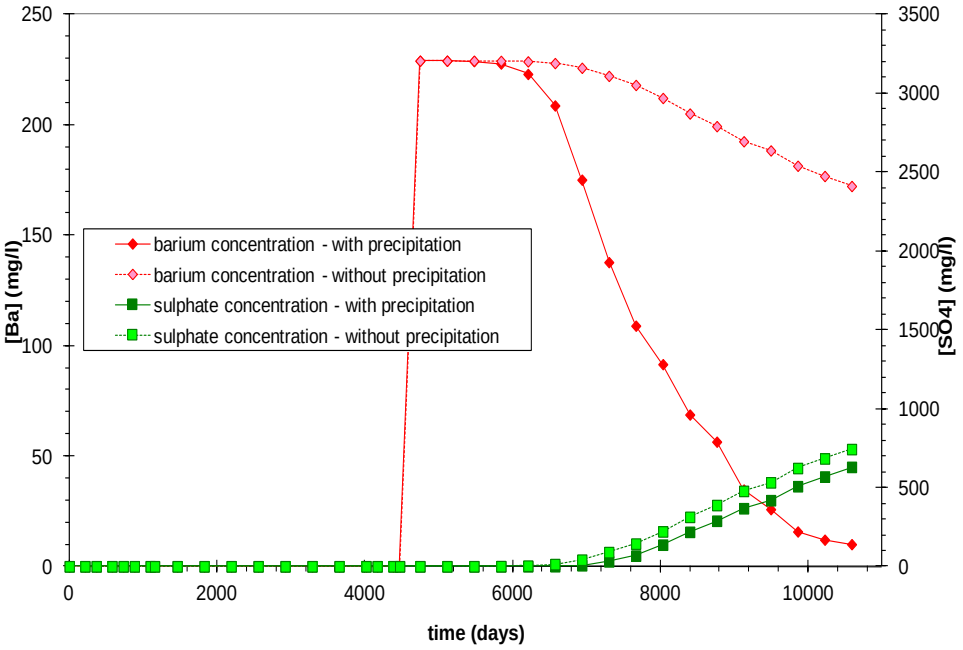

Figure 6.53: Barium and sulphate production with instantaneous precipitation and without precipitation as a function of time for well A1Z, with initial formation water barium concentration set to 229 mg/l.

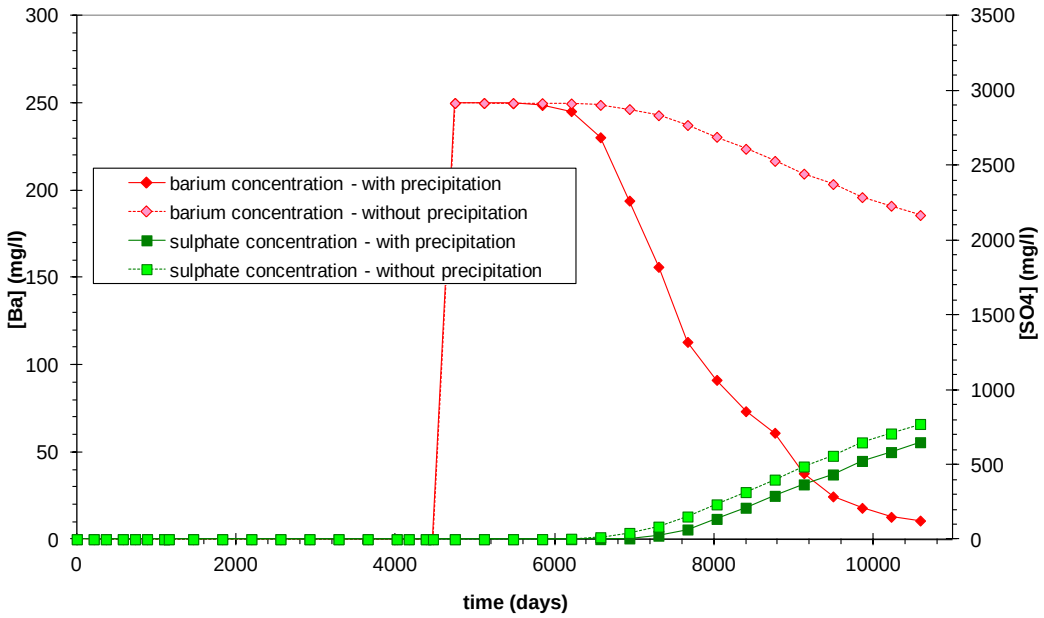

Figure 6.54: Barium and sulphate production with instantaneous precipitation and without precipitation as a function of time for well A1Z, with initial formation water barium concentration set to 250 mg/l.

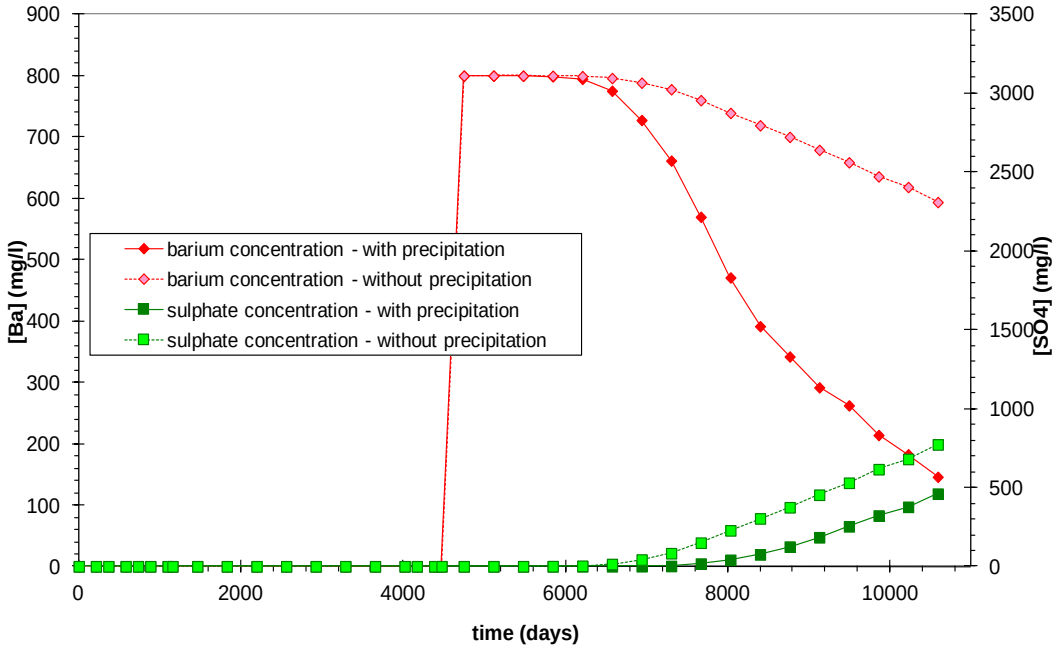

Figure 6.55: Barium and sulphate production with instantaneous precipitation and without precipitation as a function of time for well A1Z, with initial formation water barium concentration set to 800 mg/l.

Well A5:-

The following figures show the results for well A5 for different concentrations of barium; 45, 80, 229, 250 and 800 mg/l in contrast of well A1Z. All the figures indicate that the barium dropped to zero after 400 days and remained zero till the end of the simulation period for Well A5. Furthermore, it is observed that the sulphate before and after precipitation remained the same in all different concentrations of barium, with sulphate concentration ultimately reading 2900 mg/l. The main contribution to the produced water was mainly from the injected sea water not from aquifer water. Therefore, the different barium concentrations in this case did not change much the results, primarily because the well is in the oil leg and far away from water oil contact.

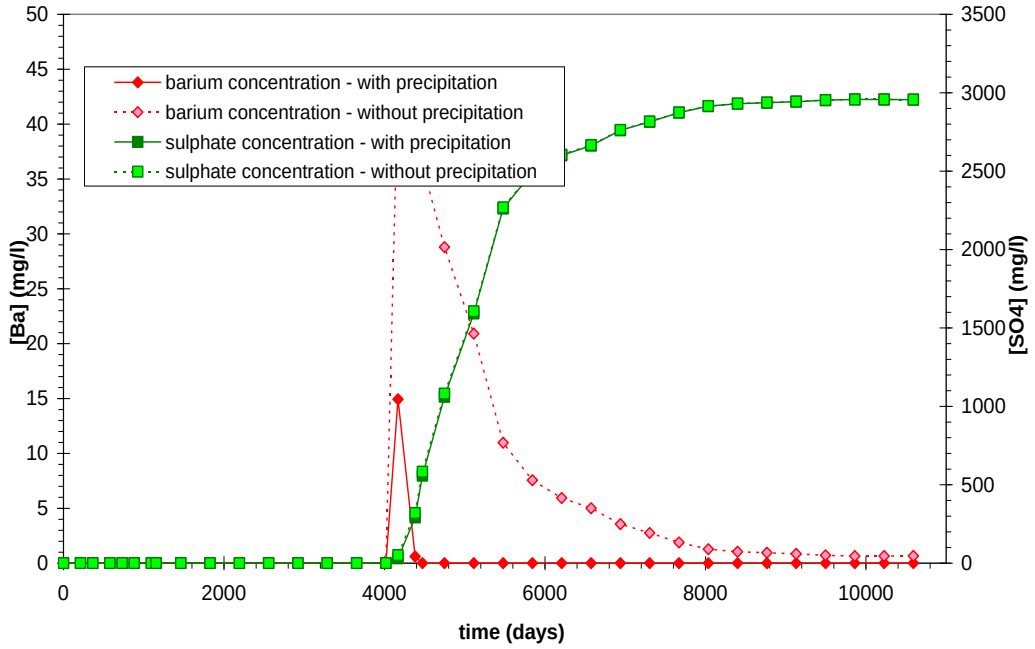

Figure 6.56: Barium and sulphate production with instantaneous precipitation and without precipitation as a function of time for well A5 with initial formation water barium concentration set to 45 mg/l.

.

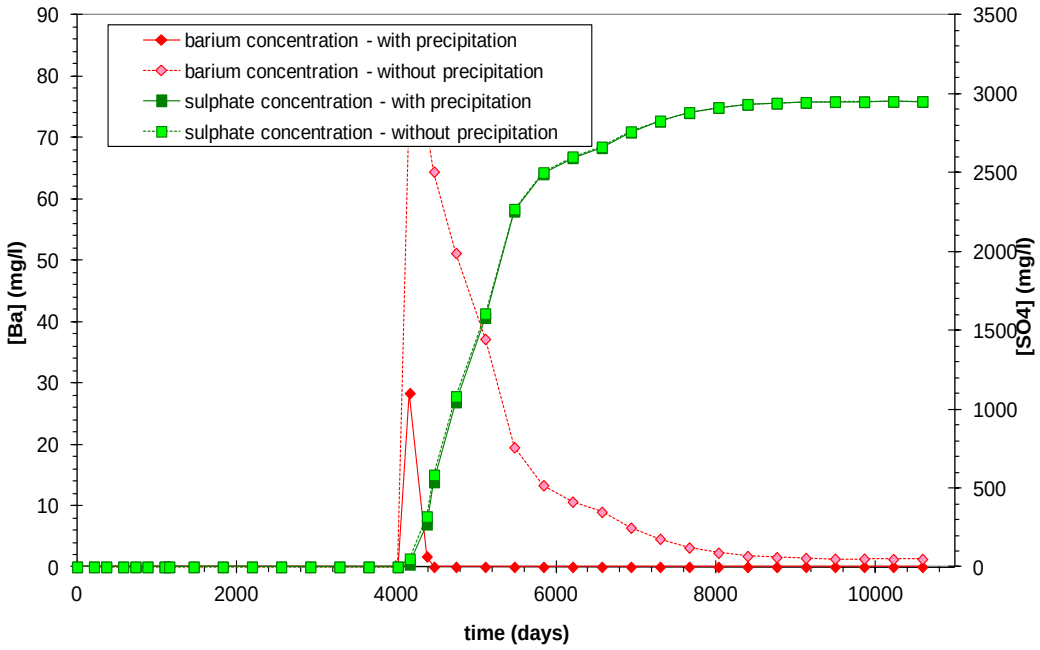

Figure 6.57: Barium and sulphate production with instantaneous precipitation and without precipitation as a function of time for well A5 with initial formation water barium concentration set to 80 mg/l.

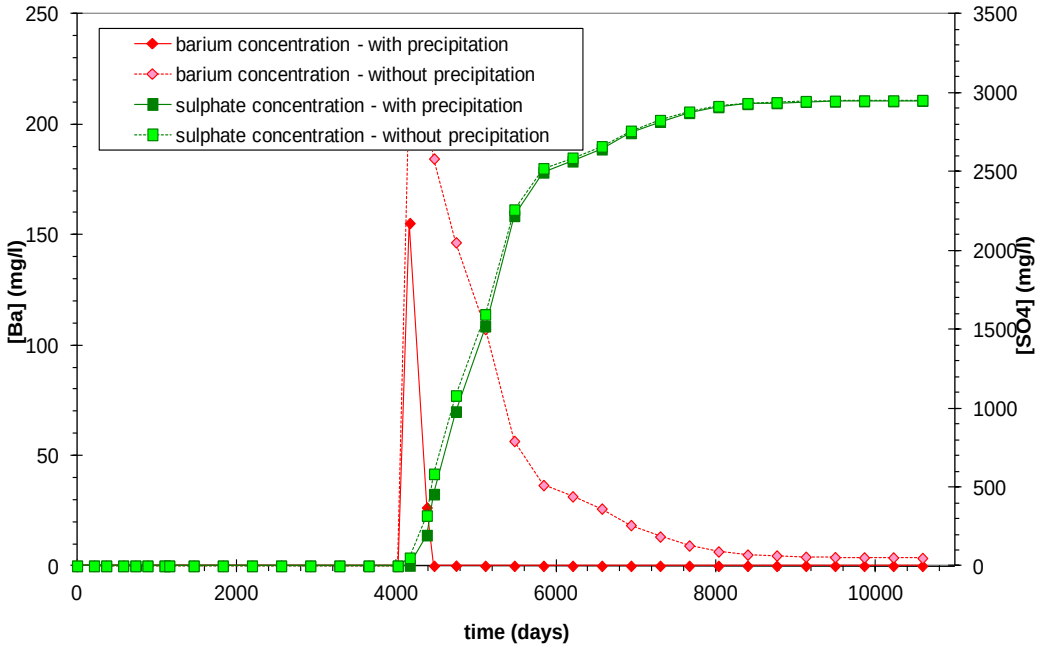

Figure 6.58: Barium and sulphate production with instantaneous precipitation and without precipitation as a function of time for well A5 with initial formation water barium concentration set to 229 mg/l.

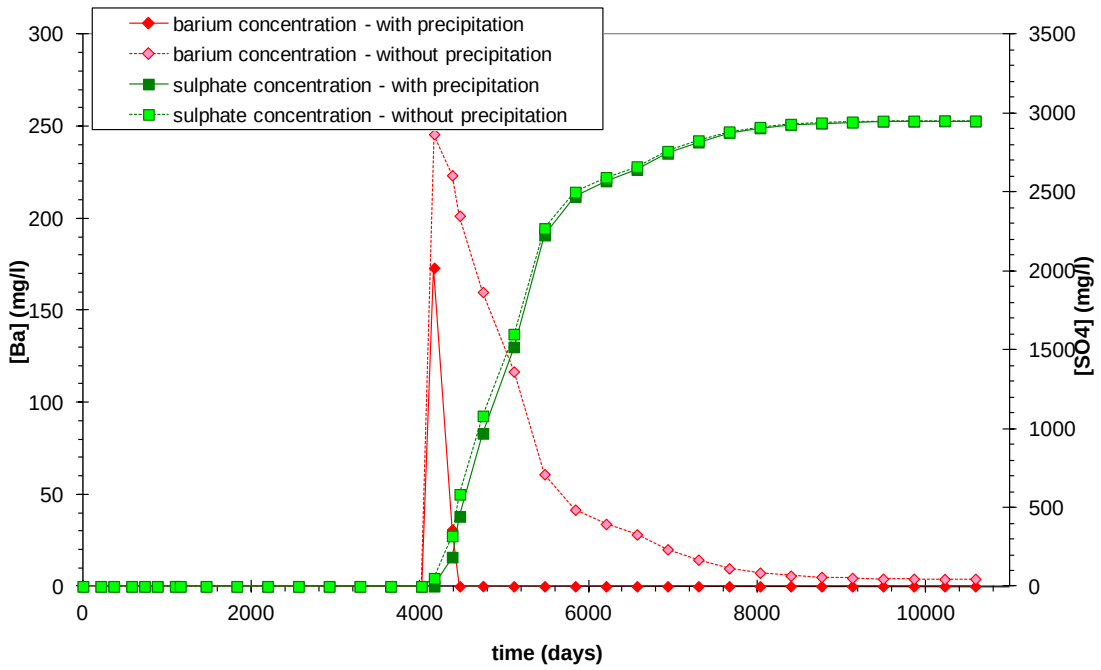

Figure 6.59: Barium and sulphate production with instantaneous precipitation and without precipitation as a function of time for well A5 with initial formation water barium concentration set to 250 mg/l.

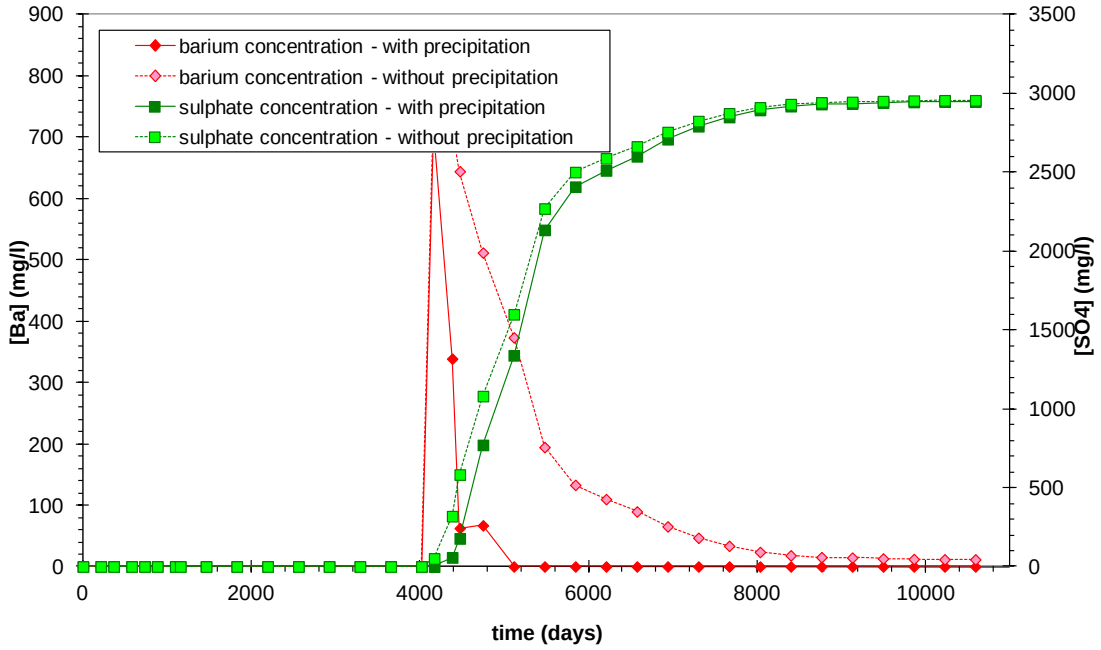

Figure 6.60: Barium and sulphate production with instantaneous precipitation and without precipitation as a function of time for well A5 with initial formation water barium concentration set to 800 mg/l.

WELL B5-Z

The following figures are the results of well B5-Z for different concentrations of barium; 45, 80, 229, 250 and 800 mg/l. All the figures indicate that after precipitation the barium dropped to a low level after 400 days and dropped to zero after 5000 days until the end of the simulation period. It is observed that before and after precipitation the sulphate is the same for all different concentrations of barium. The main contribution to the produced water was mainly from the injected sea water and not from the aquifer water. Therefore, the different barium concentrations in this case did not change much the results, because the well is in the oil leg and far away from water oil contact.

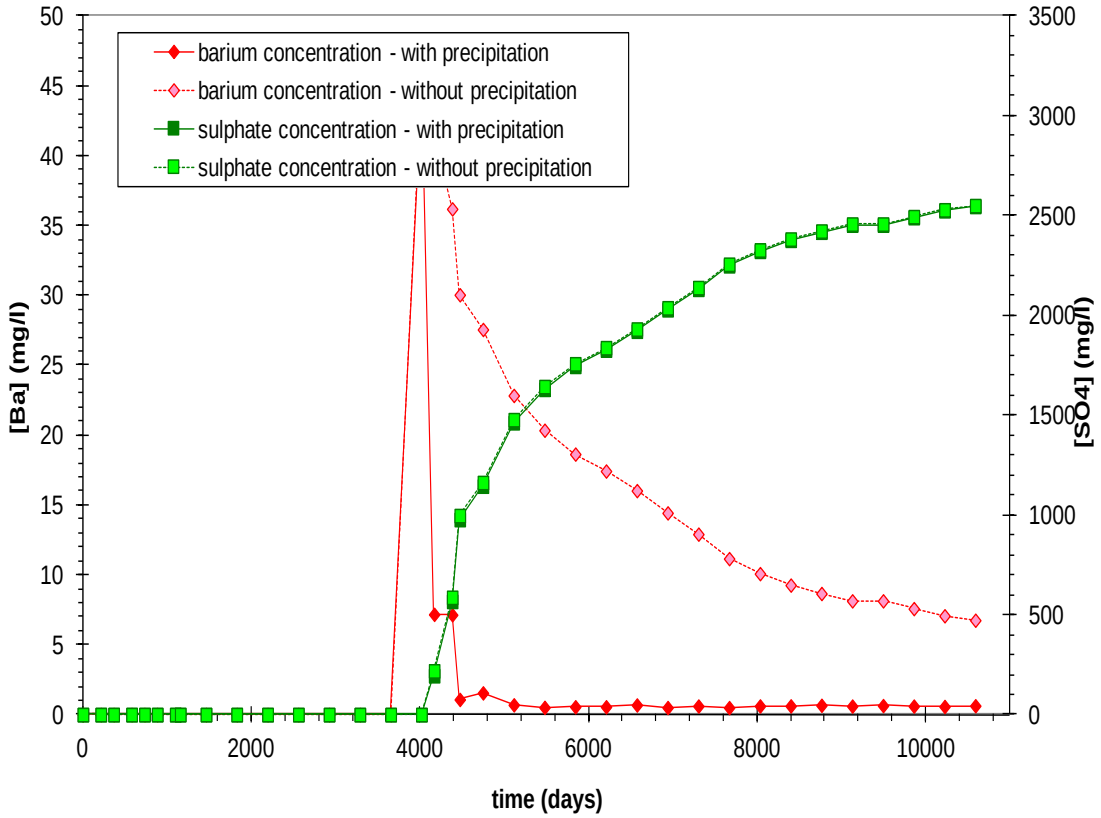

Figure 6.61: Barium and sulphate production with instantaneous precipitation and without precipitation as a function of time for well B5-Z with initial formation water barium concentration set to 40 mg/l.

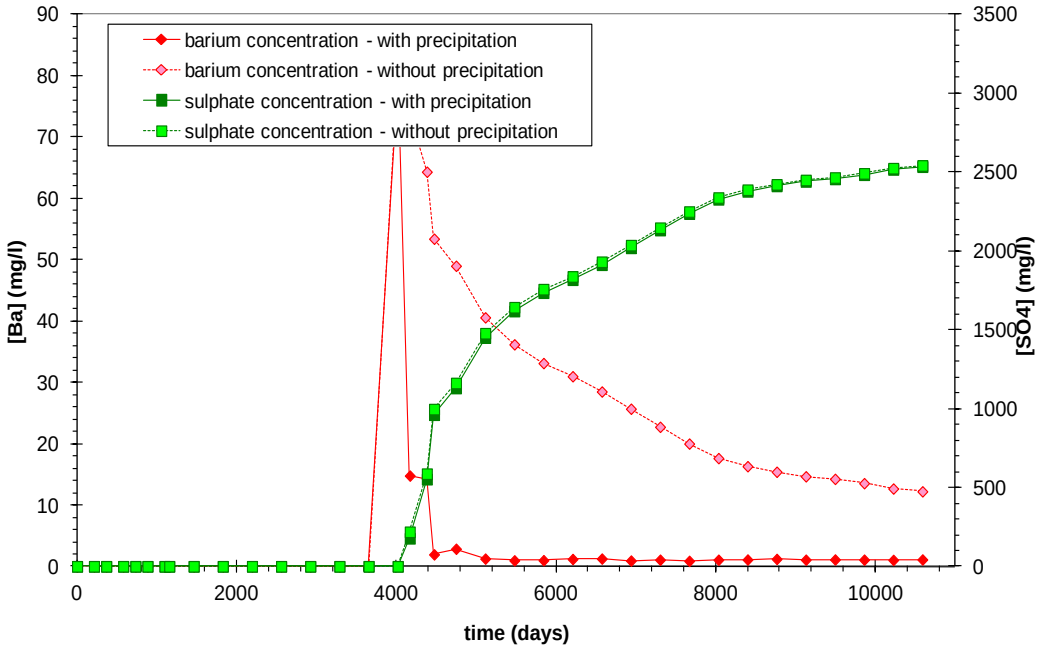

Figure 6.62: Barium and sulphate production with instantaneous precipitation and without precipitation as a function of time for well B5-Z with initial formation water barium concentration set to 80 mg/l.

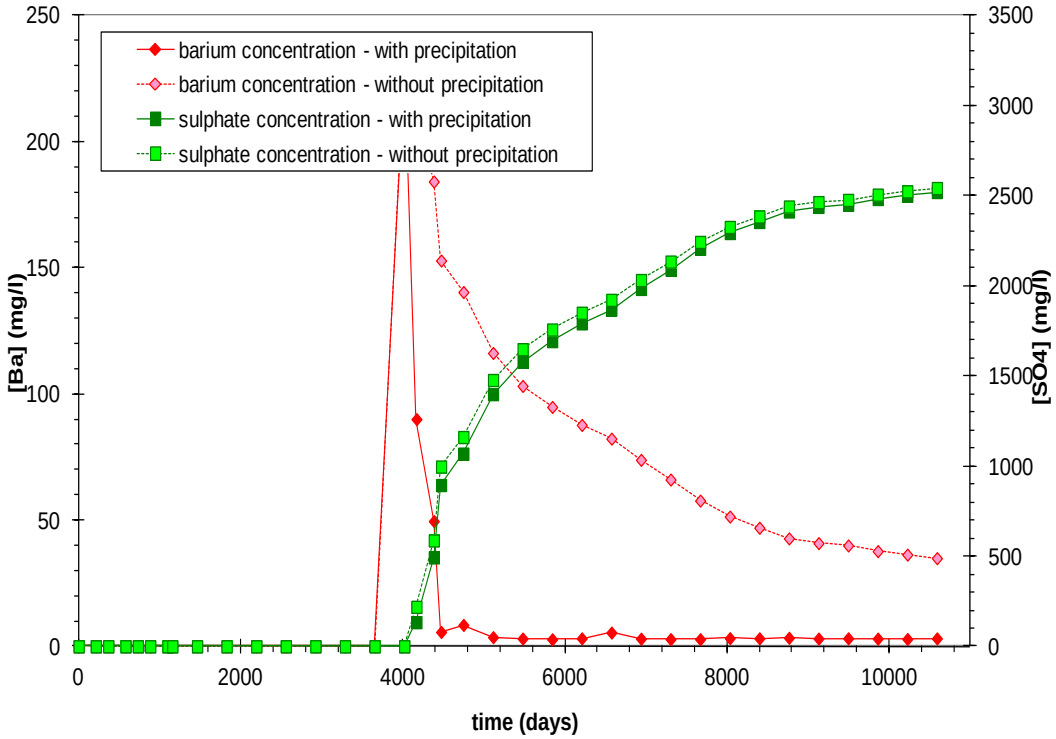

Figure 6.63: Barium and sulphate production with instantaneous precipitation and without precipitation as a function of time for well B5-Z with initial formation water barium concentration set to 229 mg/l.

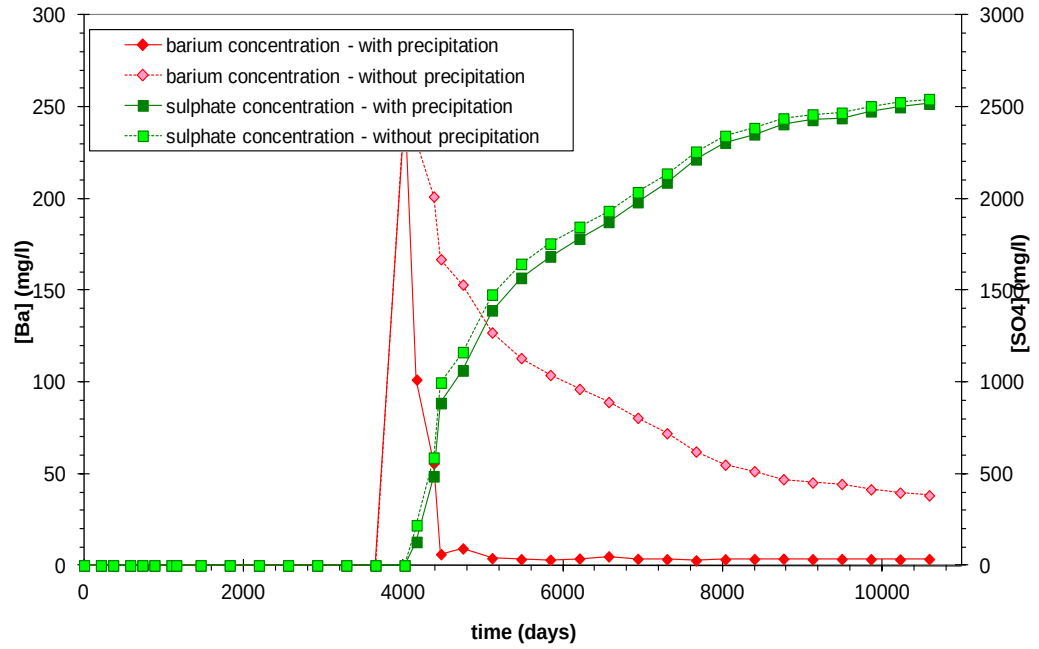

Figure 6.64: Barium and sulphate production with instantaneous precipitation and without precipitation as a function of time for well B5-Z with initial formation water barium concentration set to 250 mg/l.

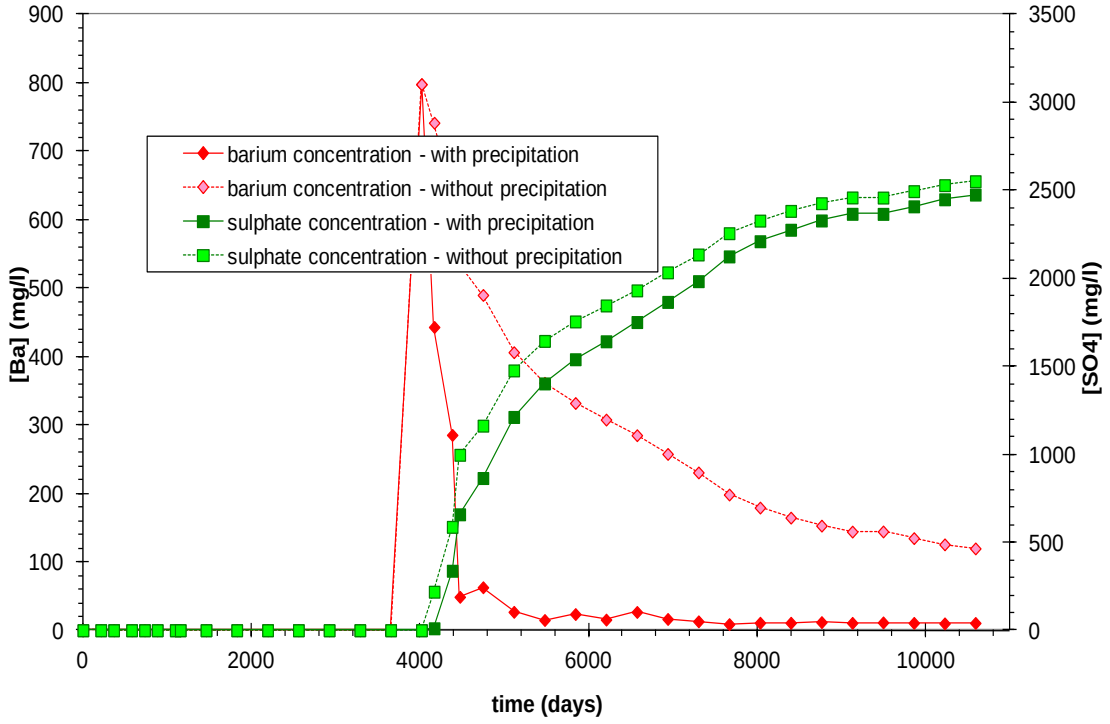

Figure 6.65: Barium and sulphate production with instantaneous precipitation and without precipitation as a function of time for well B5-Z with initial formation water barium concentration set to 800 mg/l.

WELL D9-Z

The following figures are the results for well D9-Z for different concentrations of barium; 45, 80, 229, 250 and 800 mg/l. All the figures indicate after seawater breakthrough the barium increased and then dropped to zero very rapidly in the interval from 6000 days up to 8000 days. However, it is observed that in the case with barium concentration levels of 800 mg/l, there was significant sulphate depletion of around 200 mg/l.

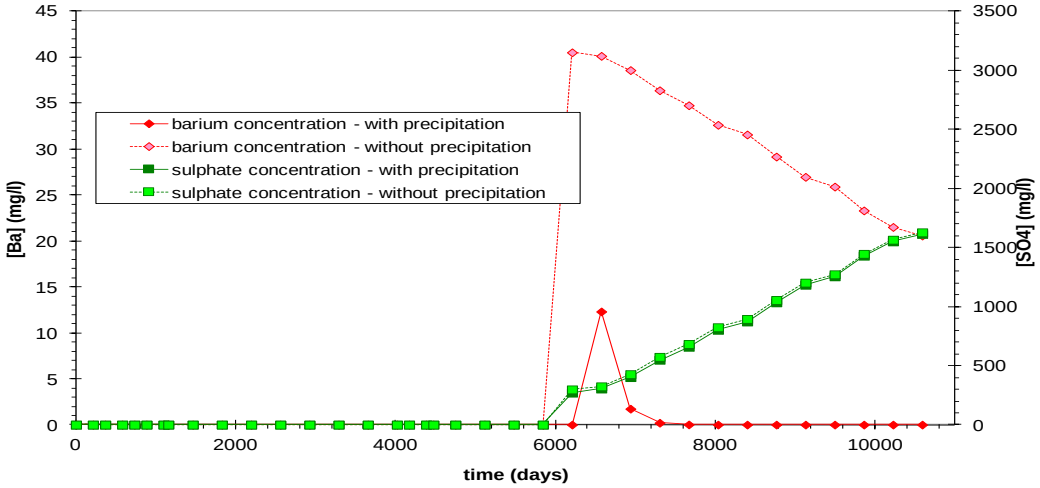

Figure 6.66: Barium and sulphate production with instantaneous precipitation and without precipitation as a function of time for well D9-Z with initial formation water barium concentration set to 45 mg/l.

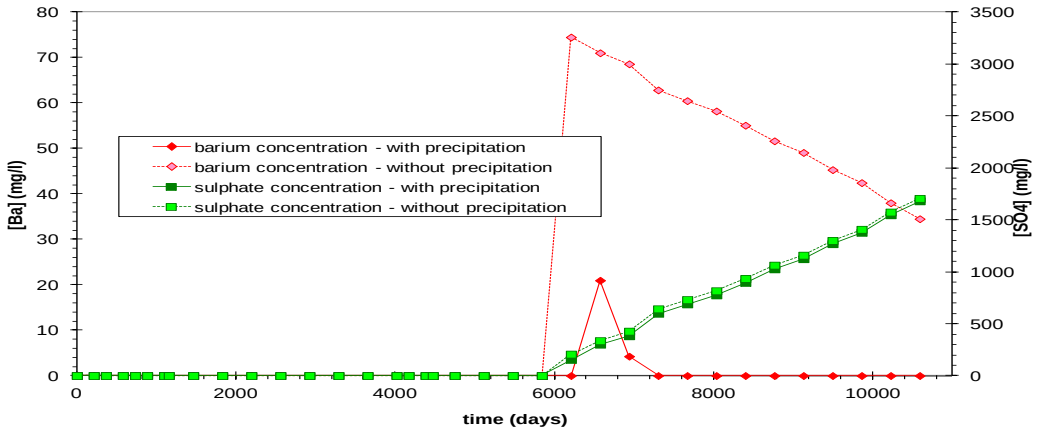

Figure 6.67: Barium and sulphate production with instantaneous precipitation and without precipitation as a function of time for well D9-Z with initial formation water barium concentration set to 80 mg/l.

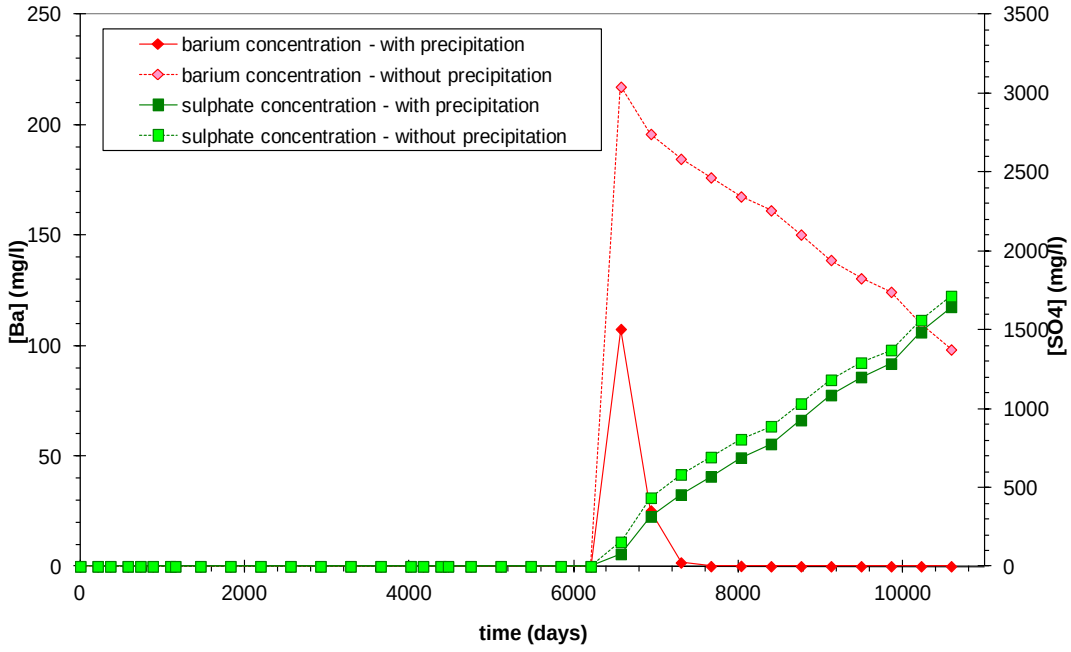

Figure 6.68: Barium and sulphate production with instantaneous precipitation and without precipitation as a function of time for well D9-Z with initial formation water barium concentration set to 229 mg/l.

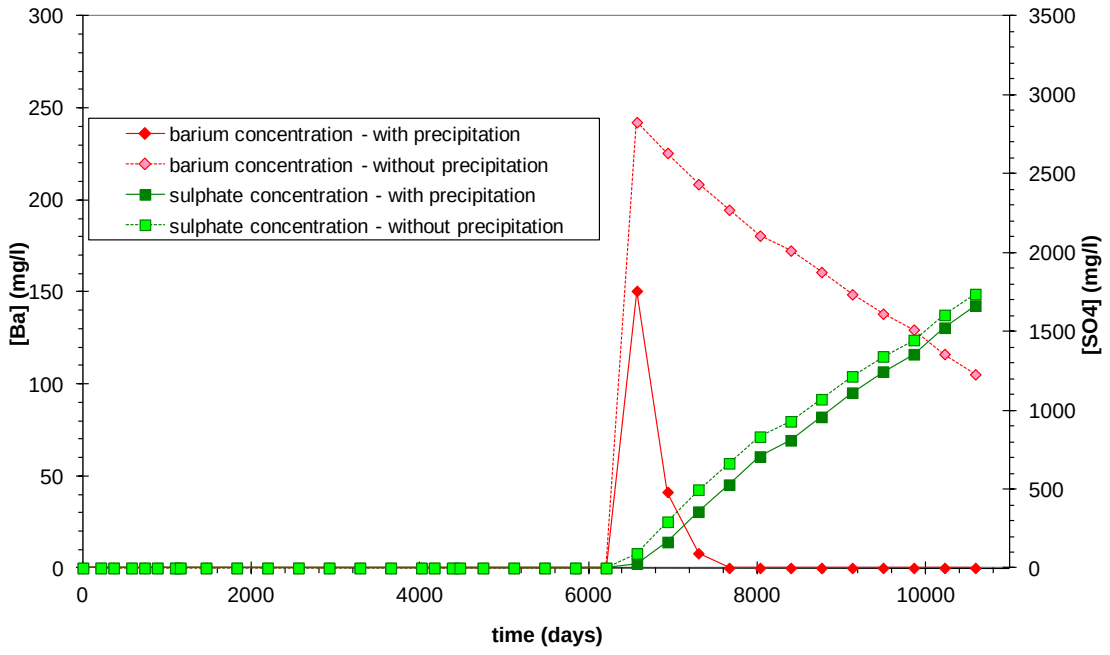

Figure 6.69: Barium and Sulphate production with instantaneous precipitation and without precipitation as a function of time for well D9-Z with initial formation water barium concentration set to 250 mg/l.

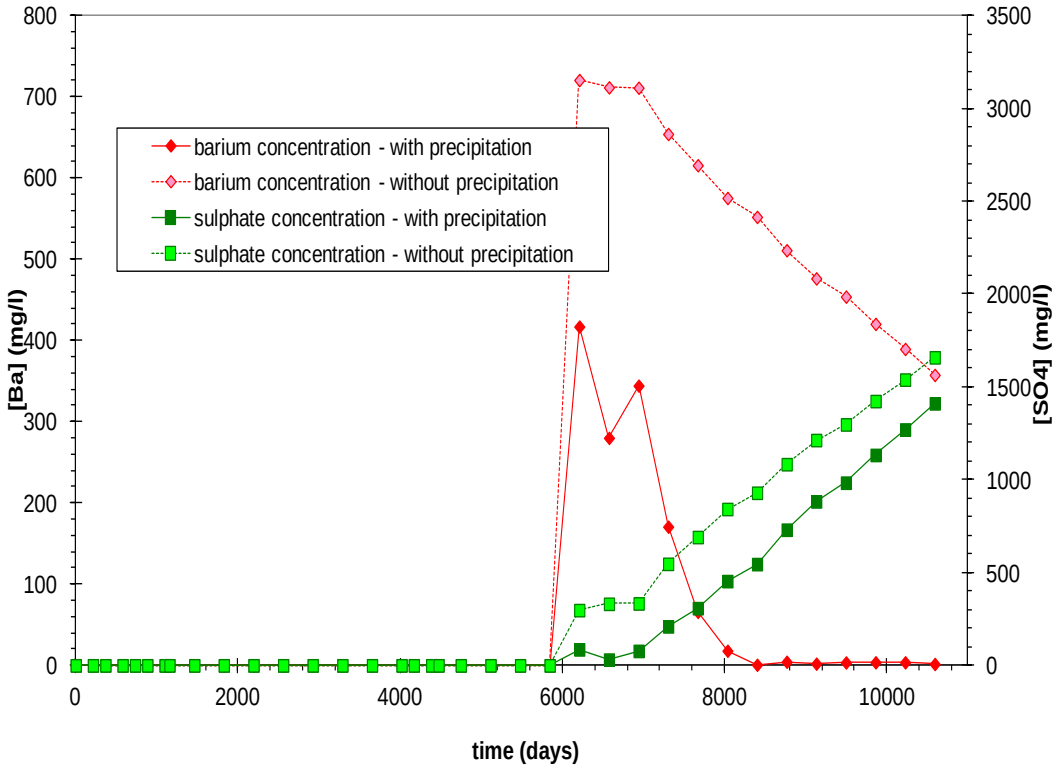

Figure 6.70: Barium and sulphate production with instantaneous precipitation and without precipitation as a function of time for well D9Z with initial formation water barium concentration set to 800mg/l.

6.5 CONCLUSIONS

In this chapter we presented the results of using the streamline model to simulate $BaSO_4$ precipitation in a real field scenario. Whereas conventional finite difference models tend to overestimate the amount of in situ mixing, in this model the extent of numerical dispersion and therefore the numerical error is reduced, and hence it is expected that the calculated produced ion concentrations should be more accurate. This means that in wells where there has not been significant in situ mixing, barium and sulphate ions may be co-produced in high concentrations, leading to a significant scaling risk. In a finite different simulation, such a scenario might be difficult to identify, due to the effect of numerical dispersion. On the other hand, when the streamline simulation shows significant ion dilution, then it is likely that would be a real effect, and not just an artifact of the model. Wells A1Z, A2, B6 and especially B3 show significant co-production of barium and sulphate ions. This occurs for long periods of time in well B3 (over 6000 days) and at high water production rates (rising to 18000 stb/d) and thus this well has the most significant scaling risk of all.

On the other hand, Wells A3, A5, A6 and D6 only co-produce barium and sulphate for a relatively short period of time, and it is expected that well B2 would co-produce hardly any of the scaling ions. That this conclusion is arrived at using streamline simulators gives greater confidence that it is in fact true.

CHAPTER 7: CONCLUSIONS AND FUTURE WORK

7.1 COMPARISON BETWEEN FINITE DIFFERENCE AND STREAMLINE SIMULATION

The purpose of this study was to use different methods to model $BaSO_4$ scale in a streamline simulation to avoid the numerical dispersion errors that arise from using the different finite difference methods in conventional simulators. The use of streamline simulations has become more common in the industry, the attraction being mainly the significant savings in computation time and the reduction in numerical dispersion. In this study, a finite difference based model (ECLIPSE) and a streamline simulator (FrontSim) have been compared for tracking the flow of injected water through a series of one, two and three-dimensional systems to address the problem of numerical dispersion exhibited by finite difference methods, particularly when predicting injected water breakthrough times. Recent calculations using FDM have been performed regarding injected, connate and aquifer water mixing in waterflooding and its consequences in scale dropout within the reservoir. In this work, those conclusions have been closely used as a framework to contrast with streamline simulation. Basic 1D, 2D and 3D geometries and model studies have confirmed the numerical dispersion problem with FDM when compared with streamline modelling. These differences lead to the following conclusions concerning dispersion in a waterflood simulation, where there is a mixing of injected and formation water and temperature tracking in the reservoir:

- In 1D linear waterflood displacements, FrontSim has effectively shown minimal numerical dispersion, producing similar results to ECLIPSE with grid block sizes that are approximately 100 times bigger.
- Streamline simulation is more effective and faster than Finite Difference Modelling for simulation of oilfield scaling processes, and can be used with very find grid blocks and with lower run times.

- The results clearly show that streamline simulations can be an effective substitute or complementary tool in alleviating the issues regarding numerical dispersion that are inherent in standard simulators, and which cannot be corrected when modeling brine mixing and scale precipitation. As streamline simulation maintains sharp fronts, this can help gain a better insight into where the problem scaling may be arising. This is crucial when the aim is to avert a drop in productivity that could occur because of scale.

- Numerical calculations in a 2D areal model have shown that injected water will arrive at the producer at different times, determined by the areal flow paths taken by the streamlines. Hence, the mixing of different brines is expected in the near production wellbore region for an extended period, which can lead to continuous scale deposition. Similar effects regarding brine mixing at the producers have been quoted for 2D heterogeneous model. FrontSim results for the 2D areal systems always produced sharper brine mixing zones than finite difference solutions.

7.2 SCALE MODELLING IN STREAMLINE SIMULATION

- The tracer code inside the streamline simulator FrontSim has been previously modified by adding a simple scale deposition model so that we can model the scale deposition and predict where and when the scale will be formed: thus we can better plan ahead to implement a squeeze treatment operation. We have shown by means of simple one-dimensional, two-dimensional models and later three-dimensional models that we can produce the type of behaviour that we would expect in a reservoir where we have incompatible formation and injected waters. The methodology was then applied to real data in Field X, and observations and learnings recorded.

- We note that in the 2D model significant scale deposition is predicted as the stream lines converge near the producer. In addition, the mapping process between streamlines and the grid introduces some numerical dispersion which will cause diffusion of the ions perpendicular to the streamlines creating additional mixing and therefore scale deposition.

- We applied the technique to Field X, obtaining results that show that when water is initially produced, the concentration of barium is in line with the concentration in the connate water. After a period of time the barium concentration begins to decline, but faster than would be expected simply from the injected water replacing connate water in the producer. Furthermore, the sulphate levels are lower than would be expected purely from brine mixing, indicating that scale is being formed in the formation. The barium levels and sulphate levels remain lower than expected throughout the life of the well. It is worth noting that the barium and sulphate ions are sometimes being produced from different layers. This is because some layers have a higher permeability than others (example well B7). This means that although there is potential for significant scale formation in the well, the actual mixing close to the well and therefore the region where scale formation can damage the well is relatively narrow.

7.3 FUTURE WORK

The modelling could be developed and expanded in a variety of ways. One of the weaknesses of the model is that the scale is in effect deposited immediately between time steps. This can produce a situation where certain cells have no scale deposits. This is because the boundary between injected and connate waters passes over the cell entirely in one time step. If the advection of both tracers was simulated concurrently the amount of scale deposited at intermediate points along the streamline could be calculated, which would give a superior depiction of the scale deposition. Furthermore, only the rate at which equilibrium is reached is dependent on the tracer concentrations at present. It would be possible to introduce velocity dependence quite easily to the scale formation rate if the scaling calculation was conducted as part of the tracer tracking step. It would also be possible to make the rate temperature dependent by connecting the scale formation rate to the temperature option.

A more robust thermodynamic model, including calculation of the solubility product for scales with higher solubility would be a significant improvement. The thermodynamic model could also take account of the impact of other ions on the solubility product.

Finally, we could also let the mass of scale formed operate as a modifier on both the pore volume in the cell and the permeability within the cells and/or the transmissibility between cells. These adjustments would probably best be controlled by adding additional tables to the input that would link the changes in scale density and temperature to the changes in permeability and the scale formation rate in that order. Alternatively, the impact of scale deposition in the near wellbore zone could be allowed to impact the well skin by means of a look up table.

APPENDIX A: A COMPREHENSIVE ANALYSIS FOR THE REMAINING WELLS IN FIELD-X WITH BARIUM CONCENTRATIONS OF 250 MG/L

WELL-A4Z

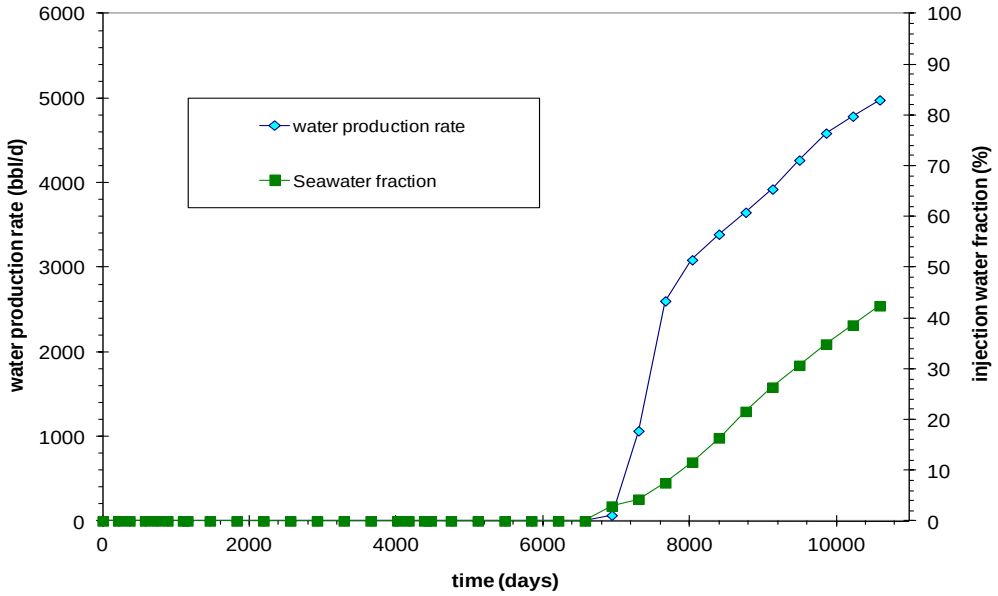

Figure A.1: Water Production rate and percentage of the injected water produced as function of time for well A4Z.

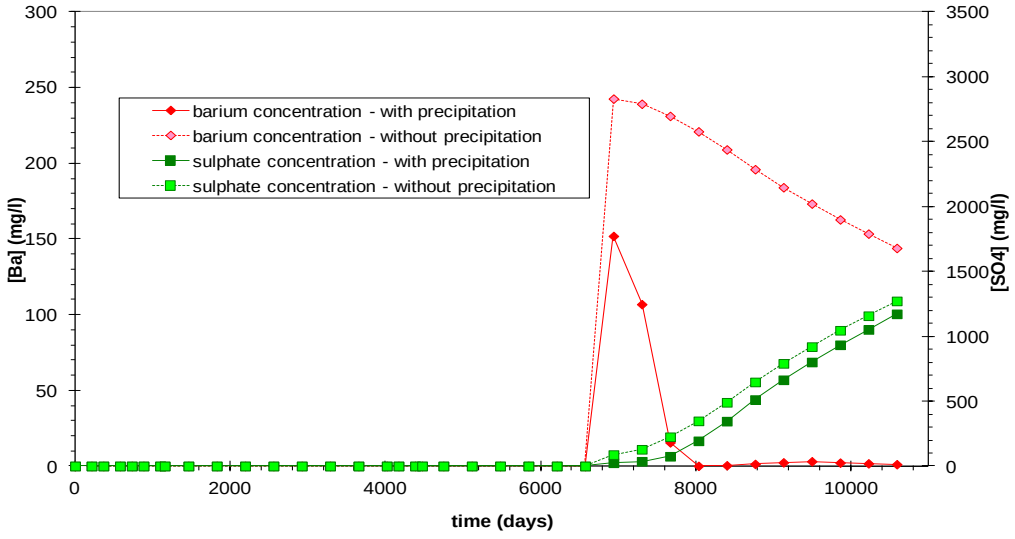

Figure A.2: Barium and sulphate production with instantaneous precipitation and without precipitation as a function of time for well A4Z.

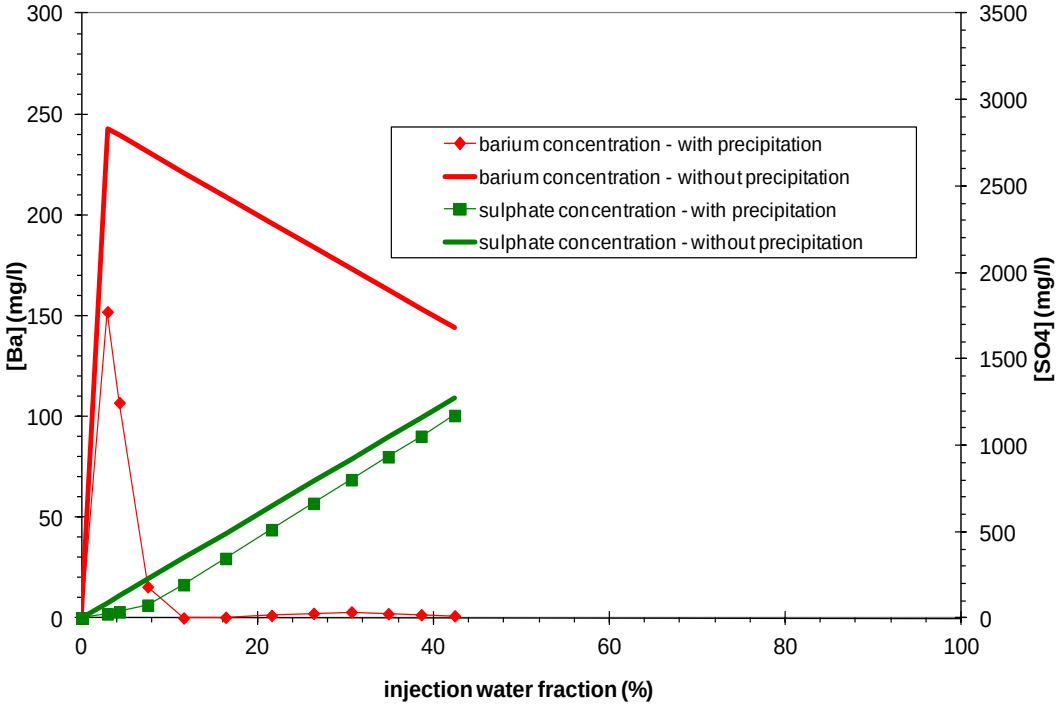

Figure A.3: The produced concentration of barium and sulphate ions as a function of the produced fraction of sea water for well A4Z.

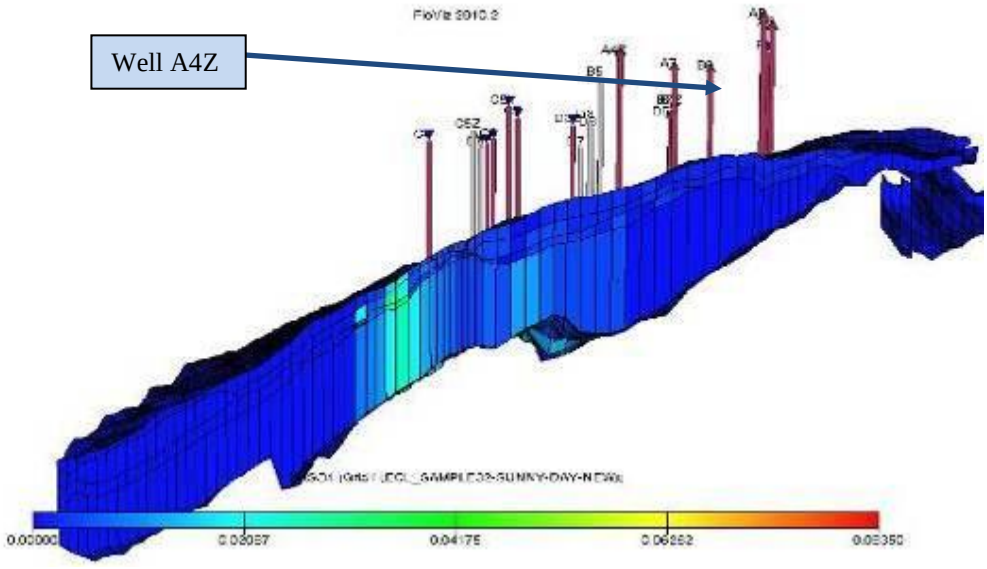

Figure A.4: The 3D section of Field X indicates $BaSO_4$ location for well A4Z.

WELL-A7

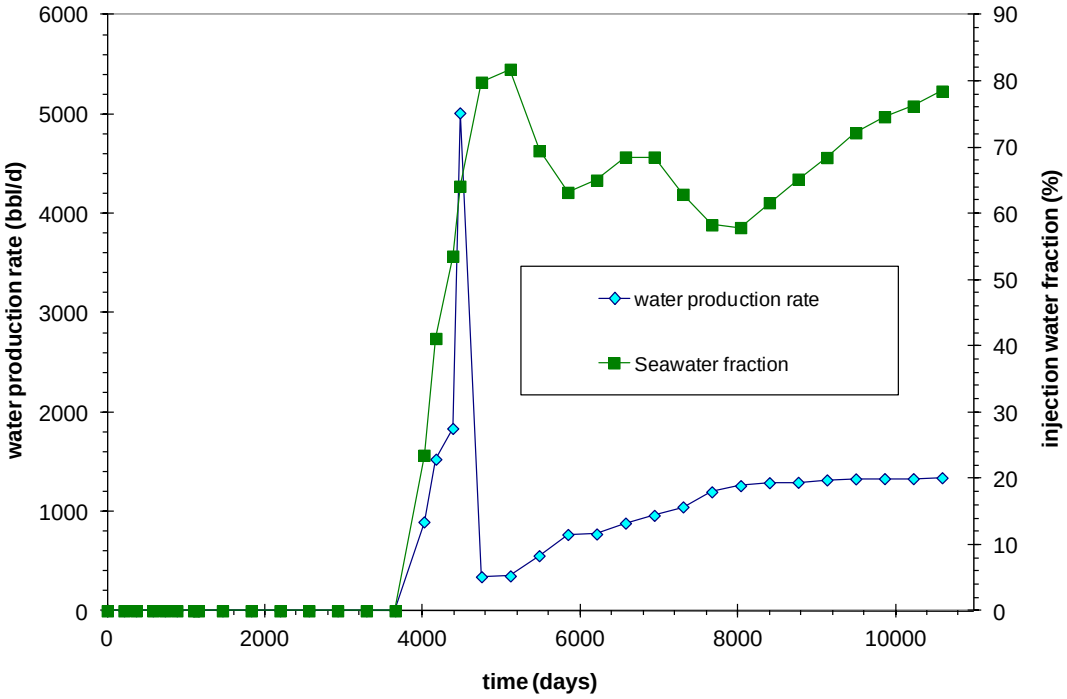

Figure A.5: Water production rate and percent of injected water produced as function of time for well A7.

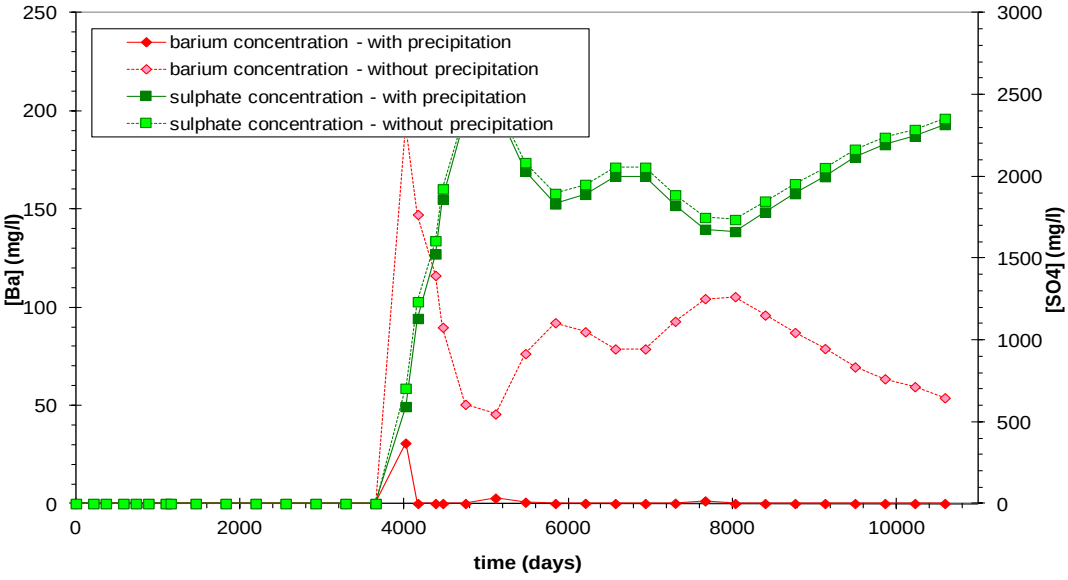

Figure A.6: Barium and sulphate production with instantaneous precipitation and without precipitation as a function of time for well A7.

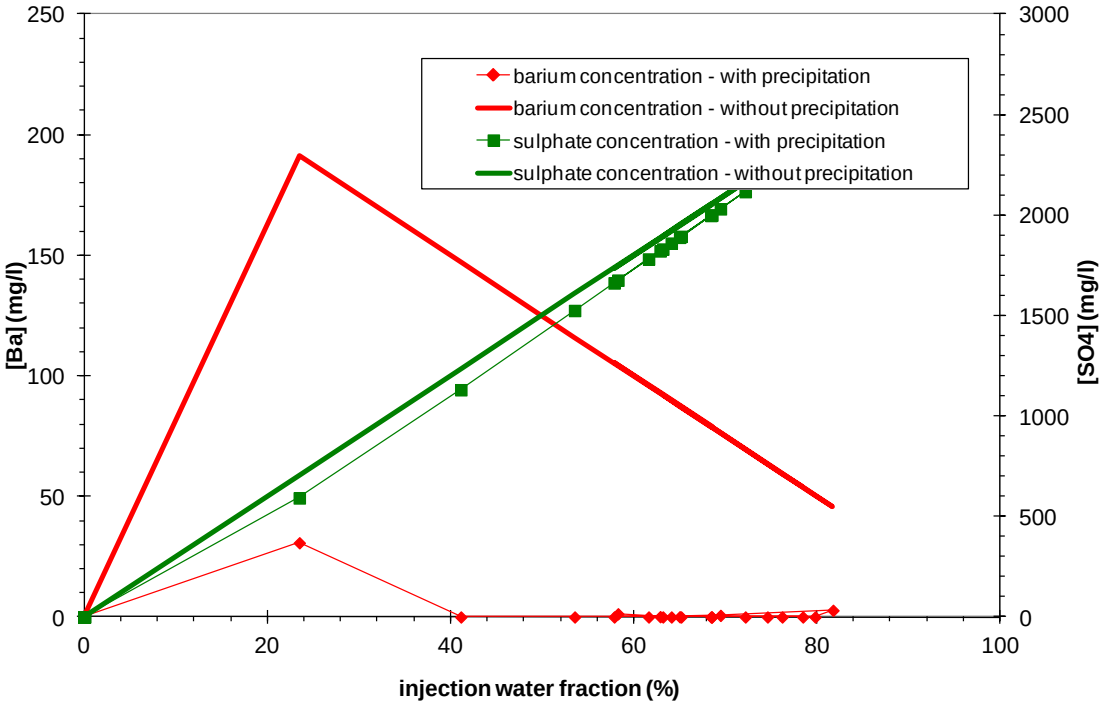

Figure A.7: The produced concentration of barium and sulphate ions as a function of the produced fraction of seawater for well A7

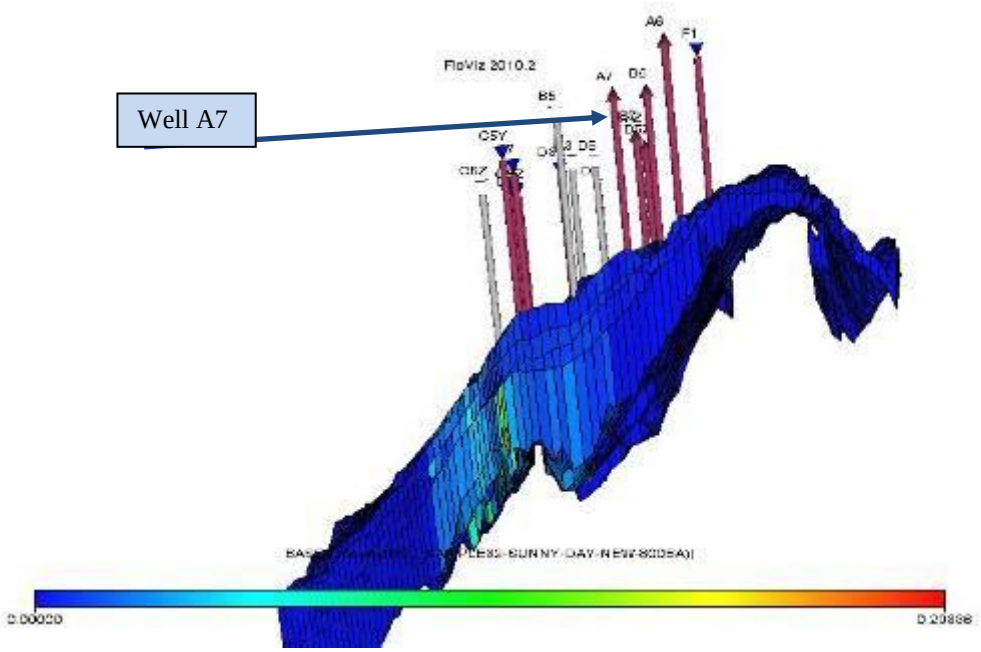

Figure A.8: The 3D section of Field X indicates $BaSO_4$ location for well A7.

WELL-B1

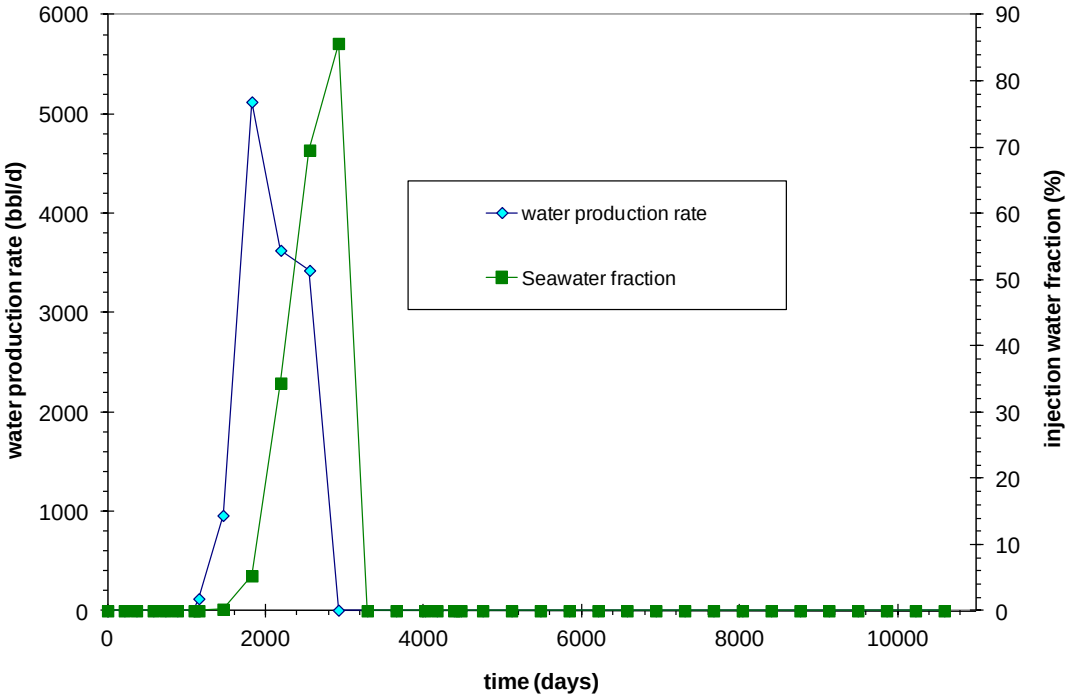

Figure A.9: Water production rate & percentage of the injected water produced as a function of time for well B1.

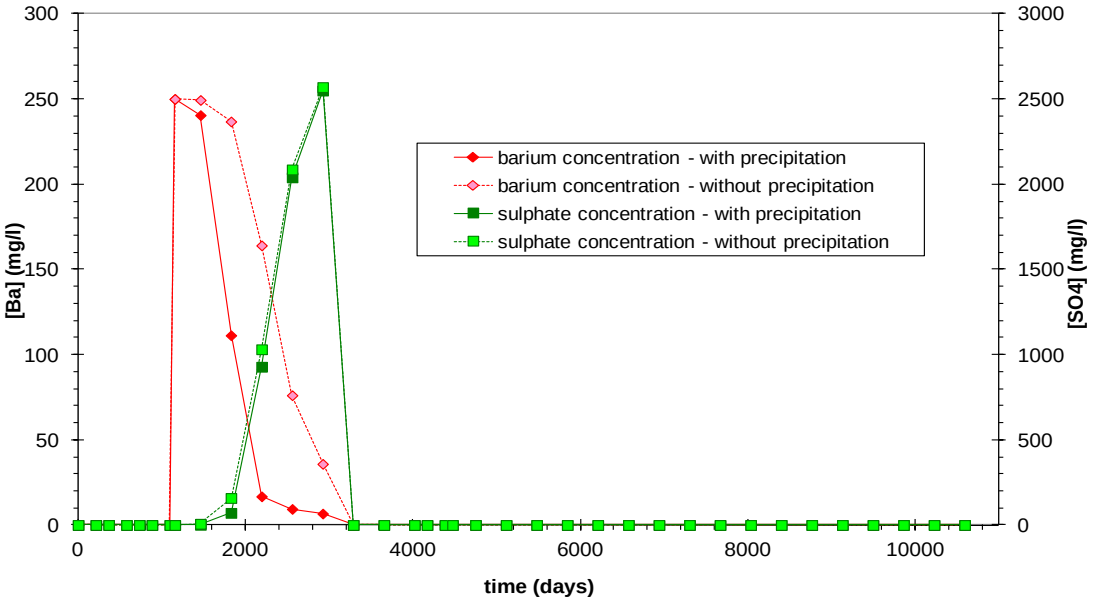

Figure A.10: Barium and sulphate production with instantaneous precipitation and without precipitation as a function of time for well B1.

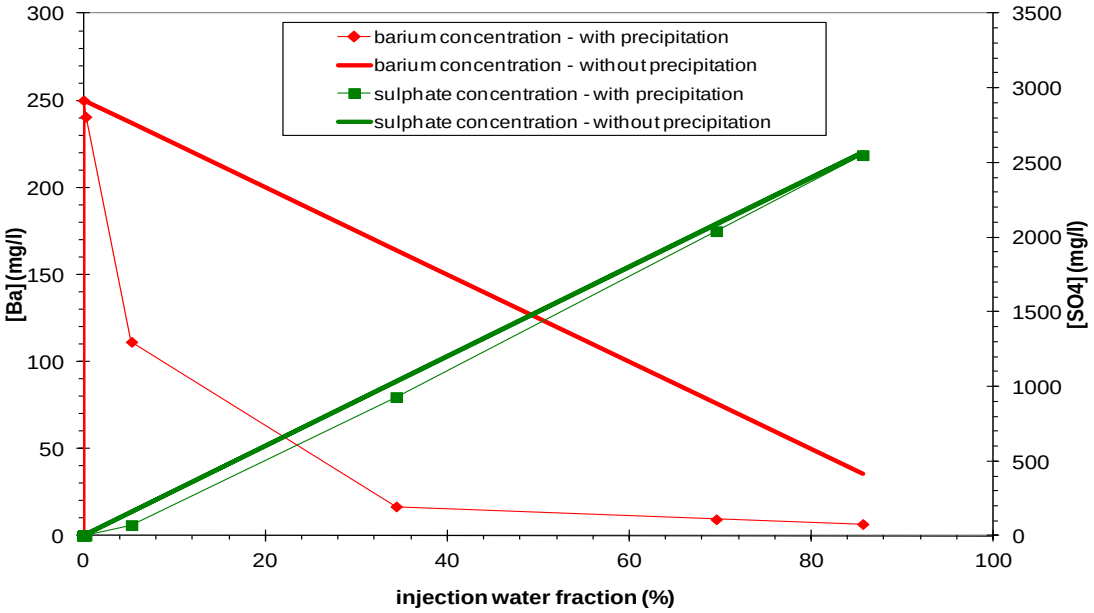

Figure A.11: The produced concentration of barium and sulphate ions as a function of the produced fraction of sea water for well B1.

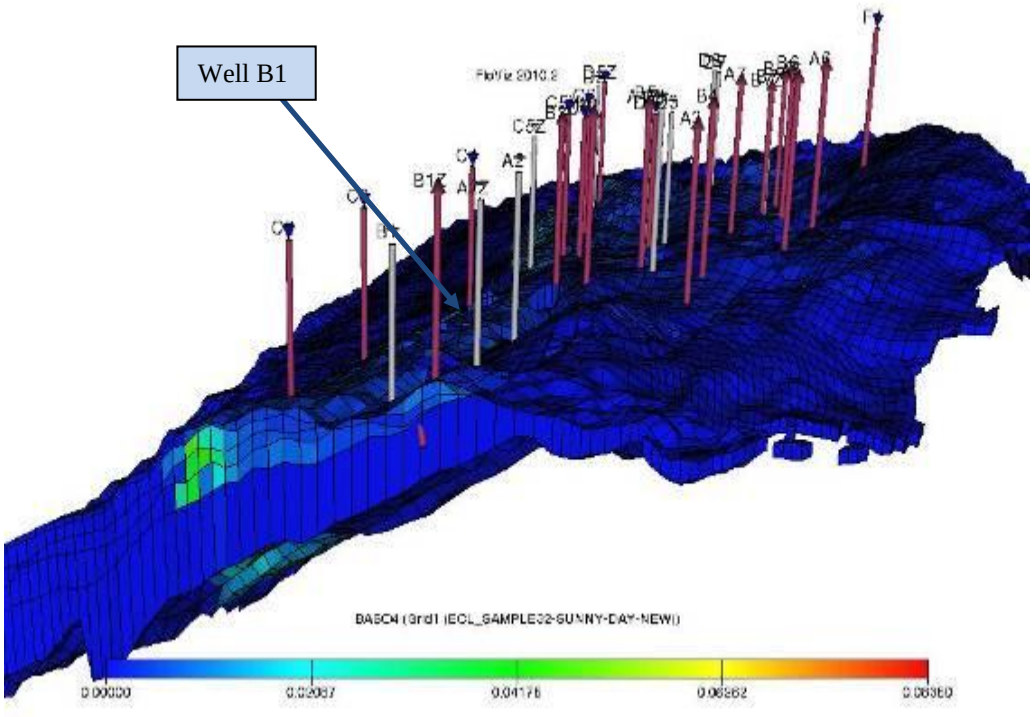

Figure A.12: The 3D section of Field X indicates $BaSO_4$ location for well B1

WELL B1Z

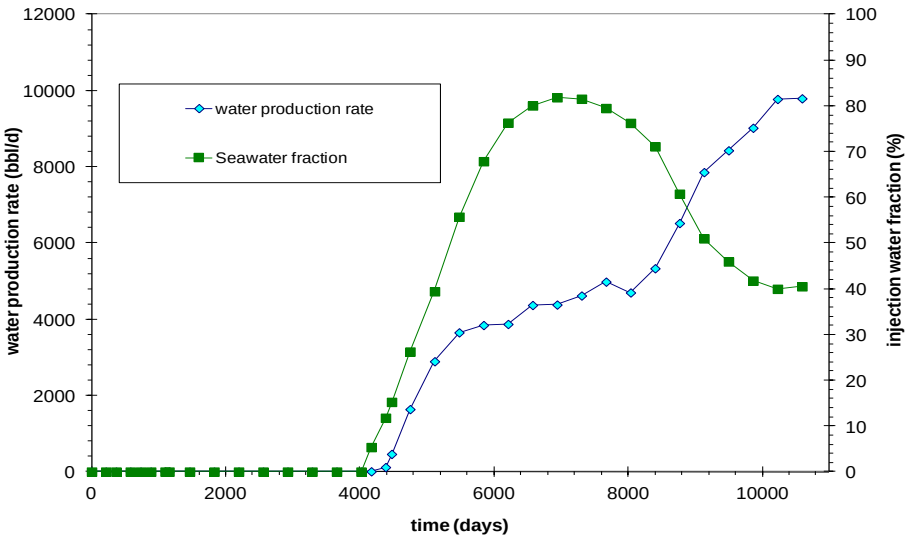

Figure A.13: Water production rate and percentage of the injected water produced as a function of time for well B1Z.

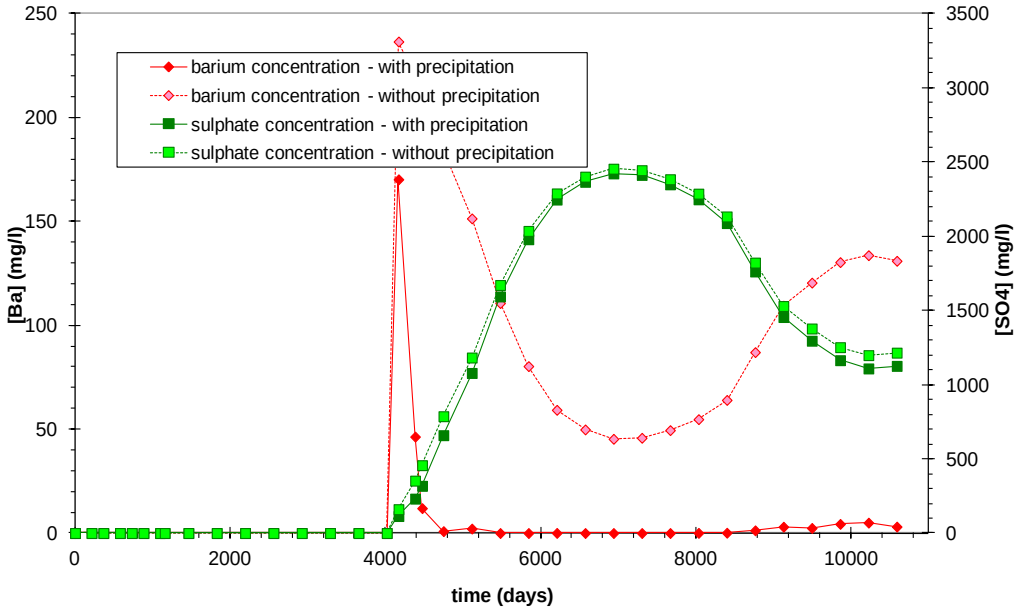

Figure A.14: Barium and sulphate production with instantaneous precipitation and without precipitation as a function of time for well B1Z.

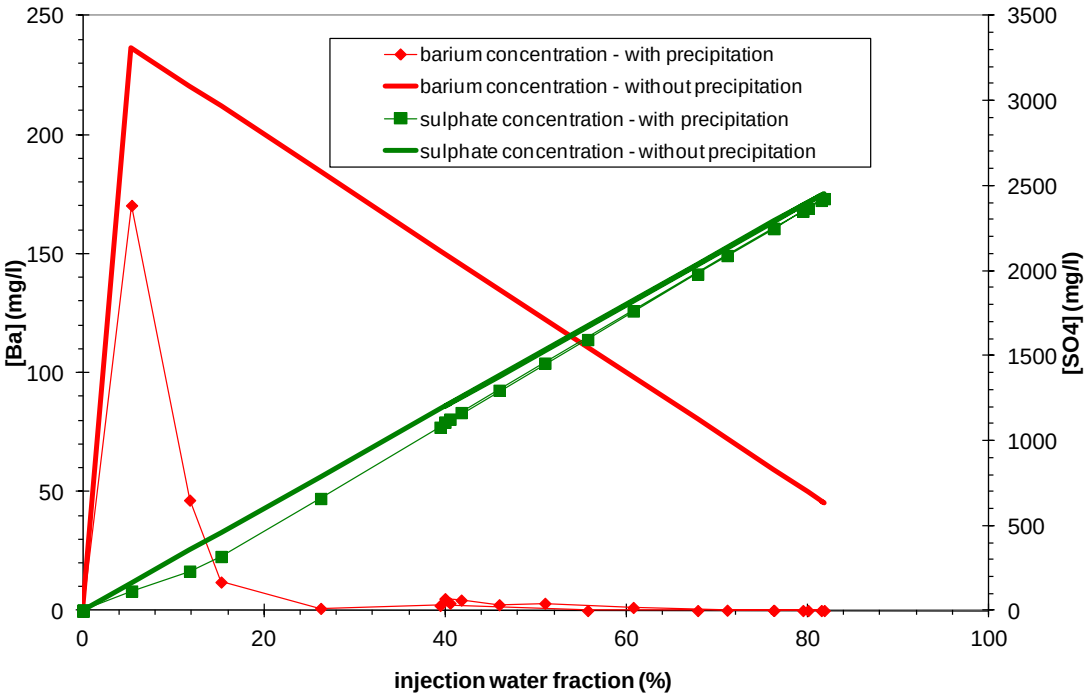

Figure A.15: The produced concentration of barium and sulphate ions as a function of the produced friction of sea water for well B1Z.

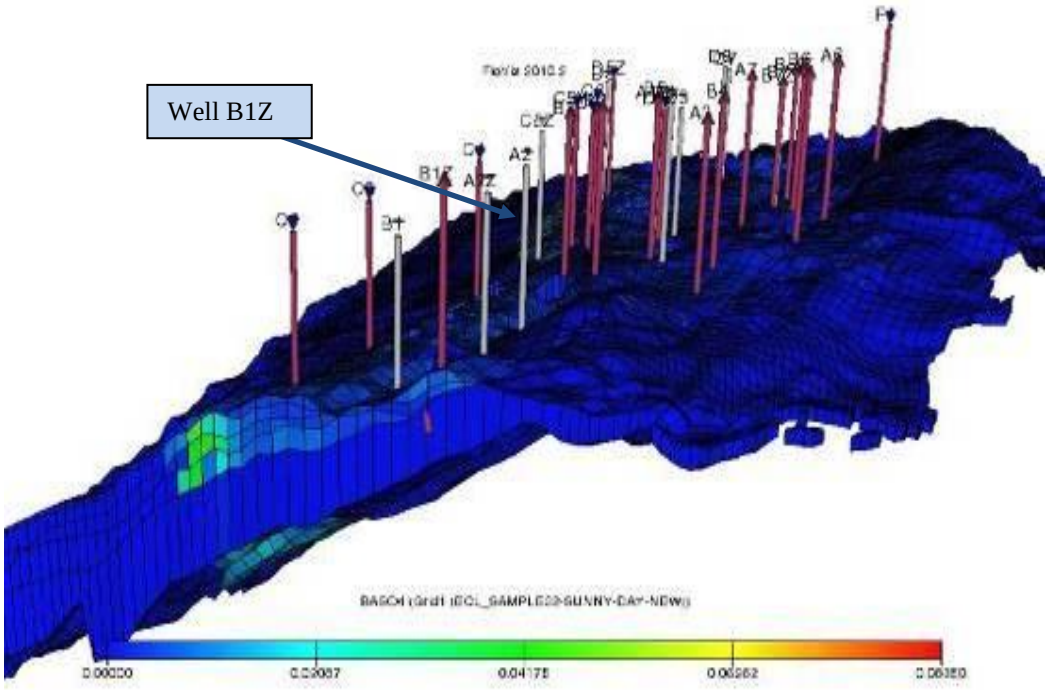

Figure A.16: The 3D section of Field X indicates $BaSO_4$ location for well B1Z.

WELL B4

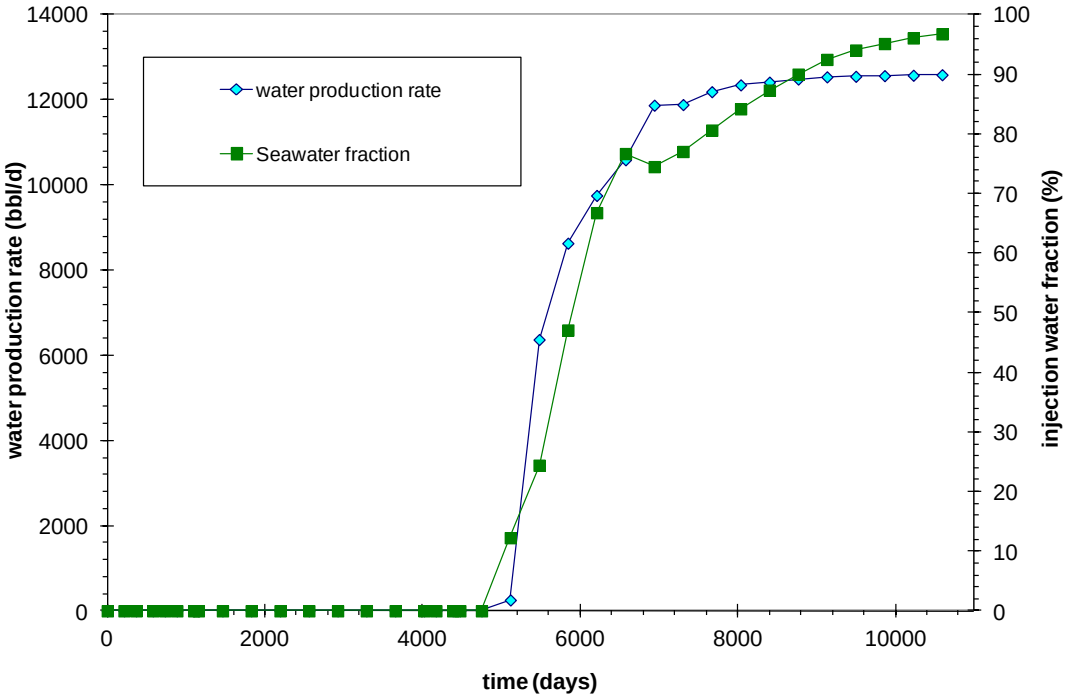

Figure A.17: Water production rate and percentage of the injected water produced as a function of time for well B4.

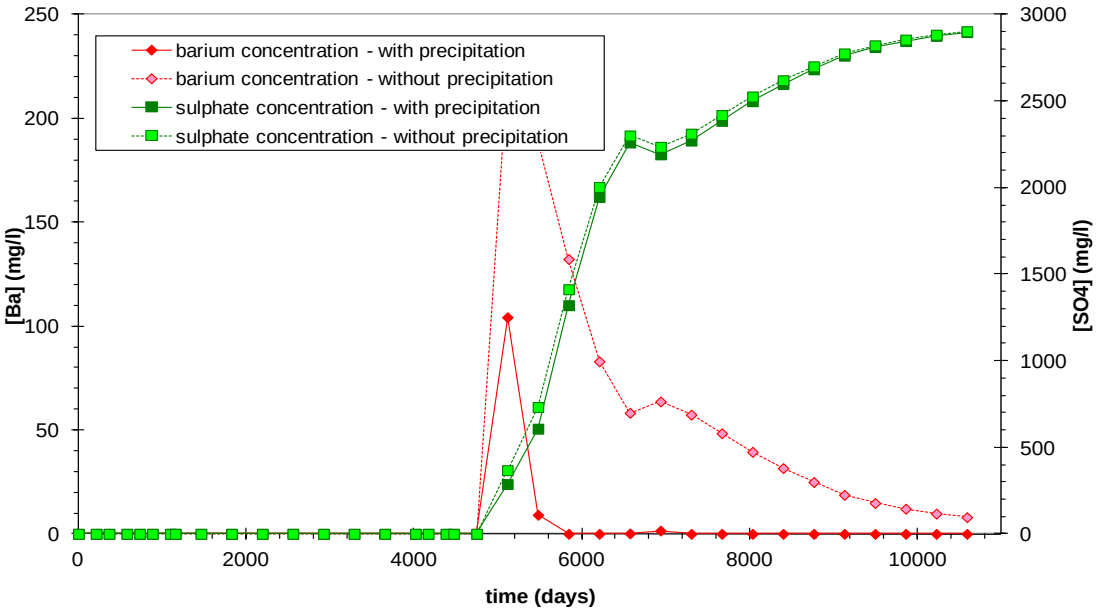

Figure A.18: Barium and sulphate production with instantaneous precipitation and without precipitation as a function of time for well B4.

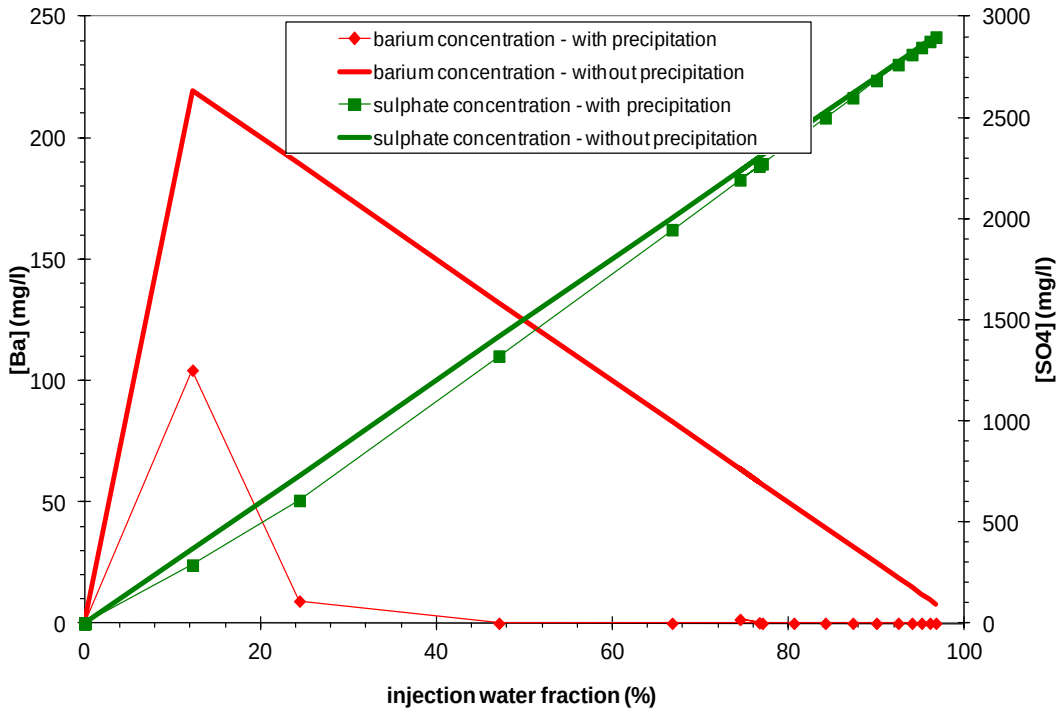

Figure A.19: The produced concentration of barium and sulphate ions as a function of the produced fraction of sea water for well B4.

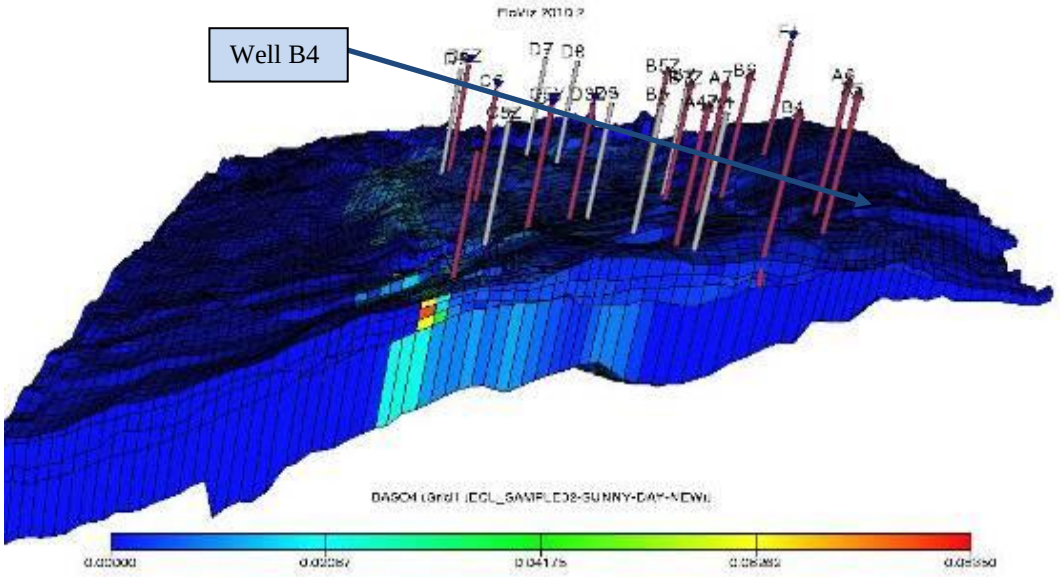

Figure A.20: The 3D section of Field X indicates $BaSO_4$ location for well B4.

WELL-B5

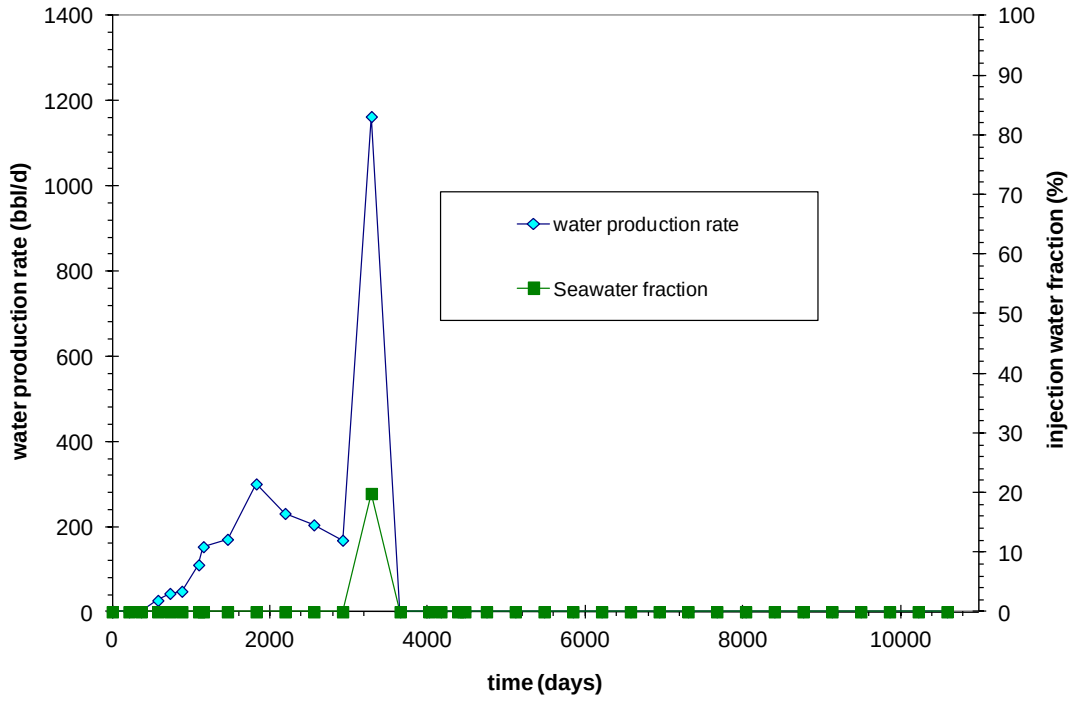

Figure A.21: Water production rate and percent of injected water produced as function of time for well B5

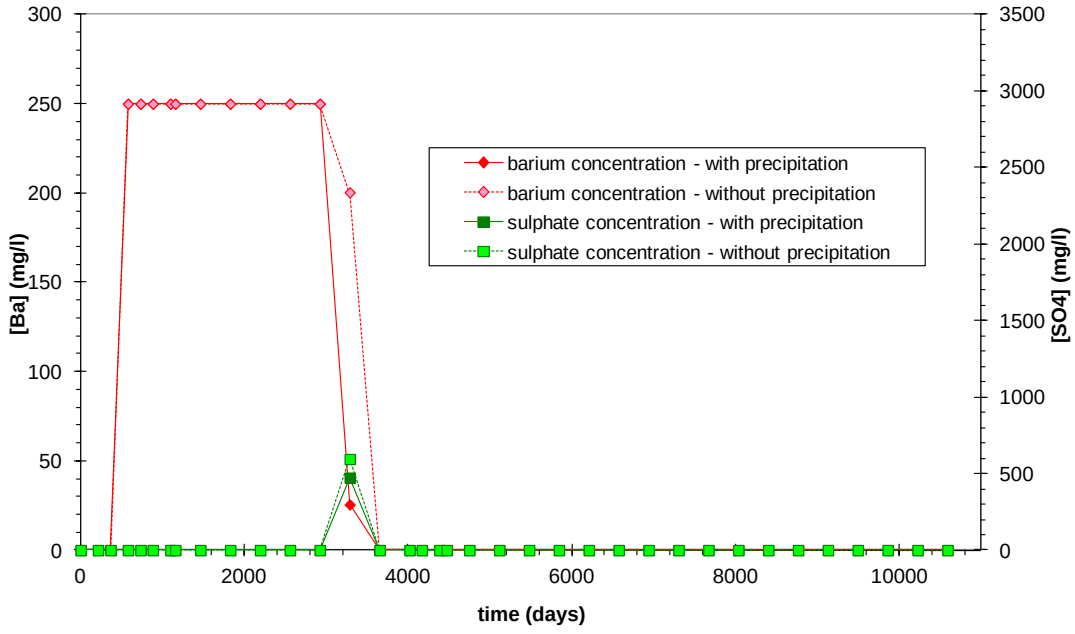

Figure A.22: Barium and sulphate production with instantaneous precipitation and without precipitation as a function of time for well B5.

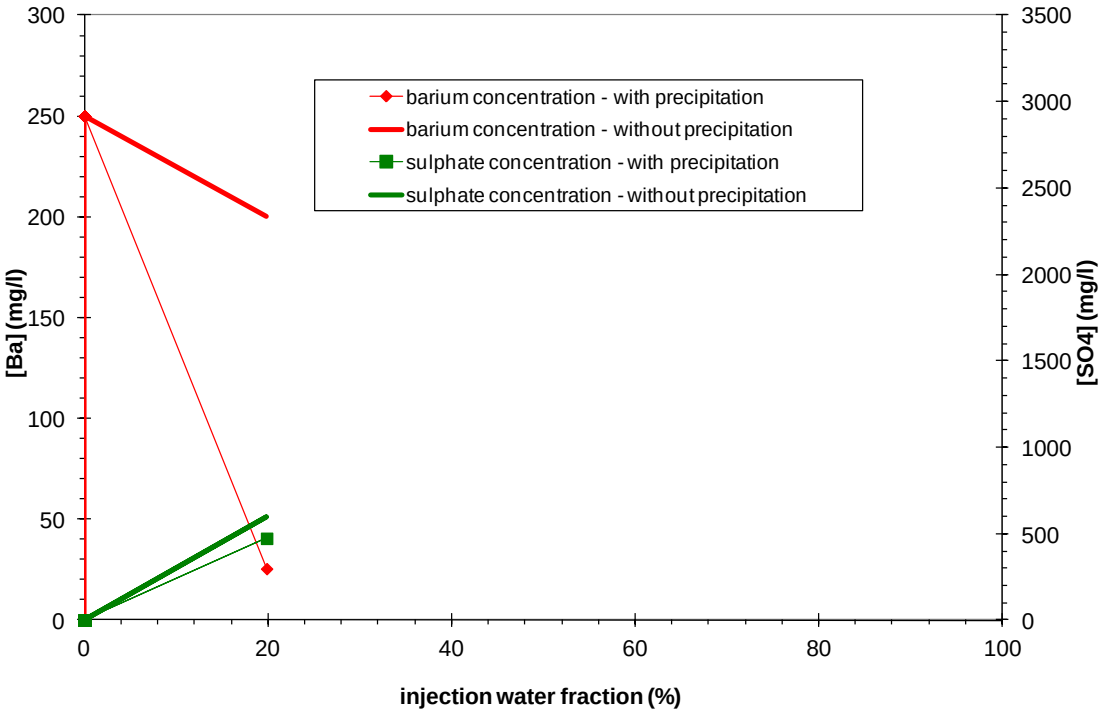

Figure A.23: The produced concentration of barium and sulphate ions as a function of the produced fraction of sea water for well B5.

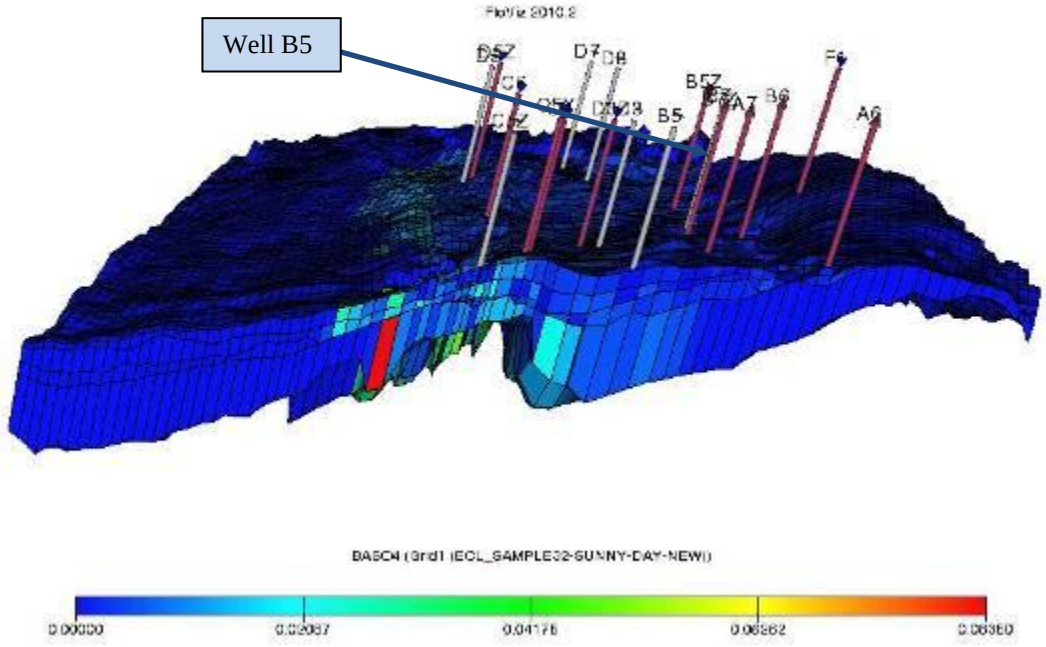

Figure A.24: The 3D section of Field X indicates $BaSO_4$ location for well B5.

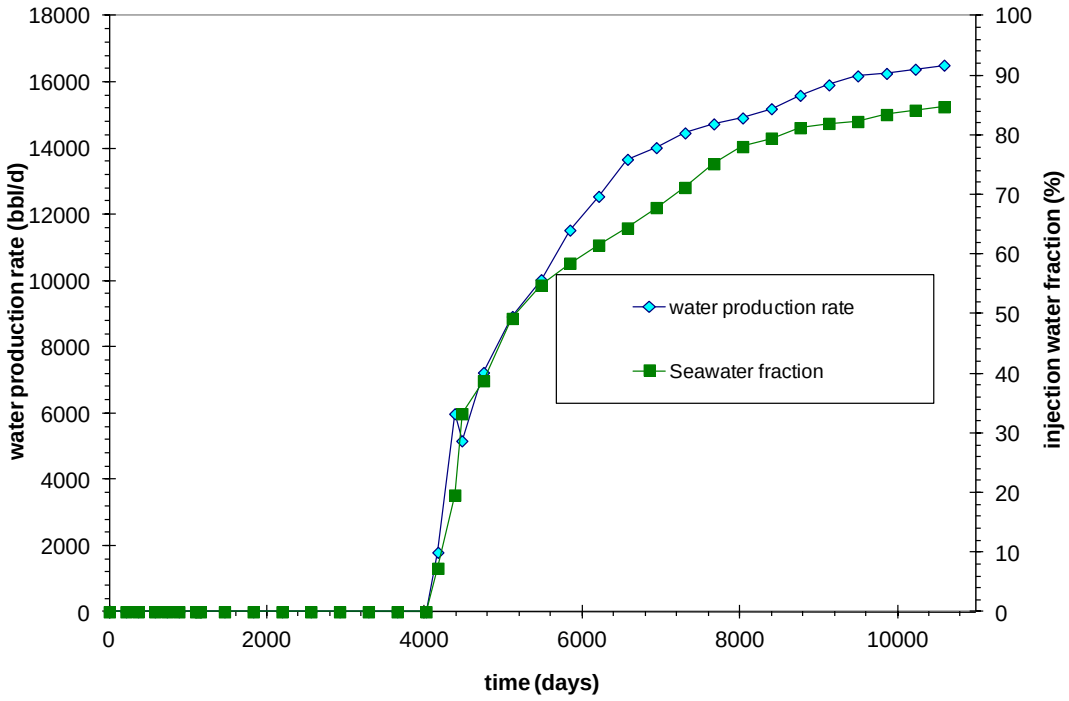

Figure A.25: Water production rate and percent of injected water produced as function of time for well B5Z.

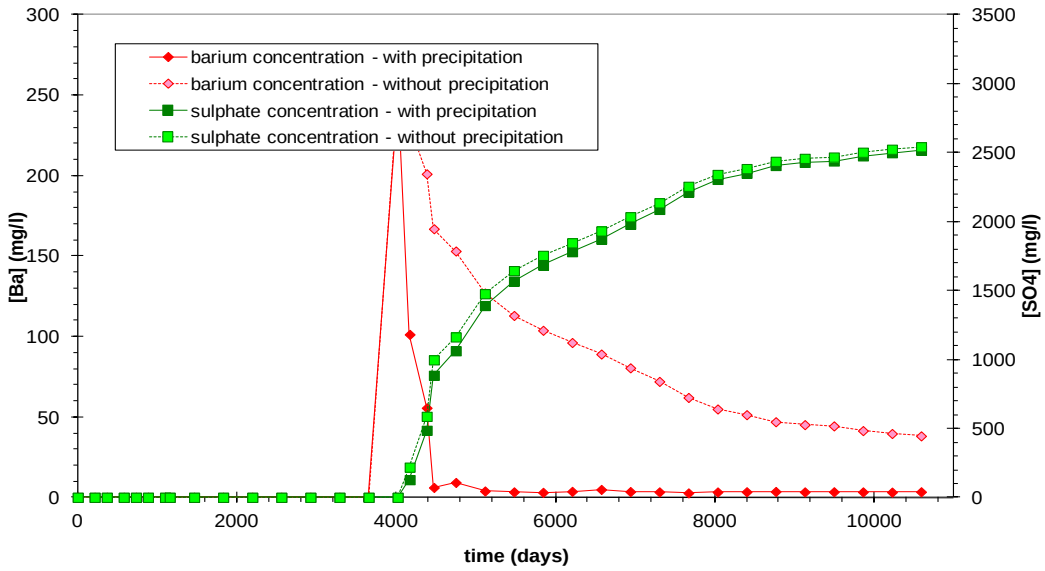

Figure A.26: Barium and sulphate production with instantaneous precipitation and without precipitation as a function of time for well B5Z.

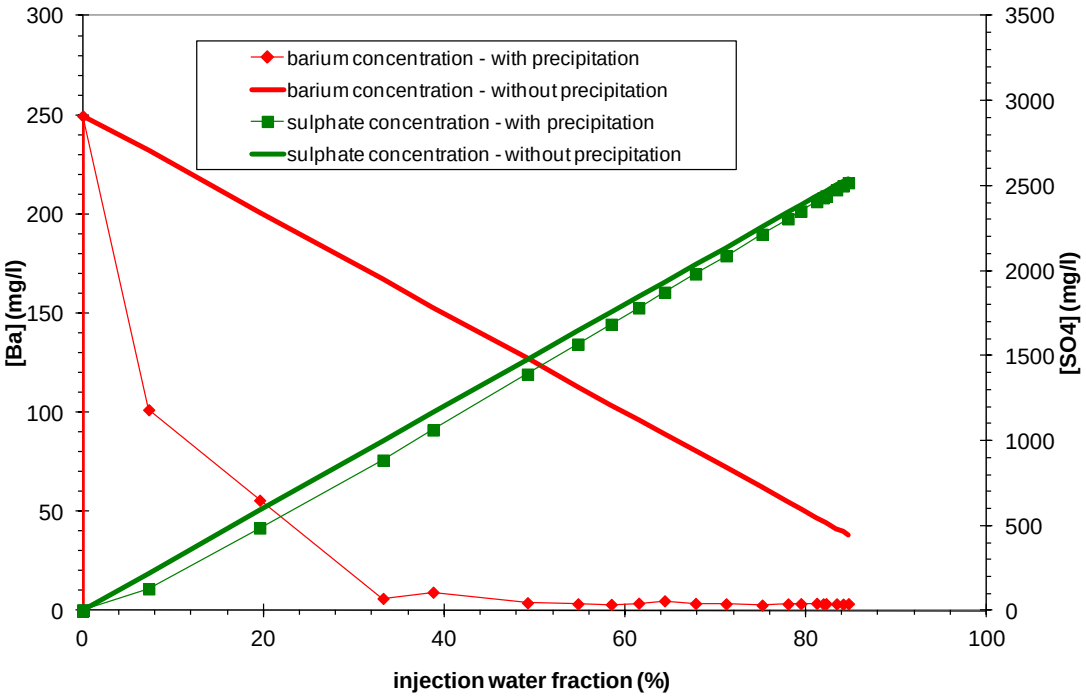

Figure A.27: The produced concentration of barium and sulphate ions as a function of the produced fraction of sea water for well B5Z.

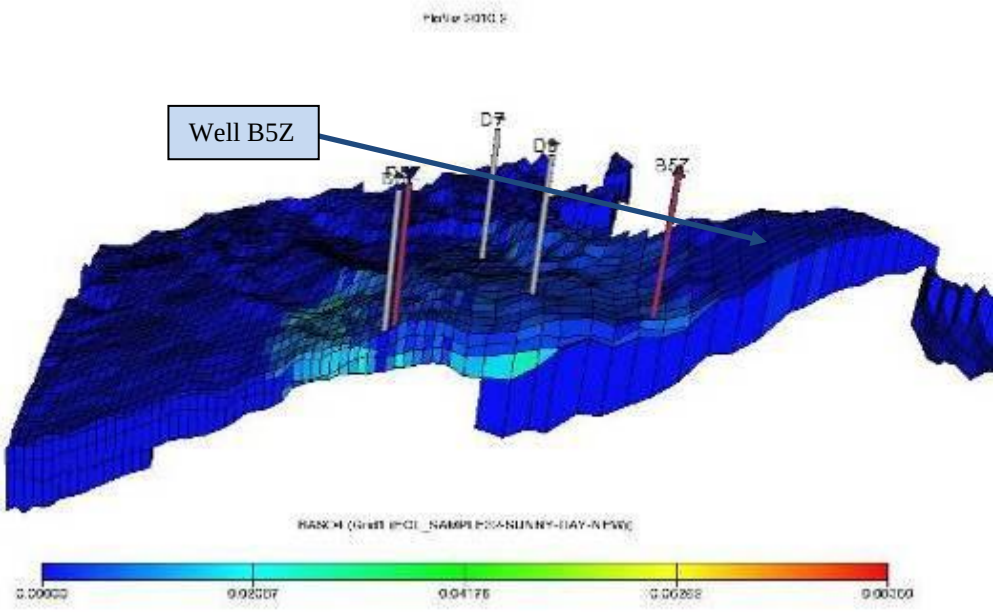

Figure A.28: The 3D section of Field-X indicates $BaSO_4$ location for well B5Z.

WELL-D9

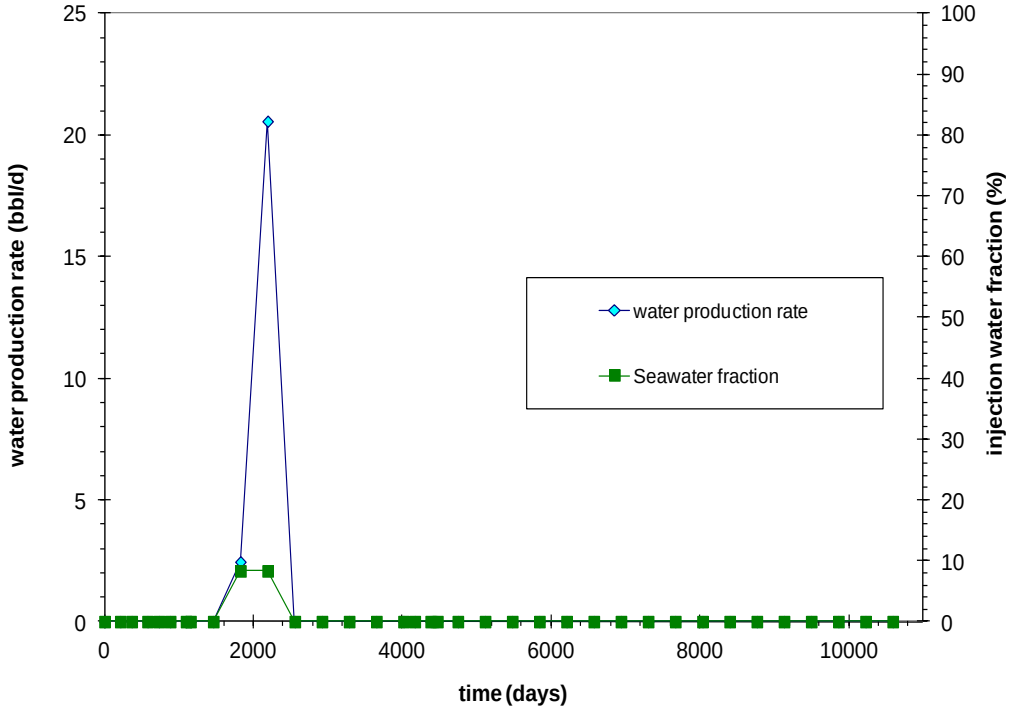

Figure 2.9: Water production rate and percent of injected water produced as function of time for well D9.

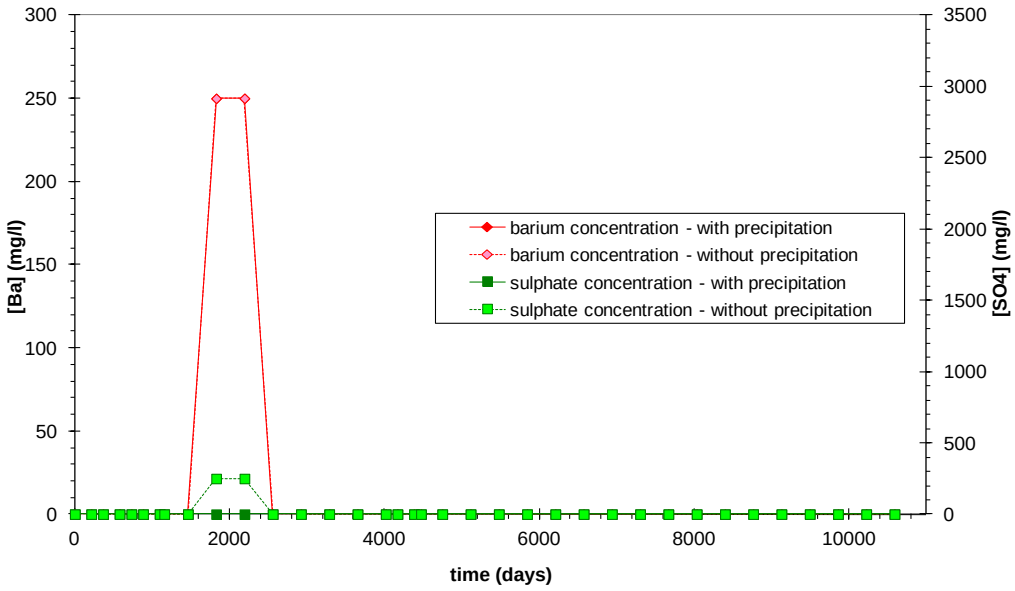

Figure A.30: Barium and sulphate production with instantaneous precipitation and without precipitation as a function of time for well D9.

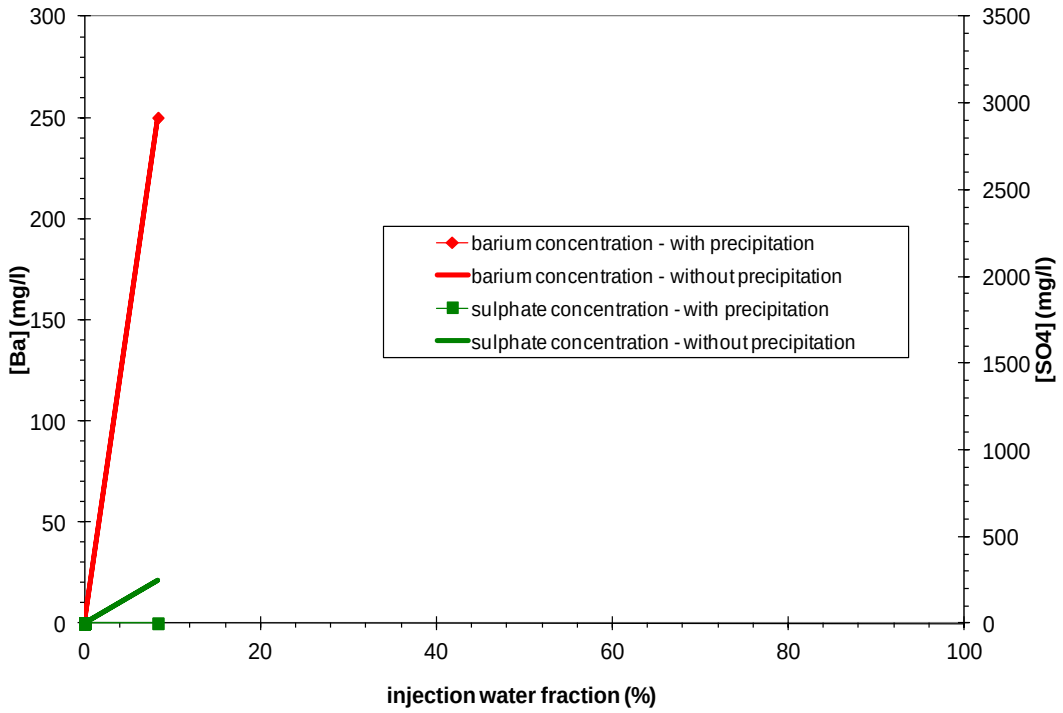

Figure A.31: The produced concentration of barium and sulphate ions as a function of the produced fraction of sea water for well D9.

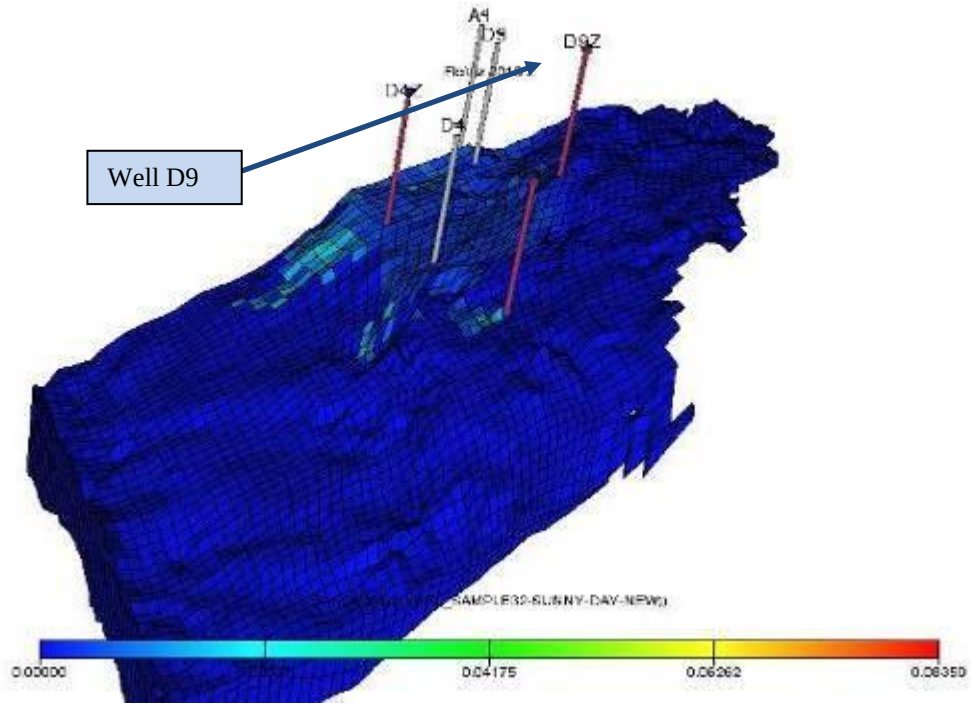

Figure A.32: The 3D section of Field X indicates $BaSO_4$ location for well D9.

WELL –D9Z

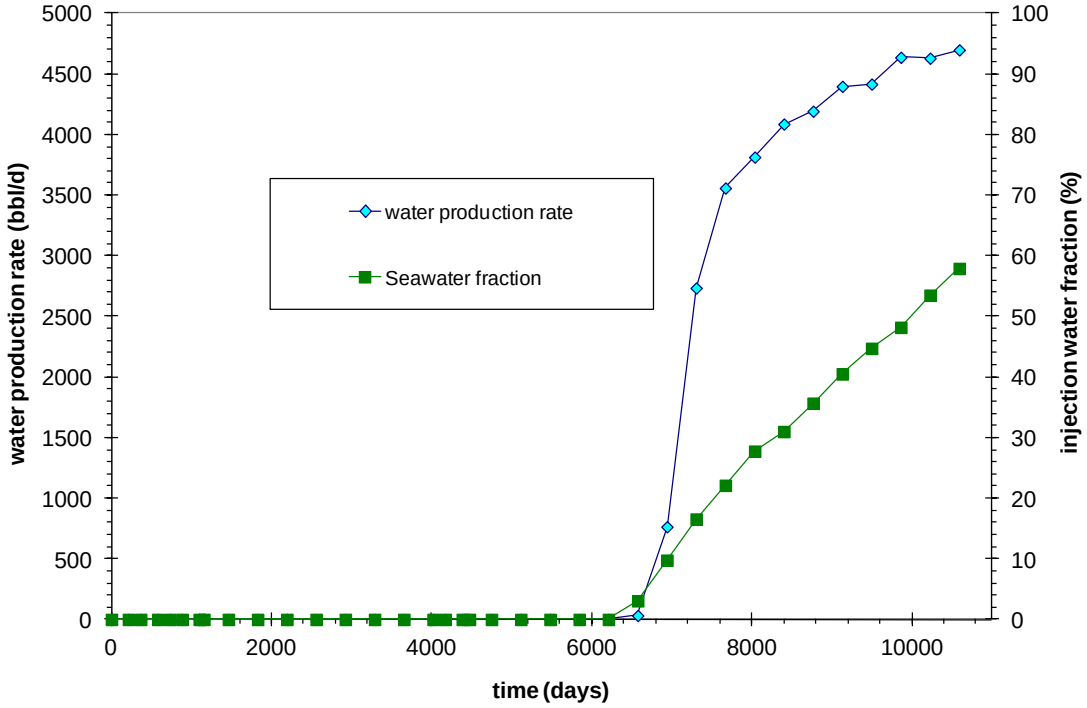

Figure A.33: Water production rate and percent of injected water produced as function of time for well D9Z**.**

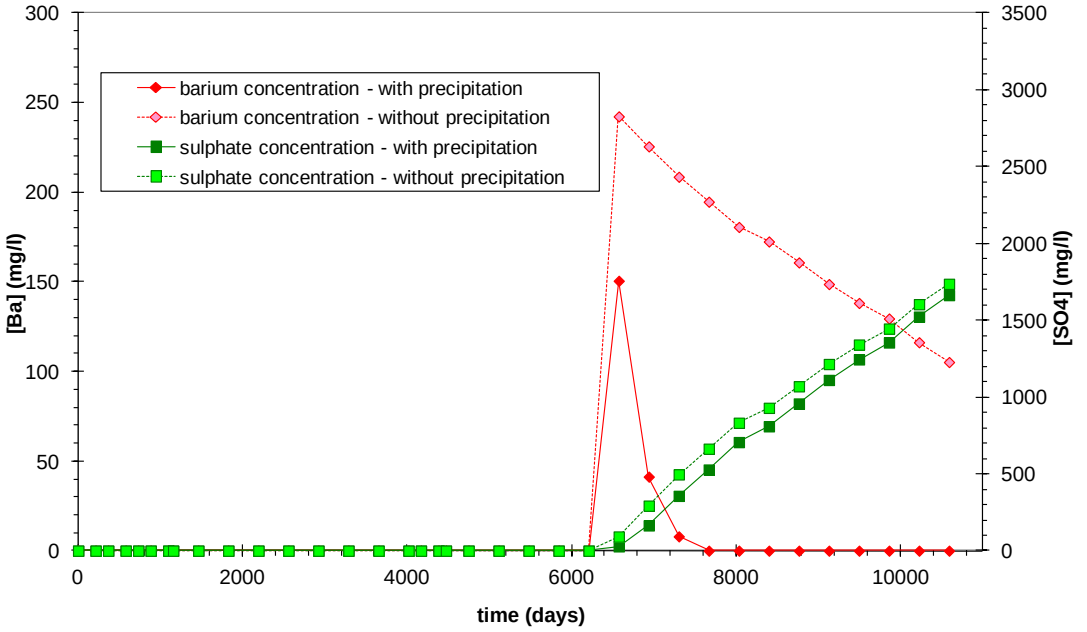

Figure A.34: Barium and sulphate production with instantaneous precipitation and without precipitation as a function of time for well D9Z.

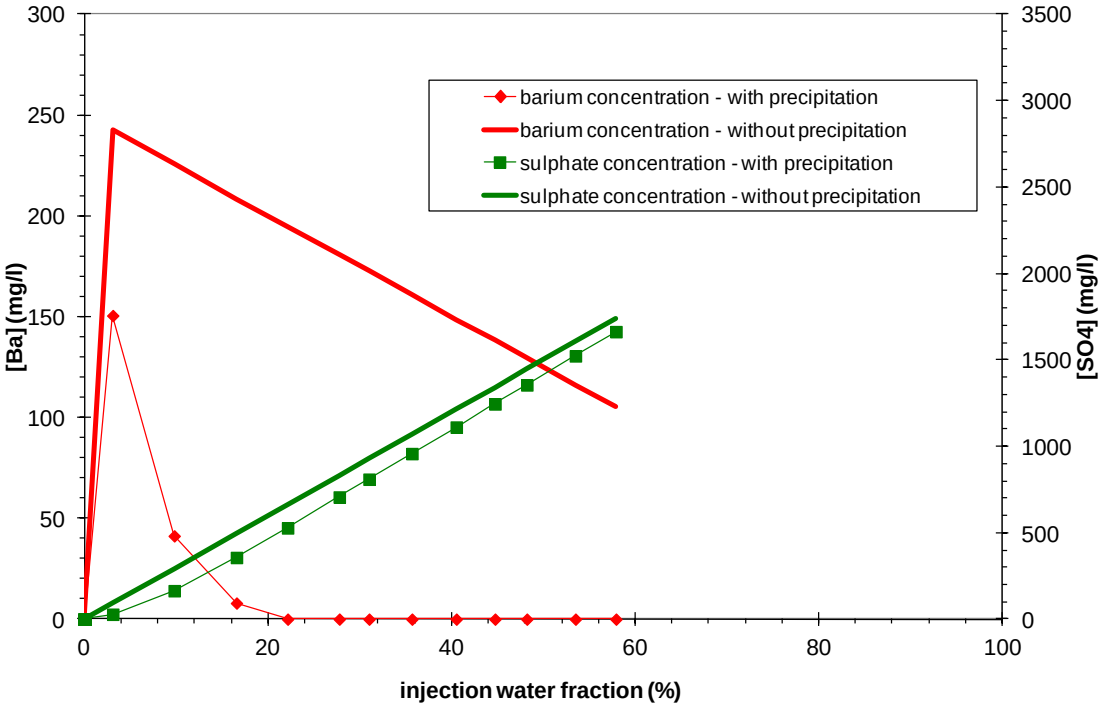

Figure A.35: The produced concentration of barium and sulphate ions as a function of the produced fraction of sea water for well D9Z.

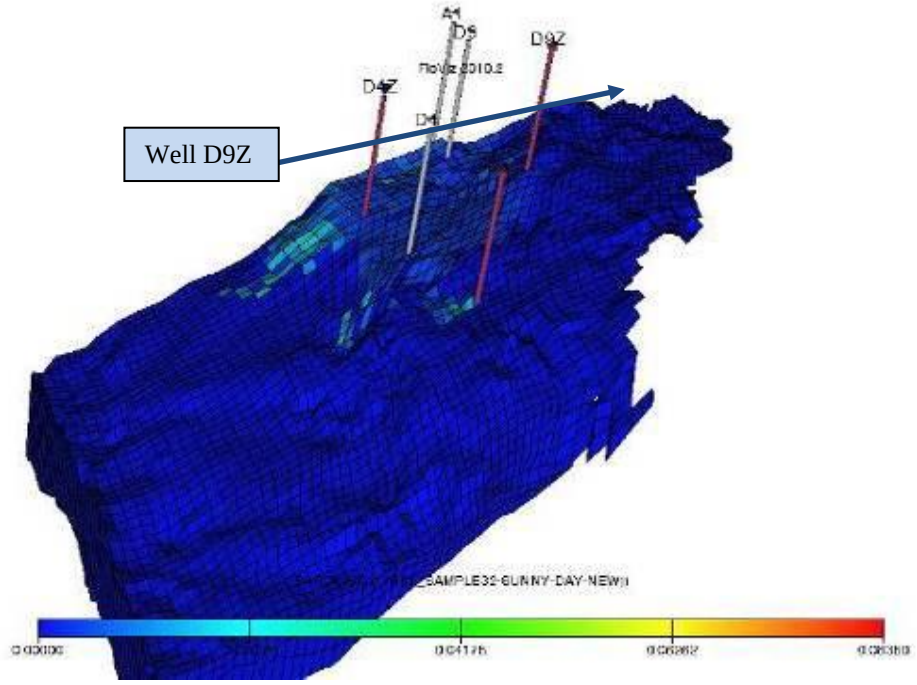

Figure A.36: The 3D section of Field X indicates $BaSO_4$ location for well D

APPENDIX B: COMPREHENSIVE ANALYSIS FOR THE OTHER WELLS IN FIELD-X WITH BARUIM CONCENTRATION OF 45, 80, 229 AND 800MG/L

Well A1Z with barium concentration of 45 mg/l.

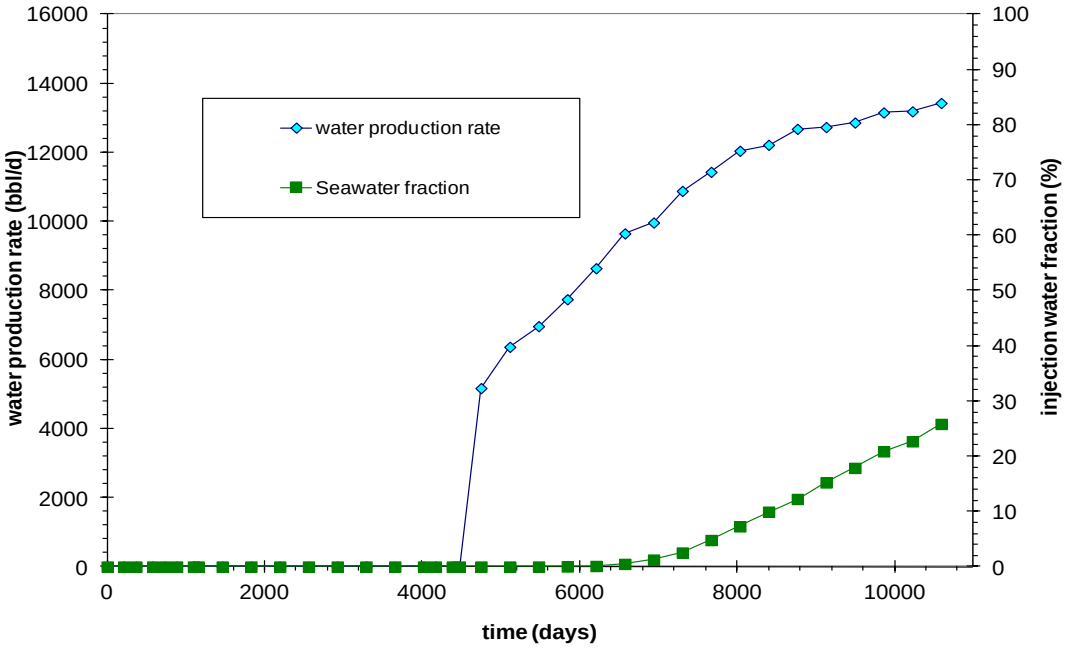

Figure B.1: Water production rate and percentage of the injected water produced as a function of time for well A1Z.

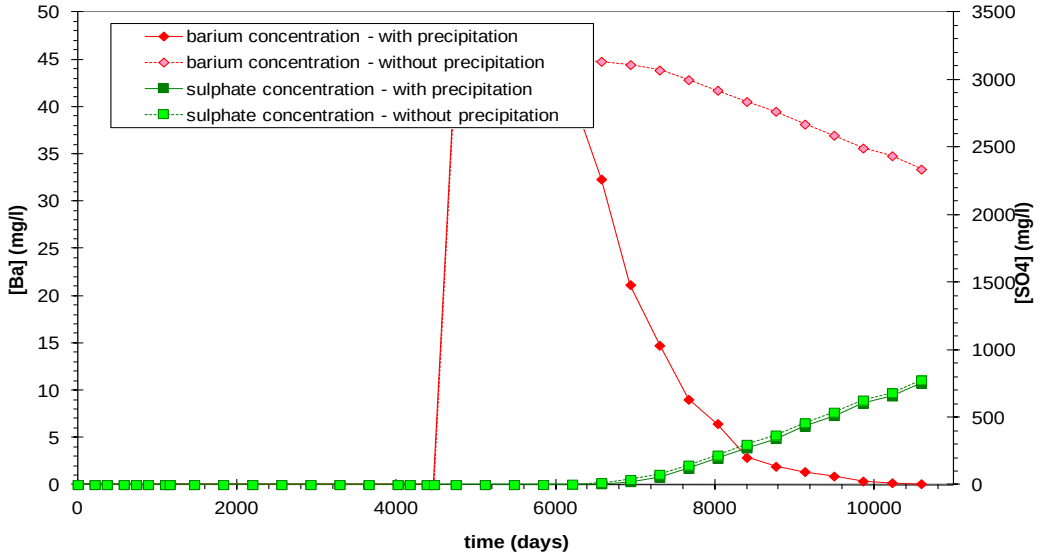

Figure B.2: Barium and sulphate production with instantaneous precipitation and without precipitation as a function of time for well A1Z.

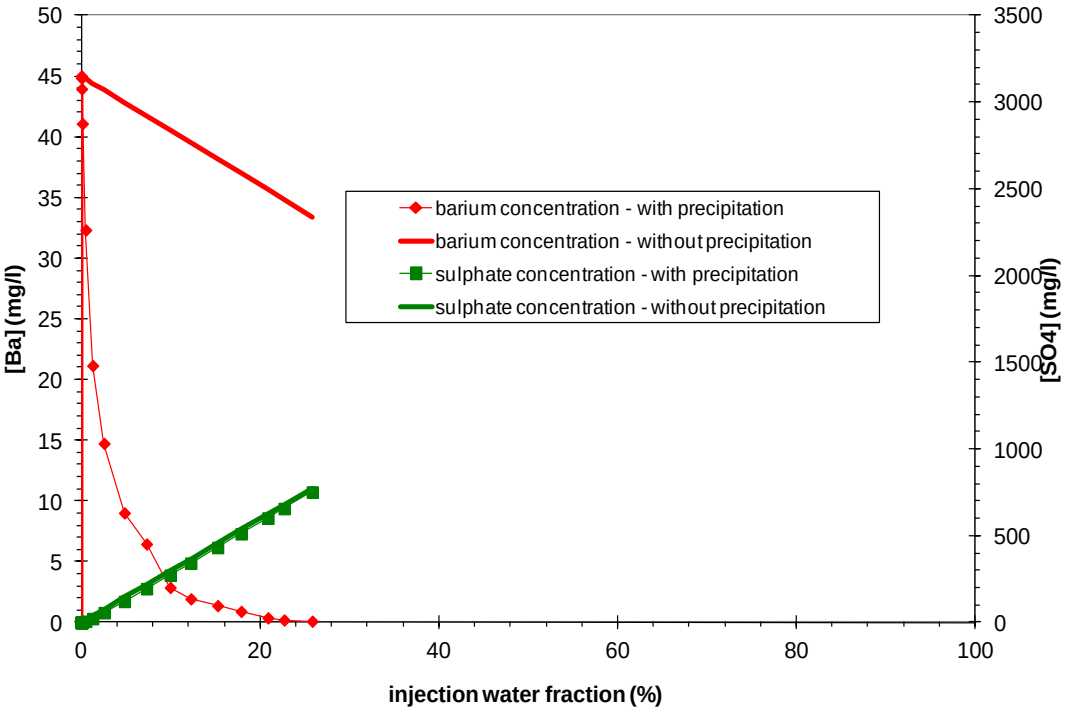

Figure B.3: The produced concentration of barium and sulphate ions as a function of the produced fraction of sea water for well A1Z.

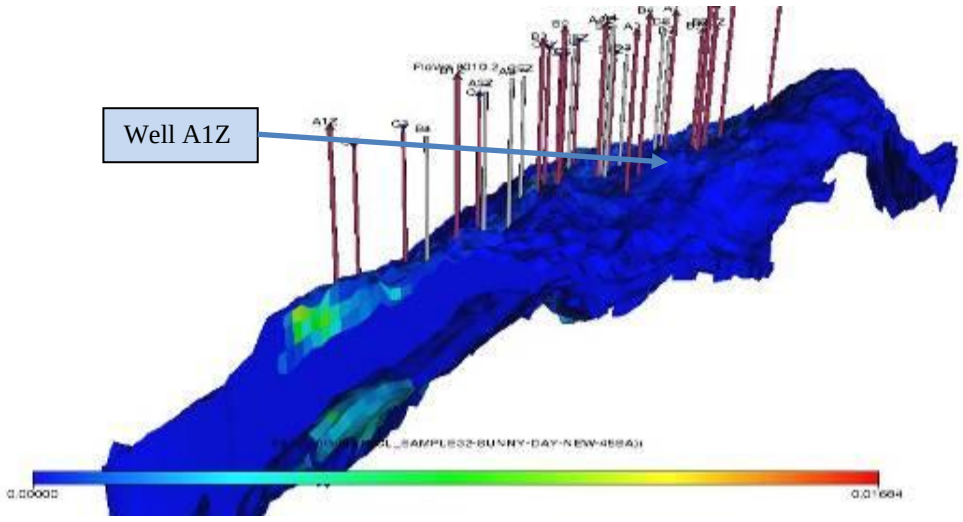

Figure B.4: The 3D section of Field X indicates $BaSO_4$ location for well A1Z.

Well A5-with barium concentration of 45 mg/l.

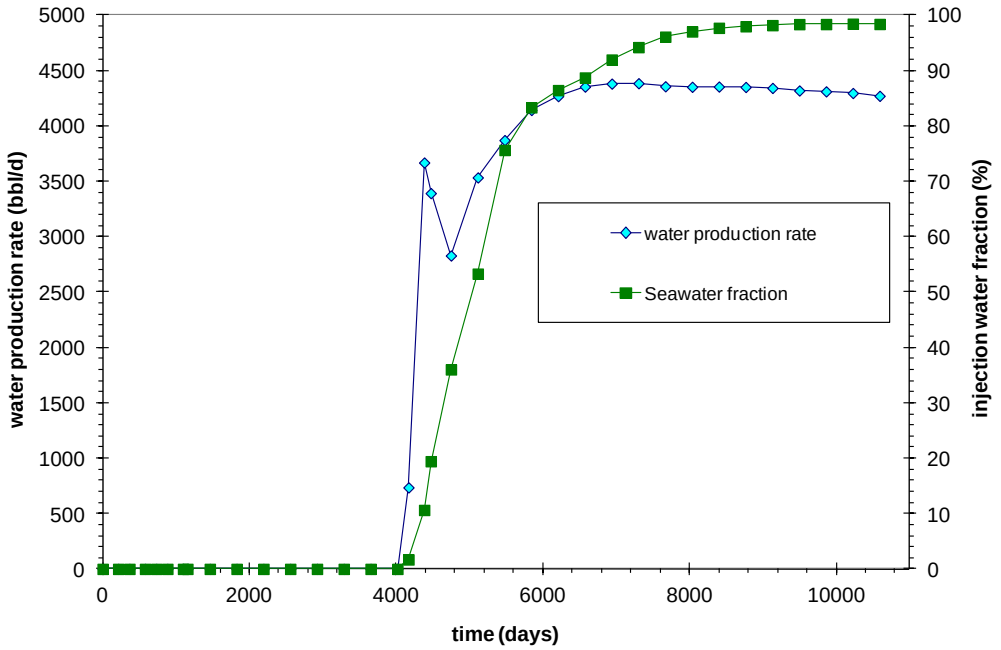

Figure B.5: Water production rate & percentage of the injected water produced as a function of time for well A5.

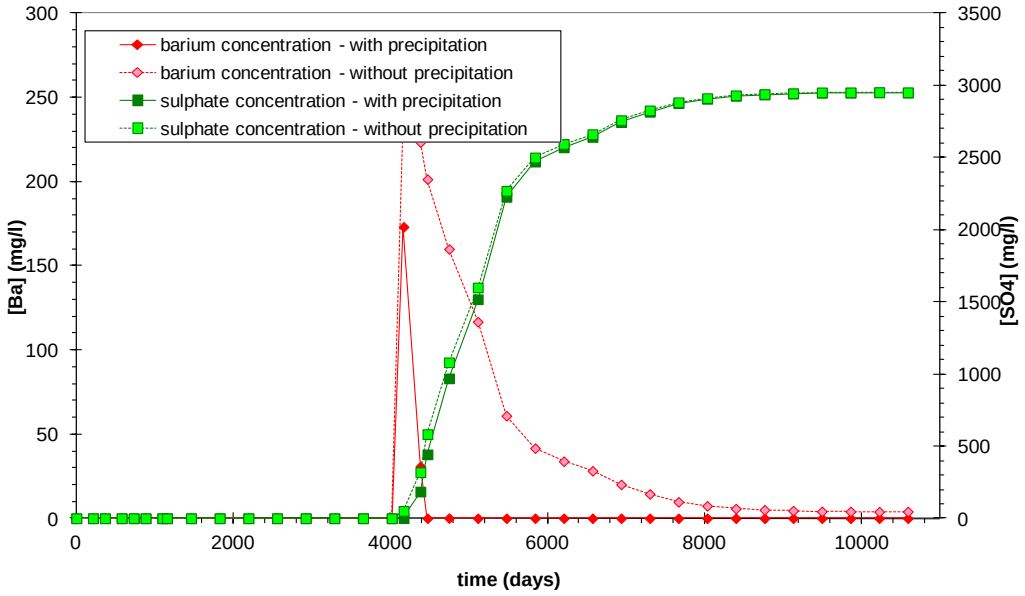

Figure B.6: Barium and sulphate production with instantaneous precipitation and without precipitation as a function of time for well A5.

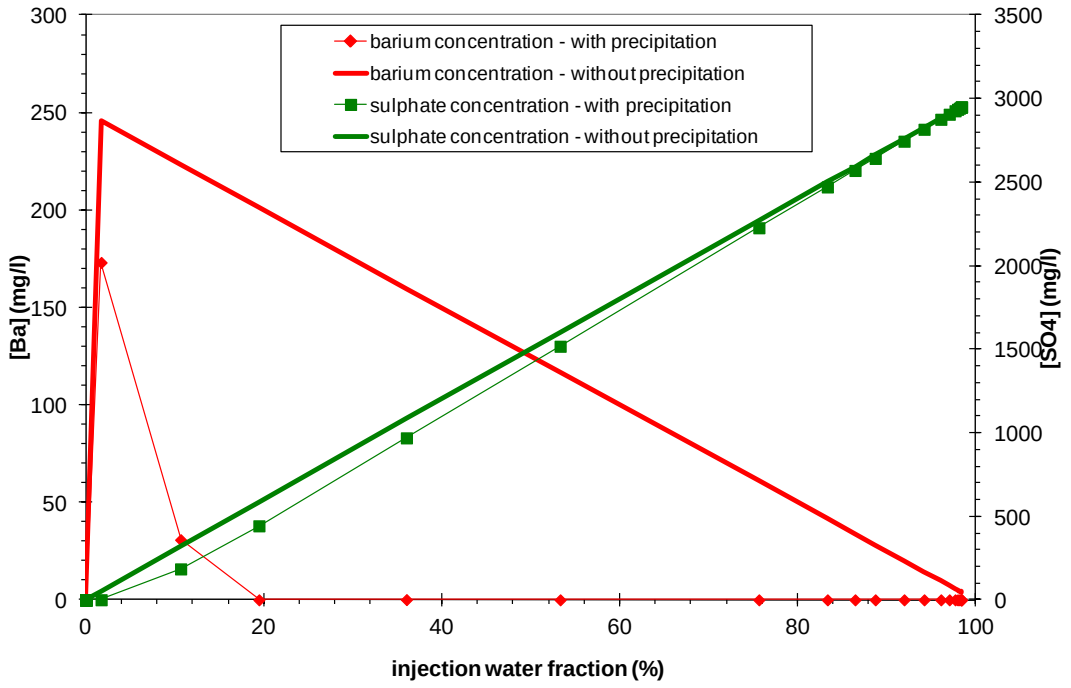

Figure B.7: The produced concentration of barium and sulphate ions as a function of the produced fraction of sea water for well A5.

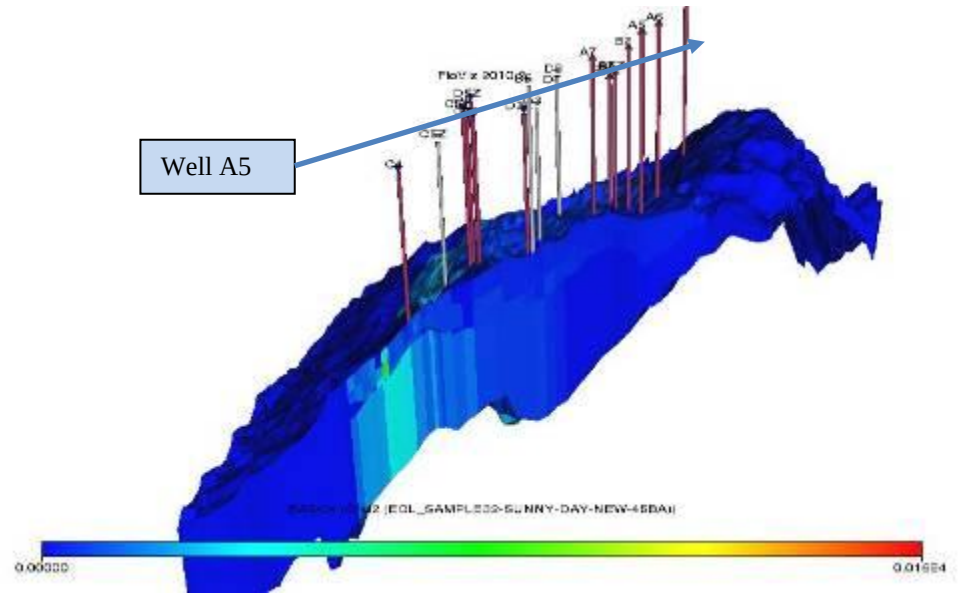

Figure B.8: The 3D section of Field X indicates $BaSO_4$ location for well A5.

Well B5Z-with barium concentration of 45 mg/l.

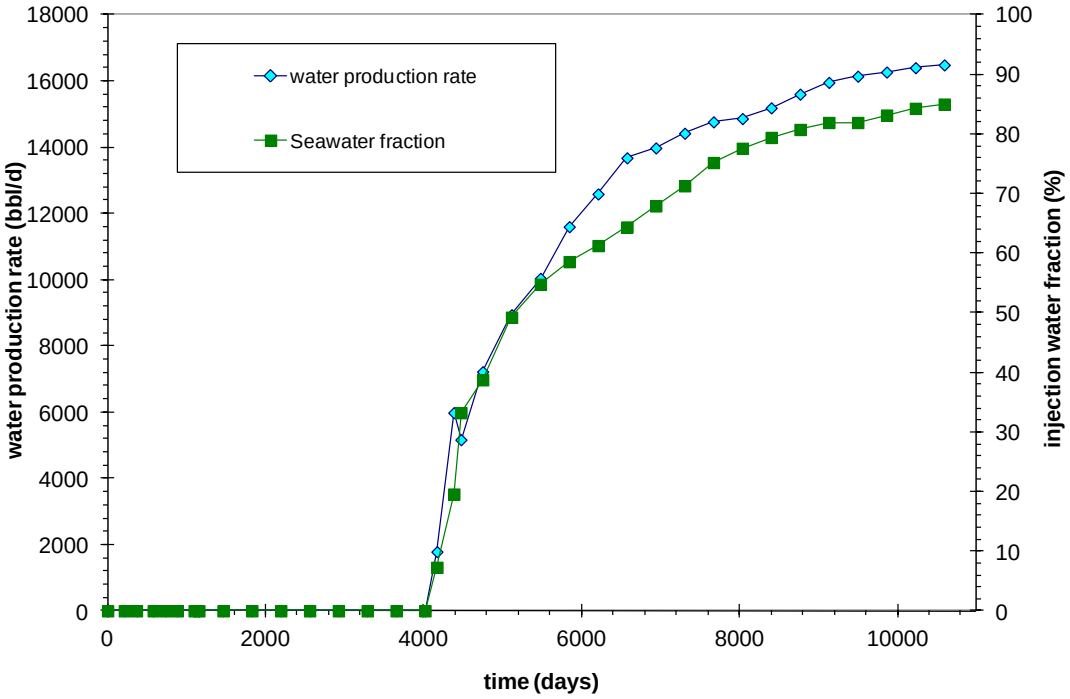

Figure B.9: Water production rate and percentage of the injected water produced as a function of time for well B5Z.

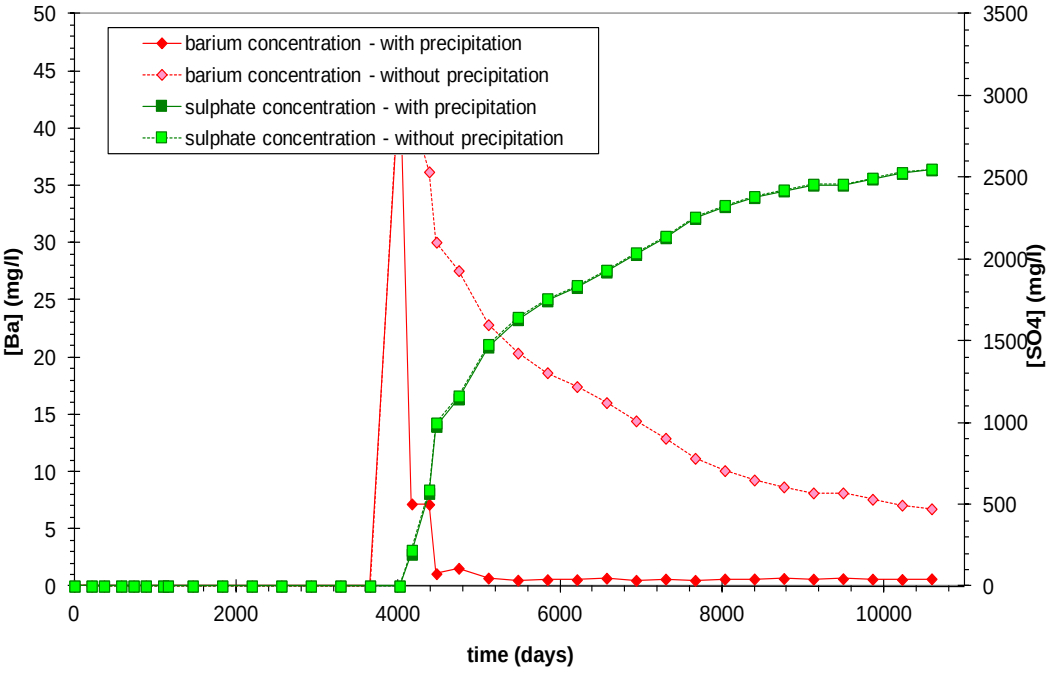

Figure B.10: Barium and sulphate production with instantaneous precipitation and without precipitation as a function of time for well B5Z.

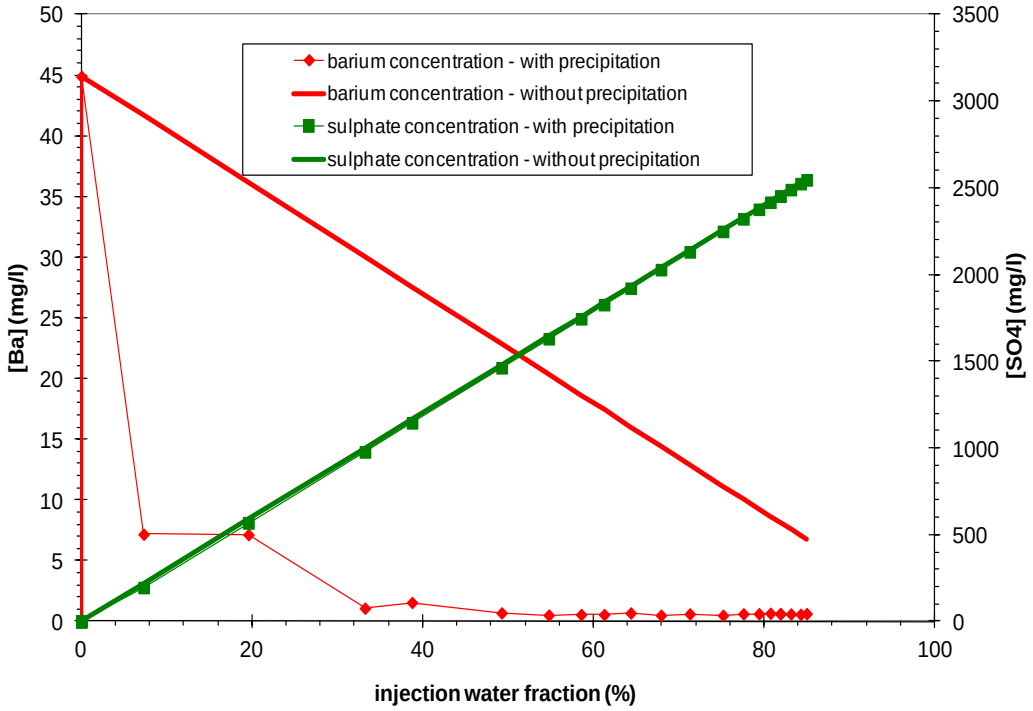

Figure B.11: The produced concentration of barium and sulphate ions as a function of the produced fraction of sea water for well B5Z.

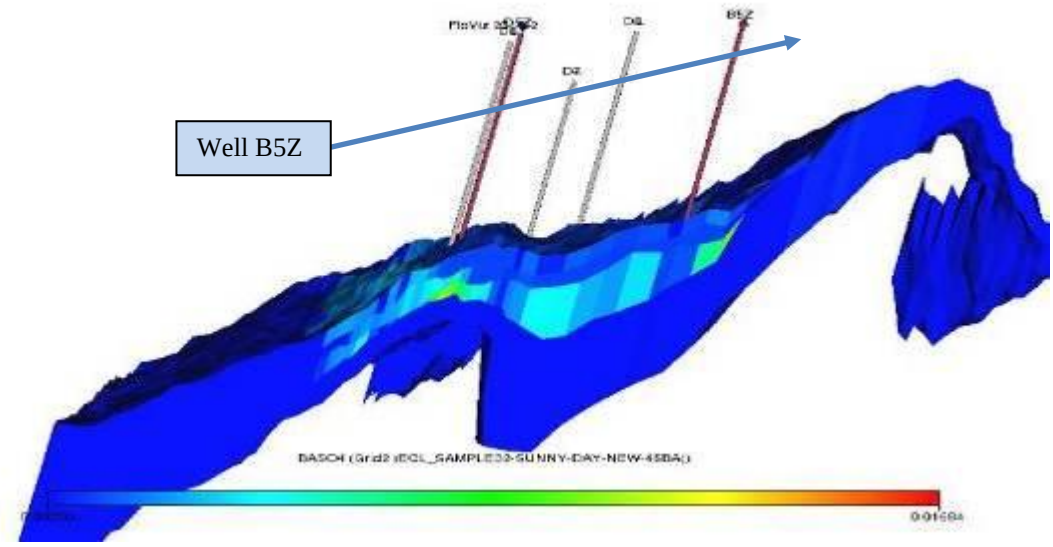

Figure B.12: The 3D section of Field X indicates $BaSO_4$ location for well B5Z.

Well D9Z -with barium concentration of 45 mg/l.

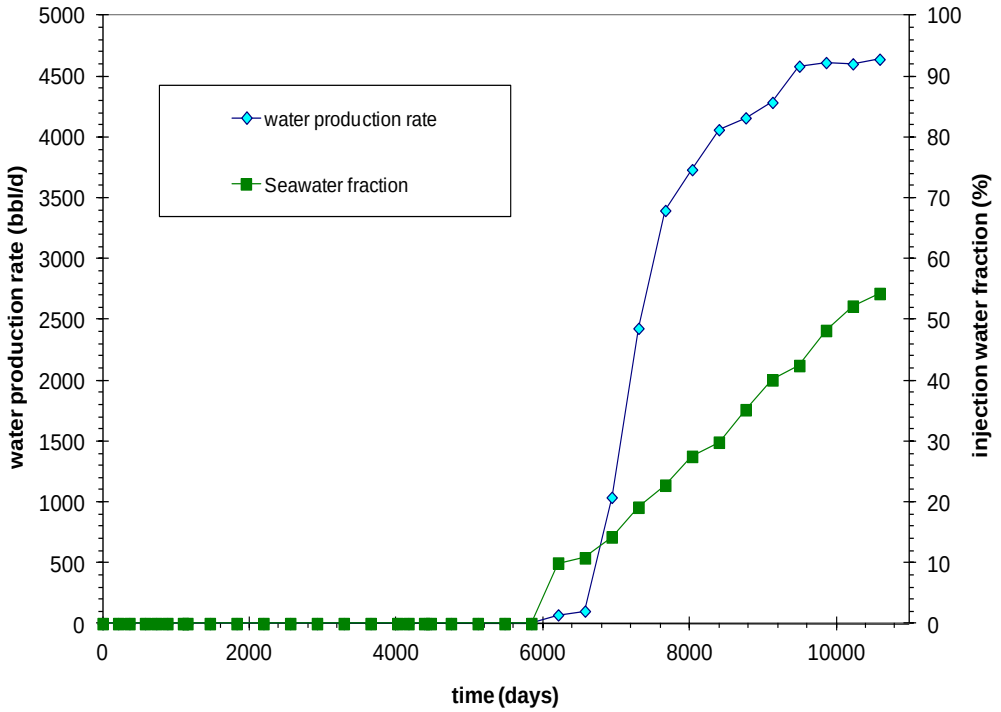

Figure B.13: Water production rate and percentage of the injected water produced as a function of time for well D9Z.

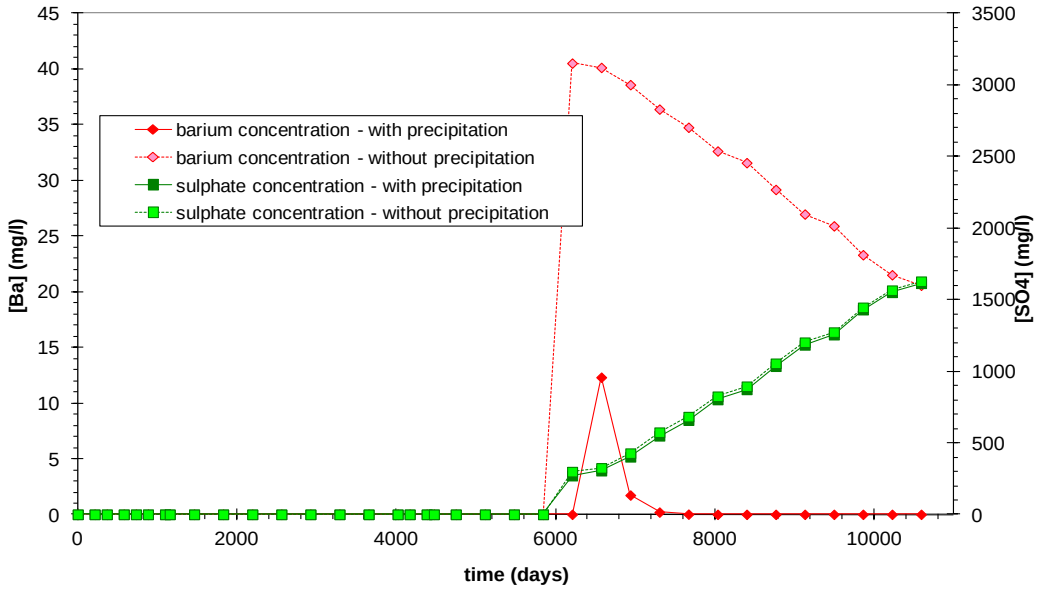

Figure B.14: Barium and sulphate production with instantaneous precipitation and without precipitation as a function of time for well D9Z.

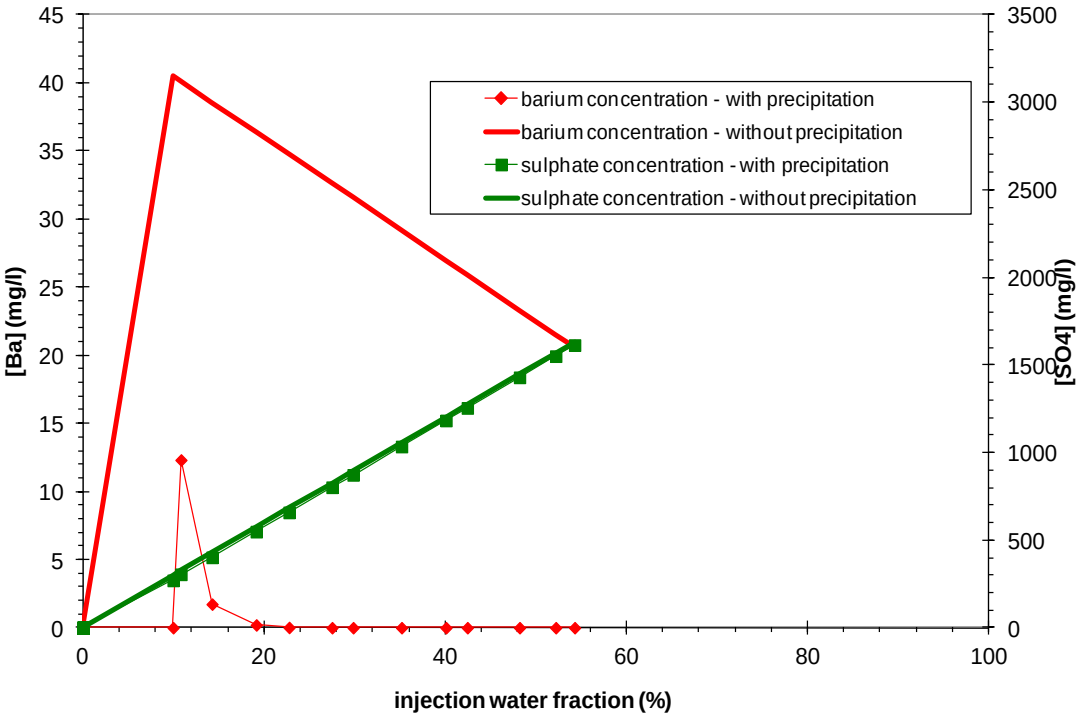

Figure B.15: The produced concentration of barium and sulphate ions as a function of the produced fraction of sea water for well D9Z

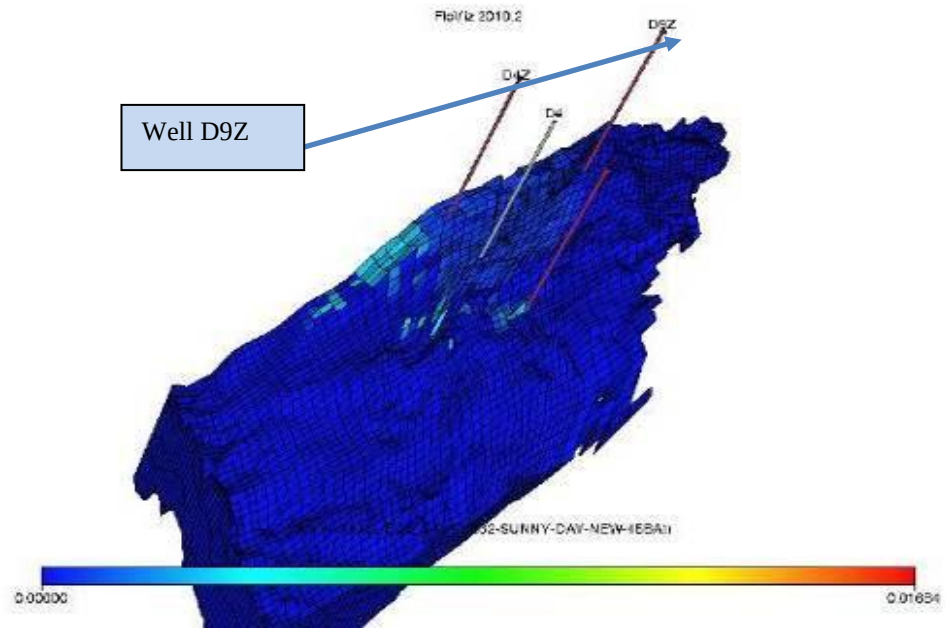

Figure B.16: The 3D section of Field X indicates $BaSO_4$ location for well D9Z.

Well A1Z-with barium concentration of 80 mg/l.

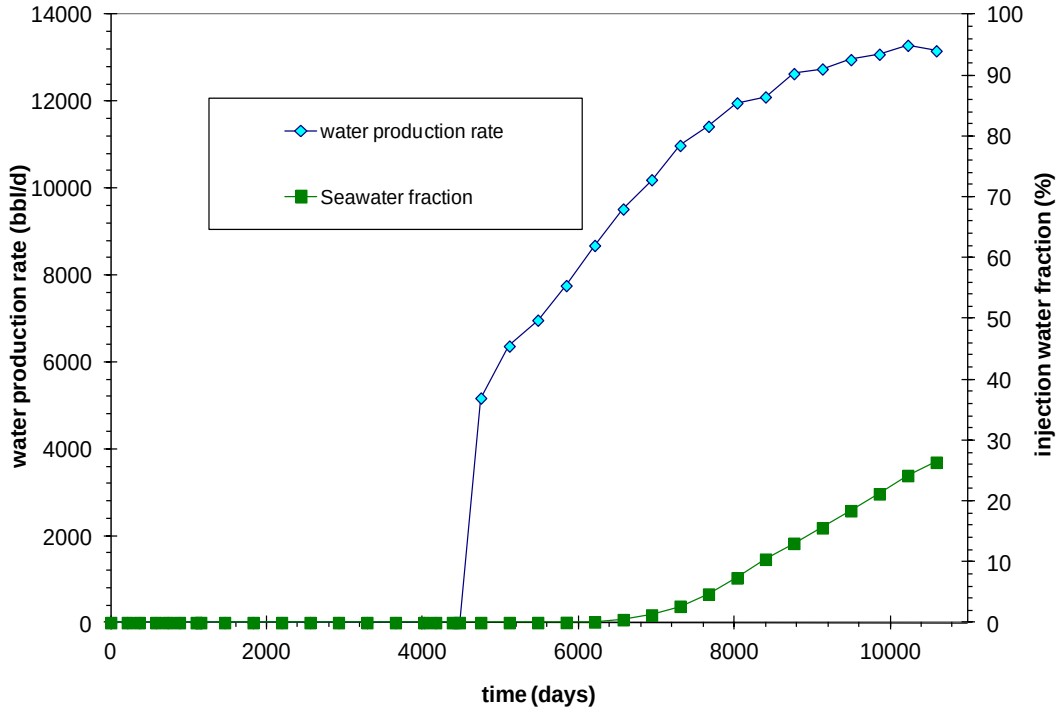

Figure B.17: Water production rate and percentage of the injected water produced as a function of time for well A1Z.

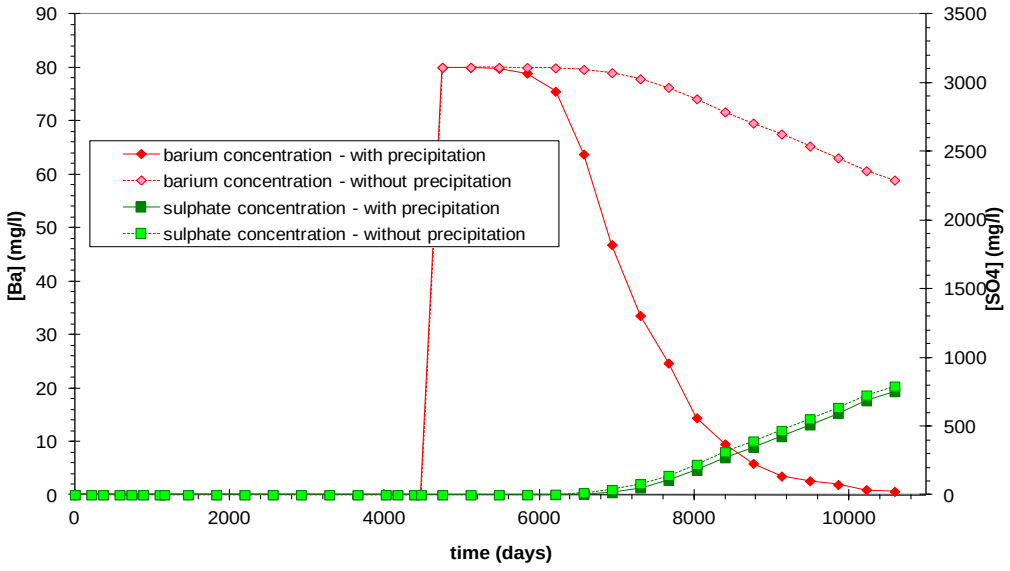

Figure B.18: Barium and sulphate production with instantaneous precipitation and without precipitation as a function of time for well A1Z.

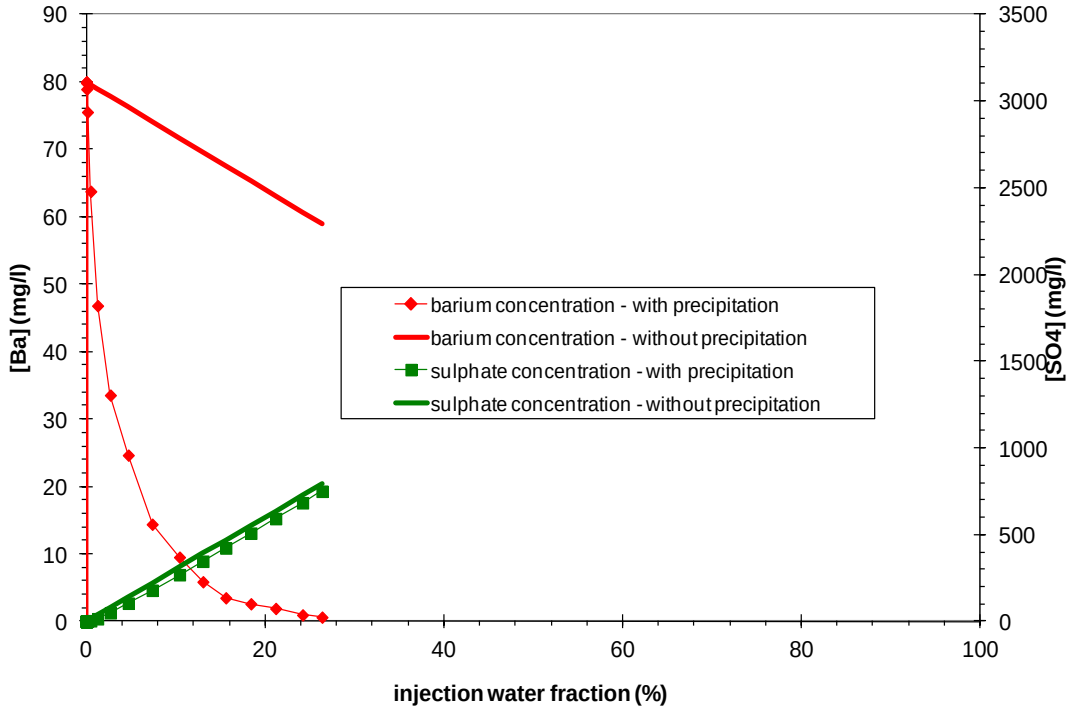

Figure B.19: The produced concentration of barium and sulphate ions as a function of the produced fraction of sea water for well A1Z.

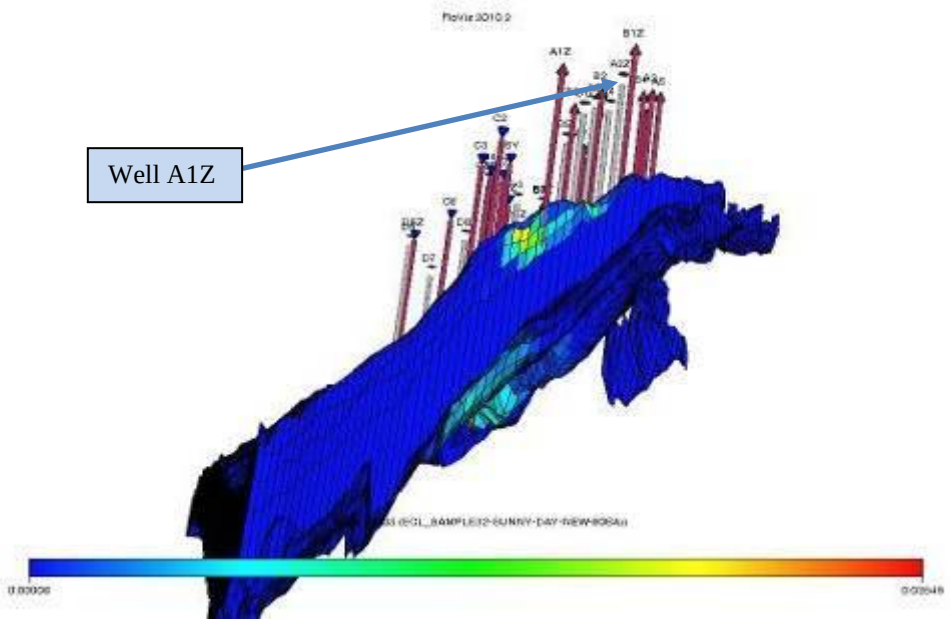

Figure B.20: The 3D section of Field X indicates $BaSO_4$ location for well A1Z.

Well A5 -with barium concentration of 80 mg/l.

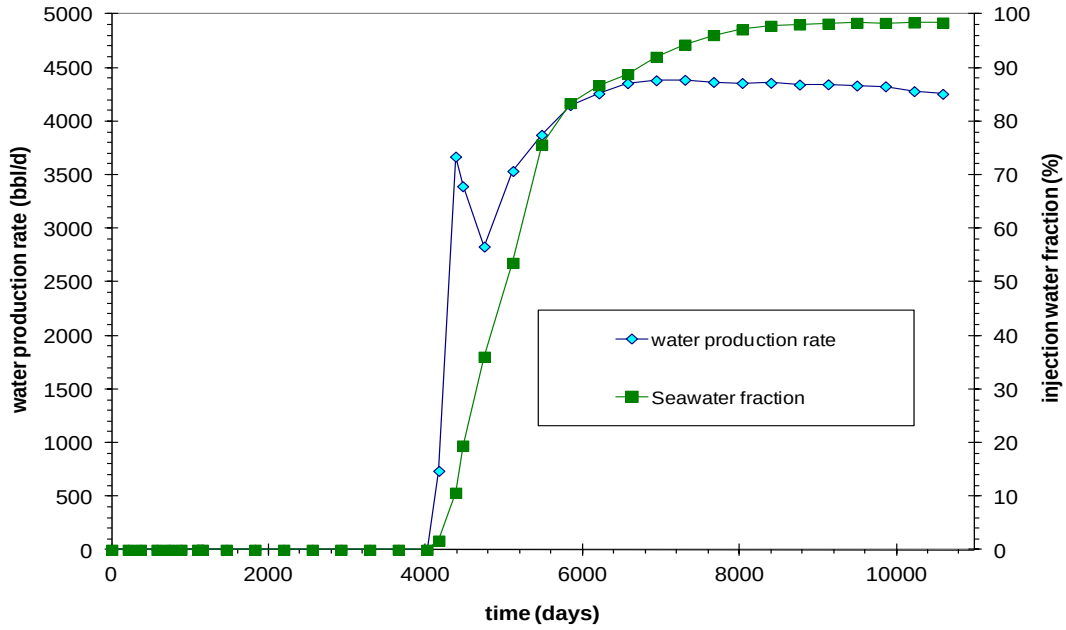

Figure B.21: Water production rate and percentage of the injected water produced as a function of time for well A5.

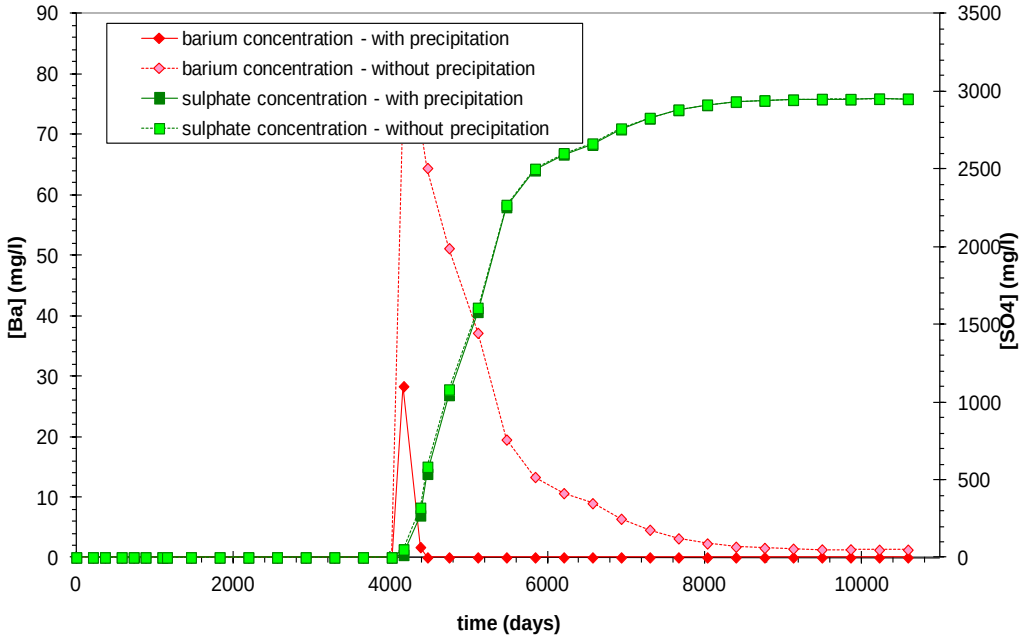

Figure B.22: Barium and sulphate production with instantaneous precipitation and without precipitation as a function of time for well A5.

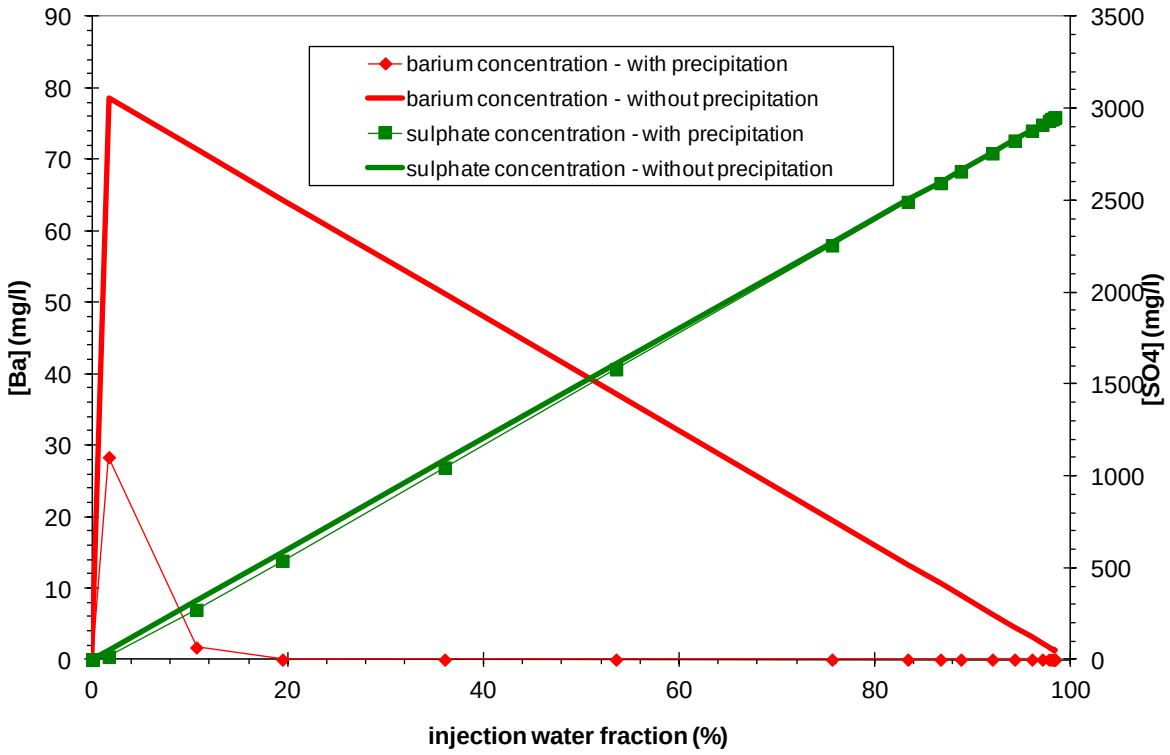

Figure B.23: The produced concentration of barium and sulphate ions as a function of the produced fraction of sea water for well A5.

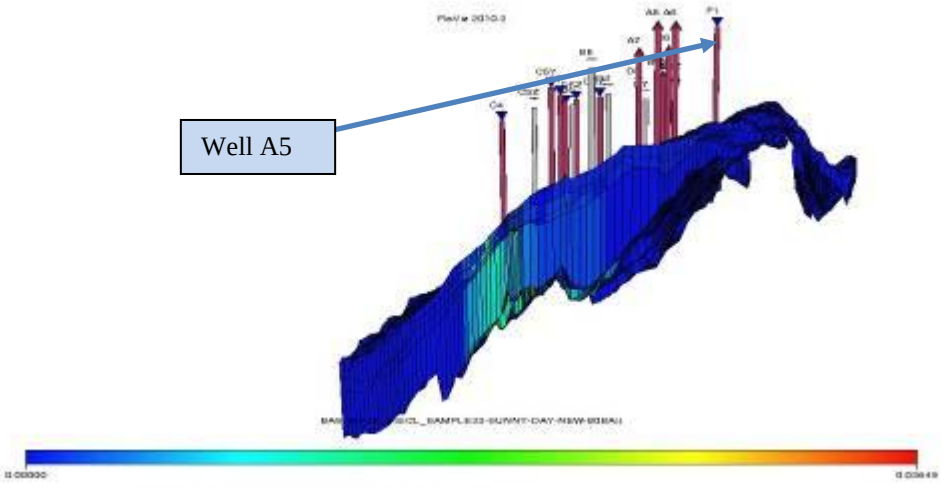

Figure B.24: The 3D section of Field X indicates $BaSO_4$ location for well A5.

Well B5Z -with barium concentration of 80 mg/l.

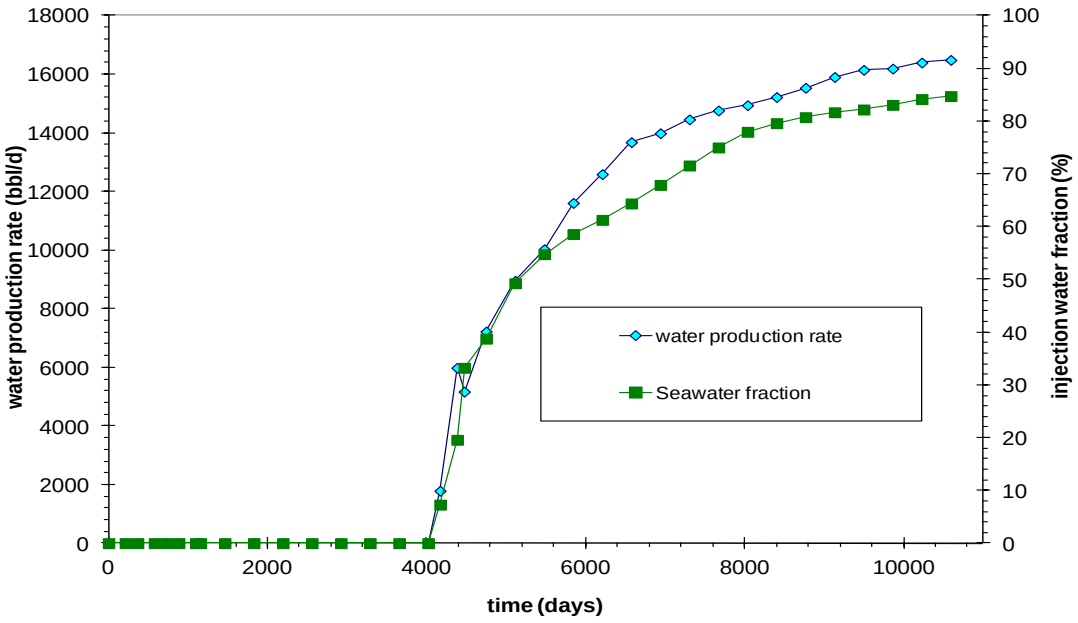

Figure B.25: Water production rate and percentage of the injected water produced as a function of time for well B5Z.

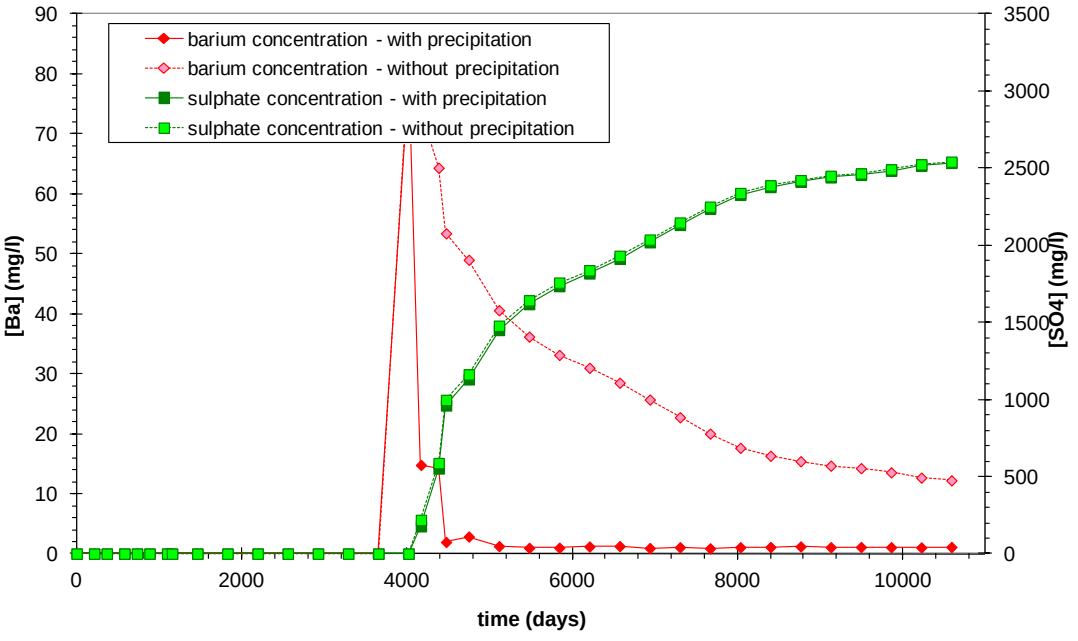

Figure B.26: Barium and sulphate production with instantaneous precipitation and without precipitation as a function of time for well B5Z.

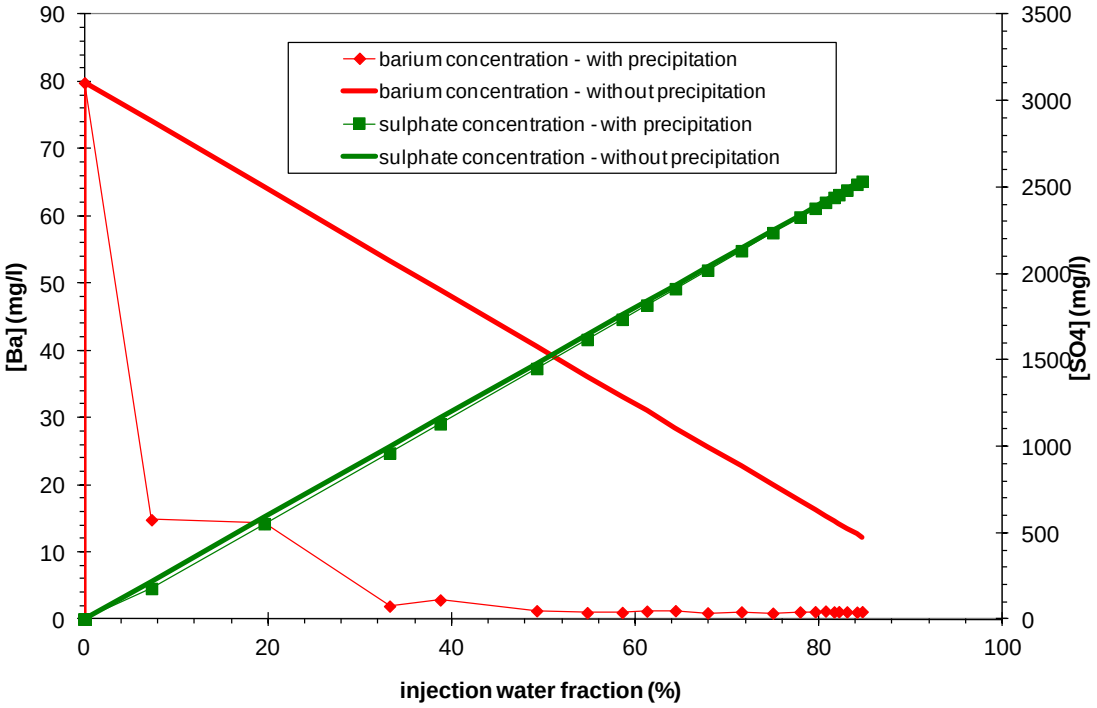

Figure B.27: The produced concentration of barium and sulphate ions as a function of the produced fraction of sea water for well B5Z.

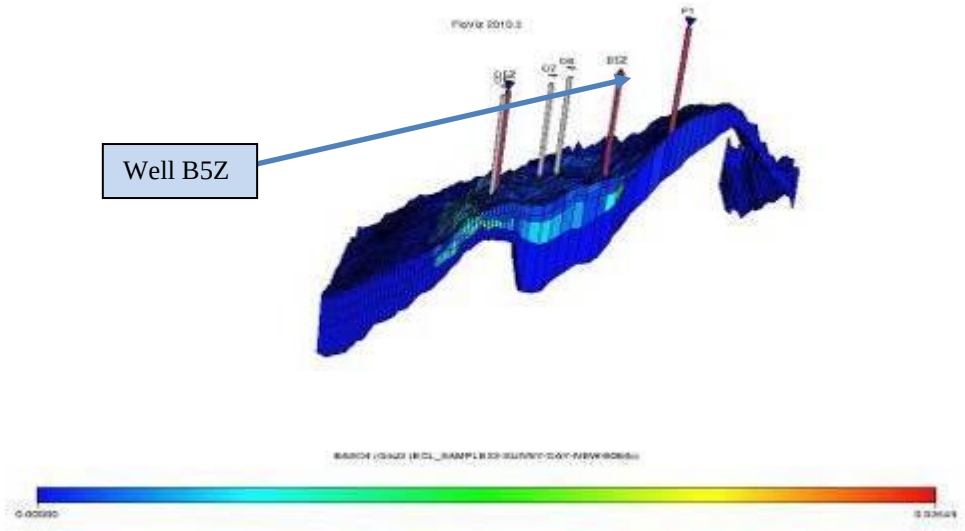

Figure B.28: The 3D section of Field X indicates $BaSO_4$ location for well B5Z.

Well D9Z -with barium concentration of 80 mg/l.

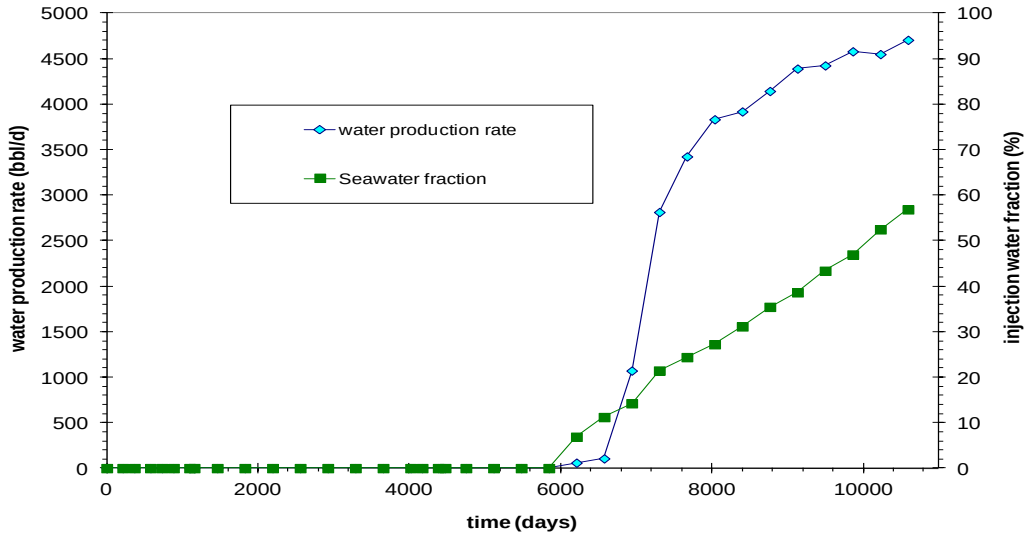

Figure B.29: Water production rate and percentage of the injected water produced as a function of time for well D9Z

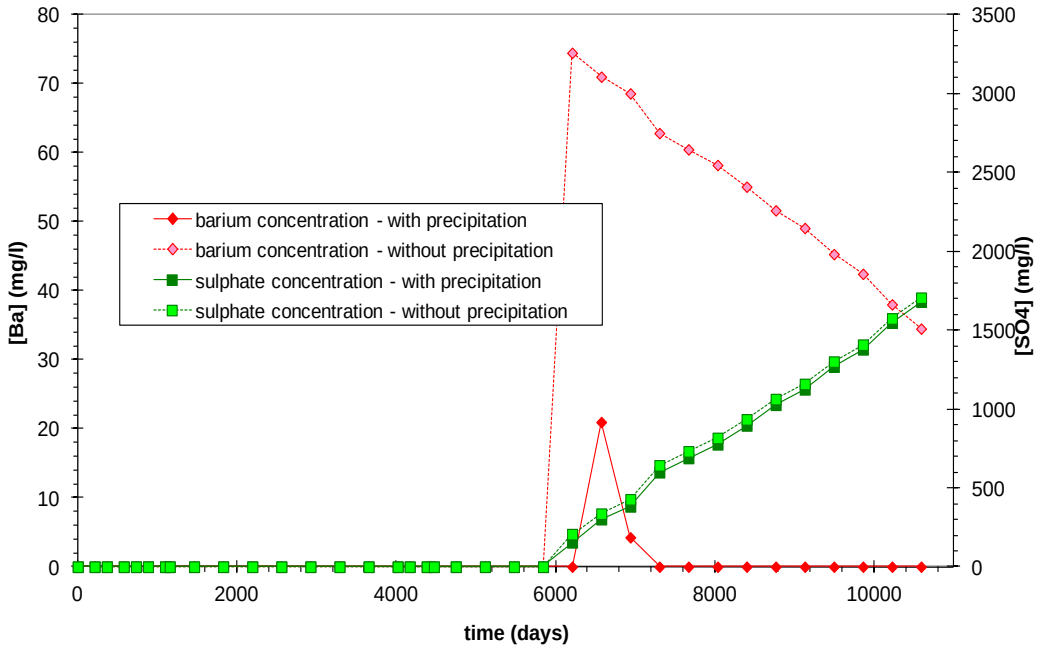

Figure B.30: Barium and sulphate production with instantaneous precipitation and without precipitation as a function of time for well D9Z.

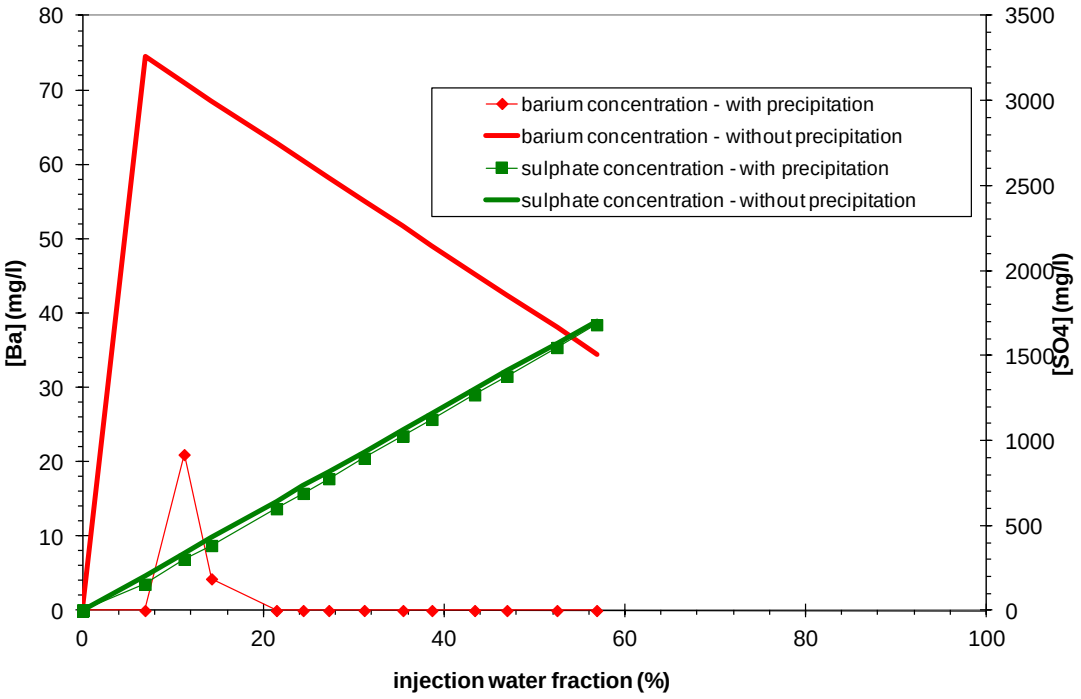

Figure B.31: The produced concentration of barium and sulphate ions as a function of the produced fraction of sea water for well D9Z.

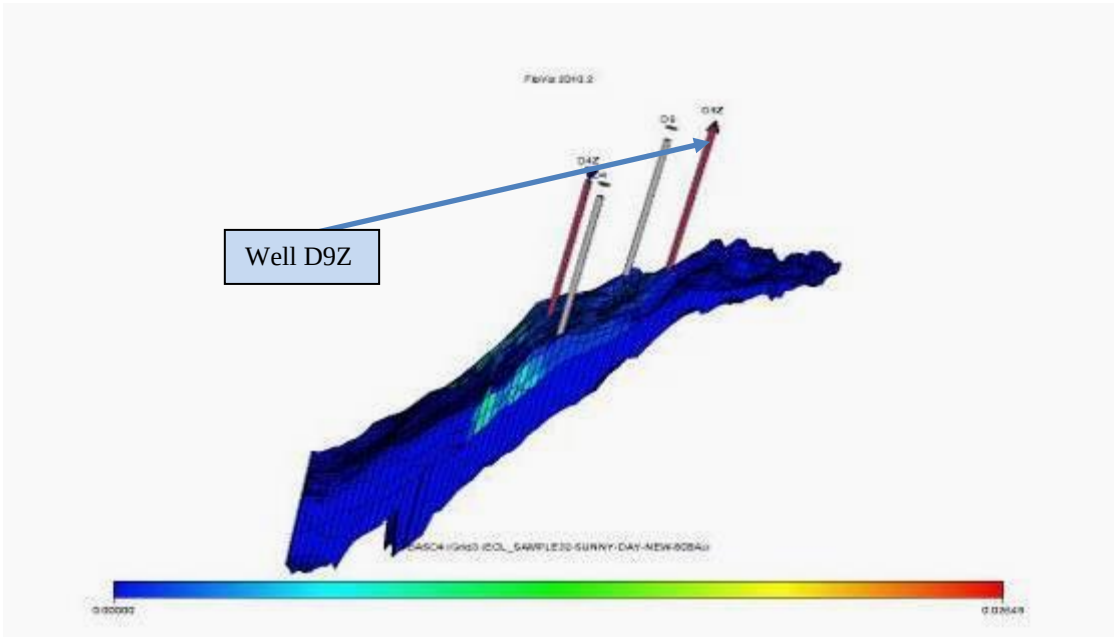

Figure B.32: The 3D section of Field X indicates $BaSO_4$ location for well D9Z.

Well A1Z -with barium concentration of 229 mg/l.

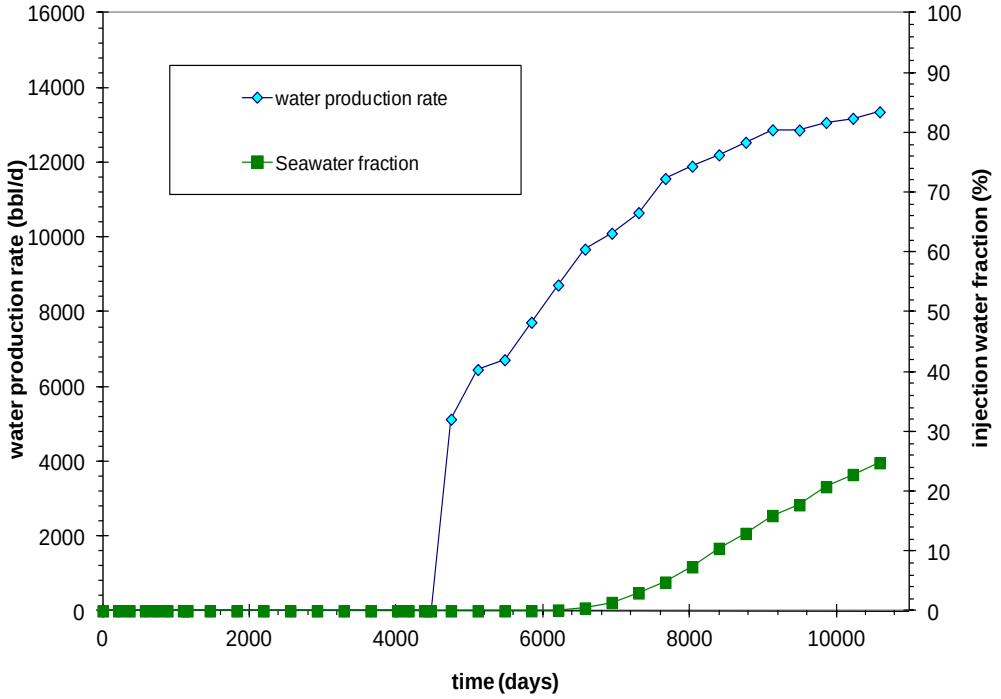

Figure B.33: Water production rate and percentage of the injected water produced as a function of time for well A1Z.

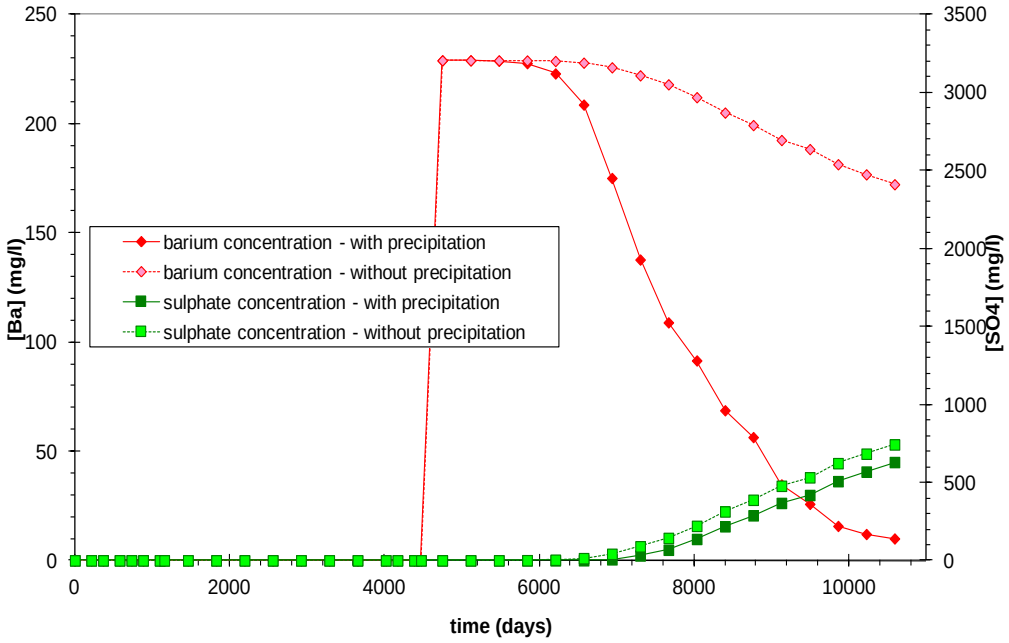

Figure B.34: Barium and sulphate production with instantaneous precipitation and without precipitation as a function of time for well A1Z.

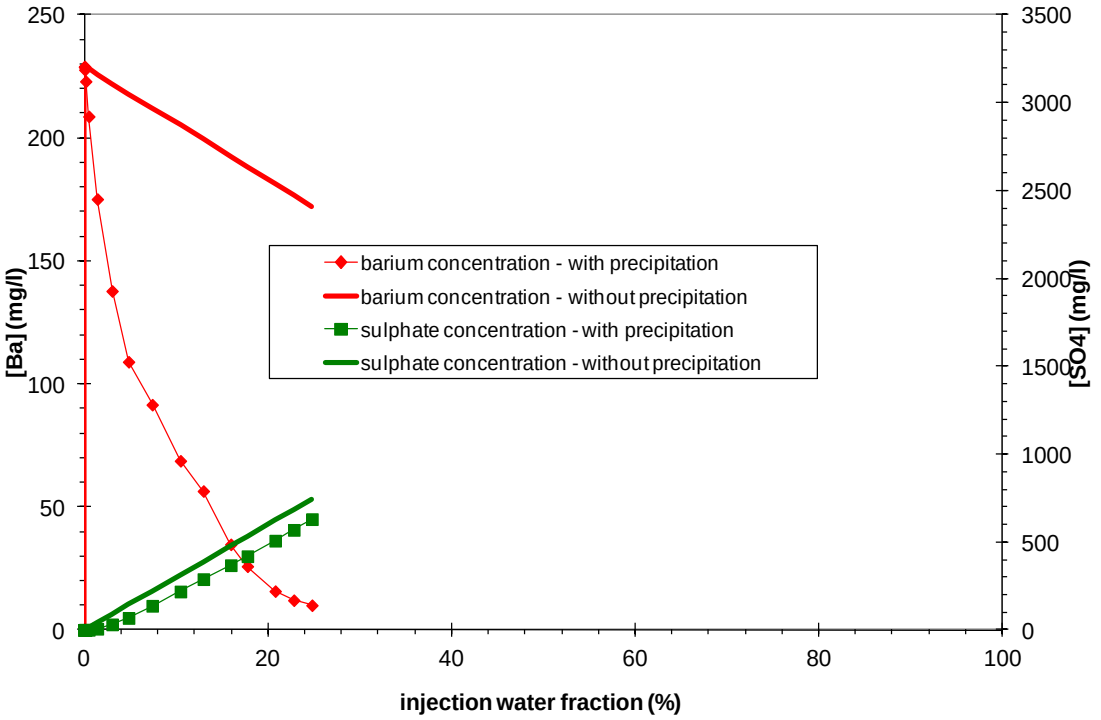

Figure B.35: The produced concentration of barium and sulphate ions as a function of the produced fraction of sea water for well A1Z.

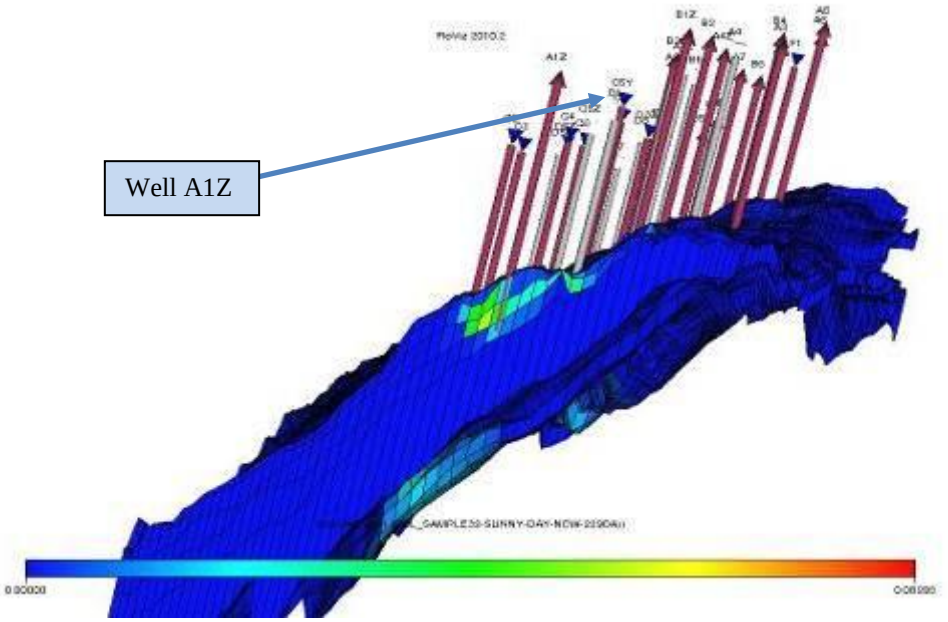

Figure B.36: The 3D section of Field X indicates $BaSO_4$ location for well A1Z.

Well A5 -with barium concentration of 229 mg/l.

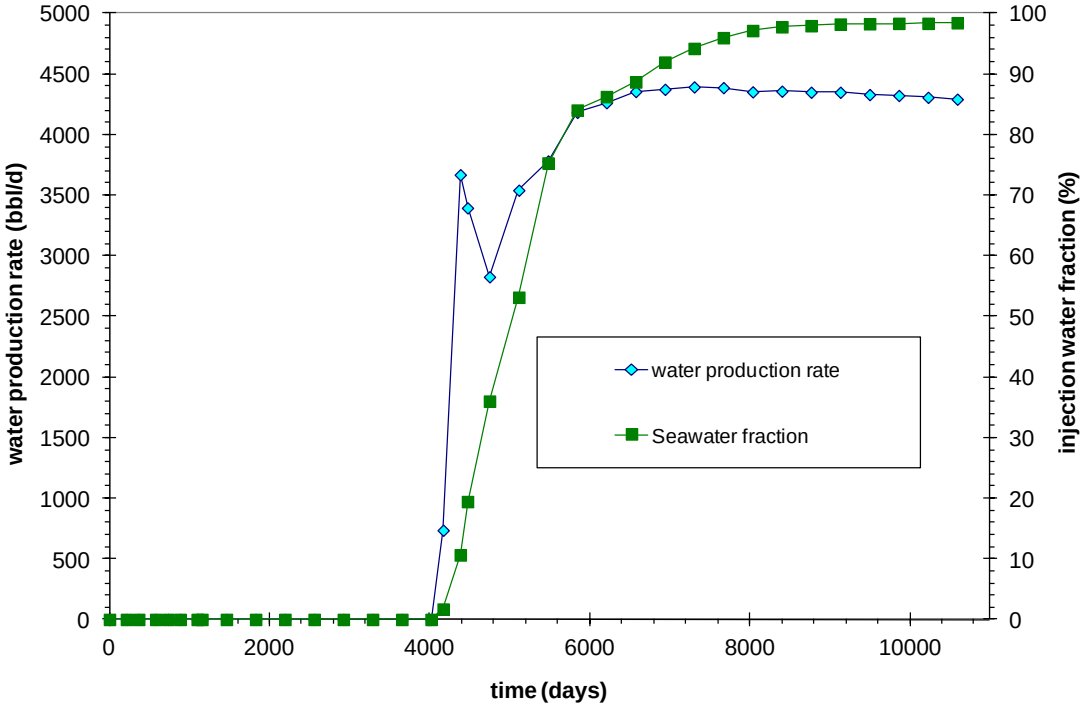

Figure B.37: Water production rate and percentage of the injected water produced as a function of time for well A5.

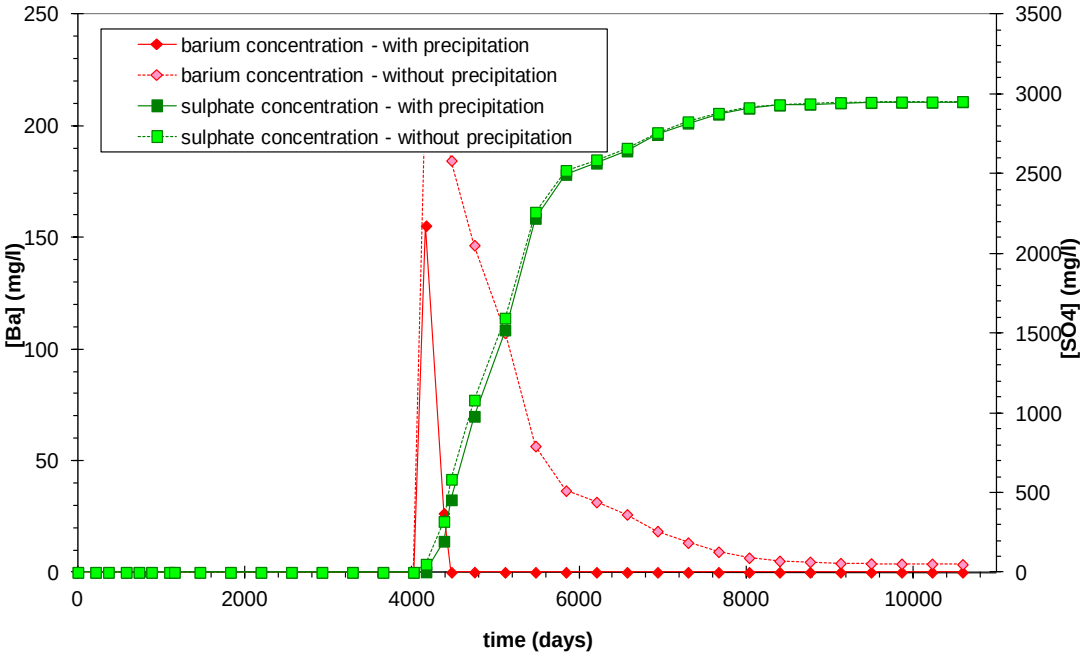

Figure B.38: Barium and sulphate production with instantaneous precipitation and without precipitation as a function of time for well A5.

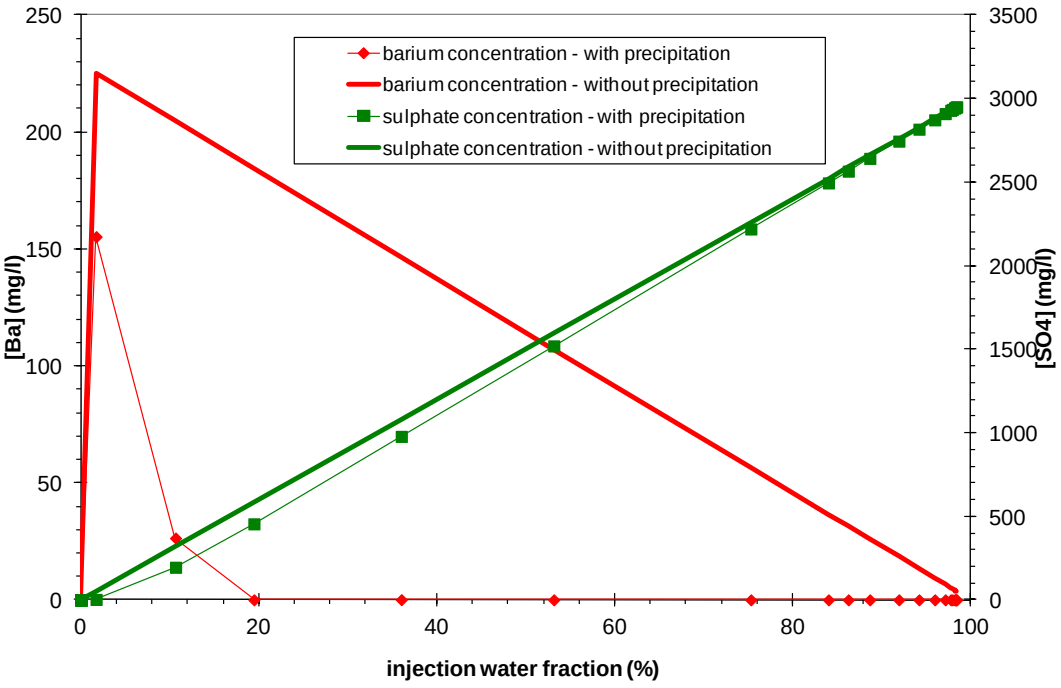

Figure B.39: The produced concentration of barium and sulphate ions as a function of the produced friction of sea water for well A5.

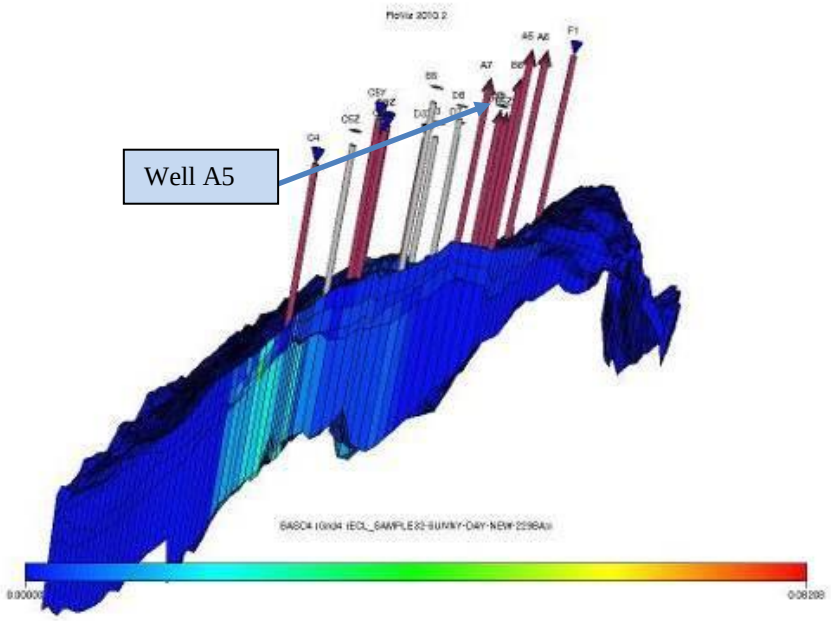

Figure B.40: The 3D section of Field X indicates $BaSO_4$ location for well A5.

Well B5Z -with barium concentration of 229 mg/l.

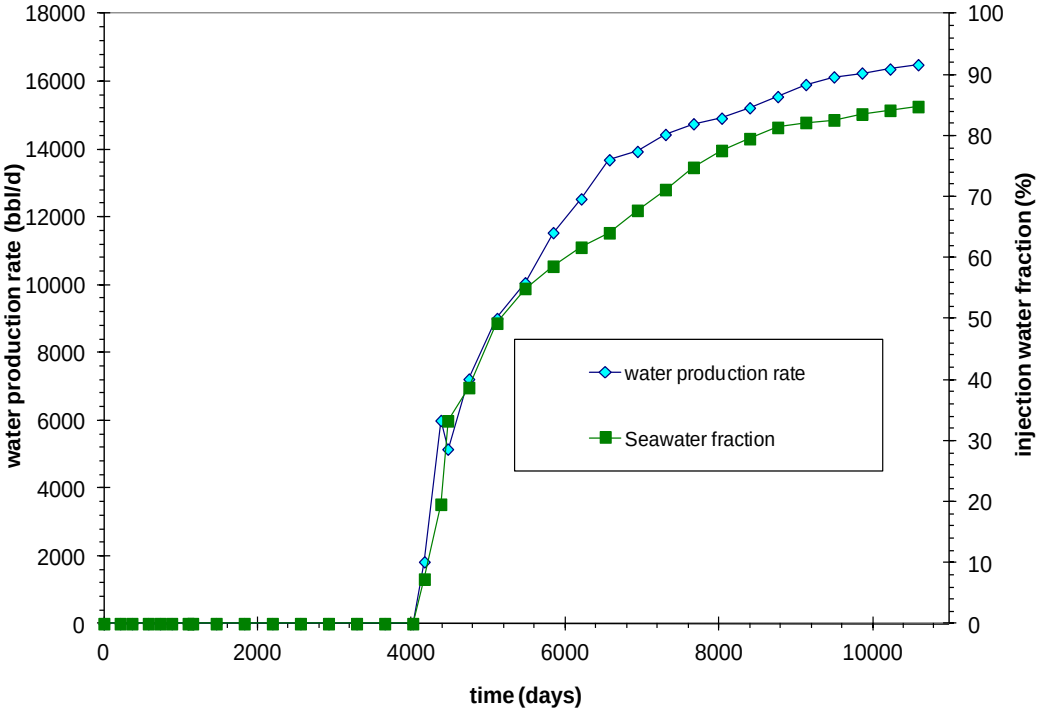

Figure B.41: Water production rate and percentage of the injected water produced as a function of time for well B5Z.

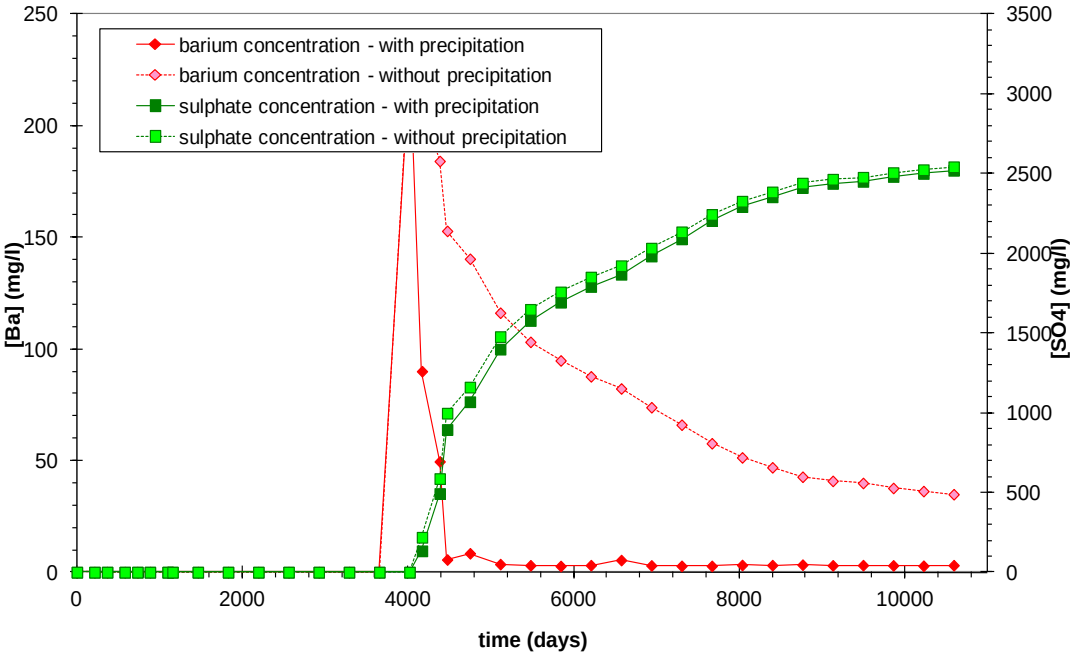

Figure B.42: Barium and sulphate production with instantaneous precipitation and without precipitation as a function of time for well B5Z.

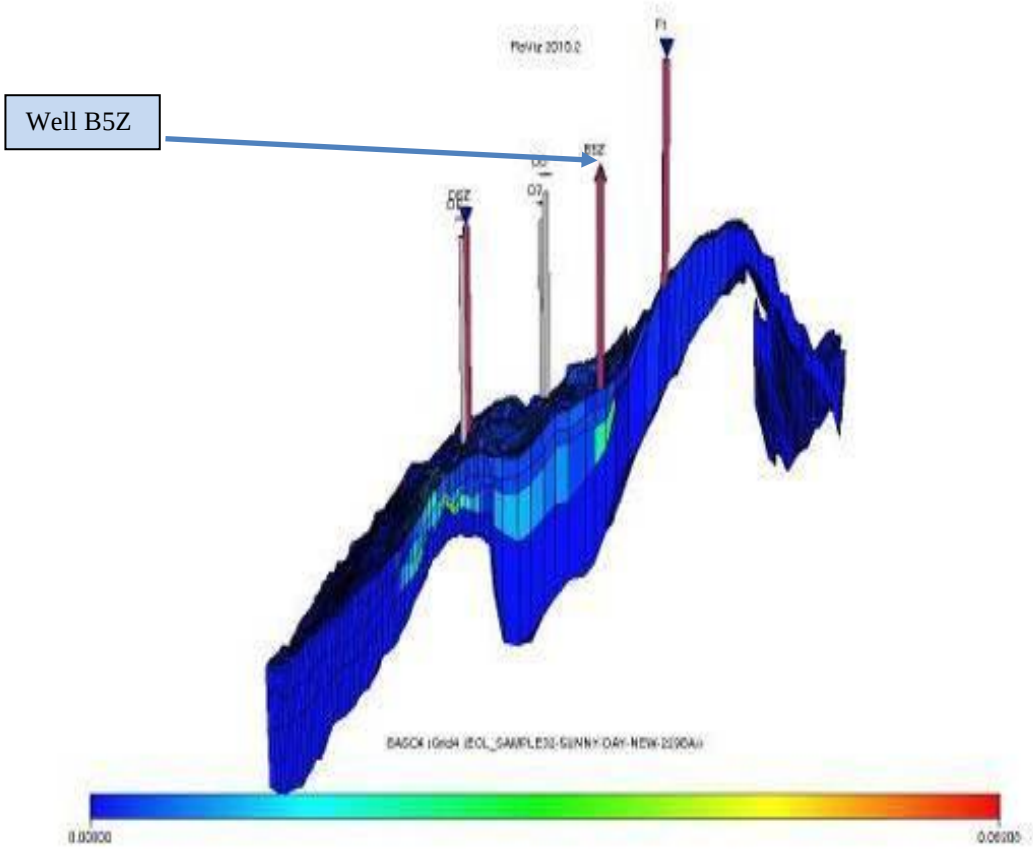

Figure B.43: The 3D section of Field X indicates $BaSO_4$ location for well B5Z.

Well D9Z -with barium concentration of 229 mg/l

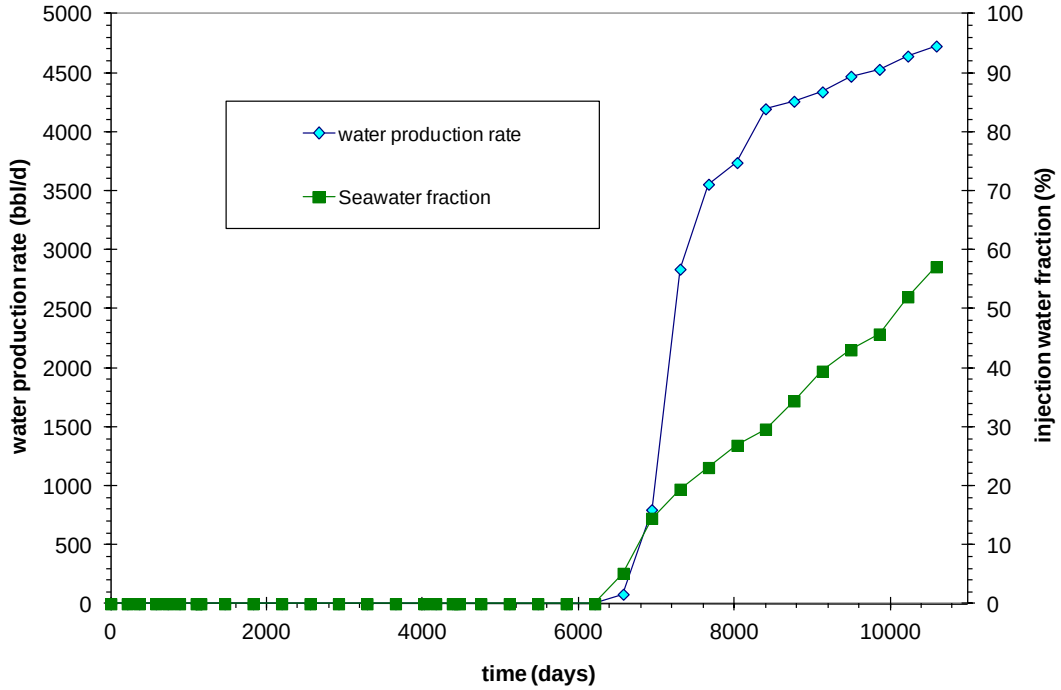

Figure B.44: Water production rate and percentage of the injected water produced as a function of time for well D9Z

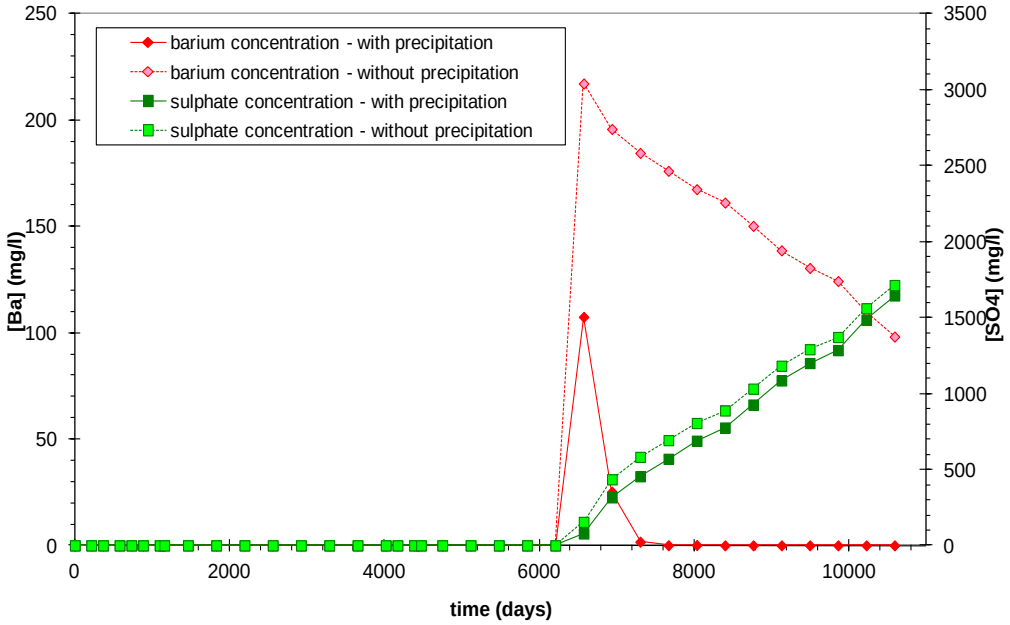

Figure B.45: Barium and sulphate production with instantaneous precipitation and without precipitation as a function of time for well D9Z.

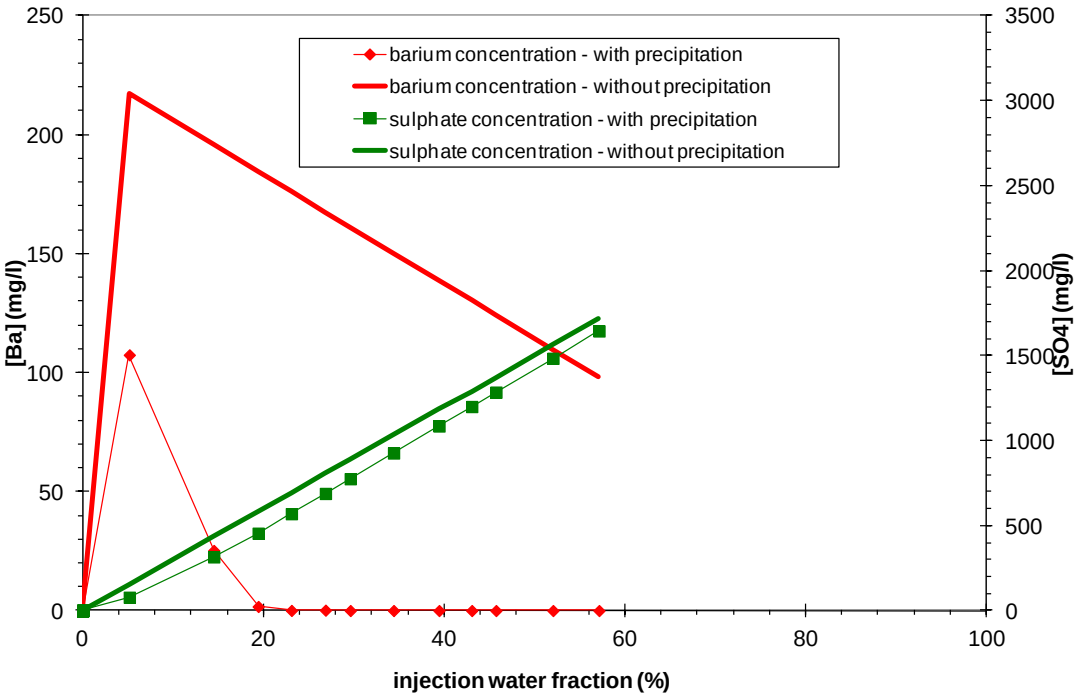

Figure B.46: The produced concentration of barium and sulphate ions as a function of the produced fraction of sea water for well D9Z.

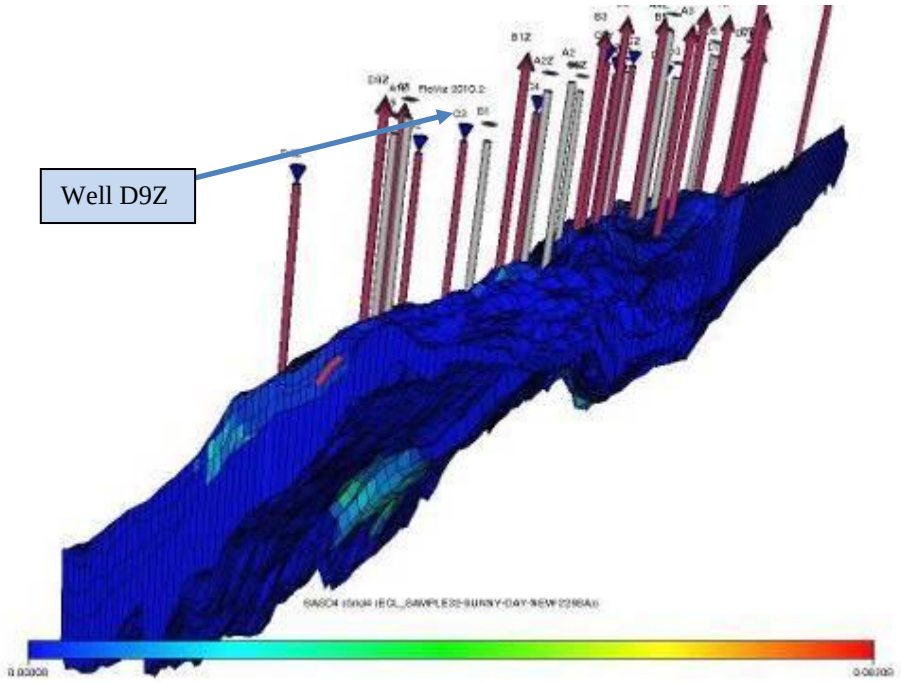

Figure B.47: The 3D section of Field X indicates $BaSO_4$ location for well D9Z.

Well A1Z -with barium concentration of 800 mg/l.

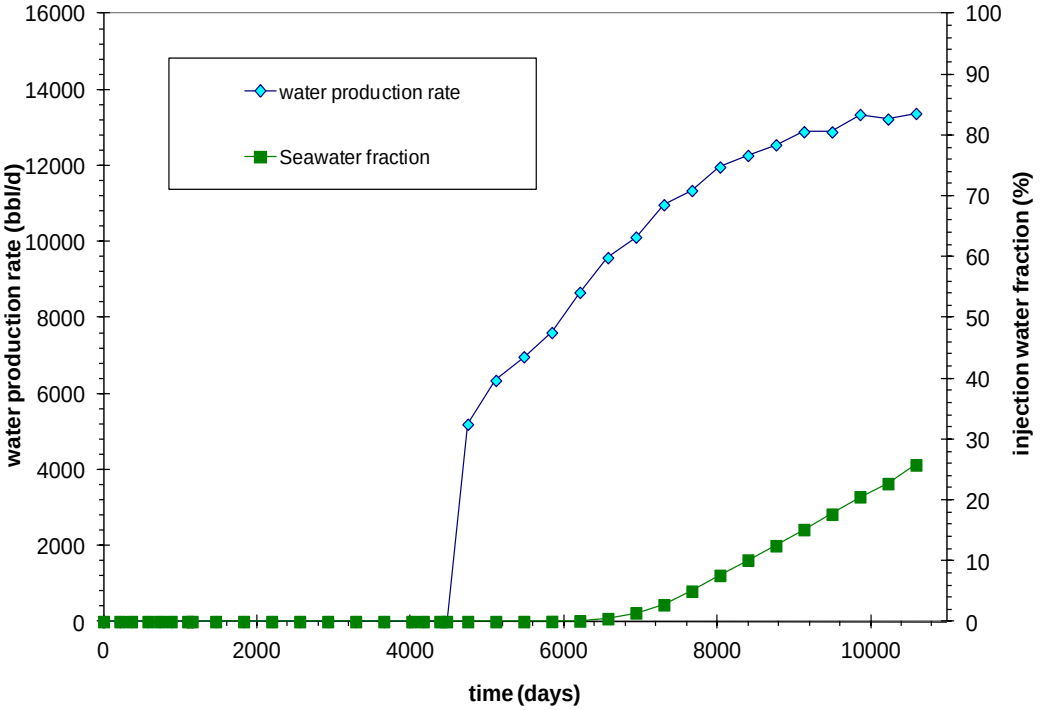

Figure B.48: Water production rate and percentage of the injected water produced as function of time for well A1Z.

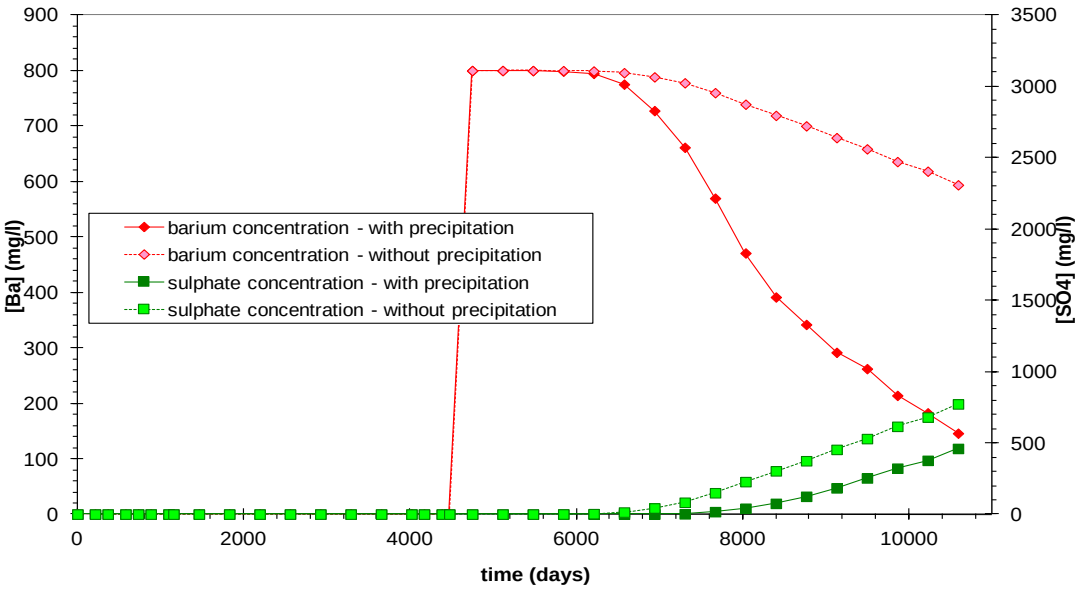

Figure B.49: Barium and sulphate production with instantaneous precipitation and without precipitation as a function of time for well A1Z.

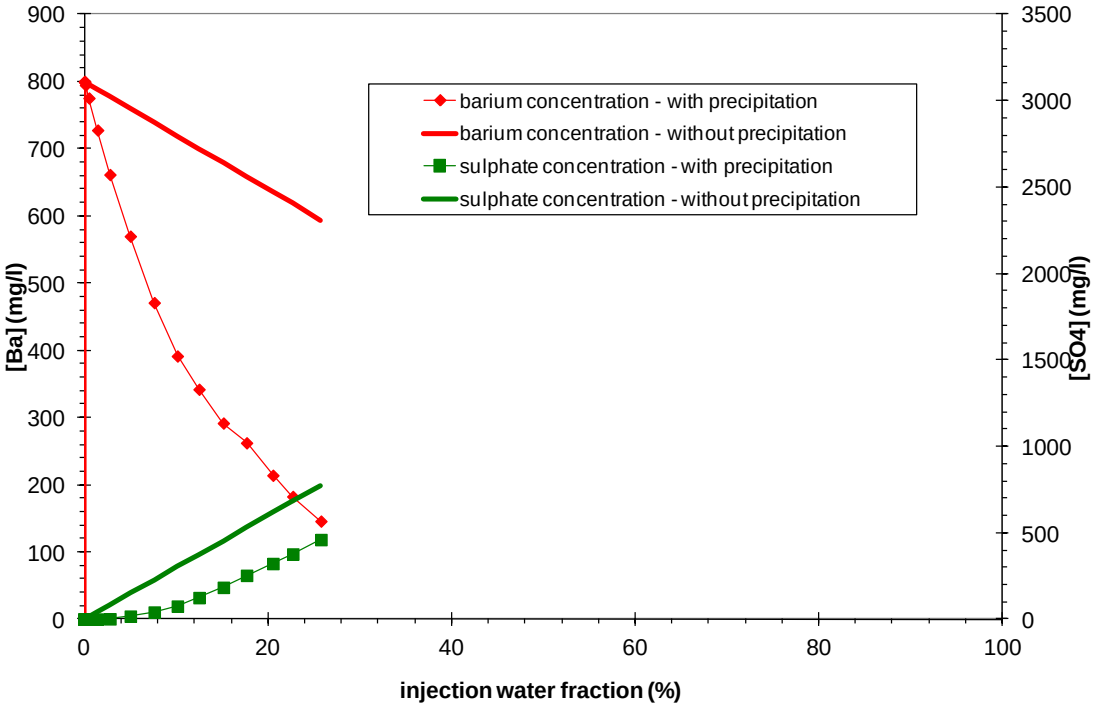

Figure B.50: The produced concentration of barium and sulphate ions as a function of the produced fraction of sea for well A1Z.

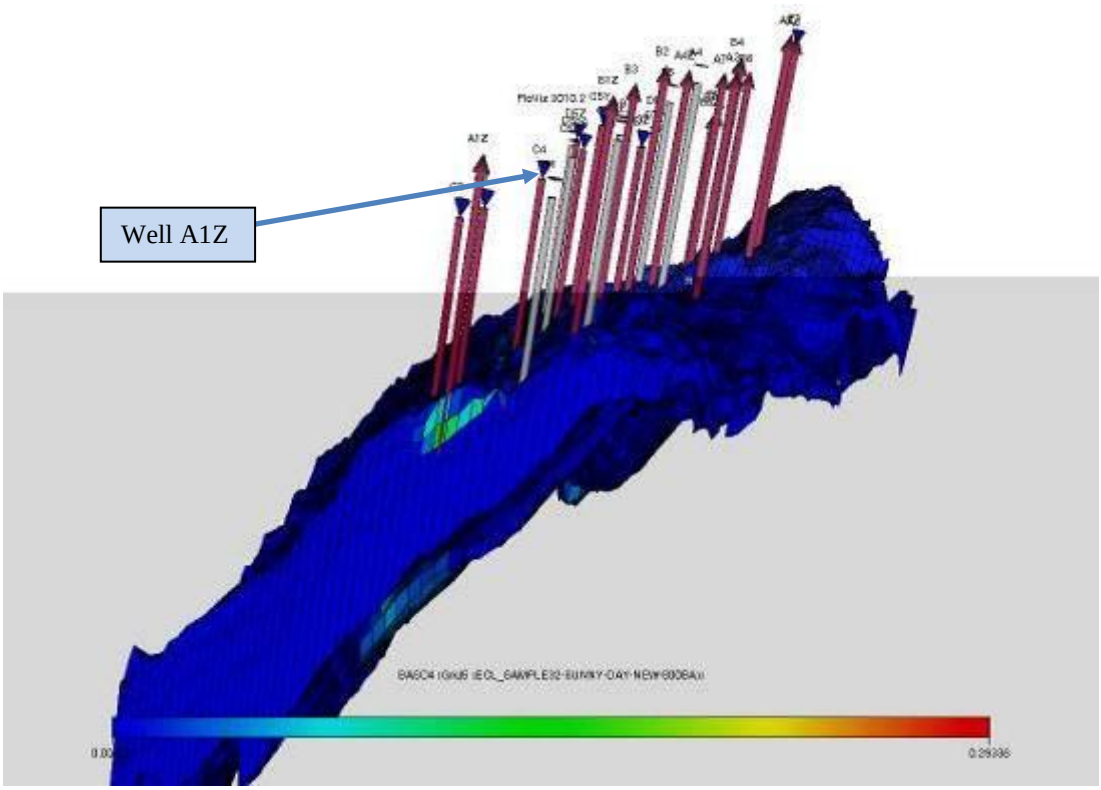

Figure B.51: The 3D section of Field X indicates $BaSO_4$ location for well A1Z.

Well A5 -with Barium concentration of 800 mg/l

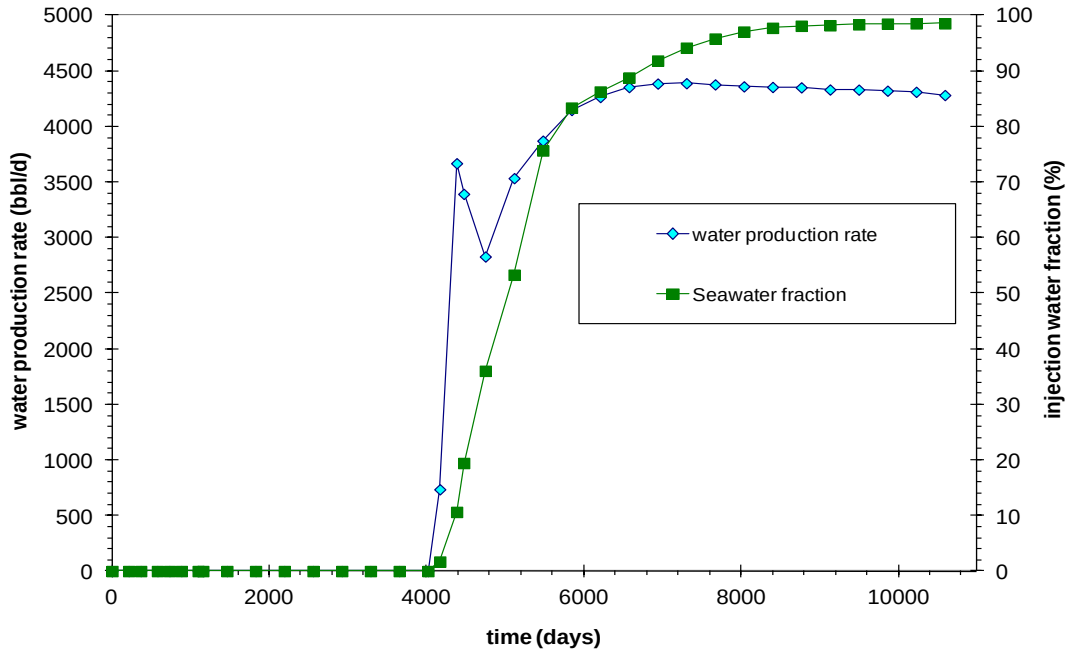

Figure B.52: Water production rate & percentage of the injected water produced as a function of time for well A5.

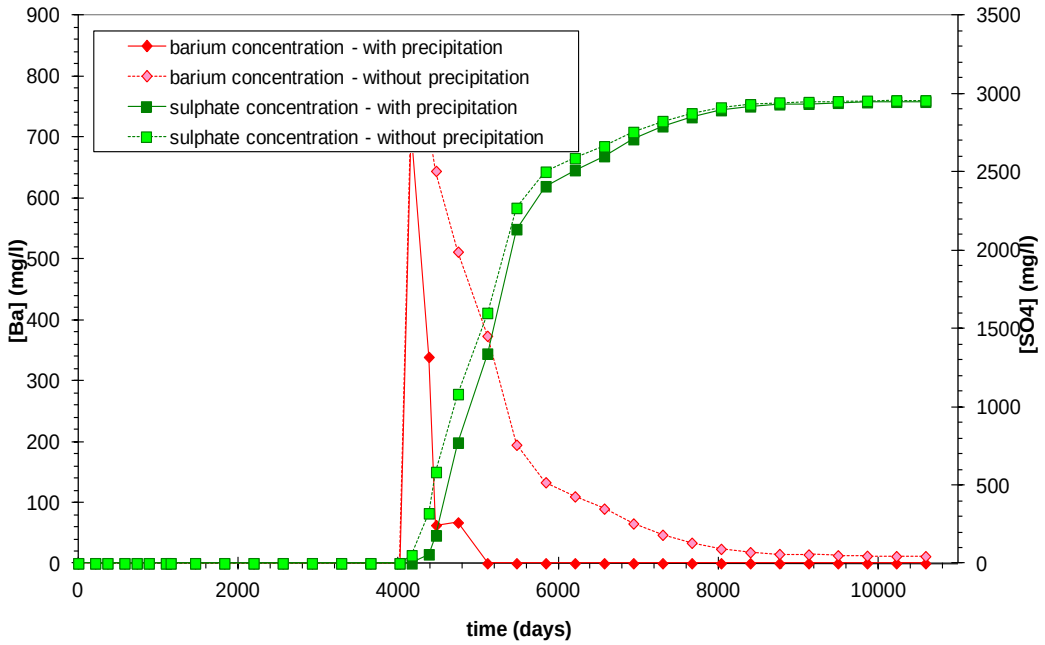

Figure B.53: Barium and sulphate production with instantaneous precipitation and without precipitation as a function of time for well A5.

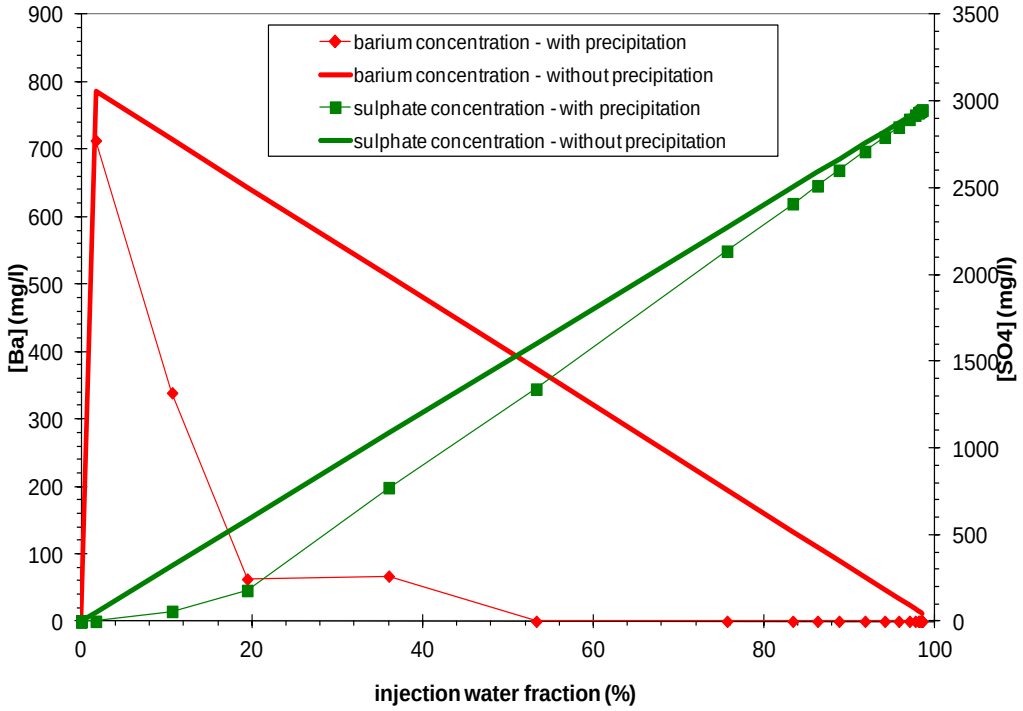

Figure B.54: The produced concentration of barium and sulphate ions as a function of the produced fraction of sea water for well A5.

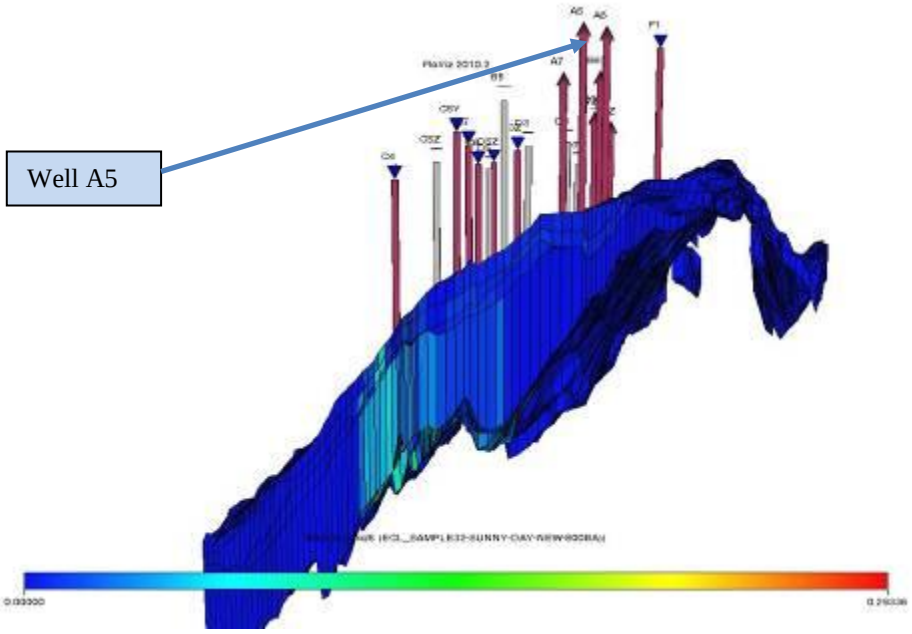

Figure B.55: The 3D section of Field X indicates $BaSO_4$ location for well A5.

Well B5Z -with barium concentration of 800 mg/l.

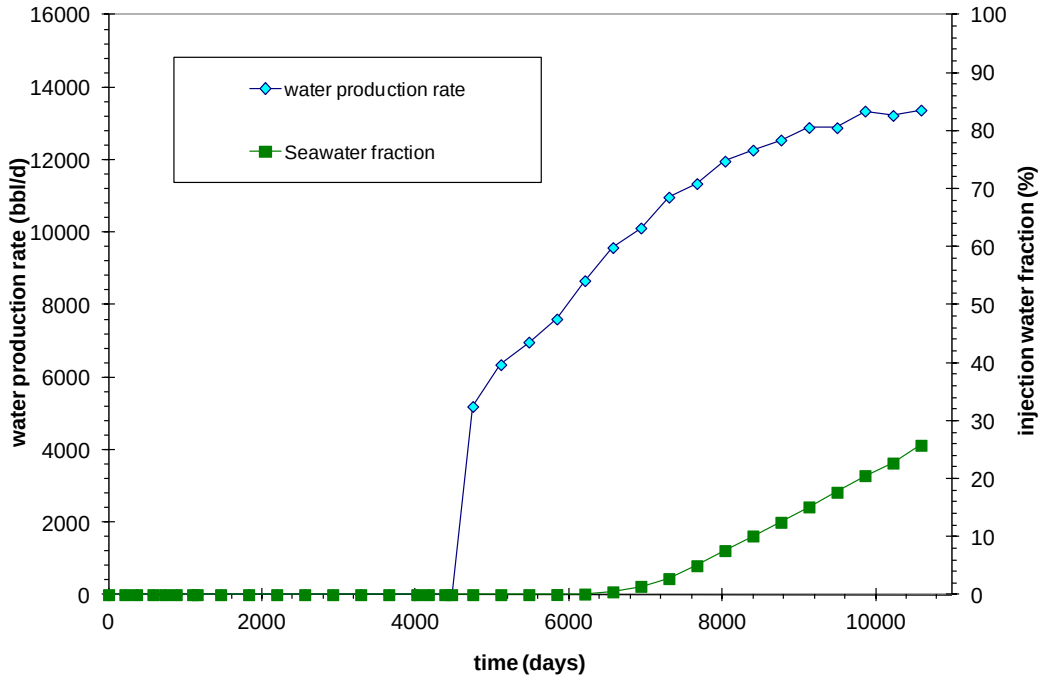

Figure B.56: Water production rate and percentage of the injected water produced as a function of time for well B5Z.

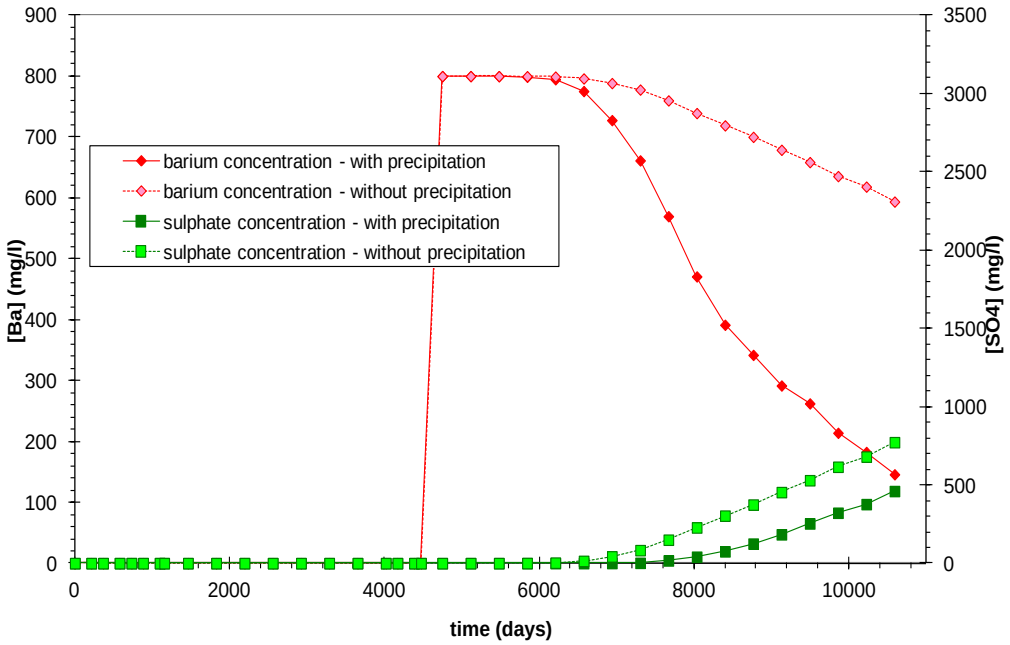

Figure B.57: Barium and sulphate production with instantaneous precipitation and without precipitation as a function of time for well B5Z.

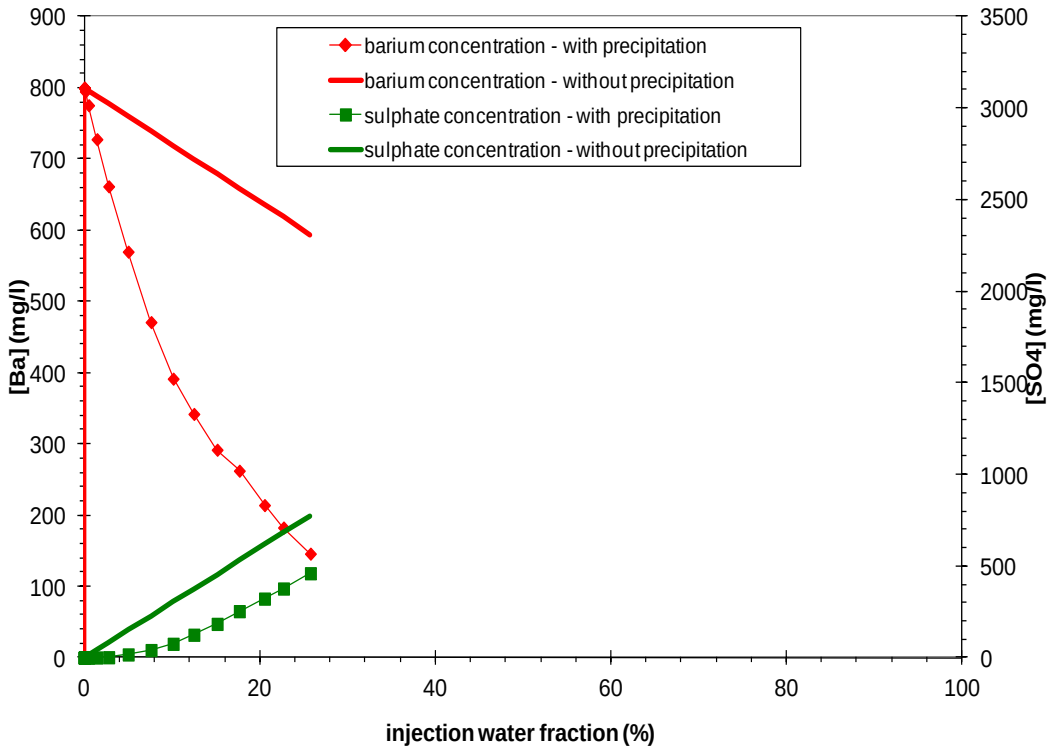

Figure B.58: The produced concentration of barium and sulphate ions as a function of the produced fraction of sea water for well B5Z.

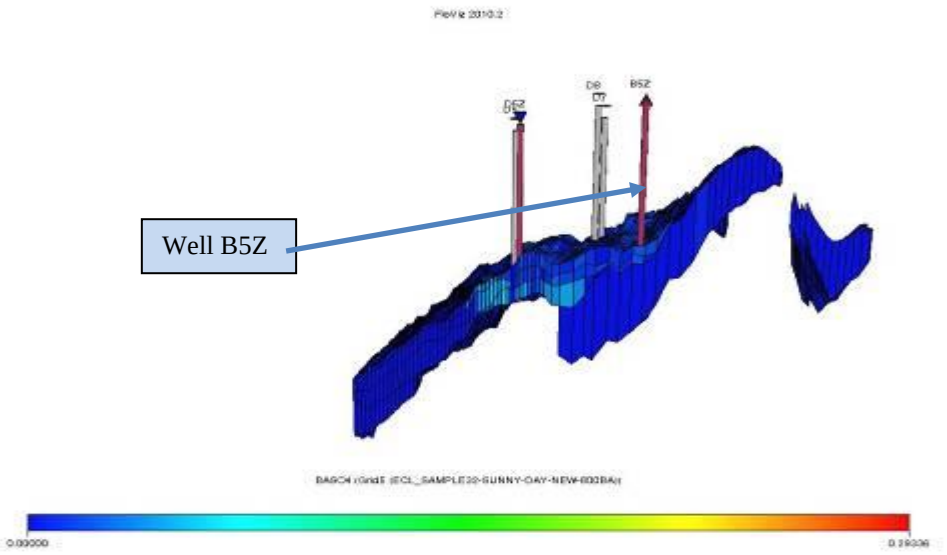

Figure B.59: The 3D section of Field X indicates $BaSO_4$ location for well B5Z.

Well D9Z -with barium concentration of 800 mg/l.

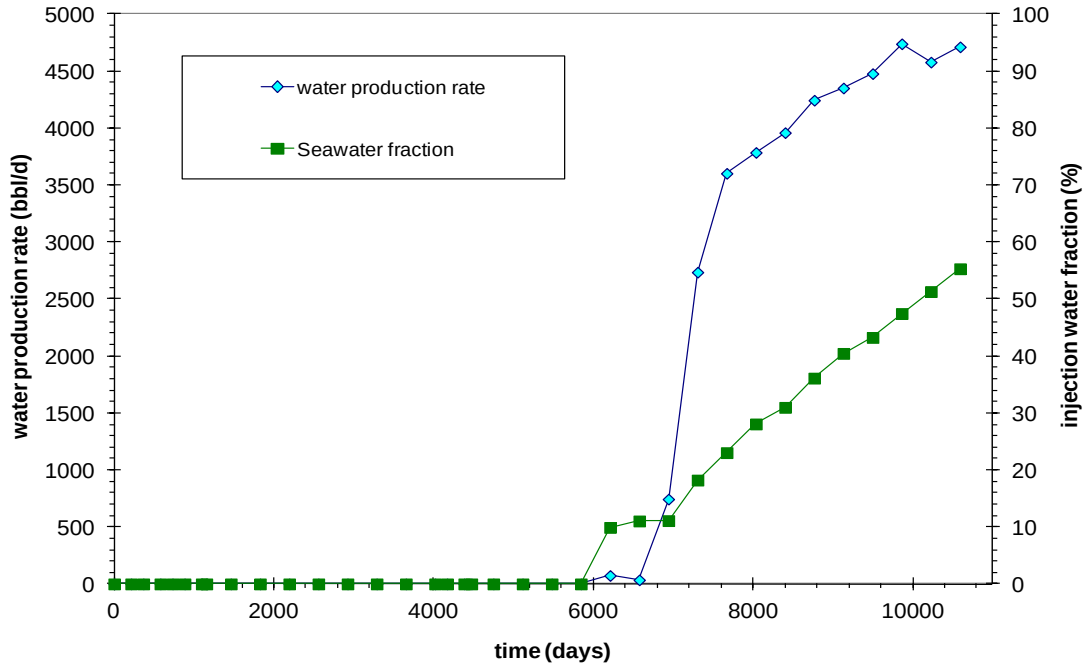

Figure B.60: Water production rate and percentage of the injected water produced as a function of time for well D9Z.

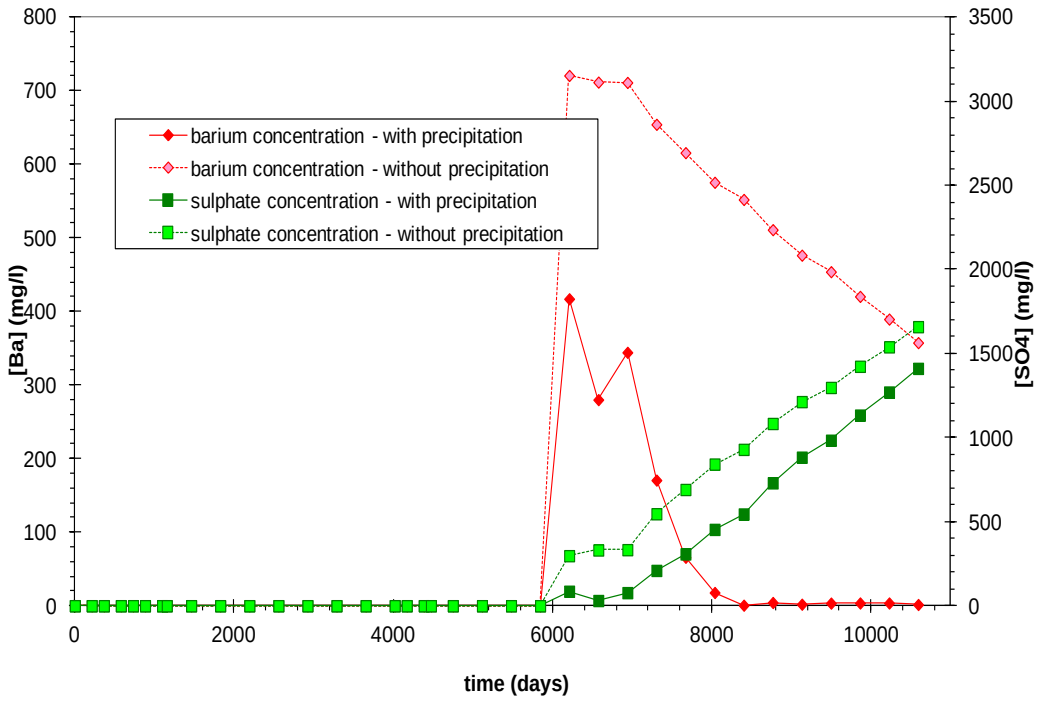

Figure B.61: Barium and sulphate production with instantaneous precipitation and without precipitation as a function of time for well D9Z.

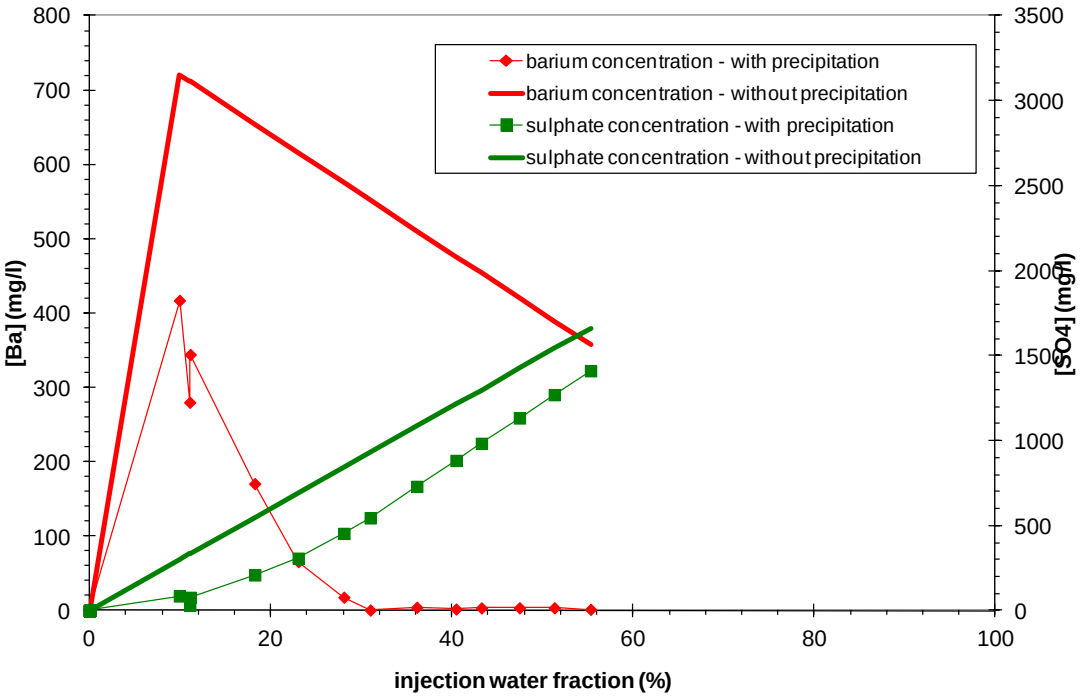

Figure B.62: The produced concentration of barium and sulphate ions as a function of the produced fraction of sea water for well D9Z.

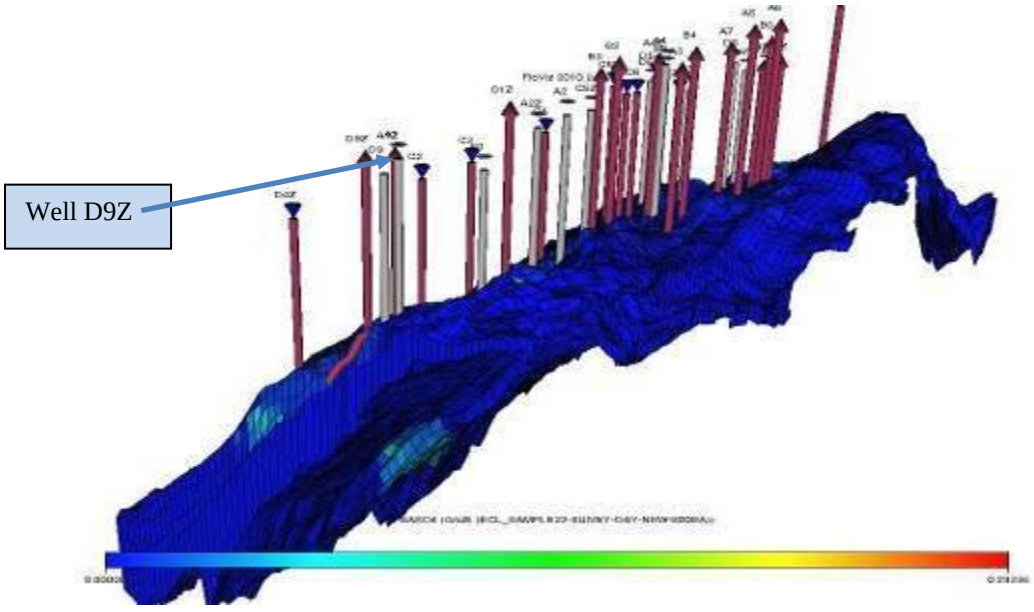

Figure B.63: The 3D section of Field X indicates $BaSO_4$ location for well D9Z.

APPENDIX C: DATA FILE USED IN THE FIELD X ANALYSIS

The data file used in Field X. Scale specific parts highlighted.

RUNSPEC

FRONTSIM

TITLE

Mp13 area review

DIMENS

86 154 5 /

FIELD

OIL

WATER

START

1 JAN 1983 /

GRID

GRIDFILE

2 /

INIT

INCLUDE

ecl_sample32_gri.inc /

PROPS

FSSCALE

-- TRACER1 TRACER 2 MM1 MM2 INTERACTION T-DEPENDENT MAX T1 MAX T2

BA SO_4 137.8 96 'LINEAR' 0 250 3000 / -- DEFAULT

-- TRACER CONC IN PPM

TSVCBA

0 0

1 1 /

TSVC SO_4

0 0

1 1 /

PVDO

500 1.561 0.295

2000 1.524 0.34

2500 1.513 0.355

3000 1.503 0.37

3500 1.492 0.385

4000 1.482 0.4

4500 1.472 0.414

5000 1.461 0.429

5500 1.451 0.445

6000 1.441 0.46

6653 1.428 0.479

7000 1.421 0.49

7500 1.411 0.505

8000 1.401 0.52 /

PVTW

6676 1.03 3.07e-06 0.31 /

RSCONSTT

0.775 0 /

ROCK

6676 5e-06 /

DENSITY

51.615 63.024 0.0624 /

SOF2

0.369 0

0.5102 0.25

0.6515 0.5

0.7928 0.75

0.934 1 /

0.351 0

0.4895 0.25

0.628 0.5

0.7665 0.75

0.905 1 /

0.301 0

0.4297 0.25

0.5585 0.5

0.6873 0.75

0.816 1 /

0.1 0

0.125 0.25

0.15 0.5

0.175 0.75

0.2 1 /

SWFN

0.066 0 0

0.35 0 0

0.4202 0.165 0

0.4905 0.33 0

0.5608 0.495 0

0.631 0.66 0

1 1 0 /

0.095 0 0

0.35 0 0

0.4248 0.165 0

0.4995 0.33 0

0.5742 0.495 0

0.649 0.66 0

1 1 0 /

0.184 0 0

0.35 0 0

0.4372 0.09425 0

0.5245 0.1885 0

0.6118 0.28275 0

0.699 0.377 0

1 1 0 /

0.8 0 0

0.825 0.05975 0

0.85 0.1195 0

0.875 0.17925 0

0.9 0.239 0

1 1 0 /

TRACER

Ba WAT /

SO_4 WAT /

SW WAT / -- SEA WATER

FW WAT /-- Formation water

/

REGIONS

INCLUDE

ecl_sample32_reg.inc /

SOLUTION

TBLKFBa

66220*250 /

TBLKFSO_4

66220*0 /

TBLKFFW

66220*250 /

TBLKFSW

66220*0 /

EQUIL

10006.6 6653 10387 /

SUMMARY

WTPRSO_4

/

WTPRBA

/

WTPTSO_4

/

WTPTBA

/

WTPRSW

/

WTPRFW

/

WTPTSW

/

WTPTFW

/

WWPR

/

-- Field average pressure

FPR

-- Field water cut

FWCT

-- Bottomhole pressure of all wells

WBHP

/

-- Field Oil Production Rate

```
FOPR
-- Field Water Production Rate
FWPR
-- Field Oil Production Total
FOPT
-- Field Water Production Total
FWPT
EXCEL
SCHEDULE
TUNEFSPR
1 0.01 4* /
TUNEFSSA
 2 0.500000 1* 1* NO 1* 1* 1*
-- Warning: SUSPEND NOCLOSEWELL keyword not converted
INCLUDE
 ecl_sample32_sched-sunny-day-new.inc /

RPTRST
--  'BASIC=3'  'POT'  'FIP=3'   'FREQ=3'   /
  3 4* 1 /
TUNEFSPR
 1 /
WELSPECS
 A1        NN          52    46  1*  LIQ  3* 1* 3* /
 A1Z       NN          53    47  1*  LIQ  3* 1* 3* /
 A2        NC          46    65  1*  LIQ  3* 1* 3* /
 A2Z       NC          46    56  1*  LIQ  3* 1* 3* /
```

A3 CR 29 71 1* LIQ 3* 1* 3* /

A4 CR 32 77 1* LIQ 3* 1* 3* /

A4Z CR 33 78 1* LIQ 3* 1* 3* /

A5 CR 25 80 1* LIQ 3* 1* 3* /

A6 CC 21 87 1* LIQ 3* 1* 3* /

A7 CC 30 93 1* LIQ 3* 1* 3* /

B1 NC 50 55 1* LIQ 3* 1* 3* /

B1Z NN 45 51 1* LIQ 3* 1* 3* /

B2 NC 46 56 1* LIQ 3* 1* 3* /

B3 CR 40 74 1* LIQ 3* 1* 3* /

B4 CR 28 75 1* LIQ 3* 1* 3* /

B5 CC 34 87 1* LIQ 3* 1* 3* /

B5Z SS 30 117 1* LIQ 3* 1* 3* /

B6 SC 27 99 1* LIQ 3* 1* 3* /

B7 SC 29 109 1* LIQ 3* 1* 3* /

B7Z SC 30 108 1* LIQ 3* 1* 3* /

C2 NC 58 59 1* LIQ 3* 1* 3* /

C3 NC 57 70 1* LIQ 3* 1* 3* /

C4 NC 51 81 1* LIQ 3* 1* 3* /

C5Y CC 40 90 1* LIQ 3* 1* 3* /

C5Z CC 45 90 1* LIQ 3* 1* 3* /

C6 SC 42 106 1* LIQ 3* 1* 3* /

C7 CC 38 93 1* LIQ 3* 1* 3* /

D3 SC 34 101 1* LIQ 3* 1* 3* /

D3Z SC 35 101 1* LIQ 3* 1* 3* /

D4 NN 57 31 1* LIQ 3* 1* 3* /

D4Z NN 61 39 1* LIQ 3* 1* 3* /

```
D5       SS        46   117  1*  LIQ  3* 1* 3* /
D5Z      SS        46   118  1*  LIQ  3* 1* 3* /
D6       NN        49    21  1*  LIQ  3* 1* 3* /
D7       SS        41   133  1*  LIQ  3* 1* 3* /
D8       SS        35   122  1*  LIQ  3* 1* 3* /
D9       NN        52    43  1*  LIQ  3* 1* 3* /
D9Z      NC        47    29  1*  LIQ  3* 1* 3* /
F1       LK        24   111  1*  LIQ  3* 1* 3* /
/

COMPDAT
A1        52   46    1    1 1* 1*  1*  0.71  1*  1*  1*  Z  /
A1        52   46    2    2 1* 1*  1*  0.71  1*  1*  1*  Z  /
A1        52   46    3    3 1* 1*  1*  0.71  1*  1*  1*  Z  /
A1        52   45    4    4 1* 1*  1*  0.71  0  1*  1*  Z  /
A1Z       53   47    1    1 1* 1*  1*  0.71  1*  1*  1*  Z  /
A1Z       53   47    2    2 1* 1*  1*  0.71  0  1*  1*  Z  /
A1Z       53   47    3    3 1* 1*  1*  0.71  0  1*  1*  Z  /
A1Z       53   47    4    4 1* 1*  1*  0.71  0  1*  1*  Z  /
A2        46   65    2    2 1* 1*  1*  0.71  1*  1*  1*  Z  /
A2        46   65    3    3 1* 1*  1*  0.71  1*  1*  1*  Z  /
A2        46   65    4    4 1* 1*  1*  0.71  1*  1*  1*  Z  /
A2        47   65    5    5 1* 1*  1*  0.71  0  1*  1*  Z  /
A2Z       46   56    2    2 1* 1*  1*  0.71  1*  1*  1*  Z  /
A2Z       46   56    3    3 1* 1*  1*  0.71  1*  1*  1*  Z  /
A2Z       46   56    4    4 1* 1*  1*  0.71  1*  1*  1*  Z  /
A2Z       46   56    5    5 1* 1*  1*  0.71  0  1*  1*  Z  /
```

```
A3      28   71    1    1 1* 1*  1*  0.71  0  1*  1*  Z  /
A3      28   71    2    2 1* 1*  1*  0.71  0  1*  1*  Z  /
A3      28   71    4    4 1* 1*  1*  0.71  0  1*  1*  Z  /
A3      28   71    5    5 1* 1*  1*  0.71  1*  1*  1*  Z  /
A4      32   77    1    1 1* 1*  1*  0.71  0  1*  1*  Z  /
A4      32   77    2    2 1* 1*  1*  0.71  0  1*  1*  Z  /
A4      32   77    4    4 1* 1*  1*  0.71  0  1*  1*  Z  /
A4      31   76    5    5 1* 1*  1*  0.71  1*  1*  1*  Z  /
A4Z     33   78    5    5 1* 1*  1*  0.71  1*  1*  1*  Z  /
A5      25   80    1    1 1* 1*  1*  0.71  0  1*  1*  Z  /
A5      24   80    2    2 1* 1*  1*  0.71  0  1*  1*  Z  /
A5      24   80    5    5 1* 1*  1*  0.71  1*  1*  1*  Z  /
A6      21   87    1    1 1* 1*  1*  0.71  0  1*  1*  Z  /
A6      21   87    2    2 1* 1*  1*  0.71  0  1*  1*  Z  /
A6      21   88    5    5 1* 1*  1*  0.71  1*  1*  1*  Z  /
A6      20   88    5    5 1* 1*  1*  0.71  1*  1*  1*  Z  /
A7      30   93    1    1 1* 1*  1*  0.71  0  1*  1*  Z  /
A7      30   93    2    2 1* 1*  1*  0.71  0  1*  1*  Z  /
A7      30   93    4    4 1* 1*  1*  0.71  1*  1*  1*  Z  /
A7      30   93    5    5 1* 1*  1*  0.71  0  1*  1*  Z  /
B1      50   55    2    2 1* 1*  1*  0.71  1*  1*  1*  Z  /
B1      50   55    3    3 1* 1*  1*  0.71  1*  1*  1*  Z  /
B1      50   55    4    4 1* 1*  1*  0.71  0  1*  1*  Z  /
B1      50   55    5    5 1* 1*  1*  0.71  0  1*  1*  Z  /
B1Z     45   51    1    1 1* 1*  1*  0.71  0  1*  1*  Z  /
B1Z     45   50    2    2 1* 1*  1*  0.71  1*  1*  1*  Z  /
B1Z     45   50    3    3 1* 1*  1*  0.71  1*  1*  1*  Z  /
```

B1Z 45 50 4 4 1* 1* 1* 0.71 1* 1* 1* Z /

B1Z 44 49 5 5 1* 1* 1* 0.71 1* 1* 1* Z /

B2 37 72 2 2 1* 1* 1* 0.71 1* 1* 1* Z /

B2 37 71 4 4 1* 1* 1* 0.71 1* 1* 1* Z /

B3 40 74 1 1 1* 1* 1* 0.71 0 1* 1* Z /

B3 40 74 2 2 1* 1* 1* 0.71 1* 1* 1* Z /

B3 40 74 4 4 1* 1* 1* 0.71 1* 1* 1* Z /

B3 40 74 5 5 1* 1* 1* 0.71 1* 1* 1* Z /

B4 28 75 1 1 1* 1* 1* 0.71 1* 1* 1* Z /

B4 28 74 2 2 1* 1* 1* 0.71 0 1* 1* Z /

B4 28 74 4 4 1* 1* 1* 0.71 0 1* 1* Z /

B5 34 87 1 1 1* 1* 1* 0.71 1* 1* 1* Z /

B5 34 87 2 2 1* 1* 1* 0.71 1* 1* 1* Z /

B5 34 87 4 4 1* 1* 1* 0.71 1* 1* 1* Z /

B5 34 87 5 5 1* 1* 1* 0.71 0 1* 1* Z /

B5Z 30 118 1 1 1* 1* 1* 0.71 1* 1* 1* Z /

B5Z 30 118 2 2 1* 1* 1* 0.71 1* 1* 1* Z /

B5Z 30 118 5 5 1* 1* 1* 0.71 0 1* 1* Z /

B6 27 100 2 2 1* 1* 1* 0.71 0 1* 1* Z /

B6 27 100 4 4 1* 1* 1* 0.71 1* 1* 1* Z /

B6 27 100 5 5 1* 1* 1* 0.71 0 1* 1* Z /

B7 29 109 1 1 1* 1* 1* 0.71 1* 1* 1* Z /

B7 29 109 2 2 1* 1* 1* 0.71 1* 1* 1* Z /

B7 29 110 4 4 1* 1* 1* 0.71 1* 1* 1* Z /

B7 29 110 5 5 1* 1* 1* 0.71 0 1* 1* Z /

B7Z 29 108 1 1 1* 1* 1* 0.71 0 1* 1* Z /

B7Z 29 108 2 2 1* 1* 1* 0.71 0 1* 1* Z /

B7Z 29 108 4 4 1* 1* 1* 0.71 1* 1* 1* Z /

C2 58 59 1 1 1* 1* 1* 0.71 1* 1* 1* Z /

C2 58 59 2 2 1* 1* 1* 0.71 1* 1* 1* Z /

C2 58 58 2 2 1* 1* 1* 0.71 1* 1* 1* Z /

C2 58 58 3 3 1* 1* 1* 0.71 0 1* 1* Z /

C2 58 58 4 4 1* 1* 1* 0.71 0 1* 1* Z /

C2 58 58 5 5 1* 1* 1* 0.71 0 1* 1* Z /

C3 57 70 1 1 1* 1* 1* 0.71 1* 1* 1* Z /

C3 57 69 2 2 1* 1* 1* 0.71 0 1* 1* Z /

C3 58 69 3 3 1* 1* 1* 0.71 0 1* 1* Z /

C3 58 69 4 4 1* 1* 1* 0.71 0 1* 1* Z /

C3 58 69 5 5 1* 1* 1* 0.71 0 1* 1* Z /

C4 51 81 1 1 1* 1* 1* 0.71 1* 1* 1* Z /

C4 51 81 2 2 1* 1* 1* 0.71 1* 1* 1* Z /

C4 51 81 3 3 1* 1* 1* 0.71 1* 1* 1* Z /

C4 52 81 5 5 1* 1* 1* 0.71 0 1* 1* Z /

C5Y 40 90 1 1 1* 1* 1* 0.71 1* 1* 1* Z /

C5Y 40 90 2 2 1* 1* 1* 0.71 1* 1* 1* Z /

C5Y 40 90 4 4 1* 1* 1* 0.71 1* 1* 1* Z /

C5Y 40 90 5 5 1* 1* 1* 0.71 0 1* 1* Z /

C5Z 45 90 2 2 1* 1* 1* 0.71 1* 1* 1* Z /

C5Z 45 90 4 4 1* 1* 1* 0.71 0 1* 1* Z /

C5Z 45 90 5 5 1* 1* 1* 0.71 0 1* 1* Z /

C6 42 106 1 1 1* 1* 1* 0.71 1* 1* 1* Z /

C6 42 106 2 2 1* 1* 1* 0.71 1* 1* 1* Z /

C6 42 107 2 2 1* 1* 1* 0.71 1* 1* 1* Z /

C6 42 107 4 4 1* 1* 1* 0.71 0 1* 1* Z /

C6 42 107 5 5 1* 1* 1* 0.71 0 1* 1* Z /

C7 38 93 1 1 1* 1* 1* 0.71 1* 1* 1* Z /

C7 38 93 2 2 1* 1* 1* 0.71 1* 1* 1* Z /

C7 38 93 4 4 1* 1* 1* 0.71 1* 1* 1* Z /

C7 38 93 5 5 1* 1* 1* 0.71 1* 1* 1* Z /

D3 34 101 1 1 1* 1* 1* 0.71 1* 1* 1* Z /

D3 34 101 2 2 1* 1* 1* 0.71 1* 1* 1* Z /

D3 34 101 4 4 1* 1* 1* 0.71 1* 1* 1* Z /

D3 34 101 5 5 1* 1* 1* 0.71 0 1* 1* Z /

D3Z 35 101 1 1 1* 1* 1* 0.71 0 1* 1* Z /

D3Z 35 101 2 2 1* 1* 1* 0.71 0 1* 1* Z /

D3Z 35 101 4 4 1* 1* 1* 0.71 1* 1* 1* Z /

D4 57 31 1 1 1* 1* 1* 0.71 1* 1* 1* Z /

D4 57 31 2 2 1* 1* 1* 0.71 1* 1* 1* Z /

D4 57 31 3 3 1* 1* 1* 0.71 1* 1* 1* Z /

D4 57 31 4 4 1* 1* 1* 0.71 0 1* 1* Z /

D4Z 61 39 1 1 1* 1* 1* 0.71 1* 1* 1* Z /

D4Z 61 39 2 2 1* 1* 1* 0.71 1* 1* 1* Z /

D4Z 61 40 3 3 1* 1* 1* 0.71 1* 1* 1* Z /

D4Z 61 40 4 4 1* 1* 1* 0.71 0 1* 1* Z /

D5 46 118 1 1 1* 1* 1* 0.71 1* 1* 1* Z /

D5 46 118 2 2 1* 1* 1* 0.71 0 1* 1* Z /

D5 46 118 4 4 1* 1* 1* 0.71 1* 1* 1* Z /

D5Z 45 118 1 1 1* 1* 1* 0.71 1* 1* 1* Z /

D5Z 45 118 2 2 1* 1* 1* 0.71 1* 1* 1* Z /

D5Z 45 118 4 4 1* 1* 1* 0.71 1* 1* 1* Z /

D6 49 21 1 1 1* 1* 1* 0.71 1* 1* 1* Z /

```
D6        49   21    2    2 1* 1*  1*  0.71  1*  1*  1*  Z  /
D6        49   21    3    3 1* 1*  1*  0.71  1*  1*  1*  Z  /
D6        49   21    5    5 1* 1*  1*  0.71  0  1*  1*  Z  /
D7        41  133    1     1 1* 1*  1*  0.71  1*  1*  1*  Z  /
D7        41  133    2     2 1* 1*  1*  0.71  1*  1*  1*  Z  /
D7        41  133    4     4 1* 1*  1*  0.71  0  1*  1*  Z  /
D8        35  122    1     1 1* 1*  1*  0.71  0  1*  1*  Z  /
D8        35  122    2     2 1* 1*  1*  0.71  1*  1*  1*  Z  /
D8        35  122    4     4 1* 1*  1*  0.71  1*  1*  1*  Z  /
D9        52   43    2    2 1* 1*  1*  0.71  1*  1*  1*  Z  /
D9        52   43    3    3 1* 1*  1*  0.71  1*  1*  1*  Z  /
D9        52   43    4    4 1* 1*  1*  0.71  1*  1*  1*  Z  /
D9        52   43    5    5 1* 1*  1*  0.71  0  1*  1*  Z  /
D9Z       47   35    1     1 1* 1*  1*  0.71  1*  1*  1*  Z  /
D9Z       47   34    1     1 1* 1*  1*  0.71  1*  1*  1*  Z  /
D9Z       47   33    2     2 1* 1*  1*  0.71  1*  1*  1*  Z  /
D9Z       47   32    2     2 1* 1*  1*  0.71  1*  1*  1*  Z  /
D9Z       47   31    3     3 1* 1*  1*  0.71  1*  1*  1*  Z  /
F1        24  111    5     5 1* 1*  1*  0.71  1*  1*  1*  Z  /
/
DATES
 1 AUG 1983 /
/
WCONPROD
 D3       1* LRAT 3* 21802.1 1* 2500 /
 D4       1* LRAT 3* 10445 1* 2500 /
 D5       1* LRAT 3* 9952.58 1* 2500 /
```

D6 1* LRAT 3* 3883.22 1* 2500 /

D7 1* LRAT 3* 8250.02 1* 2500 /

D8 1* LRAT 3* 37.22 1* 2500 /

D9 1* LRAT 3* 20252.6 1* 2500 /

/

WECON

D3 10 1* 0.99 1* 1* /

D4 10 1* 0.99 1* 1* /

D5 10 1* 0.99 1* 1* /

D6 10 1* 0.99 1* 1* /

D7 10 1* 0.99 1* 1* /

D8 10 1* 0.99 1* 1* /

D9 10 1* 0.99 1* 1* /

/

DATES

1 JAN 1984 /

/

WCONPROD

A2 1* LRAT 3* 867.23 1* 2500 /

B5 1* LRAT 3* 23485.7 1* 2500 /

D3 1* LRAT 3* 25846.8 1* 2500 /

D4 1* LRAT 3* 5966.82 1* 2500 /

D5 1* LRAT 3* 12096.9 1* 2500 /

D6 1* LRAT 3* 8766.96 1* 2500 /

D7 1* LRAT 3* 7907.97 1* 2500 /

D8 1* LRAT 3* 6483.47 1* 2500 /

D9 1* LRAT 3* 21950.2 1* 2500 /

```
/

WECON

 A2      10 1* 0.99 1* 1* /

 B5      10 1* 0.99 1* 1* /

 D3      10 1* 0.99 1* 1* /

 D4      10 1* 0.99 1* 1* /

 D5      10 1* 0.99 1* 1* /

 D6      10 1* 0.99 1* 1* /

 D7      10 1* 0.99 1* 1* /

 D8      10 1* 0.99 1* 1* /

 D9      10 1* 0.99 1* 1* /

/

DATES

 1 AUG 1984 /

/

WCONPROD

 A2      1* LRAT 3* 24704.5 1* 2500 /

 B5      1* LRAT 3* 32979 1* 2500 /

 C2      1* LRAT 3* 2075.7 1* 2500 /

 D3      1* LRAT 3* 18627.8 1* 2500 /

 D5      1* LRAT 3* 9348.38 1* 2500 /

 D6      1* LRAT 3* 7024.77 1* 2500 /

 D7      1* LRAT 3* 4270.68 1* 2500 /

 D8      1* LRAT 3* 11482.6 1* 2500 /

 D9      1* LRAT 3* 16288.9 1* 2500 /

/

WCONINJE
```

C6 WATER 1* RATE 18804.2 1* 8500 /

D4 WATER 1* RATE 15159.2 1* 8500 /

/

WTRACER

C6 SO_4 3000 /

C6 SW 3000 /

D4 SO_4 3000 /

D4 SW 3000 /

/

WECON

A2 10 1* 0.99 1* 1* /

B5 10 1* 0.99 1* 1* /

C2 10 1* 0.99 1* 1* /

D3 10 1* 0.99 1* 1* /

D5 10 1* 0.99 1* 1* /

D6 10 1* 0.99 1* 1* /

D7 10 1* 0.99 1* 1* /

D8 10 1* 0.99 1* 1* /

D9 10 1* 0.99 1* 1* /

/

DATES

1 JAN 1985 /

/

WCONPROD

A2 1* LRAT 3* 15184.2 1* 2500 /

B3 1* LRAT 3* 1918.96 1* 2500 /

B5 1* LRAT 3* 30976 1* 2500 /

C2 1* LRAT 3* 10000.6 1* 2500 /

C4 1* LRAT 3* 13337.8 1* 2500 /

D3 1* LRAT 3* 17646 1* 2500 /

D6 1* LRAT 3* 5993.33 1* 2500 /

D7 1* LRAT 3* 2751.93 1* 2500 /

D8 1* LRAT 3* 12214.1 1* 2500 /

D9 1* LRAT 3* 17389.6 1* 2500 /

/

WCONINJE

C6 WATER 1* RATE 41120.5 1* 8500 /

D4 WATER 1* RATE 19088.2 1* 8500 /

D5 WATER 1* RATE 15017.8 1* 8500 /

/

WTRACER

D5 SO_4 3000 /

D5 SW 3000 /

/

WECON

A2 10 1* 0.99 1* 1* /

B3 10 1* 0.99 1* 1* /

B5 10 1* 0.99 1* 1* /

C2 10 1* 0.99 1* 1* /

C4 10 1* 0.99 1* 1* /

D3 10 1* 0.99 1* 1* /

D6 10 1* 0.99 1* 1* /

D7 10 1* 0.99 1* 1* /

D8 10 1* 0.99 1* 1* /

```
 D9       10 1* 0.99 1* 1* /

/

DATES

 1 JUN 1985 /

/

COMPDAT

 C2        58   58    3    3 1* 1*  1*  0.71  1*  1*  1*  Z  /

 C2        58   58    4    4 1* 1*  1*  0.71  1*  1*  1*  Z  /

 C2        58   58    5    5 1* 1*  1*  0.71  1*  1*  1*  Z  /

 C4        52   81    5    5 1* 1*  1*  0.71  1*  1*  1*  Z  /

/

WCONPROD

 A2       1* LRAT 3* 17108.6 1* 2500 /

 B1       1* LRAT 3* 15319.1 1* 2500 /

 B3       1* LRAT 3* 24451.8 1* 2500 /

 B5       1* LRAT 3* 25700.9 1* 2500 /

 C3       1* LRAT 3* 5345.63 1* 2500 /

 C5Z       1* LRAT 3* 793.54 1* 2500 /

 D3       1* LRAT 3* 12275.4 1* 2500 /

 D6       1* LRAT 3* 2717.15 1* 2500 /

 D7       1* LRAT 3* 2028.88 1* 2500 /

 D8       1* LRAT 3* 6462.38 1* 2500 /

 D9       1* LRAT 3* 13702.5 1* 2500 /

/

WCONINJE

 C2       WATER 1* RATE 43391 1* 8500 /

 C4       WATER 1* RATE 16667.7 1* 8500 /
```

C6 WATER 1* RATE 45130.4 1* 8500 /

D4 WATER 1* RATE 18822 1* 8500 /

D5 WATER 1* RATE 0 1* 8500 /

D5Z WATER 1* RATE 12618 1* 8500 /

/

WTRACER

C2 SO_4 3000 /

C2 SW 3000 /

C4 SO_4 3000 /

C4 SW 3000 /

D5Z $SO_{4\ 3000}$ /

D5Z SW 3000 /

/

WECON

A2 10 1* 0.99 1* 1* /

B1 10 1* 0.99 1* 1* /

B3 10 1* 0.99 1* 1* /

B5 10 1* 0.99 1* 1* /

C3 10 1* 0.99 1* 1* /

C5Z 10 1* 0.99 1* 1* /

D3 10 1* 0.99 1* 1* /

D6 10 1* 0.99 1* 1* /

D7 10 1* 0.99 1* 1* /

D8 10 1* 0.99 1* 1* /

D9 10 1* 0.99 1* 1* /

/

DATES

```
 1 JAN 1986 /

/

WCONPROD

 A2       1* LRAT 3* 17484.8 1* 2500 /

 A3       1* LRAT 3* 1742.68 1* 2500 /

 B1       1* LRAT 3* 20972.7 1* 2500 /

 B3       1* LRAT 3* 27357.5 1* 2500 /

 B5       1* LRAT 3* 25795.4 1* 2500 /

 C3       1* LRAT 3* 8205.4 1* 2500 /

 C5Z      1* LRAT 3* 1786.01 1* 2500 /

 D3       1* LRAT 3* 13557.9 1* 2500 /

 D6       1* LRAT 3* 3429.33 1* 2500 /

 D7       1* LRAT 3* 3200.46 1* 2500 /

 D9       1* LRAT 3* 16537.6 1* 2500 /

/

WCONINJE

 C2       WATER 1* RATE 32768.4 1* 8500 /

 C4       WATER 1* RATE 16554.6 1* 8500 /

 C6       WATER 1* RATE 36159 1* 8500 /

 D4       WATER 1* RATE 17264.1 1* 8500 /

 D5Z      WATER 1* RATE 21895.2 1* 8500 /

/

WECON

 A2       10 1* 0.99 1* 1* /

 A3       10 1* 0.99 1* 1* /

 B1       10 1* 0.99 1* 1* /

 B3       10 1* 0.99 1* 1* /
```

B5 10 1* 0.99 1* 1* /

C3 10 1* 0.99 1* 1* /

C5Z 10 1* 0.99 1* 1* /

D3 10 1* 0.99 1* 1* /

D6 10 1* 0.99 1* 1* /

D7 10 1* 0.99 1* 1* /

D9 10 1* 0.99 1* 1* /

/

DATES

1 MAR 1986 /

/

COMPDAT

C3 57 69 2 2 1* 1* 1* 0.71 1* 1* 1* Z /

C3 58 69 3 3 1* 1* 1* 0.71 1* 1* 1* Z /

C3 58 69 4 4 1* 1* 1* 0.71 1* 1* 1* Z /

C3 58 69 5 5 1* 1* 1* 0.71 1* 1* 1* Z /

A2 47 65 5 5 1* 1* 1* 0.71 1* 1* 1* Z /

/

WCONPROD

A2 1* LRAT 3* 8898.31 1* 2500 /

A3 1* LRAT 3* 1616.31 1* 2500 /

A5 1* LRAT 3* 5797.38 1* 2500 /

B1 1* LRAT 3* 11611.4 1* 2500 /

B3 1* LRAT 3* 15802 1* 2500 /

B5 1* LRAT 3* 17235.5 1* 2500 /

B7 1* LRAT 3* 25052.1 1* 2500 /

C5Z 1* LRAT 3* 0 1* 2500 /

D3 1* LRAT 3* 12191.3 1* 2500 /

D6 1* LRAT 3* 5331.46 1* 2500 /

D7 1* LRAT 3* 6395.28 1* 2500 /

D8 1* LRAT 3* 0 1* 2500 /

D9 1* LRAT 3* 15904.2 1* 2500 /

/

WCONINJE

C2 WATER 1* RATE 31280.5 1* 8500 /

C3 WATER 1* RATE 25198.5 1* 8500 /

C4 WATER 1* RATE 12768.9 1* 8500 /

C5Z WATER 1* RATE 5483.55 1* 8500 /

C6 WATER 1* RATE 43268.9 1* 8500 /

D4 WATER 1* RATE 17803.8 1* 8500 /

D5Z WATER 1* RATE 23632.2 1* 8500 /

/

WTRACER

C3 SO_4 3000 /

C3 SW 3000 /

C5Z SO_4 3000 /

C5Z SW 3000 /

/

WECON

A2 10 1* 0.99 1* 1* /

A3 10 1* 0.99 1* 1* /

A5 10 1* 0.99 1* 1* /

B1 10 1* 0.99 1* 1* /

B3 10 1* 0.99 1* 1* /

```
 B5       10 1* 0.99 1* 1* /
 B7       10 1* 0.99 1* 1* /
 C5Z      10 1* 0.99 1* 1* /
 D3       10 1* 0.99 1* 1* /
 D6       10 1* 0.99 1* 1* /
 D7       10 1* 0.99 1* 1* /
 D8       10 1* 0.99 1* 1* /
 D9       10 1* 0.99 1* 1* /
/
DATES
 1 JAN 1987 /
/
COMPDAT
 A3        28   71    1    1 1* 1*  1*  0.71  1*  1*  1*  Z  /
 A3        28   71    2    2 1* 1*  1*  0.71  1*  1*  1*  Z  /
 A3        28   71    4    4 1* 1*  1*  0.71  1*  1*  1*  Z  /
/

WCONPROD
 A2       1* LRAT 3* 15648.6 1* 2500 /
 A3       1* LRAT 3* 16932.9 1* 2500 /
 A5       1* LRAT 3* 100 1* 2500 /
 B1       1* LRAT 3* 10399.4 1* 2500 /
 B3       1* LRAT 3* 24018.1 1* 2500 /
 B5       1* LRAT 3* 26604.9 1* 2500 /
 B7       1* LRAT 3* 4908.58 1* 2500 /
 D3       1* LRAT 3* 10301.8 1* 2500 /
```

D6 1* LRAT 3* 5116.14 1* 2500 /

D8 1* LRAT 3* 5160.86 1* 2500 /

D9 1* LRAT 3* 6514.68 1* 2500 /

/

WCONINJE

C2 WATER 1* RATE 20470.8 1* 8500 /

C3 WATER 1* RATE 16855.4 1* 8500 /

C4 WATER 1* RATE 4704.41 1* 8500 /

C5Z WATER 1* RATE 5593.3 1* 8500 /

C6 WATER 1* RATE 40052.8 1* 8500 /

D4 WATER 1* RATE 15923.6 1* 8500 /

D5Z WATER 1* RATE 24294.7 1* 8500 /

D7 WATER 1* RATE 5820.55 1* 8500 /

/

WTRACER

D7 SO_4 3000 /

D7 SW 3000 /

/

WECON

A2 10 1* 0.99 1* 1* /

A3 10 1* 0.99 1* 1* /

A5 10 1* 0.99 1* 1* /

B1 10 1* 0.99 1* 1* /

B3 10 1* 0.99 1* 1* /

B5 10 1* 0.99 1* 1* /

B7 10 1* 0.99 1* 1* /

D3 10 1* 0.99 1* 1* /

D6 10 1* 0.99 1* 1* /

D8 10 1* 0.99 1* 1* /

D9 10 1* 0.99 1* 1* /

/

DATES

1 JAN 1988 /

/

COMPDAT

D8 35 122 1 1 1* 1* 1* 0.71 1* 1* 1* Z /

/

WCONPROD

A2 1* LRAT 3* 17981.2 1* 2500 /

A3 1* LRAT 3* 12906.9 1* 2500 /

A5 1* LRAT 3* 1361.23 1* 2500 /

B1 1* LRAT 3* 8287.85 1* 2500 /

B3 1* LRAT 3* 19071.6 1* 2500 /

B5 1* LRAT 3* 23053.7 1* 2500 /

B7 1* LRAT 3* 27633.8 1* 2500 /

C7 1* LRAT 3* 5425.19 1* 2500 /

D3 1* LRAT 3* 4771.45 1* 2500 /

D6 1* LRAT 3* 4038.42 1* 2500 /

D8 1* LRAT 3* 6116.65 1* 2500 /

D9 1* LRAT 3* 12799.8 1* 2500 /

/

WCONINJE

C2 WATER 1* RATE 18778.8 1* 8500 /

C3 WATER 1* RATE 18062.1 1* 8500 /

C4 WATER 1* RATE 10770.2 1* 8500 /

C5Z WATER 1* RATE 6122.15 1* 8500 /

C6 WATER 1* RATE 38758.2 1* 8500 /

D4 WATER 1* RATE 14869.9 1* 8500 /

D5Z WATER 1* RATE 23724 1* 8500 /

D7 WATER 1* RATE 10365.2 1* 8500 /

/

WECON

A2 10 1* 0.99 1* 1* /

A3 10 1* 0.99 1* 1* /

A5 10 1* 0.99 1* 1* /

B1 10 1* 0.99 1* 1* /

B3 10 1* 0.99 1* 1* /

B5 10 1* 0.99 1* 1* /

B7 10 1* 0.99 1* 1* /

C7 10 1* 0.99 1* 1* /

D3 10 1* 0.99 1* 1* /

D6 10 1* 0.99 1* 1* /

D8 10 1* 0.99 1* 1* /

D9 10 1* 0.99 1* 1* /

/

DATES

1 JAN 1989 /

/

COMPDAT

A5 25 80 1 1 1* 1* 1* 0.71 1* 1* 1* Z /

A5 24 80 2 2 1* 1* 1* 0.71 1* 1* 1* Z /

B3 40 74 1 1 1* 1* 1* 0.71 1* 1* 1* Z /

D3 34 101 4 4 1* 1* 1* 0.71 0 1* 1* Z /

/

WCONPROD

A1 1* LRAT 3* 2790.67 1* 2500 /

A2 1* LRAT 3* 18076.9 1* 2500 /

A3 1* LRAT 3* 14098.2 1* 2500 /

A5 1* LRAT 3* 18277.4 1* 2500 /

A6 1* LRAT 3* 5359.53 1* 2500 /

B1 1* LRAT 3* 7832.58 1* 2500 /

B3 1* LRAT 3* 20466.6 1* 2500 /

B5 1* LRAT 3* 23745.7 1* 2500 /

B7 1* LRAT 3* 29096.1 1* 2500 /

D3 1* LRAT 3* 5.34 1* 2500 /

D6 1* LRAT 3* 1896.18 1* 2500 /

D8 1* LRAT 3* 4715.92 1* 2500 /

D9 1* LRAT 3* 0 1* 2500 /

/

WCONINJE

C2 WATER 1* RATE 14668.3 1* 8500 /

C3 WATER 1* RATE 19054.4 1* 8500 /

C4 WATER 1* RATE 9566.63 1* 8500 /

C5Z WATER 1* RATE 7055.64 1* 8500 /

C6 WATER 1* RATE 34847.1 1* 8500 /

C7 WATER 1* RATE 53148.7 1* 8500 /

D4 WATER 1* RATE 5397.09 1* 8500 /

D5Z WATER 1* RATE 20098.3 1* 8500 /

D7 WATER 1* RATE 7842.35 1* 8500 /

/

WTRACER

C7 SO_4 3000 /

C7 SW 3000 /

/

WECON

A1 10 1* 0.99 1* 1* /

A2 10 1* 0.99 1* 1* /

A3 10 1* 0.99 1* 1* /

A5 10 1* 0.99 1* 1* /

A6 10 1* 0.99 1* 1* /

B1 10 1* 0.99 1* 1* /

B3 10 1* 0.99 1* 1* /

B5 10 1* 0.99 1* 1* /

B7 10 1* 0.99 1* 1* /

D3 10 1* 0.99 1* 1* /

D6 10 1* 0.99 1* 1* /

D8 10 1* 0.99 1* 1* /

D9 10 1* 0.99 1* 1* /

/

DATES

1 JAN 1990 /

/

WCONPROD

A1 1* LRAT 3* 22182 1* 2500 /

A2 1* LRAT 3* 16989.8 1* 2500 /

A3 1* LRAT 3* 10738.2 1* 2500 /

A5 1* LRAT 3* 12325.6 1* 2500 /

A6 1* LRAT 3* 8516.18 1* 2500 /

B1 1* LRAT 3* 12.42 1* 2500 /

B3 1* LRAT 3* 16424.3 1* 2500 /

B5 1* LRAT 3* 15731 1* 2500 /

B7 1* LRAT 3* 23935.9 1* 2500 /

D3 1* LRAT 3* 0 1* 2500 /

D6 1* LRAT 3* 2992.72 1* 2500 /

D8 1* LRAT 3* 6511.78 1* 2500 /

/

WCONINJE

C2 WATER 1* RATE 20644.7 1* 8500 /

C3 WATER 1* RATE 17989.4 1* 8500 /

C4 WATER 1* RATE 7639.77 1* 8500 /

C5Y WATER 1* RATE 8962.01 1* 8500 /

C5Z WATER 1* RATE 870.9 1* 8500 /

C6 WATER 1* RATE 35433.6 1* 8500 /

C7 WATER 1* RATE 34094.1 1* 8500 /

D4 WATER 1* RATE 7016.69 1* 8500 /

D5Z WATER 1* RATE 6411.1 1* 8500 /

D7 WATER 1* RATE 7036.76 1* 8500 /

```
/

WTRACER

  C5Y SO4 3000 /

  C5Y SW 3000 /

  /

WECON

 A1      10 1* 0.99 1* 1* /

 A2      10 1* 0.99 1* 1* /

 A3      10 1* 0.99 1* 1* /

 A5      10 1* 0.99 1* 1* /

 A6      10 1* 0.99 1* 1* /

 B1      10 1* 0.99 1* 1* /

 B3      10 1* 0.99 1* 1* /

 B5      10 1* 0.99 1* 1* /

 B7      10 1* 0.99 1* 1* /

 D3      10 1* 0.99 1* 1* /

 D6      10 1* 0.99 1* 1* /

 D8      10 1* 0.99 1* 1* /

/

DATES

 1 JAN 1991 /

/

COMPDAT

 B5        34   87    5    5 1* 1*  1*  0.71  1*  1*  1*  Z  /

 A1        52   45    4    4 1* 1*  1*  0.71  1*  1*  1*  Z  /

 A4        32   77    1    1 1* 1*  1*  0.71  1*  1*  1*  Z  /

 A4        32   77    2    2 1* 1*  1*  0.71  1*  1*  1*  Z  /
```

A4 31 77 4 4 1* 1* 1* 0.71 1* 1* 1* Z /

A6 21 87 2 2 1* 1* 1* 0.71 1* 1* 1* Z /

/

WCONPROD

A1 1* LRAT 3* 23432.3 1* 2500 /

A2 1* LRAT 3* 3652.01 1* 2500 /

A3 1* LRAT 3* 14783.3 1* 2500 /

A4 1* LRAT 3* 17039.2 1* 2500 /

A5 1* LRAT 3* 15598 1* 2500 /

A6 1* LRAT 3* 13207.7 1* 2500 /

B1 1* LRAT 3* 0 1* 2500 /

B3 1* LRAT 3* 19321.4 1* 2500 /

B5 1* LRAT 3* 2111.85 1* 2500 /

B7 1* LRAT 3* 20528.9 1* 2500 /

D6 1* LRAT 3* 2182.15 1* 2500 /

D8 1* LRAT 3* 4620.79 1* 2500 /

/

WCONINJE

C2 WATER 1* RATE 23177 1* 8500 /

C3 WATER 1* RATE 15627.5 1* 8500 /

C4 WATER 1* RATE 8265.44 1* 8500 /

C5Z WATER 1* RATE 0 1* 8500 /

C5Y WATER 1* RATE 31261.8 1* 8500 /

C6 WATER 1* RATE 37635.6 1* 8500 /

C7 WATER 1* RATE 30624.1 1* 8500 /

D4 WATER 1* RATE 11367.8 1* 8500 /

D5Z WATER 1* RATE 13967.1 1* 8500 /

```
 D7       WATER 1* RATE 6290.2 1* 8500 /

/

WECON

 A1       10 1* 0.99 1* 1* /

 A2       10 1* 0.99 1* 1* /

 A3       10 1* 0.99 1* 1* /

 A4       10 1* 0.99 1* 1* /

 A5       10 1* 0.99 1* 1* /

 A6       10 1* 0.99 1* 1* /

 B1       10 1* 0.99 1* 1* /

 B3       10 1* 0.99 1* 1* /

 B5       10 1* 0.99 1* 1* /

 B7       10 1* 0.99 1* 1* /

 D6       10 1* 0.99 1* 1* /

 D8       10 1* 0.99 1* 1* /

/

DATES

 1 JAN 1992 /

/

COMPDAT

 B5         34   87    1    1 1* 1*  1*  0.71  4000  1*  1*  Z  /

 B5         34   87    2    2 1* 1*  1*  0.71  0  1*  1*  Z  /

 B5         34   87    4    4 1* 1*  1*  0.71  0  1*  1*  Z  /

 B5         34   87    5    5 1* 1*  1*  0.71  0  1*  1*  Z  /

 B7         29   109    2    2 1* 1*  1*  0.71  0  1*  1*  Z  /

 B7         29   110    4    4 1* 1*  1*  0.71  0  1*  1*  Z  /

/
```

```
WCONPROD
 A1       1* LRAT 3* 25256.4 1* 2500 /
 A2       1* LRAT 3* 0 1* 2500 /
 A3       1* LRAT 3* 17703.9 1* 2500 /
 A4       1* LRAT 3* 22540.6 1* 2500 /
 A5       1* LRAT 3* 18596.3 1* 2500 /
 A6       1* LRAT 3* 20177.8 1* 2500 /
 A7       1* LRAT 3* 7078.07 1* 2500 /
 B1Z      1* LRAT 3* 7313.99 1* 2500 /
 B3       1* LRAT 3* 18109.2 1* 2500 /
 B5       1* LRAT 3* 0 1* 2500 /
 B7       1* LRAT 3* 12911.1 1* 2500 /
 D6       1* LRAT 3* 1711.77 1* 2500 /
 D8       1* LRAT 3* 324.25 1* 2500 /
/
WCONINJE
 C2       WATER 1* RATE 24826 1* 8500 /
 C3       WATER 1* RATE 9363.65 1* 8500 /
 C4       WATER 1* RATE 7950.52 1* 8500 /
 C5Y      WATER 1* RATE 37275.2 1* 8500 /
 C6       WATER 1* RATE 40561.5 1* 8500 /
 C7       WATER 1* RATE 47485.1 1* 8500 /
 D4       WATER 1* RATE 20316 1* 8500 /
 D5Z      WATER 1* RATE 23085.6 1* 8500 /
 D7       WATER 1* RATE 5767.93 1* 8500 /
/
WECON
```

```
 A1       10 1* 0.99 1* 1* /
 A2       10 1* 0.99 1* 1* /
 A3       10 1* 0.99 1* 1* /
 A4       10 1* 0.99 1* 1* /
 A5       10 1* 0.99 1* 1* /
 A6       10 1* 0.99 1* 1* /
 A7       10 1* 0.99 1* 1* /
 B1Z      10 1* 0.99 1* 1* /
 B3       10 1* 0.99 1* 1* /
 B5       10 1* 0.99 1* 1* /
 B7       10 1* 0.99 1* 1* /
 D6       10 1* 0.99 1* 1* /
 D8       10 1* 0.99 1* 1* /
/
DATES
 1 JAN 1993 /
/
COMPDAT
 A6         21   87    1    1 1* 1*  1*  0.71  1*  1*  1*  Z  /
 B7         29  109    2    2 1* 1*  1*  0.71  1*  1*  1*  Z  /
 B7         29  110    4    4 1* 1*  1*  0.71  1*  1*  1*  Z  /
 C2         58   59    3    3 1* 1*  1*  0.71  0  1*  1*  Z  /
 C2         58   59    4    4 1* 1*  1*  0.71  0  1*  1*  Z  /
/
WCONPROD
 A1       1* LRAT 3* 19429.8 1* 2500 /
 A3       1* LRAT 3* 15308 1* 2500 /
```

A4 1* LRAT 3* 21127 1* 2500 /

A5 1* LRAT 3* 18119.5 1* 2500 /

A6 1* LRAT 3* 17785.2 1* 2500 /

A7 1* LRAT 3* 10625.8 1* 2500 /

B1Z 1* LRAT 3* 14591.1 1* 2500 /

B3 1* LRAT 3* 17549.3 1* 2500 /

B5Z 1* LRAT 3* 7554.67 1* 2500 /

B7 1* LRAT 3* 10349 1* 2500 /

D6 1* LRAT 3* 2565.22 1* 2500 /

D8 1* LRAT 3* 0 1* 2500 /

/

WCONINJE

C2 WATER 1* RATE 15079 1* 8500 /

C3 WATER 1* RATE 19359.9 1* 8500 /

C4 WATER 1* RATE 11648.7 1* 8500 /

C5Y WATER 1* RATE 47050.3 1* 8500 /

C6 WATER 1* RATE 30181.7 1* 8500 /

C7 WATER 1* RATE 38073.9 1* 8500 /

D3Z WATER 1* RATE 9293.04 1* 8500 /

D4 WATER 1* RATE 17810.2 1* 8500 /

D5Z WATER 1* RATE 22511.5 1* 8500 /

D7 WATER 1* RATE 1993.1 1* 8500 /

/

WTRACER

D3Z SO_4 3000 /

```
  D3Z SW 3000 /
  /
WECON
 A1       10 1* 0.99 1* 1* /
 A3       10 1* 0.99 1* 1* /
 A4       10 1* 0.99 1* 1* /
 A5       10 1* 0.99 1* 1* /
 A6       10 1* 0.99 1* 1* /
 A7       10 1* 0.99 1* 1* /
 B1Z      10 1* 0.99 1* 1* /
 B3       10 1* 0.99 1* 1* /
 B5Z      10 1* 0.99 1* 1* /
 B7       10 1* 0.99 1* 1* /
 D6       10 1* 0.99 1* 1* /
 D8       10 1* 0.99 1* 1* /
/
DATES
 1 JAN 1994 /
/
COMPDAT
 C2         58   59    3    3 1* 1*  1*  0.71  1*  1*  1*  Z  /
 C2         58   59    4    4 1* 1*  1*  0.71  1*  1*  1*  Z  /
/
WCONPROD
 A1       1* LRAT 3* 14318.7 1* 2500 /
 A2Z      1* LRAT 3* 396.78 1* 2500 /
 A3       1* LRAT 3* 16577 1* 2500 /
```

A4 1* LRAT 3* 20107.7 1* 2500 /

A5 1* LRAT 3* 21070.2 1* 2500 /

A6 1* LRAT 3* 4525.88 1* 2500 /

A7 1* LRAT 3* 6680.36 1* 2500 /

B1Z 1* LRAT 3* 12443.6 1* 2500 /

B3 1* LRAT 3* 19242.6 1* 2500 /

B5Z 1* LRAT 3* 24103.9 1* 2500 /

B6 1* LRAT 3* 5713.77 1* 2500 /

B7 1* LRAT 3* 0 1* 2500 /

B7Z 1* LRAT 3* 9724.56 1* 2500 /

/

WCONINJE

C2 WATER 1* RATE 29084.5 1* 8500 /

C3 WATER 1* RATE 17190.5 1* 8500 /

C4 WATER 1* RATE 9187.55 1* 8500 /

C5Y WATER 1* RATE 52723.7 1* 8500 /

C6 WATER 1* RATE 34429.6 1* 8500 /

C7 WATER 1* RATE 50822.9 1* 8500 /

D3Z WATER 1* RATE 26367.3 1* 8500 /

D4 WATER 1* RATE 0 1* 8500 /

D4Z WATER 1* RATE 4279.06 1* 8500 /

D5Z WATER 1* RATE 17547.8 1* 8500 /

D7 WATER 1* RATE 0 1* 8500 /

/

WTRACER

D4Z SO_4 3000 /

```
  D4Z SW 3000 /
  /
WECON
 A1       10 1* 0.99 1* 1* /
 A2Z      10 1* 0.99 1* 1* /
 A3       10 1* 0.99 1* 1* /
 A4       10 1* 0.99 1* 1* /
 A5       10 1* 0.99 1* 1* /
 A6       10 1* 0.99 1* 1* /
 A7       10 1* 0.99 1* 1* /
 B1Z      10 1* 0.99 1* 1* /
 B3       10 1* 0.99 1* 1* /
 B5Z      10 1* 0.99 1* 1* /
 B6       10 1* 0.99 1* 1* /
 B7       10 1* 0.99 1* 1* /
 B7Z      10 1* 0.99 1* 1* /
/
DATES
 1 JUN 1994 /
/
COMPDAT
 A6         21    87     5     5 1* 1*  1*  0.71  0  1*  1*  Z  /
 A6         20    87     5     5 1* 1*  1*  0.71  0  1*  1*  Z  /
/
WCONPROD
 A1       1* LRAT 3* 14318.7 1* 2500 /
 A2Z      1* LRAT 3* 396.78 1* 2500 /
```

A3 1* LRAT 3* 16577 1* 2500 /

A4 1* LRAT 3* 20107.7 1* 2500 /

A5 1* LRAT 3* 21070.2 1* 2500 /

A6 1* LRAT 3* 4525.88 1* 2500 /

A7 1* LRAT 3* 6680.36 1* 2500 /

B1Z 1* LRAT 3* 12443.6 1* 2500 /

B3 1* LRAT 3* 19242.6 1* 2500 /

B5Z 1* LRAT 3* 24103.9 1* 2500 /

B6 1* LRAT 3* 5713.77 1* 2500 /

B7Z 1* LRAT 3* 9724.56 1* 2500 /

/

WCONINJE

C2 WATER 1* RATE 29084.5 1* 8500 /

C3 WATER 1* RATE 17190.5 1* 8500 /

C4 WATER 1* RATE 9187.55 1* 8500 /

C5Y WATER 1* RATE 52723.7 1* 8500 /

C6 WATER 1* RATE 34429.6 1* 8500 /

C7 WATER 1* RATE 50822.9 1* 8500 /

D3Z WATER 1* RATE 26367.3 1* 8500 /

D4Z WATER 1* RATE 4279.06 1* 8500 /

D5Z WATER 1* RATE 17547.8 1* 8500 /

/

WECON

A1 10 1* 0.99 1* 1* /

A2Z 10 1* 0.99 1* 1* /

A3 10 1* 0.99 1* 1* /

A4 10 1* 0.99 1* 1* /

A5 10 1* 0.99 1* 1* /

A6 10 1* 0.99 1* 1* /

A7 10 1* 0.99 1* 1* /

B1Z 10 1* 0.99 1* 1* /

B3 10 1* 0.99 1* 1* /

B5Z 10 1* 0.99 1* 1* /

B6 10 1* 0.99 1* 1* /

B7Z 10 1* 0.99 1* 1* /

/

DATES

1 JAN 1995 /

/

WCONPROD

A1 1* LRAT 3* 8022.48 1* 2500 /

A2Z 1* LRAT 3* 0 1* 2500 /

A3 1* LRAT 3* 17732.4 1* 2500 /

A4 1* LRAT 3* 18497.5 1* 2500 /

A5 1* LRAT 3* 12560.2 1* 2500 /

A6 1* LRAT 3* 5518.66 1* 2500 /

A7 1* LRAT 3* 11297.5 1* 2500 /

B1Z 1* LRAT 3* 11600.3 1* 2500 /

B3 1* LRAT 3* 20180.7 1* 2500 /

B5Z 1* LRAT 3* 17102.1 1* 2500 /

B6 1* LRAT 3* 22678.2 1* 2500 /

B7Z 1* LRAT 3* 18017.9 1* 2500 /

/

WCONINJE

C2 WATER 1* RATE 24406 1* 8500 /

C3 WATER 1* RATE 9365 1* 8500 /

C4 WATER 1* RATE 7160.95 1* 8500 /

C5Y WATER 1* RATE 59351.9 1* 8500 /

C6 WATER 1* RATE 36852 1* 8500 /

C7 WATER 1* RATE 48226.4 1* 8500 /

D3Z WATER 1* RATE 30790 1* 8500 /

D4Z WATER 1* RATE 16488.1 1* 8500 /

D5Z WATER 1* RATE 23834.6 1* 8500 /

/

WECON

A1 10 1* 0.99 1* 1* /

A2Z 10 1* 0.99 1* 1* /

A3 10 1* 0.99 1* 1* /

A4 10 1* 0.99 1* 1* /

A5 10 1* 0.99 1* 1* /

A6 10 1* 0.99 1* 1* /

A7 10 1* 0.99 1* 1* /

B1Z 10 1* 0.99 1* 1* /

B3 10 1* 0.99 1* 1* /

B5Z 10 1* 0.99 1* 1* /

B6 10 1* 0.99 1* 1* /

B7Z 10 1* 0.99 1* 1* /

/

DATES

1 APR 1995 /

/

WCONPROD

A1 1* LRAT 3* 0 1* 2500 /

A1Z 1* LRAT 3* 13950.5 1* 2500 /

A3 1* LRAT 3* 21500.3 1* 2500 /

A4 1* LRAT 3* 0 1* 2500 /

A4Z 1* LRAT 3* 9737.69 1* 2500 /

A5 1* LRAT 3* 4440.06 1* 2500 /

A6 1* LRAT 3* 4181.08 1* 2500 /

A7 1* LRAT 3* 1353.3 1* 2500 /

B1Z 1* LRAT 3* 12980.8 1* 2500 /

B2 1* LRAT 3* 2275.68 1* 2500 /

B3 1* LRAT 3* 20475.1 1* 2500 /

B4 1* LRAT 3* 12734.9 1* 2500 /

B5Z 1* LRAT 3* 16990.9 1* 2500 /

B6 1* LRAT 3* 13447.4 1* 2500 /

B7Z 1* LRAT 3* 9497.9 1* 2500 /

D9Z 1* LRAT 3* 4922.01 1* 2500 /

/

WCONINJE

C2 WATER 1* RATE 23444.1 1* 8500 /

C3 WATER 1* RATE 10560.1 1* 8500 /

C5Y WATER 1* RATE 50905 1* 8500 /

C6 WATER 1* RATE 33316.1 1* 8500 /

C7 WATER 1* RATE 44160.4 1* 8500 /

D3Z WATER 1* RATE 27307.9 1* 8500 /

D4Z WATER 1* RATE 17407.9 1* 8500 /

D5Z WATER 1* RATE 20725.2 1* 8500 /

F1 WATER 1* RATE 2940.4 1* 8500 /

/

WTRACER

F1 SO_4 3000 /

F1 SW 3000 /

/

WECON

A1 10 1* 0.99 1* 1* /

A1Z 10 1* 0.99 1* 1* /

A3 10 1* 0.99 1* 1* /

A4 10 1* 0.99 1* 1* /

A4Z 10 1* 0.99 1* 1* /

A5 10 1* 0.99 1* 1* /

A6 10 1* 0.99 1* 1* /

A7 10 1* 0.99 1* 1* /

B1Z 10 1* 0.99 1* 1* /

B2 10 1* 0.99 1* 1* /

B3 10 1* 0.99 1* 1* /

B4 10 1* 0.99 1* 1* /

B5Z 10 1* 0.99 1* 1* /

B6 10 1* 0.99 1* 1* /

B7Z 10 1* 0.99 1* 1* /

D9Z 10 1* 0.99 1* 1* /

/

DATES

1 JAN 1996 /

/

-- end history match

-- START PREDICTION

DATES

1 JAN 1997 /

1 JAN 1998 /

1 JAN 1999 /

1 JAN 2000 /

1 JAN 2001 /

1 JAN 2002 /

1 JAN 2003 /

1 JAN 2004 /

1 JAN 2005 /

1 JAN 2006 /

1 JAN 2007 /

1 JAN 2008 /

1 JAN 2009 /

1 JAN 2010 /

1 JAN 2011 /

1 JAN 2012

REFERENCES

Batycky, R.P., Blunt, M.J., and Thiele, M.R.: "A 3D Field Scale Streamline-Based Reservoir Simulator," SPERE (1997) 12, No. 4, 246–254.

Benton W.J., Collins I.R.,Grimsey I.M., Parkinson G.M., Rodger S.A.[1993],*'Nucleation ,Growth and Inhibition of Barium Sulphate–controlled Modification with Organic and Inorganic additives* '; Faraday Discussion , 95,281-297.

Bertero, L., Chierici, G.L., Gotardi, G., Mesini, E. and Mormino, G.: "Chemical Equilibrium Models: Their Use in Simulating the Injection of Incompatible Waters," SPE Reservoir Engineering, pp.288-294, Feb.1998.

Bratvedt, F., Gimse, T., and Tegnander,c.:"*Streamline computation for porous media flow including gravity*, "Transport Porous Med.(1996)25,63.

Butler J.C. and Sorrel C.A. [1971],*'Thermal Expansion and Orthorhombic-Cubic transition of Barium Sulphate and Strontium Sulphate* '; High Temperature Science 3,389-400.

Chernov A.A.[1973],*'Annual Review Of Material Science* '; Vol. 3, Palo Alto, California. 397,Ann. Rev .Inc

Coleman, M.: "*Novel Methods for Determining Chemical Compositions of Oil-Zone Waters and Relevance to Scale Prediction*", presented at the 1999 1st SPE Symposium *Oilfield Scale: Field Applications and Novel Solutions*, Aberdeen, Scotland, Jan. 27-28.

Collins I.R. [1999],*'Surface Electrical Properties of Barium Sulphate Modified by Adsorption of poly α,β Aspartic Acid* '; Journal of Colloids and Interfacial Science 212,535-544.

Davey R.J ,Balck S.N, Bromely R.A., Cottier D., Dobbos B. and Rout J.E [1991],*'Molecular Design Based On Recognition at inorganic Surface* ';Nature

353,549.

Datta-Gupta, A.: "*Accurate Resolution of Physical Dispersion in the Multidimensional Numerical Modelling of Miscible and Chemical Displacements*," SPERE (1990) 15, No. 4, 581–588.

Datta-Gupta, A.: *"Streamline Simulation: A Technology Update," SPE Distinguished* Author Series, JPT (December 2000) 68–73.

Datta-Gupta, A. and King, M.J.: "*A Semianalytic Approach to Tracer Flow Modelling in Heterogeneous Permeable Media*," Adv. Water Resour. (1995) 18, No. 1, 9.

Datta-Gupta, A. et al.: "*A Symmetric Positive Definite Formulation of a Three Dimensional Micellar/ Polymer Simulator*," SPERE (1986) 1, No. 6, 622–632.

Datta-Gupta, A. et al.: "*High Resolution Monotonic Schemes for Reservoir Fluid Flow Simulation,"* In Situ (1991) 15, 3, 289–317.

Datta-Gupta, A. et al.: "A Type-Curve Approach to Analyzing Two-Well Tracer Tests," SPEFE (1995) 10, No. 1, 40.

Datta-Gupta, A. et al.: *"Streamlines, Ray Tracing and Production Tomography: Generalization to Compressible Flow*," Pet. Geosci. (2001) 7, S75–S86 (special supplement on Geostatistics).

Datta-Gupta, A. and King, M.J., [2007], "*Streamline Simulation :Theory and practice*" SPE Textbook Series Volume 11.

Deer, Howie R.A. and Zussman [1992], '*An Introduction to the Rock-Forming Minerals*'; (2nd Edition Longman Group UK.).

Emanuel, A.S. and Milliken, W.J.: "*The Application of Streamtube Techniques to Full Field Waterflood Simulation*," paper SPE 30758 in Proceedings of the 1995 SPE

Annual.

ECLIPSE 100 99A, Reference Manual; Technical Description, Schlumberger GeoQuest Reservoir Technologies, 1999.

Fischer R.B [1995],'*Precipitation of Barium Sulphate*: *Investigation by electron Microscopy* '; Analytical Chemistry 23, 11.

FrontSim 99A, User Guide, Schlumberger GeoQuest Reservoir Technologies, 1999.

Gallardo V., Zurita L., Ontiveros A. and Duran J.D.G. [2000],*'Interfacial Properties of Barium Sulphate Suspension* and *Implication in Their Stability* '; Journal of Pharmaceutical Science 89, 9, September.

Gautier, Y., Blunt, M.J. and Christie, M.A.: "*Nested Gridding and Streamline Simulation for Fast Reservoir Performance Prediction*," paper SPE 51931 in Proceedings of the 1999 Reservoir Simulation Symposium, Houston, Texas.

Hennessy A. J. B., Graham G.M. [2002],' *The Effect of Additives on the Crystallization of calcium with Barium Sulfate* '; Journal of Crystal Growth , 237-239, 2153-2159.
Hertman. P, Perdok.G.[1995], '*Acta Crystallographica ,'On Relation Between Structure and Morphology Crystals* II';8,521.

Hertman. P, Perdok.G.[1995], '*Acta Crystallographica ,'On Relation Between Structure and Morphology Crystals* I';8,59

Hinrichsen, C.J. and Edgerton, M.C.: "*Preventing Scale Deposition in Oil Production Facilities*," presented at the 1998 IBC Fourth International Conference on Advances in Solving Oilfield Scaling, Aberdeen, Scotland, Jan. 28-29

Lantz, R.B.: "*Quantitative Evaluation of Numerical Diffusion (Truncation Error*)," paper SPE 2811, 1981.

Liu S.T. and Nancolls G.H. [1976], *'Scanning Electron Microscopic and kinetic Studies of the Crystallization and Dissolution of Barium Sulphate Crystal* '; Journal of Crystal Growth 33, 11-20

Lolo Mari, T., Bratvedt, K., Crane, M., Milliken, W.J., and Tyrie J.: "*The Use of Streamline Simulation in Reservoir Management: Methodology and Case Studies*," paper SPE 63157 to be presented at the 2000 SPE Annual Technical Conference and Exhibition, Dallas, Texas, Oct. 1-4.

Lugo N., **"***Impact Of Injection Regime On Brine Mixing In The Reservoir And In Situ Scale Deposition*", MSc project, Heriot Watt University,

Mackay, E.J., Matharu, A.P., Sorbie, K.S., Jordan, M.M. and Tomlins, R.: "*Modelling of Scale Inhibitor Treatments in Horizontal Wells: Application to the Alba Fiel*d," paper SPE 39452 presented at the 1998 SPE International Symposium on Formation Damage Control, Lafayette, Louisiana, Feb. 18-19.

Mackay, E.J. and Sorbie, K.S.[1998] "*Modelling Scale Inhibitor Squeeze Treatments in High Cross flow Horizontal Wells,"* paper SPE 50418 presented at the 1998 SPE Third International Conference on Horizontal Well Technology, Calgary, Alberta, Nov. 1-4.

Mackay, E.J. and Sorbie, K.S.: "*An Evaluation of Simulation Techniques for Modelling Squeeze Treatments*," paper SPE 56775 presented at the 1999 SPE Annual Conference and Exhibition, Houston, Texas, Oct. 3-6

Mackay E.J., Sorbie K.S. "*Brine Mixing in waterflood reservoirs and the implications for scale prevention*", paper SPE9 60193, paper presented to the 2000 SPE symposium Oilfield Scale, Aberdeen, 26-27 January.

Mackay, E.J. and Sorbie, K.S.: "*Brine Mixing in Waterflooded Reservoirs and the Implications for Scale Prevention,"* paper SPE 60193 presented at the 2000 2nd International Symposium on Oilfield Scale, Aberdeen, UK, Jan. 26-27.

Mackay, E.J., Matharu, A.P., Sorbie, K.S., Jordan, M.M., and Tomlins, R, [2000] "*Modelling Scale-Inhibitor Treatments in Horizontal Wells: Application to the Alba Field*" paper SPE 63013, SPE Prod. & Facilities, 15 (2) 107-114.

Mackay, E.J.: "*Modelling of In-Situ Scale Deposition: the Impact of Reservoir and Well Geometries and Kinetic Reaction Rates*" paper SPE 81830, SPE Prod. & Facilities (February 2003) 18 (1) 45-56.

Mackay, E.J.: "*Predicting In-Situ Sulphate Scale Deposition and the Impact on Produced Ion Concentrations*", Trans IChemE (March 2003) 81 (A) 326-332.

Mackay, E.J., Jordan, M.M. and Torabi, F.: "*Predicting Brine Mixing deep Within the Reservoir, and the Impact on Scale Control in Marginal and Deepwater Developments*" paper SPE 85104, SPE Prod. & Facilities (Aug 2003) 18 (3) 210-220.

Mackay E.J., Graham G.M.: "*The Use of Flow models in Assessing the Risk of Scale Drainage*", paper SPE80252, presented at the 2003 SPE symposium on Oilfield Chemistry, Houston, 20-21 February.

Mackay, E.J., Jordan, M.M., Feasey, N., Shah, D., Kumar, P. and Ali, S.,[2003],' *Integrated Risk Analysis for Scale Management in Deepwater Developments"* by paper SPE 87459, SPE Prod. & Facilities, 20 (2) 138-154.

Mackay, E.J., Jordan, M.M., Feasey, N., Shah, D., Kumar, P. and Ali, S.: "*Integrated Risk Analysis for Scale Management in Deepwater Developments*" paper SPE 87459, SPE Journal of Production Technology (August 2004) 58 (8) 49-51. Also in SPE Prod. & Facilities (May 2005) 20 (2) 138-154.

Marchisio D.L., Barresi A.A., Garbero M., Vanni M. and Baldi G. [2002], '*Study of the aggregation in Barium Sulphate Precipitation* ', 15-18 September.

Markov .I.V. [1996],'Crystal *Growth for Beginner; Fundamental of Nucleation, Crystal Gross and Expitaxy,* ; World Scientific Publishing ,2nd Edition.

Mellor J.W. [1922],*'A Comprehensive Treatise on Inorganic and Theatrical Chemistry*'; Vol. 1,590.

Oddo, J.E. and Tomson, M.T [1994],*'why Scale Forms in the oil Field and methods to prevent it* '; SPE Production and Facilities, 47-54.

Ostwald, W. [1896],' Lehrbruck der Allgemeinen Chemie', vol.2,Part 1.Leipzing,Germany.

Peddibhotla, S., Datta-Gupta, A. and Xue, G.: "*Multiphase Streamline Modelling in Three Dimensions*: *Further Generalizations and a Field Application*," paper SPE 38003 in Proceedings of the 1997 14th Reservoir Simulation Symposium, Dallas, Texas, Jun. 8-11.

Pina C. M., Enders M. and Putnis A [2000],' *The Composition of Solid Solutions Crystallising from Aqueous Solutions: The influence of superstation and Growth Mechanism* 'Chemical Geology, 168,195-210.

Pollok ,DW .,"*Semianalytical compostion of path lines for finite difference method* ," Ground water , 26(6), 743-750(1988)

Redfren S. E. and parker S. C. [1998],*'Atomic Simulation of the effect of calcium and Strontium Defect on the Surface Structure and Stability of Barium Sulphate* '; J. Chem. Soc.: Faraday Trans., 94(14)..

Simon Day, Tim Griffin [1998],*'Redevelopment and Management of the Magnus Field for Post-Plateau Production*'; paper SPE 49130 presented annual technical conference and exhibition held in New Orland, Louisiana, 27-30 Sep. 1998.

Sorbie, K.S., Todd, A.C., Wat, R.M.S. and McClosky, T.: "*Derivation of Scale* Inhibitor Isotherms for Sandstone Reservoirs," presented at the Royal Society of Chemistry Symposium Session "Chemicals in the Oil Industry," Imperial College, London, Apr. 9-11, 1991

Sorbie, K.S. and Mackay, E.J.: "*Mixing of Injected, Connate and Aquifer Brines in waterflooding and its Relevance to Oilfield Scaling*" Journal of Petroleum Science and Engineering (July2000)27(1-2) 85-106

Sorbie, K.S. and Mackay, E.J.: "*Mixing of Injected, Connate and Aquifer Brines in Waterflooding and its Relevance to Oilfield Scaling*," Journal of Petroleum Science and Engineering 27, Elsevier, pp.85-106, 2000.

Sweeney F. M. and Cooper S. D.: "*The Development of a Novel Scale Inhibitor for Severe Water Chemistries,"* paper SPE 25159 presented at the 1993 SPE International Symposium on Oilfield Chemistry, New Orleans, LA, U.S.A., March 2-5

Thiele, M.R., Batycky, R.P. and Blunt, M.J.: "*A 3D Field Scale Streamline with Gravity and Changing Well Conditions*," paper SPE 36726 in Proceedings of the 1996 SPE Annual Technical Conference and Exhibition, Denver, Colorado, Oct. 6-9.

Thiele, M.R., Batycky, R.P. and Blunt, M.J.: "*A Streamline-Based 3D Field-Scaled* Compositional Reservoir Simulator," paper SPE 38889 presented at the 1997 SPE Annual Conference and Exhibition, San Antonio, Texas, Oct. 5-8.

Tim P. Moulds, Phillip Trussell [2010],*'Post-Plateau Production Mangament in Magnus Field*'; paper SPE 134953 presented annual technical conference and exhibition held in Florence, Italy, 19-22 Sep. 2010.

Vetter O. J. G.[1975],'*Oilfield Scale- Can we Handel it* ?'; Journal of Petroleum Technology 259, 1515-1523.

White, R, Brookley, J and Menzies, N, "*Practical Experiences of Gel Diversion Technique and an Overview of Scale Management for the Alba Field*", SPE Symposium Oilfield Scale: Field Applications and Novel Solutions, Aberdeen, Scotland, 27 - 28 January 1999.

Weintritt, D.J., Cown, J.C. [1967],'*Unique Characteristics of Barium Sulfate Scale Deposition'*; Journal of Petroleum Technology, 19, 1381-1394.

Zhang, L.R., Sorbie, K.S. and Mackay, E.J.: "*Modelling Scale Inhibitor Squeeze Treatments in Horizontal Wells: Model Development and Application*", paper SPE 37140 presented at the 1996 SPE International Conference and Exhibition on Horizontal Well Technology, Nov. 18-20.

Yuan, M.D. and Todd, A.C.: "*Prediction of Sulphate Scaling Tendency in Oilfield Operations*," *SPE Production Engineering* (Feb. 1991) 63-72.